

Improved Condition Monitoring of Composite Insulators

A thesis submitted to The University of Manchester for the degree of

Doctor of Philosophy

in the Faculty of Engineering and Physical Sciences

2012

Elizabeth Da Silva Domingues

School of Electrical and Electronic Engineering

CONTENTS

1. INTRODUCTION.....	31
2. ASSET MANAGEMENT	34
2.1. General Definition of Asset Management.....	34
2.2. Asset Management for Electric Power Distribution System Operators (DSOs)..	37
2.2.1. Division of Asset Management in DSOs	38
2.2.2. Information Categories to Consider in Managing Electrical Assets	39
2.2.3. Levels of Asset Management Decision Process on Power Distribution Utilities	40
2.2.4. Basic Timescales of Asset Management.....	43
2.3. Maintenance, Monitoring and Condition Assessment.....	43
2.3.1. Maintenance Approaches	44
2.3.2. Asset Condition Information	46
2.3.3. Asset Degradation Analysis by Health Indices Formulation	47
2.3.4. Typical Asset Life Curves versus Probability of Failure Diagrams	55
2.4. EDF Energy Networks’ Asset Management	57
2.4.1. Generalities.....	57
2.4.2. Formulation of EDF’s Health Indices.....	61
2.5. Distribution Overhead Line Asset Management	62
2.5.1. Overhead Line Health Index Formulation	62
2.5.2. Management of Data on Distribution Overhead Line Sections.....	65
2.5.3. Challenges of Transmission and Distribution Overhead Line Asset Management.....	65
2.5.4. Experiences of Life Cycle Cost.....	66
3. COMPOSITE INSULATOR ASSET MANAGEMENT STRATEGY (AMS).....	67

3.1.	Main Objectives of Composite Insulator AMS.....	67
3.1.1.	Main Targets	68
3.2.	Inspection of Composite Insulators & Diagnostic Condition Assessment Techniques	68
3.2.1.	Visual Examination	69
3.2.2.	Main Defects and Damage Witnessed.....	74
3.2.3.	Main Diagnostic Techniques	78
3.2.4.	Diagnostic and Monitoring Techniques at EDF Energy Networks	94
3.2.5.	Quality Control of Composite Insulators.....	94
3.3.	Composite Insulator Maintenance Procedures.....	95
3.3.1.	Scheduling at Cleaning.....	96
3.3.2.	Pollution Identification.....	97
3.4.	Main Proposals for Polymer Insulator Asset Management	97
3.4.1.	Framework to Develop Condition Diagnosis of Polymer Insulators Using Visual Inspections.....	98
3.4.2.	A Supporting Matrix to Select Diagnostic or Monitoring Techniques	100
3.4.3.	A Proposal for Composite Insulators Health Index Formulation (First Step using only Visual Inspection Information).....	103
3.4.4.	General Overview of Data Base Inputs at Different Operational Stages ...	105
3.4.5.	Fundamental Documents and Knowledge to Recover and Archive	105
3.5.	EDF Energy Networks: Conditions to be Considered During AMS Development.	107
3.5.1.	Main Pollutants and Contamination Sources in EDF areas.....	107
3.5.2.	Pollution in EDF Energy Networks.....	111
3.6.	Fault Statistics from of the EDF Energy System	115
3.7.	Important Environmental Information and maps of the EDF Energy System... ..	119
3.7.1.	Solar Irradiation in the UK	119

3.7.2.	Wind maps.....	120
3.7.3.	Rain map	121
3.7.4.	Some considerations using this preliminary data taken from the environmental maps	122
3.8.	A Proposal for Future Work on Insulator Asset Management.....	123
4.	COMPOSITE INSULATORS AGED UNDER MULTISTRESS FACTORS	126
4.1.	Introduction	126
4.2.	Ageing Processes of Composite Insulators	126
4.2.1.	Composite insulators’ ageing processes activated under multistress	127
4.2.2.	Rate of Bond Breaking.....	129
4.2.3.	Influence of Ultraviolet Radiation on Insulators’ Surfaces.....	131
4.2.4.	Main Effects of Corona Discharges on the Insulators’ Surface	132
4.2.5.	Surface Tracking.....	135
4.2.6.	Ageing by Biofilms.....	137
4.3.	Ageing of EPDM and SIR Insulators.....	137
4.3.1.	Degradation and Ageing Process of EPDM Distribution Insulators	137
4.3.2.	Degradation Processes Particular to PDMS / SIR.....	139
4.3.3.	Surface Degradation of SIR under UV Stress. Comparison with EPDM..	143
5.	EPDM MV INSULATORS AGED UNDER NATURAL SERVICE CONDITIONS ..	144
5.1.	Introduction	144
5.1.1.	Experience of EPDM Insulators Aged in Service around the World	144
5.2.	Diagnosis of MV EPDM Insulators Degraded In Service	148
5.2.1.	Background and Scope of this Sub Research.....	148
5.2.2.	Insulators’ Technical Data	149
5.2.3.	Service Conditions.....	150

5.2.4.	Electric Field Distribution	157
5.3.	Diagnostic Tests and Results for Complete Insulators.....	166
5.3.1.	Visual Inspections	166
5.3.2.	Dielectric Tests.....	175
5.3.3.	Dielectric Impedance.....	178
5.4.	Diagnostic Tests and Results from Small Samples from Insulators	191
5.4.1.	Infrared Spectroscopy (FTIR) Spectrums Analysis	191
5.4.2.	Surface Microscopy, Roughness and Static Contact Angles.....	193
5.4.3.	Ranking of Insulators Condition. Summary	201
6.	DROPLETS ON POLYMERIC SURFACES UNDER THE INFLUENCE OF ELECTRICAL FIELD.....	204
6.1.	Introduction.....	204
6.2.	Main Factors Influencing Water Droplets Behaviour	205
6.2.1.	Similarities between Free droplet vs. Droplets on Hydrophobic Surfaces under Electric AC Field	205
6.2.2.	Taylor Cone, Taylor Cone Jet and Corona Discharges	206
6.2.3.	Electric Field on Material Surfaces with Water Droplet Presence	207
6.3.	Electrohydrodynamic Behaviour of Water Droplets under Electric AC Field (Different Movements)	212
6.3.1.	Stillness plus Vibration → Elongation → Fluctuation Cycle.....	213
6.3.2.	Resonance or Vibration Modes.....	213
6.3.3.	Water Droplet Located out of the Centre of the Inter-Electrode Gap.....	215
6.3.4.	Coalescence.....	216
6.3.5.	Additional Electrohydrodynamic Phenomena	216
6.3.6.	Water Droplet Distortions on Surfaces with Reduced Hydrophobicity caused by Sparks.....	217

6.3.7.	Behaviour of Water Droplets with Electrodes Directly Connected in their Volume	217
6.3.8.	Elongation and Contraction of a Droplet in AC field (Does this phenomenon exist?)	218
6.3.9.	Water Droplet Movement under DC Voltage [246-248]	219
6.3.10.	Two Droplets under DC Electric Field.....	220
6.4.	Corona Discharge Phenomena on Water Droplets	220
6.4.1.	Water Droplet Corona Onset.....	221
6.4.2.	Corona from water droplets, leakage current and early ageing state relationship.....	223
6.5.	Leakage Current Behaviour with Water Droplets Presence.....	223
6.6.	Flashover Occurrence vs. Water Droplets Presence.....	225
6.6.1.	Flashover Behaviour Applying the Similarities with the Theory of Free Droplet under Electric Field	226
6.6.2.	Phases in the Flashover Phenomena of Polymer Insulators.....	226
6.6.3.	Shapes and Location of Electrodes Used to Study Water Droplets Behaviour on Polymer Surfaces.....	227
7.	ELECTROHYDRODYNAMIC PHENOMENA ON POLYMER INSULATORS SURFACE	230
7.1.	Background and Scope of this Sub-Research.....	230
7.2.	Main Goals of this Study.....	230
7.3.	Experimental Techniques and Circuits	232
7.4.	Flashover Test under Dry conditions	236
7.4.1.	Test Procedure	236
7.4.2.	Results, Phenomena Observed and Analysis	236
7.5.	Flashover Voltage with Water Droplets on Surface	239
7.5.1.	One droplet centre between electrodes placed on surface	239

7.5.2. Single Droplet’s Flashover Mechanisms and Water Channel Formation: Elongation followed by multiple flashover discharges before a water channel is formed	242
7.6. Flashover observation between two aligned water droplets	248
7.7. Flashover observation between different cases of water droplets location, size, volume, surface condition	249
7.8. Leakage Current Pulses effect on Water Droplets Dynamics versus Surface Roughness	252
7.9. First Leakage Current Pulses on Different Water Droplets Arrangements	258
7.10. Leakage Current Pulses Patterns	263
7.11. Electric Field 3D FEM Analysis of Water Droplets under Different Condition..	268
7.12. Effects of Water Droplet Evaporation under no Electric Stress.....	270
7.12.1. Evaporation rate versus water droplet volume and conductivity	271
7.12.2. Residues on surfaces after water droplet evaporation under no electric field	273
7.13. Thermal Gradient Effect.....	276
7.14. Electrode Shape Effects on Test Results.....	277
8. CONCLUSIONS	280
9. PUBLISHED PAPERS	288
10. REFERENCES	289

List of Figures

Figure 2.1 Strategies of Asset Management for Different Degrees and Types of Risk [3]	35
Figure 2.2 Main steps to develop an AM plan and main general questions to be answered [5,6]	36
Figure 2.3 Scope of Asset Management establish by PAS 55	36
Figure 2.4 Goals of Asset Management in Power Distribution Utilities [7,9]	37
Figure 2.5 Basic feedback system for a distribution system asset management [6]	38
Figure 2.6 Asset management is based on three functions (asset owner, asset manager and asset service provider), a single process, and many decisions [4, 15]	39
Figure 2.7 Information aspects categories for management assets in power grids [18]	40
Figure 2.8 Decision Making Process: (a) in an AM Approach (Source: Cigre WG 23/19-14, 2002); (b) model including maintenance strategies simulation taking into account an ad-hoc approach based on technical and economic evaluation and an asset management approach	41
Figure 2.9 Risk assessment algorithm: basic philosophy [4]	42
Figure 2.10 Reliability-Risk Based Maintenance (a) Strategy; (b) Maintenance philosophy scheme [6]	45
Figure 2.11 Reliability Centre Maintenance (RCM) Simplification - A proposal using asset grouping [25]	46
Figure 2.12 Main blocks of information required for an asset condition based model (Source: KEMA)	47
Figure 2.13 Critical objectives of health index	48
Figure 2.14 Benefits of implementing a health index	49
Figure 2.15 Developing a health index using a pragmatic approach	50
Figure 2.16 Health Index Formulation (Source: Kinectrics)	50
Figure 2.17 Participants involved on the end-of-life criteria definition (Source: Kinectrics)	51
Figure 2.18 Examples of Health Index profiles [9]	54
Figure 2.19 Typical assets failure curves [31]	55
Figure 2.20 Estimation of Probability of Failure (POF) (Source: Kinectrics)	56

Figure 2.21 Relating Asset Condition and Failure Probability to Effective Age (Source: Kinectrics).....	56
Figure 2.22 Health Index and POF, (a) Scaling categories of health index as reflected on the age curve, (b) Health Index scaling categories and probabilities of failure (Source: Kinectrics).....	57
Figure 2.23 EDF Energy’s asset knowledge process (2008) [33,38].....	58
Figure 2.24 Policy Inspection and Maintenance Life Cycle of the EDF Power Networks	58
Figure 2.25 Plan Overview of the EDF Energy Networks’ Asset Management [38].....	59
Figure 2.26 Relation Probability of Failure versus Health Index (Source EA Technology)	62
Figure 2.27 Extension of the health index from poles to an overhead line	63
Figure 3.1 Gorur’s Visual Inspection Guide.....	78
Figure 3.2 Hydrophobicity classification following the STRI Guide 1-92	79
Figure 3.3 Patrol Position to maximize the overall view of the insulators [51]	80
Figure 3.4 IR Thermography on polymer insulators [60,61].....	81
Figure 3.5 Corona discharges detected on polymer insulators using IR and UV integration [60].....	82
Figure 3.6 Defects on HDPE insulators detected using X-rays [67].....	82
Figure 3.7 Defects on polymer suspension insulators detected using X-rays [70]	83
Figure 3.8 FEM Simulation of E field distribution in a 33 kV polymer insulator with no defects and with voids at the fibre glass core/polymer interface (calculations 0.01 mm away from the insulator surface) [70].....	83
Figure 3.9 Electric field distribution (in laboratory) of a healthy and a defective insulator removed from service having a 42 cm long visible defect at the HV end (Source: www.positronpower.com).....	84
Figure 3.10 E-field distribution (FEM simulation) along a 40 kV insulator under dry and wet condition [71].....	84
Figure 3.11 Leakage current sensors installed by (a) Celpe, Brazil, to monitor leakage current over a peak threshold on 69 kV EPDM insulators; (b) EPRI prototype, USA.	85
Figure 3.12 Leakage current patterns [79].....	86
Figure 3.13 Spectrums using laser-induced fluorescence on clean and polluted insulators (biofilms) [46]	88

Figure 3.14 Evaluation of 33 kV insulators; cases: no defects, thickness variation, presence of a void, metallic inclusion and cracks on the core using a microwaves sensor (near 24GHz) [70].....	90
Figure 3.15 Typical FTIR emission spectrum obtained from field-aged EPDM using the swabbing technique; detail of the tool to do the sampling [92,94,95].....	91
Figure 3.16 FTIR spectrum of unaged and aged (by corona discharges) silicon rubber [94,95].....	91
Figure 3.17 Test Stations of Insulators [101-104].....	93
Figure 3.18 Aspects to be covered by a plan to ensure quality [108].....	94
Figure 3.19 Documents to collect and to keep in the insulators data base.....	95
Figure 3.20 Robot developed to wash insulators. View of the truck and patrol members [110].....	96
Figure 3.21 Framework to develop the condition diagnosis of polymer insulators using visual inspection supported by non expensive equipments.....	99
Figure 3.22 Action to be taken when an alarm is triggered after a monitoring process is concluded.....	100
Figure 3.23. General ageing state estimator of composite insulators. Different conditions and processes. (A. Tzimas, E. Da Silva, S. Rowland [114]).....	100
Figure 3.24 Composite Insulators Asset Database Information.....	105
Figure 3.25 General Steps to Cover and Information to keep Updated.....	106
Figure 3.26 Regions in which EDF Energy Networks operates.....	107
Figure 3.27 Reduction of NO _x and SO _x in England over recent decades	110
Figure 3.28. Main pollutants emissions (2007 maps) over the EDF Energy served areas [157].....	112
Figure 3.29. Aggregated information with the three main contaminant components of acid rain (2007) over EDF served areas	113
Figure 3.30 Main sources of NO _x and SO _x (2008) surrounding EDF Energy Networks (source: <i>European Pollutant Release and Transfer Register</i>)	114
Figure 3.31 Solar irradiation over the UK [158-161]	119
Figure 3.32 Annual mean wind speed and influence introduced by the maritime, equator, continental and arctic winds [162, 163].....	120
Figure 3.33 UK maximum wind speeds [163]	121

Figure 3.34 Rain Annual Average.....	121
Figure 3.35. Concentration of NH_4^+ over UK (<i>Source: Defra</i>).....	122
Figure 3.36 Future Work Plan Overview for Insulator Asset Management (Proposal)..	124
Figure 3.37 Steps to elaborate an Asset Management Plan for composite insulators used on Distribution Aerial Lines	125
Figure 3.38 Different aspects and factors to consider when planning monitoring frequency and replacement plans.....	125
Figure 4.1 Main factors influencing composite insulators performance	126
Figure 4.2 Reaction acting synergistically on composite insulators	127
Figure 4.3 Two stages to describe outdoor polymer’s surface ageing mechanisms	129
Figure 4.4 Very early ageing stage: electrohydrodynamic is added in parallel with the two processes generate by microdischarges [167].....	129
Figure 4.5 Main processes activated by UV radiation on polymer’s surface	132
Figure 4.6 Chemical oxidation reactions [170].....	132
Figure 4.7 Consequences of corona discharges on polymer surface.....	133
Figure 4.8 Some important processes associated/connected with corona discharges on polymer surfaces.....	135
Figure 4.9 Main concepts and processes associated with surface tracking	136
Figure 4.10 Main microorganisms in biofilms and consequences of them on polymer surface ageing.....	137
Figure 4.11 Undesirable effects of biofilms [180]	137
Figure 4.12 Damage on SIR surface under partial discharges and hydrophobicity recovery [184].....	142
Figure 5.1 Structure of the 11 kV insulators diagnosis results presentation.....	148
Figure 5.2 Geographical location of the three areas where insulators where recovered .	150
Figure 5.3 Satellite view showing the surrounding area including two power plants (The distance between the Recovery Area and each plant is approximately 3 km).....	151
Figure 5.4 Satellite view of the installation location where insulators from Circuit I and II where recovered	151
Figure 5.5 Satellite view of the installation location where insulators from Circuit III where recovered	152
Figure 5.6 Satellite view of the installation location where insulators from Circuit IV where recovered	152

Figure 5.7 Insulators’ geographical orientation connected in tension (horizontal, dead-end).....	152
Figure 5.8 Detail of the connections of Circuit I recovered insulators.....	156
Figure 5.9 Circuit II insulators connection detail.....	156
Figure 5.10 Detail of the connections of Circuit III recovered insulators.....	156
Figure 5.11 Detail of the connections of Circuit IV recovered insulators.....	156
Figure 5.12 Electric field distribution along the insulators under Circuit I connection...	159
Figure 5.13 Close up of electric field distribution along Circuit I’ insulators. Lines a to f show where the figures 5.15 (a to f) were determined.....	159
Figure 5.14 Electric field along Circuit I’s insulators, V/m versus position (cm). Line at: (a) top part of the core, (b) bottom part of the core, (c) between upper sheds’ tips, (d) between bottoms sheds’ tips, (e) Shed 1 surface, (f) Shed 5 surface (See a-f locations in the Figure 5.13).....	160
Figure 5.15 Electric field distribution along the insulators under Circuit II and Circuit III connection.....	161
Figure 5.16 Close up of electric field distribution along Circuit II and Circuit III’s insulators. Lines a to f show where the Figure 5.17 (a to f) were determined.....	161
Figure 5.17 Electric field along Circuit II and II’s insulators, V/m versus position: Line at: (a) upper part of the core, (b) bottom part of the core, (c) between upper sheds’ tips, (d) between bottoms sheds’ tips, (e) Shed 1 surface, (f) Shed 5 surface (See a-f locations in the Figure 5.16).....	162
Figure 5.18 Electric field distribution along the insulators under Circuit IV arrangement.....	163
Figure 5.19 Close up of electric field distribution along Circuit II and Circuit III’s insulators. Lines a to f show where the Figure 5.21 (a to f) were determined.....	164
Figure 5.20 Electric potential distribution along the insulators of Circuit IV (Volts).....	164
Figure 5.21 Electric field along Circuit I’s insulators, V/m versus position: Line at: (a) upper part of the core, (b) bottom part of the core, (c) between upper sheds’ tips, (d) between bottoms sheds’ tips, (e) Shed 1 surface, (f) Shed 5 surface (See a-f locations in the Figure 5.19).....	165
Figure 5.22 Hydrophobicity condition of a new similar EPDM insulator.....	166
Figure 5.23 Insulators’ areas definition.....	166

Figure 5.24 Void in the interface polymer/socket end fitting	166
Figure 5.25 View of the (a) East face, (b) West face, and (c) Spots on North face	167
Figure 5.26 View of the Circuit I insulators after spraying to see hydrophobicity classification. Both sides have the same condition (HC7).....	167
Figure 5.27 Drying differences between darker and lighter areas, the lighter side dried first	168
Figure 5.28 High roughness on the surface of an insulator	168
Figure 5.29 Some hydrophobicity was recovered after four months in only one of the insulators.....	168
Figure 5.30 Lighter and darker areas are identified	169
Figure 5.31 Undulation in some sheds (South-West facing sheds).....	169
Figure 5.32 Hydrophobicity, (a) Classification equal to HC7, (b) a small hydrophobic area is detected.....	169
Figure 5.33 Pollution on the core on the red phase insulator bottom side and on the rims, (b) Close-up of the area, (c) Pollution on the second shed of the red phase insulator	170
Figure 5.34 Possible evidence of flashover at the South-West facing end fitting	170
Figure 5.35 Ochre, sand-like contaminant at the bottom of the sheds; (a) dry conditions, (b) wet conditions	171
Figure 5.36 Undulations detected in some sheds close to the South side terminal; high level of corrosion on metal end-fittings.....	171
Figure 5.37 Severe erosion is detected in the interface polymer/end-fitting seals.....	171
Figure 5.38 Local pollution in one of the sheds. Contaminant deposition detail, a less polluted ring is surrounding the rim of the sheds.....	172
Figure 5.39 Organic pollution deposition; (a) green biofilm layers and bird droppings, (b) darker spots	172
Figure 5.40 Biofilms on the sheds and core combined with other contaminants	173
Figure 5.41 Hydrophilic surfaces. Biofilms get completely wet	173
Figure 5.42 (a) Cow hairs on spider webs; (b) misalignment between metal end-fitting and polymer	173
Figure 5.43 Differences between end-fittings (a) Circuit IV; (b) Circuit I.....	173
Figure 5.44 Insulator arrangement for dielectric tests.....	176

Figure 5.45 Example of the voltage (brown) and leakage current (green) waveforms taken (New insulator under wet conditions), Scales: $V = 0.5 \text{ kV/div}$ ($V_{\text{test}} \approx 1.8 \text{ kV}$); $I = 95 \mu\text{A/div}$	177
Figure 5.46 Impedance or admittance estimation.....	180
Figure 5.47 (a) Insulator’s RC parallel model; (b) Active and reactive components of the impedance; (c) Z' versus Z'' diagram (Cole-Cole plot); (d) Circle equation of the circle showed in (c)	180
Figure 5.48 Cole-Cole plots of more complex dielectric behaviours [205, 206]	181
Figure 5.49 Impedance spectroscopy test system and sample connections	182
Figure 5.50 Total impedance under dry conditions	183
Figure 5.51 Total impedance under wet conditions.....	184
Figure 5.52 Total impedance of 28 kV thermoplastic insulator, new and aged in laboratory	185
Figure 5.53 Total impedance under dry conditions using lineal axes.....	185
Figure 5.54 Total impedance under wet conditions using lineal axes	186
Figure 5.55 Cole-Cole Plots (Impedance: Reactance versus Resistance) of new insulator	187
Figure 5.56 Cole-Cole Plots (Impedance: Reactance versus Resistance) of the three insulators recovered on location II (poles R, W and B).....	187
Figure 5.57 Cole-Cole Plots (Admittance: susceptance versus conductance) of new insulator, (a) Dry, (b) Wet conditions	187
Figure 5.58 Cole-Cole Plot (Admittance: susceptance versus conductance) of three insulators, poles R, W and B, recovered from location II (named Circuit II insulators) under dry conditions.....	188
Figure 5.59 Cole-Cole Plots (Admittance: susceptance versus conductance) of insulators recovered from Circuit I, Circuit II and their comparison with new insulator under dry conditions	188
Figure 5.60 Resistance and Reactance versus frequency of two identical new insulators with two different formulations.....	190
Figure 5.61 Cole-Cole of two identical new insulators with two different formulations .	191
Figure 5.62 Areas for the asymmetrical conditions study.....	191

Figure 5.63 Changes in hydrocarbons groups and in alumina fillers along the insulators	193
Figure 5.64 New insulator surface detail	194
Figure 5.65 Surface of Circuit I insulator samples.....	194
Figure 5.66 Surface of Circuit II insulator samples	195
Figure 5.67 Surface of Circuit III insulator samples	195
Figure 5.68 Surface of Circuit IV insulator samples.....	196
Figure 5.69 Close up of the circled area in the Figure 5.68, IV D S sample	196
Figure 5.70 Roughness arithmetic mean, Ra [μm].....	197
Figure 5.71 Roughness arithmetic mean focusing the differences between (a) lighter-top and darker bottom side of the insulators; (b) geographical orientation.....	197
Figure 5.72 Profile: depth of greatest valleys (V_h) and peaks (P_h) and total height of profile ($T_h = P_h + V_h$).....	198
Figure 5.73 Static contact angle, SCA (sessile drop method).....	198
Figure 5.74 Static contact angle variation versus surface roughness	199
Figure 5.75 Static contact angle variation versus surface roughness considering sky-facing and ground-facing surfaces	200
Figure 5.76 Static contact angle values, insulator Circuit I, (a) surface facing North, (b) surface facing South	201
Figure 5.77 Circuit II and Circuit IV insulators ranking using the state estimator proposed on chapter 3.....	203
Figure 6.1 Factors influencing the behaviour of water droplets on polymer surfaces under electric field stress	205
Figure 6.2 Taylor cone jet.....	207
Figure 6.3 Main factors that influence the enhancement of \bar{E}	207
Figure 6.4 Normal and tangential electric field on one droplet located on a polymer insulator surface	208
Figure 6.5 Comparison between the electric field on (a) hemispherical and (b) ellipsoidal droplet [223].....	209
Figure 6.6 Electric field between two symmetrical droplets at the centre of an interelectrode gap	209
Figure 6.7 3D FEM mesh of three droplets unaligned (equidistant in a triangular disposition) [227]	210

Figure 6.8 Shape of a droplet located on the upper part of a shed (a), at the bottom part (b) and at the core (c).....211

Figure 6.9 Electric field on the sheds at (a) the potential side and (b) the ground side of an insulator covered by water droplets [233].....211

Figure 6.10 Configuration simulated: polluted surface plus droplets. (a) Basic model, (b) Electric field distribution, (c) \bar{E} magnitude along the lines shown in (a) [234]211

Figure 6.11 Enhancement of \bar{E} when water droplets coalescence.....212

Figure 6.12 Water droplet distortion at 50 Hz and resonance frequency, 19 Hz214

Figure 6.13 Water droplet distortion in two different materials214

Figure 6.14 Vibration modes of a water droplet located on a hydrophobic surface under AC field [241].....215

Figure 6.15 Behaviour of a water droplet located at the end of an insulator under an AC field [240]216

Figure 6.16 Basic patterns of electrically stressed water droplets [167].....217

Figure 6.17 Distorted shapes found in non-hydrophobic surfaces217

Figure 6.18 Electrodes inside the droplets and protusions218

Figure 6.19 Waveform of voltage and current218

Figure 6.20 Water droplet’s behaviour with different diameters at $V_{\max+}$ and $V_{\max-}$ [238]219

Figure 6.21 Water droplet behaviour following the voltage cycle with agreement in the literature [223]219

Figure 6.22 (a) Asymmetrical distortion, (b) Return to symmetric position.....220

Figure 6.23 Droplets on silicon surface under DC voltage, (a) Negative, (b) Positive ...220

Figure 6.24 Corona onset voltage vs. volume and water conductivity223

Figure 6.25 Onset as a function of air pressure for a water droplet in a divergent field..223

Figure 6.26 Relation of corona discharges under water droplet presence with early stages of degradation223

Figure 6.27 Typical leakage current waveform , (a) Before dry band arcs under AC field, (b) During dry band arc under AC field, (c) Tracking under AC field, (I) AC, (II) DC+ and (III) DC.....224

Figure 6.28 Vibration of water droplets, leakage current waveform and frequency analysis225

Figure 6.29 Dry band arc activity between water droplets, leakage current waveform and frequency analysis	225
Figure 6.30 Expected flashover voltage (U) vs. drop volume (V) [220].....	227
Figure 6.31 Flashover mechanisms	228
Figure 7.1 Main proposed goals to achieve with this study.....	231
Figure 7.2 Scheme of the general test system implemented.....	232
Figure 7.3 View of the main components and instruments used	233
Figure 7.4 Components to collect and synchronized the voltage and leakage current signals with high speed camera frames (buffer and a protection circuit boxes are not included in the image).....	233
Figure 7.5 View of sample test bases, electrodes, and one side of the mirrors systems. A second mirror was placed in front of this one to reflect the image to the camera for some experiments	234
Figure 7.6(b) High speed camera images/videos synchronized with the voltage and leakage current signals.....	235
Figure 7.7 Sub-scheme for UV camera and signals recording on the oscilloscope	235
Figure 7.8 Sub-scheme for temperature measurement approximation on sample surface (for comparison with the general environmental conditions surrounding the test area) ..	235
Figure 7.9 Electrodes shape and location on the surface	236
Figure 7.10 Corona Onset Voltage for one centre droplet with different conductivities of the water and volume.....	240
Figure 7.11 Flashover voltage for one centre droplet with different conductivities of the water and volume	241
Figure 7.12 Flashover voltage versus water droplet location, conductivity and volume .	242
Figure 7.13 Voltage and leakage current followed by a flashover at 94.86 msec at the positive V_{peak} . At the top current pulses are shown; at the bottom a ten times magnification of the current pulses is presented	243
Figure 7.14 Voltage behaviour between 120ms and 380ms	244
Figure 7.15 Voltage signals between 380ms and 490ms where multiple dry band arcs are observed	244
Figure 7.16 Images of the movements after corona inception, and flashover, gap 25mm, 50 μ l droplet.....	246
Figure 7.17 Voltage and leakage current signal for flashovers over two droplets.....	248

Figure 7.18 Images of the flashovers of two droplets aligned with the electric field.....248

Figure 7.19 Flashover between two water droplets (75 ml) not aligned with the electric field249

Figure 7.20 Flashover between two water droplets (25 ml) not aligned with the electric field251

Figure 7.21 Flashover between three water droplets (25 ml) not aligned with the electric field252

Figure 7.22 Some configurations under study (changes in droplets size means different volume).....253

Figure 7.23 Droplets movements: displacements, coalescence, vibration, and ejections (Roughness: A: 0.45 μ m, B: 0.72 μ m and C: 0.93 μ m).....254

Figure 7.24 Elongation versus roughness (Roughness: A: 0.45 μ m, B: 0.72 μ m and C: 0.93 μ m)255

Figure 7.25 Effect of roughness on the hydrophobicity of solid surface following Young/Wenzel/Cassie concepts.....256

Figure 7.26 Water droplets on porous surfaces [272].....258

Figure 7.27 Oscilloscope signals: voltage and current pulses; Voltage scale: 10 kV/div; Current scale: 500 μ A/div; Time scale: 2 msec/div, (a) One droplet, 25 μ l, deionized; (b) One droplet, 25 μ l, 500 μ S/cm.....258

Figure 7.28 Information to collect from each current pulse’s excel file recorded from each configuration.....259

Figure 7.29 Typical current pulse view after data is recorded and plotted; table shows all the information taken from the pulses plots259

Figure 7.30 Main charts produced for each experiment recorded. These figures will show how many pulses occur for each water droplets configuration studied during 100 msec, sequence of pulses, peaks magnitude, phase, duration and charge of each one.....260

Figure 7.31 Example of one graphic created using the data extracted from the signals recorded (examples shown on Figure 7.27 and Figure 7.29). First peaks detected versus deionized water droplet volume.....261

Figure 7.32 Example of one graphic created using the data extracted from the signals recorded (examples shown on Figure 7.27 and Figure 7.29). First peaks detected versus water droplet volume for two different conductivities.....262

Figure 7.33 First positive and negative peaks for distilled water droplets with four different volumes and placed on different positions in the interelectrode gap	262
Figure 7.34 First positive and negative peak for 50 µl water droplets with two different conductivities	263
Figure 7.35 Charge of the first positive and negative peaks for a 25 µl, deionized water droplet, placed on centre, close to potential electrode and close to ground electrode.	263
Figure 7.36 Changes on current pulses envelopes with elapse time (5 sec each graphic) for 50 µl, deionized water droplet	265
Figure 7.37 Changes on current pulses envelopes with elapse time (5 sec each graphic) for 25 µl, 500 µS/cm, water droplet.....	267
Figure 7.38 Three-dimensional electric field FEM simulations examples.....	268
Figure 7.39 Enhancement factors (E_{\max}/E_0) for water droplets with different contact angle	270
Figure 7.40 100, 150 and 200 µl water droplets: (a) top view, and (b) front view, recorded using one camera and one mirror arrangement	271
Figure 7.41 Time to dried sessile water droplets with different volumes and conductivities (21°C, 34% humidity and 767.31mmHg).....	271
Figure 7.42 Conductive water droplets (0.5 mS/cm) dimensional factor ($D_{\text{factor}} = \text{base}_{\text{wd}}/\text{height}_{\text{wd}}$)	272
Figure 7.43 Water droplets dimensions at 0 min and after 40 min after been placed on surface (water conductivity = 0.5 mS/cm).....	273
Figure 7.44 25 µl tap water droplet evaporation process.....	274
Figure 7.45 Evaporation process of 25 µl tap water droplet placed on the first evaporated water droplet stain	274
Figure 7.46 Crystallization during evaporation of saturated NaCl droplets. Hydrophilic surface: (a) growth of cubic crystal at the liquid-air interface, (b) ringlike crystalline deposit surrounded by a small spreading film. Hydrophobic surface: (c) crystallization pattern, (d) close-up of the cauliflowerlike morphology on the border [282].....	275
Figure 7.47 Effect of thermal gradient on water droplets dynamic and forces.....	276
Figure 7.48 Sources of thermal gradients on polymer insulators surface.....	277
Figure 7.49 (a) Electrode cross-section shapes under study (d; diameter; d': base; h: height; l: length; t: thickness, all in mm); (b) Electric field intensity with semicircle bar	

electrodes and a centred water droplet under 15 kV. LX: height for the analysis (L1 = 0 mm; L2 = 1 mm; L3 = 2 mm; L4 = 3 mm; L5 = 0.5 mm)278

Figure 7.50 (a) Electric field enhance factors (F) along the material surface; (b) Contact angle versus applied voltage (Ground electrode side)278

Figure 7.51 (a) Changes of flashover voltages caused by different electrodes shapes; (b) Leakage current and pulses at leakage current signal278

Figure 7.52 Water droplet dimensions versus applied voltage. D1 is the drop length on the axis between the electrodes, H is the droplet height and D2 is the width of the droplet parallel to the length of the electrodes279

Figure 8.1 Proposal for the early ageing stage of polymer insulators281

Figure 8.2 Early stage diagram including additional loops. In black is presented the original diagram found in [167], in blue the additional proposed steps.....282

List of Tables

Table 2.1 Main asset information to collect.....	40
Table 2.2 DSO’s asset management timescale	43
Table 2.3 Condition factors and their relative degree of importance	51
Table 2.4 General Health Index categories and descriptions.....	54
Table 2.5 Condition rates used to formulate Health Index at EDF Power Networks	61
Table 2.6 Different condition criteria, weights and scores for a distribution overhead line’s health index [8]	64
Table 3.1 Classification and description of Composite Insulator Deterioration.....	70
Table 3.2 Classification and description of Composite Insulator Damage.....	72
Table 3.3 Other process to consider for the ageing of composite insulators	74
Table 3.4 Main insulators regions where defects and damages are developed.....	75
Table 3.5 Conditions to replace or not a polymer insulator using visual inspection	76
Table 3.6 Conditions and its extension along the insulators.....	77
Table 3.7 Insulator condition and maintenance priority rating (by EPRI)	78
Table 3.8 Minimum DC surface resistance with different polymer housings, pollution and hydrophobicity [80,83]	87
Table 3.9 Main physicochemical techniques used to diagnose composite insulators.....	92
Table 3.10 Classification of the Diagnosis Techniques Normally Used to Study Composite Insulators	102
Table 3.11 Composite Insulators’ Condition Rating (CR)	103
Table 3.12 CR Scores Weighting Empirical Proposal	104
Table 3.13 Main Pollution Sources of Elements Affecting Polymer Insulator Surface...	108
Table 3.14 Main contaminants which activate metal corrosion.....	111
Table 3.15 Failures caused by known weather conditions	115
Table 3.16 Failures by 100 Km of 11 kV lines by weather conditions	115
Table 3.17 Failures caused by human error	116
Table 3.18 Failures caused by ageing or corrosion	116
Table 3.19 Failures per 100 Km of 11 kV lines by ageing or wear	116
Table 3.20 Failures caused by trees, animals and possible sources of pollution	117

Table 3.21 Failures per 100 Km of 11 kV lines caused by trees and animals	117
Table 3.22 Number of interruptions by voltage levels and networks	117
Table 3.23 Number of failure with unknown reason or cause reported.....	117
Table 4.1 Properties of dry band arc and corona discharges [172].....	133
Table 4.2 Differences in the ageing process under UV stress on EPDM and SIR	143
Table 5.1. Characteristics of the Insulators under Study (Source: www.wt-henley.com)	149
Table 5.2 Insulators qualification tests and used standards (Source: www.wt-henley.com)	149
Table 5.3 Geographical location and estimated time in service	150
Table 5.4 Main Environmental Conditions	153
Table 5.5 Dungeness National Grid Test Station main conditions (Circuit III conditions)	155
Table 5.6 Potential and ground connections of each circuit.....	157
Table 5.7 Summary of the main visual conditions, deterioration and damage detected..	174
Table 5.8. Insulators diagnosis using visual inspection (STRI Guides 1 and 5 [43, 44, 194, 195]).....	175
Table 5.9 Dielectric Tests Results	176
Table 5.10 Properties of leakage current under wet conditions	177
Table 5.11 Values of capacitance and resistance using Schering Bridge	189
Table 5.12 Values of the parameter R [Ω], C [F], obtained from the dielectric spectroscopy test	189
Table 5.13 Severity of service condition, loss of properties and degradation level	202
Table 6.1 Enhance Factors of Electric Field [227, 229-232]	210
Table 6.2 Some electrodes used in the literature for water droplets under electric field stress studies	229
Table 7.1 Flashovers occurrence time and details crossing over the water droplet.....	245
Table 7.2 Electric field enhancement factor for different basic configurations	269

ABSTRACT

Improved Condition Monitoring of Composite Insulators

by

Elizabeth Da Silva Domingues

Although the cost of investment in power lines insulators is 3 - 5% of the total cost of the installation, the impact of their performance on reliability, failure costs, maintenance routines, etc in power systems is tens of times higher. Composite insulators were introduced 50 years ago and have been used around the world with consistently good experience. Low weight, easy handling, good performance under high pollution, low maintenance costs, and resistance to vandalism are some of their advantages. Nevertheless, acid rain, salty dust deposition, corona discharges, ozone, UV radiation, and humidity among other factors, deteriorate the quality of the polymeric housing reducing their hydrophobicity. The synergistic action of ageing factors is extremely complex and the whole degradation process may change when any one variable is slightly modified. Many studies have been carried out to increase understanding of the physicochemical processes which control the electrical and mechanical stability of polymers during in-service ageing with the objective of predicting remaining life-times.

Vital areas of knowledge about polymer insulators are still incomplete and lacking; three of them are: (1) early stages of degradation in service under different environmental conditions, (2) monitoring and diagnosis techniques suitable for distribution installations and (3) steps to establish an insulators management plan based on condition and risk of failure.

In this research these three topics are covered. A full review of literature about management of electrical distribution assets is included, followed by a specific plan developed for monitoring, diagnosis and ranking of insulators mainly supported by visual inspections. Diagnosis of medium voltages EPDM insulators recovered from service aged under different conditions is done using both traditional techniques and, uniquely, dielectric impedance. The relationship between surface roughness and static contact angle is also used to characterize insulators' surfaces. Early stages of degradation are studied focusing the experimental work to evaluate the electrohydrodynamic processes which occur on new samples under different conditions, giving special attention to leakage current pulse analysis, electric field enhancement, and resistance/capacitive behaviour including phase of leakage current.

Results from each specific topic offer additional understanding of polymer insulators degradation providing insight to monitoring, diagnosis and management. Additionally, results open new topics in which new investigations are proposed.

DECLARATION

No portion of the work referred to in this thesis has been submitted in support of an application for another degree or qualification of this or any other university or other institute of learning.

COPYRIGHT

The author of the thesis (including any appendices and/or schedules to this thesis) owns any copyright in it (the “Copyright”) and s/he has given The University of Manchester the right to use such Copyright for any administrative, promotional, educational and/or teaching purposes.

Copies of this thesis, either in full or in extracts, may be made only in accordance with the regulations of the John Rylands University Library of Manchester. Details of these regulations may be obtained from the Librarian. This page must form part of any such copies made.

The ownership of any patents, designs, trademarks and any and all other intellectual property rights except for the Copyright (the “Intellectual Property Rights”) and any reproductions of copyright works, for example graphs and tables (“Reproductions”), which may be described in this thesis, may not be owned by the author and may be owned by third parties. Such Intellectual Property Rights and Reproductions cannot and must not be made available for use without the prior written permission of the owner(s) of the relevant Intellectual Property Rights and/or Reproductions.

Further information on the conditions under which disclosure, publication and exploitation of this thesis, the Copyright and any Intellectual Property Rights and/or Reproductions described in it may take place is available from the Head of the School of Electrical and Electronic Engineering.

ACKNOWLEDGEMENT

First, I would like to sincerely thank Prof Simon Rowland, who was always an amazing supervisor during these years. His patience and qualities as a person made my time here much nicer, easier and happier.

I would like to thank EDF Energy (nowadays UK Power Networks) for funding this project and the support of Eng Mathieu Michel and Eng Brendan Lyon.

This thesis has meant some hard time in a nice environment... I thus would like to address many thanks to all the fellows from the University of Manchester that helped me enjoy this thesis, and in particular: Prof Ian Cotton and Mr Frank Hogan for his support, time and friendship; Brucey for being the happier face and voice in the lab and my personal helper with my English grammar and idioms (specially the important ones!), Antonios, Xin, Kostas, Viddy, Ricardo and Ilias for being good friends and big motivation to go to work.

Special thanks to members of the staff and support personal: Mrs Marie Davies (Postgraduate -Research- Admissions & Administrator), Mrs Bernadette Bellingham (Project Administrative Assistant), Mr John Branwell (Chief Mechanical Technician), Mr Paul Mulherin (IS Officer), Dr Ralf Wagenblast (IS Manager), and Mr Stephen Hannam (Stores Technician) for all their support, happy mood and responsiveness to any request. Also I would like to include two very nice ladies: Mrs Pam and Sue for all their daily work to keep tidy offices and labs rooms.

It is also important to give tons of thanks to my Venezuelan friends; these are my colleagues, professors and chosen family. Thanks to you I am, in good measure, who I am.

Dedicated to:

Julio...Without his love, companion, support, strength, caring, cooking, dedication, and patience this degree would never be done... You are someone special in all senses.

My Mom... because you are always with me.

My Dad, my sister Mary, Migue, Ale and Andrea... because I love you.

Joy... our four legs angel.

Abbreviations and acronyms

A, amperes
AC, Alternating Current
ACA, Asset Condition Assessment
ACS, Automation Control System
AE, Acoustic Emission
AM, Asset Management
AMS, Asset Management Strategy
ANSI, American National Standards Institute
ATH, Aluminium Trihydroxide or Alumina Trihydrate
ACS, Automatic Control System
BS, British Standard
°C, centigrade
CBM, Condition Based Maintenance
CI, Customer Interruptions
Circuit I, location I from where insulators were recovered
Circuit II, location II from where insulators were recovered
Circuit III, location III from where insulators were recovered
Circuit IV, location IV from where insulators were recovered
cm, centimeters
CML, Customer Minutes Lost
CMMS, Computerized Maintenance Management Software
CPF_i, Condition Parameter Factor i
CPS, Condition Parameter Score
CR, Condition Ratings
DBM, Duty Based Maintenance
DC, Direct Current
DSO's, Distribution System Operators
DST, Data Transfer Solution
Ē, electric field
EAM, Enterprise Asset Management
EDF, Electricity of France
EDX, Energy Dispersive X-ray
EPDM, Ethylene Propylene Diene Monomer
EPN, Easter Power Networks
EPRI, Electrical Power Research Institute
ERP, Enterprise Resource Planning
ESDD, Equivalent Salt Deposit Density
EVA, Ethylene Vinyl Acetate
f, frequency
FEM, Finite Element Analysis
FMEA, Failure Mode and Effect Analysis
fps, frames per second
FRC, Fiberglas Reinforced Core

FTIR, Fourier Infrared Spectroscopy
F/m, farads per meter
GC/MS, Gas Chromatography / Mass Spectroscopy
GIS, Geospatial Information System
GPC, Gel Permeation Chromatography
HC_i, hydrophobicity classification level following STRI guide
HDPE, High Density Polyethylene
HI, Health Index
HNO₂, nitrous acid
HNO₃, nitric acid
HV, High Voltage
Hz, Hertz
IAM, Institute of Asset Management (UK)
IEC, International Electrotechnical Commission
IEEE, Institute of Electrical and Electronic Engineers
IR, Infrared Radiation
IT, Information Technology
kHz, kilohertz
km, kilometers
KPI, Key Performance Indicator
kV, kilovolts
kV/cm, kilovolt per centimetre, electric field units
kWh/m², kilowatt-hour per square kilometer
LIF, Laser-Induced Fluorescence
LMW, Low Molecular Weight
LPN, London Power Networks
LV, Low Voltage
μl, microlitre
m/s, metre per second
MV, Medium Voltage
MW, megawatts
NCI, Non Ceramic Insulators
NO, nitric oxide
NO₂, nitrogen dioxide
NO₃⁻, nitrate ion
NO_x, nitro oxides
OMS, On-line Messenger Service
PAS, Publicly Available Specification
PDMS, Polydimethylsiloxane
Ph, greatest peaks (roughness)
PM, Preventive Maintenance
POF, Probability Of Failure
Ra, arithmetic value of roughness
RS, Raman Spectroscopy
RCAM, Reliability-Centred Asset Maintenance
RCM, Reliability Centre Maintenance
RTU, Remote Terminal Units
RTV, Rubber Thermal Vulcanized
SAM, unit for high speed camera and images synchronization

SCA, Static Contact Angle
SCADA, Supervisory Control And Data Acquisition
SCM, Supply Chain Management
SE, South East
SEM, Scanning Electron Microscopy
SIR, Silicone Rubber
SO_x, sulphur oxides
SPN, South-East Power Networks
STRI, Swedish Transmission Research Institute
T&D, Transmission and Distribution
TBM, Time Based Maintenance
TGA, Thermogravimetric Analysis
Th, total height of profile (Th = Ph + Vh)
T_M, melting temperature
TOMP, toxic organic micro-pollutants
UV, Ultraviolet Radiation
V_h, greatest valleys (roughness)
VOC, volatile organic compounds
Ω, ohm
WCP, Weight of Condition Parameter
WCPF, Weight of Condition Parameter Factor
XPS, X-ray Photoelectron Spectroscopy
Y, dielectric impedance
Y', real component of dielectric impedance, conductance
Y'', imaginary component of dielectric impedance, susceptance
Z, dielectric impedance
Z', real component of dielectric impedance, resistance
Z'', imaginary component of dielectric impedance, reactance
α_m, data availability coefficient for condition parameter (=1 when data available, =0 when data unavailable)
β_n, data availability coefficient for condition factor (=1 when data available, =0 when data unavailable).
θ_s, contact angle
μA/div, microamps per division
μS/cm, microsiemens per centimetre

1. INTRODUCTION

The degradation of composite insulators represents one prime factor that can significantly influence power network reliability, performance and maintenance costs and constitutes one of the most important topics in dielectrics research. Polymer insulators introduce significant advantages compared with the traditional technologies of glass or ceramic. High tensile strength-to-weight ratio, good performance under pollution conditions, presenting an unattractive target for vandalism, and ease of transport, handling and storage, are only some of them. Comprehension of their ageing processes, during early, medium and late life, is fundamental to improving the technology and to giving utilities and other users the tools to develop their monitoring, maintenance and replacement plans before failures of these components start to occur. Considerable effort has gone into understanding the ageing of the polymer insulators, but much work is still necessary to achieve this goal.

One of the main advantages of polymer insulators is their high surface hydrophobicity under severe environmental conditions but, as with any organic materials, silicone rubber (SiR) and ethylene propylene diene monomer (EPDM) used for outdoor applications, are susceptible to ageing by solar ultraviolet radiation (UV), increasing the oxidation level and roughness. For distribution power lines, the stress generated by environmental factors is the fundamental key to explain their ageing but only the synergistic action of environmental conditions and electric stress can explain the ageing of composite insulators used on overhead transmission lines.

Under wet conditions (rain or moisture), water droplets with different conductivities (after pollutants are dissolved) will be formed and under electric field stress the inception voltage of corona discharges can be reached. This is mainly seen around the triple edge (air-water-polymer perimeter) leading to material surface deterioration. The electric field intensity also produces different water droplet movements which cause changes to their shapes (extension, vibration, undulation, and resonance), location (displacement and ejection), quantity (increased by ejection, decreased by coalescence or evaporation), and volume (evaporation, coalescence, ejection). As a consequence of these, sharp edges at the

triple contact line are observed. Roughness, inclination, surface energy gradients and temperature gradients influence the final shape of the droplets and, therefore, the corona activity level. With time, loss of hydrophobicity occurs and partial arcs, known as dry band arcs between non-uniform wet layers result. These are key ageing phenomena. Therefore, it is an indispensable matter to improve the diagnosis and monitoring techniques, their applicability, and the definition of different modes of failure so that these elements can inform good asset management policies.

Corona discharge activity is reflected as leakage current pulses and they constitute the main ageing phenomena in the early ageing of outdoor insulators. Corona discharges on polymer surfaces have low intensity and reduced heat in comparison with dry band arcs but they are in closer contact with the surface and can last for longer periods and result in changes to the hydrophobicity, roughness profile and oxidation rate. Providing a further insight into this phenomenon is one of the aims of this work. Results from systematic measurements taken using digital instrumentation to record simultaneously signals and visible images under AC 50 Hz voltage, are compared.

This current work focuses three different topics going from macro-scale aspects of (a) polymer insulator asset management, and (b) diagnosis of MV EPDM degraded in service to a micro-scale with (c) a study of water droplet behaviour and associated corona current activity.

The main concepts for asset management policies for composite insulators, emphasizing diagnosis techniques, degradation identification, an ‘alarm’ flowchart system and ageing estimators are introduced to produce a proposal which suits the distribution overhead lines of one major power utility. A full visual guide including the main published works has been compiled and numerical limits on properties are incorporated to rank insulators in service. Detailed lists of steps within an asset management plan for insulators based on conditioning and risk were prepared and a methodology for future calculation of health indices is established following the procedures which already exist in the EDF Energy for other equipment.

The main ageing factors and mechanisms of MV insulators are presented and different diagnosis techniques are used to evaluate the ageing state of samples recovered from four

different locations. Visual and microscopic inspections, physicochemical analysis, electrical tests, including a new approach of dielectric impedance evaluation on full samples were used. This part included identification of a direct relationship between roughness on surfaces and the static contact angle where differences between ageing environmental conditions can be detected.

Using images recorded using a high speed camera, deformation of water droplets under an electric field, looking at the front and top views simultaneously, were classified and the most representative shapes were simulated using finite element analysis to study the influence of these deformations on the electric field enhancement and their effect on corona current pulses. Each one of the frames was taken in synchrony with voltage and leakage current signals, allowing the evaluation of water droplet behaviour and leakage current pulses. Using UV camera and the voltage and leakage current signals captured by a digital oscilloscope, the behaviour of the first five cycles (100 ms) after the first corona current pulse occurs were studied. For selected cases a phase-resolved diagram of current pulse activity during some tens of seconds were also registered. Analyzing all this information, properties such as peak magnitude, polarity and phase, duration times, and charge are analyzed. Parameters such as droplet volume, water conductivity, number of droplets, location along the inter-electrode gap, time to recover hydrophobicity, and surface roughness were changed to evaluate their influence on the leakage current pulse behaviour.

2. ASSET MANAGEMENT

In this chapter the main concepts related to asset management focused on power distribution utilities are summarized. A review of the different approaches, strategies and standards commonly used are presented. The relevance of different levels of information, maintenance options, condition monitoring, diagnostic data and health index formulation focusing are also summarized. This chapter covers the main concepts needed to define an asset management plan for polymer insulators.

2.1. General Definition of Asset Management

Asset Management (AM) is a concept derived from the financial industry and means any activity or action used to get the most of something and it is typically centred on decisions about appropriate maintenance for existing assets and about investments in new assets, bearing in mind that this depends on the organization and its particular concerns. The British Standard PAS 55-1 defines asset management as: “The systematic and coordinated activities and practices through which an organization optimally manages its physical assets, and their associated performance, risks and expenditures over their lifecycle for the purpose of achieving its organizational strategic plan or, more simply, the optimum way of managing assets to achieve a desired and sustainable outcome” [2].

Many techniques derived from AM are applicable to the electricity industry; of particular importance is the treatment of reliability and risk management. However, electric power assets are complex because they have non-financial aspects of performance and risk, require maintenance and/or replacement, and are part of an intricate interconnected system [3, 4].

Three different approaches are used for a single asset (Figure 2.1): (i) ignore the asset until it fails and then replace it (for assets that cause little or no problems when they fail); (ii) run the asset for a specific time and then maintain/replace it (for assets for which: failure can be predicted, failure can cause a major problem, no good test exists to check their condition, or the cost of maintenance or replacement is moderate); and (iii) monitor/test the condition of the asset and take care of it (when the risk of failure grows over a specific threshold, for costly assets or critical assets for which failure is catastrophic). A

combination of life-extending treatments with frequent monitoring can be used for very expensive assets [3]. The approach chosen will depend on the general condition and performance associated with an asset, this means: its condition, probability of failure, cost of failure, maintenance or replacement, monitoring and testing.

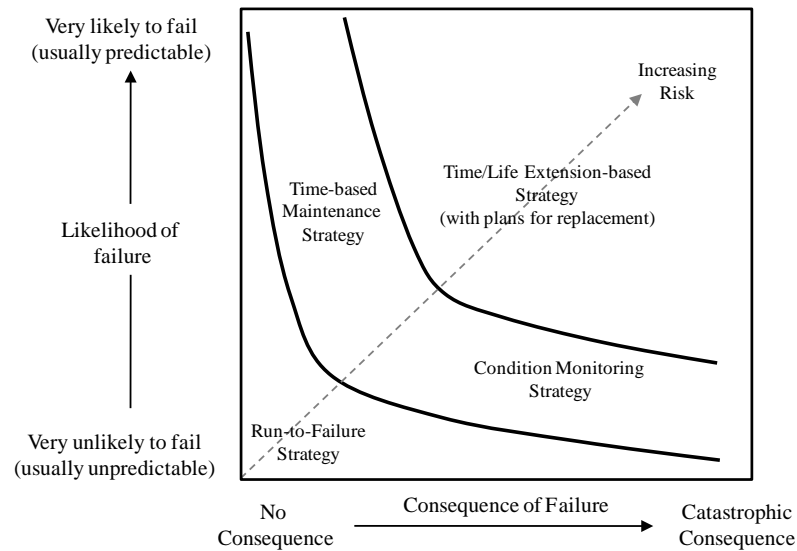


Figure 2.1 Strategies of Asset Management for Different Degrees and Types of Risk [3]

When a simple asset management is extrapolated for a group of assets, there are some specific actions or steps to follow answering particular questions for the main three levels involved: asset knowledge, calculations/models/protocols involving the system network, and decision-making [5, 6] (see

Figure 2.2). A proper asset management plan introduces three main general benefits as it: extends the horizon life of the assets, reduces the gap between the type of service provided with the one expected, and reduces the overall costs.

The UK has been a pioneer in asset management standardization development, in response to demand from industry for a ‘formal way’ for carrying out asset management. The Publicly Available Specification, PAS 55, is a standard’s requirements specification for the optimal management of physical infrastructure assets produced by the British Institute of Asset Management (IAM). First published in 2004, it is rapidly becoming an accepted international benchmark for good practice in whole life cycle, optimized asset management. The 2008 update involved contributions from 50 organizations from 15 industries in 10 countries.

In November 2009 the International Standards Organization agreed to adopt PAS 55 as the basis for a forthcoming ISO standard for good practices in asset management. It is applicable to any organization where physical assets are a key or critical factor in achieving effective service delivery [2]. It contains a framework of 21 “good practices” and is specifically intended to assess how well core physical assets, such as lines and stations, are managed. The scope presented by PAS 55 is presented in the Figure 2.3. The exercise of comparing company processes with PAS 55 good practices provides credible evidence of an organization’s Asset Management competence.

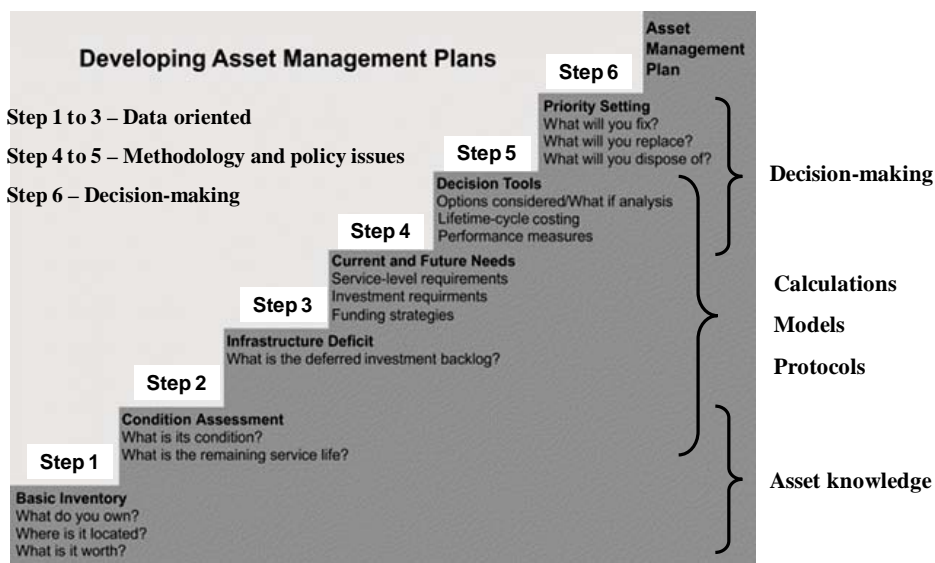


Figure 2.2 Main steps to develop an AM plan and main general questions to be answered [5,6]

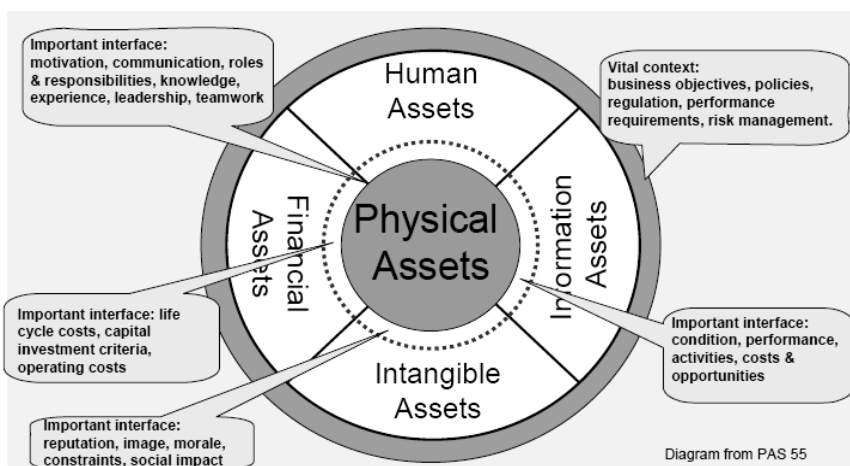


Figure 2.3 Scope of Asset Management establish by PAS 55

2.2. Asset Management for Electric Power Distribution System Operators (DSOs)

Brown [4] says “Asset management is a corporate strategy that seeks to balance performance, cost, and risk. Since reliability is the primary driver of discretionary cost, the goal of distribution asset management is to balance reliability, cost, and risk. Achieving this balance requires the alignment of corporate goals, management decisions, and technical decisions. It also requires the corporate culture, business processes, and information systems capable of making rigorous and consistent spending decisions based on asset-level data. The result is a multi-year investment plan that maximizes shareholder value” [4]. In simpler words, asset management can be defined as the process of maximizing equipment investment return by maximizing performance and minimizing cost over the entire equipment life cycle, see Figure 2.4 [7-9]. Literature distinguishes asset management as of strategic character, as well as the need to define it as a multi criteria problem, and consider aspects not easily quantified, such as those related to the environment or the deterioration degree of some assets [9]. One of the initial works about this topic after the privatization of the electric sector in the UK can be found in [10].

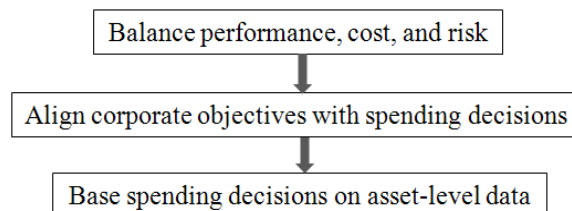


Figure 2.4 Goals of Asset Management in Power Distribution Utilities [7,9]

Ideally, a DSO’s asset management strategy will address the following main issues: the best way to monitor, maintain or replace an installed asset, the best way to expand the system to meet future needs, the best way to provide system performance from the viewpoint of customers, and the best way to specify investment capital budgets over time, given the utility's long-term financial planning objectives and requirements, whilst avoiding adverse regulatory impacts or penalties, and achieving acceptable environmental impact [11-13]. A feedback system must be working to obtain good results from an asset management strategy, as presented in Figure 2.5 [6].

In [14] the concept of Maintenance Excellence is presented as a step forward of Asset Management, in which optimization of life cycle cost and levels of reliability, availability,

maintainability and safety from the design of the assets is included. It also emphasizes the importance of personal preparation for learning, design and implementation of new management processes for maintenance.

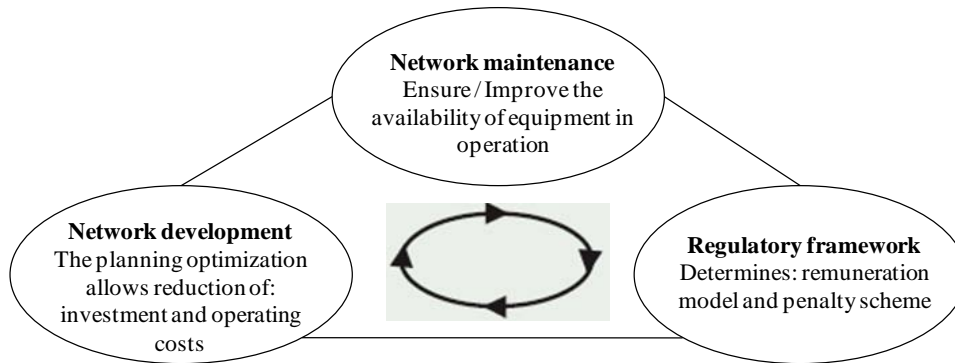


Figure 2.5 Basic feedback system for a distribution system asset management [6]

2.2.1. Division of Asset Management in DSOs

A formal division of the asset management in power distribution utilities is presented in Figure 2.6. This decoupled structure allows each asset function to have the following focus: (i) owners on corporate strategy; (ii) managers on planning and budgeting, and (iii) service providers on operational excellence [4, 6, 15].

Moreover, a robust asset management structure is supported by three pillars of competency and cross-functional expertise must be developed to create a multi supported structure. These pillars are [15]:

- *Management*: business and regulatory strategies, organizational design, performance management, process design, resource planning, decision analysis and financial risk. Risk is basically conceived as the product of two things: the probability of failure and the consequences of it happening; in this case the concern is over the business impact of an asset functional failure.
- *Engineering*: planning, design, operations, maintenance, reliability, protection, equipment health and technical risk; formal mathematical models are used.
- *Information*: system architecture, system integration, business intelligence, knowledge management, asset registry, geospatial information system (GIS), supervisory control and data acquisition (SCADA), enterprise asset management

(EAM), computerized maintenance management software (CMMS), on-line messenger service (OMS), supply chain management (SCM), etc [6, 16-18].



Figure 2.6 Asset management is based on three functions (asset owner, asset manager and asset service provider), a single process, and many decisions [4, 15]

2.2.2. Information Categories to Consider in Managing Electrical Assets

Before the restructuring process undergone by the electric sector, in an important number of countries, decisions related to asset utilization were based on their technical performance. Years later the ratio between technical performance/expenses became an important parameter in the decision process and nowadays, it is relevant to consider the effect of asset operation on the environment or its influence on the society. Having this in mind, different categories of relevant information must be considered in managing the electrical assets of a power T&D grid. Information required is summarized in Figure 2.7 [18].

As can be seen, the component ageing information is related to: the absolute age, the type, the history and the laying conditions of a network sub-component, condition assessment, ageing models, probability of failure, inventory information, network topology, available spare parts, current maintenance procedures and history of maintenance actions, history of faults, among others. Economical aspects are linked with all the technical aspects as: cost of maintenance, monitoring and testing, cost of investments for inventory and spare parts, etc, and also with the cost of faults (undelivered energy, penalties or customers' compensation, repair, critical damage to the network or environment). Additionally, aspects such public image and a feeling of safety must be considered.

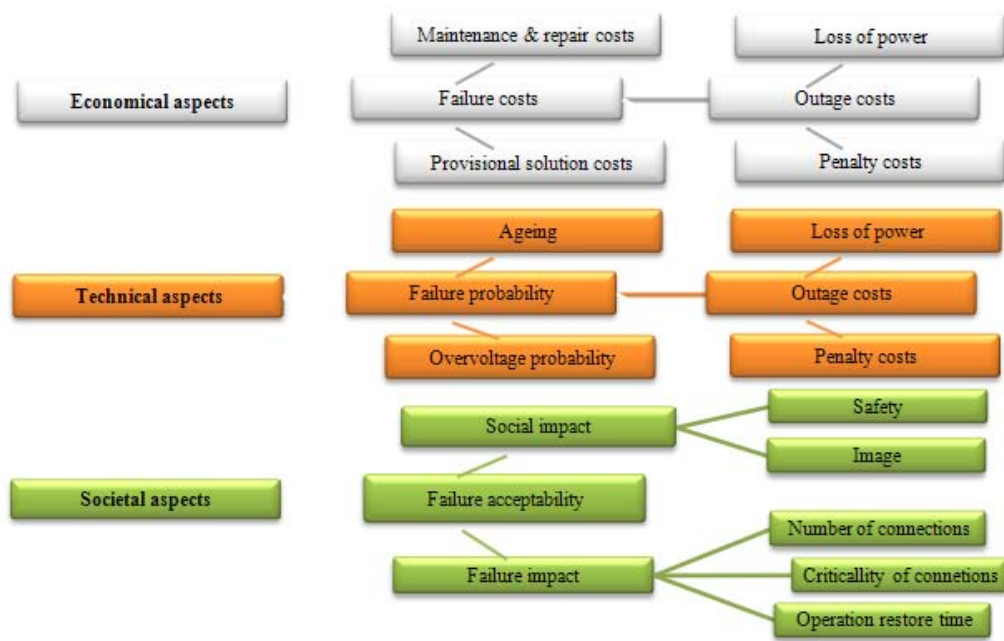


Figure 2.7 Information aspects categories for management assets in power grids [18]

Being more specific about the information required from an asset it can be also classified and organized in the way presented in the Table 2.1 [19].

Table 2.1 Main asset information to collect

TYPE OF INFORMATION	SOME EXAMPLES
Demographics	Location, voltage level, type, capacity, age (in service and manufacturer), etc.
Condition	Maintenance history, inspections, tests, loading levels, etc.
Performance	Failure history, benchmarks, etc.
Functional	Capacity ratings, obsolescence issues, safety compliance, operational conditions, etc.
Criticality	Number of customers, priority customers, load, environment, safety, etc.
Costs	O&M (operation and maintenance), refurbishment, salvage, replacement costs, etc.

2.2.3. Levels of Asset Management Decision Process on Power Distribution Utilities

Power distribution utilities require links between different parts of their structure to find all the information needed and to take decisions about the AM process to be followed. For the primary decision support process, the first level deals with the technical information of the assets and their condition assessment (mainly focused at components); the second level combines the results of the first level with the economic information on assets (mainly focus on the network or the reliability of it), and the third level uses the economic

information on business combined with the societal information, to make decisions about risk (mainly focused on the corporation), see

Figure 2.8 [9, 18].

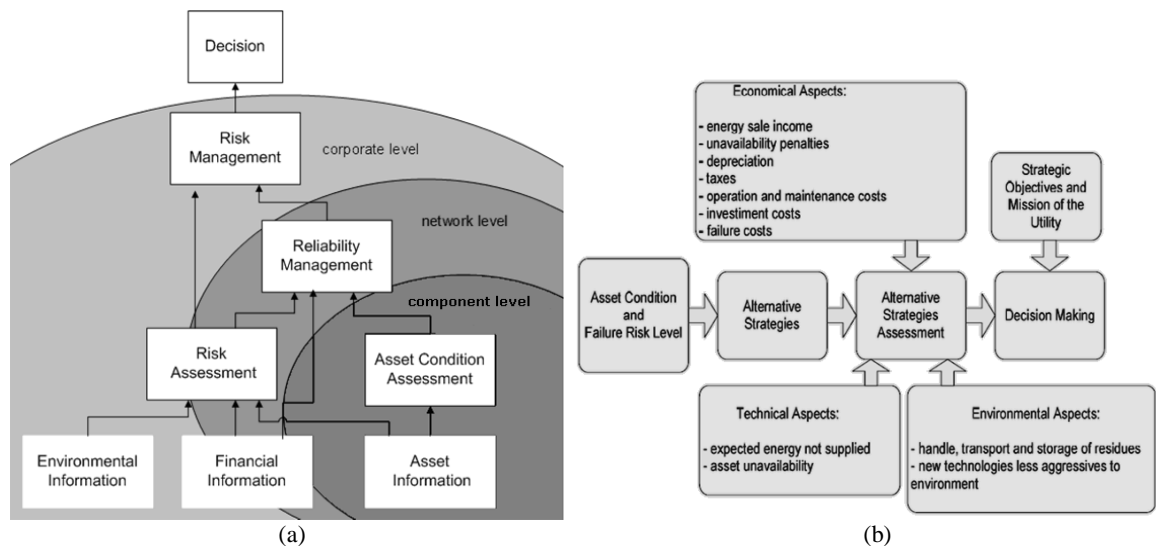


Figure 2.8 Decision Making Process: (a) in an AM Approach (Source: Cigre WG 23/19-14, 2002); (b) model including maintenance strategies simulation taking into account an ad-hoc approach based on technical and economic evaluation and an asset management approach

Processing asset information

Knowing about equipment inventory, maintenance rules, procedures performed and history, condition assessments derived from diagnostic tests results, spare parts and equipments details, in combination with failure statistics, ageing models and reliability evaluations, different scenarios and their effect on technical performance are evaluated. These scenarios normally are: replace; refurbish; change maintenance strategy (condition based, time based or corrective); monitoring/diagnosis modification; run to failure; monitoring and as before.

Processing network information

Economic data (quantification of benefits and cost) of different scenarios evaluated on asset information are compared. The analysis includes economic terms and reliability or expected lifetime as well.

Processing corporate information

The final decision is taken making the best managed risk of the different scenarios including the societal information, economic information, reliability of equipment inventory and network topology to make the risk assessment. Reliability is a major cost driver and should be the major focus of asset management initiatives within power distribution companies and Reliability Risk Management concerns itself with undesirable events such as equipment failure, poor reliability indices, etc, and its treatment requires the knowledge of asset condition, impact of maintenance and operation on equipment condition, and the impact of these on the probability of failure. It also requires: supporting information systems and business processes that allow risk mitigation in the form of inspection, maintenance, operations, replacement, and system modifications. All these must be integrated with a technical risk management program including all financial aspects, regulatory and legal affairs and public relations [4, 15]. A basic risk assessment algorithm is presented as an example in the Figure 2.9. This part of the asset management process involves important formal modelling and quantification and different approaches can be found in the literature.

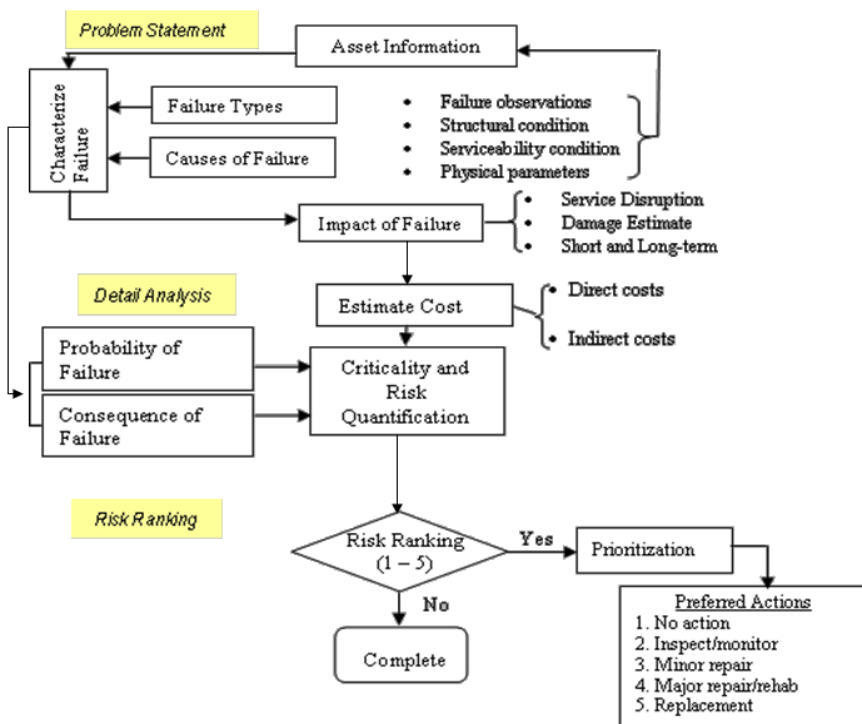


Figure 2.9 Risk assessment algorithm: basic philosophy [4]

2.2.4. Basic Timescales of Asset Management

One of the critical points that experience has shown is that asset management strongly depends on the coordination of time scales because this plays a critical role in the success of strategic decisions [6, 17]. The basic timescale of asset management for DSO's has three main components as summarized in Table 2.2

Table 2.2 DSO's asset management timescale

<p>Short Term: real time to weeks → <i>Covering the operational management where a secure and reliable operation, monitoring and control, and full restoration of the system are done</i></p>	<ul style="list-style-type: none"> • System monitoring and tracking of asset conditions: using SCADA to monitor, control and collect data in real time. This is transmitted using remote terminal units (RTUs) and storage to the Distribution Management System where the system is managed. Here the failures are identified and patrols can be dispatched. Using Geographic Information System (GIS) the spatial information can be stored, including asset condition, customer complaints, among others. • Fault restoration: Automation control system (ACS) is implemented to improve the continuity of supply, making possible a better way to isolate and restore the service. Here the network topology must be appropriated.
<p>Mid Term: monthly and seasonal → <i>covering the maintenance management with optimal maintenance strategy and optimal outage plan</i></p>	<ul style="list-style-type: none"> • Optimal maintenance strategy. Corrective, preventive and predictive. Preventive can be time based (TBM) or condition based (CBM). Reliability centred maintenance (RCM) includes the reliability concept on preventive maintenance; this involves mathematical models. • A comprehensive asset database which includes information on periodic inspections, diagnostic tests or condition monitoring is mandatory. This must be integrated with the GIS and a robust IT platform, preferably favoring open standards. • Optimal outage plan option or optimization of voluntary disconnection aiming for preventive maintenance to minimize interruptions.
<p>Long Term: yearly and beyond → <i>covering strategic planning</i></p>	<ul style="list-style-type: none"> • Associated with the identification of asset enhancement and development planners required to meet target levels of service.

2.3. Maintenance, Monitoring and Condition Assessment

The management of power distribution infrastructure is critical for insuring the service with quality, reliability and at a reasonable cost. In general, power distribution companies have a large inventory of assets, some of which are close to or over 50 years in age; in the majority of the cases utilities do not have the data necessary for managing the assets and initially the maintenance was normally decentralized. With restructuring there was a reduction in the workforce, and as one result the knowledge base of infrastructure problems has been largely lost because the information was not stored in formal recorded files.

Condition Monitoring is taken to mean the use of advanced technologies in order to determine equipment condition, and potentially predict failure. Condition Monitoring is most frequently used as a Predictive or Condition-Based Maintenance technique. However, there are other Predictive Maintenance techniques that can also be used,

including the use of the Human Senses (look, listen, feel, smell etc.), Machine Performance Monitoring, and Statistical Process Control techniques.

2.3.1. Maintenance Approaches

Asset age is nowadays far less important than its actual condition. This forced the utilities to change from a time based maintenance (TBM) to a condition based one (CBM) [6, 20-23]. A derived approach is also considered as duty based maintenance (DBM) when a duty cycle criteria (specific number of operations, hours run, etc) is taken into account [13]. The adoption of Reliability Centred Maintenance (RCM) was part of the initial effort to incorporate economic analysis in T&D planning after its success in the aircraft, military and nuclear sectors. RCM is a method which relates reliability to preventive maintenance (is a *qualitative* systematic development of a preventive maintenance (PM) strategy); documents PM decisions; allows non-critical assets to operate until failure, and builds a reasonable defensive strategy against failure. Figure 2.10 (a) presents the main RCM steps and objectives. RCM is fundamentally focused on preserving system function where critical components for system reliability are prioritized for PM measures but, one limitation use to be that it is not capable of showing the benefits of maintenance for system reliability and costs. The fusion between reliability and component maintenance is rarely put in practice and the main reason seems to be the lack of suitable data and a reluctance to use theoretical tools to address the practical problem of maintenance planning [20, 22, 24]. Figure 2.10(b) shows schematically the influence of the maintenance approach on its cost and equipment reliability.

In the literature a new method was published as Reliability-Centred Asset Maintenance (RCAM) [22, 24], which provides a *quantitative* relationship between PM of components and the total maintenance costs. The inclusion of mathematical models to mix the preventive maintenance (PM) with reliability offers important advances to take the final decisions but the amount of data required for this approach is even greater than the regular RCM which is already high. RCM is sometimes considered as very complex and there are examples where is not fully accepted [25]. The main criticisms are the extensive need of human and capital resources in the introduction phase and its implementation demands too much time. A simplified RCM method shown in Figure 2.11 based in a six step model and a functional block structure (all distribution networks have a similar structure with the

same functions making it possible to use the same basic documentation) is proposed in [25].

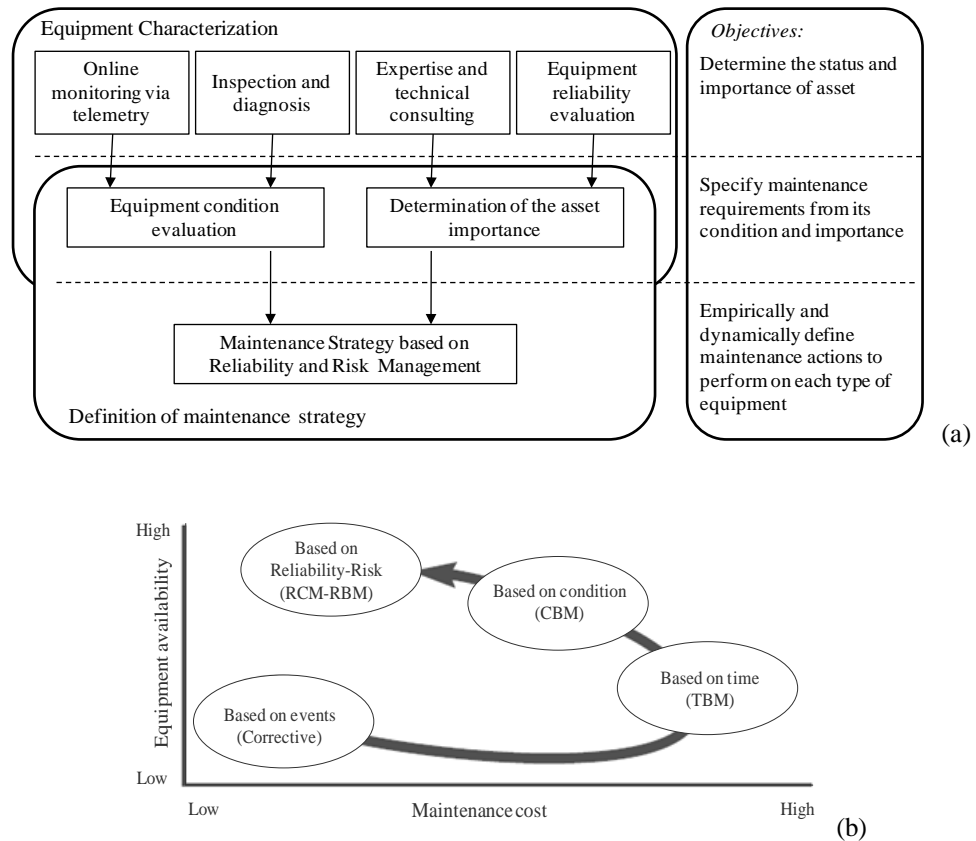


Figure 2.10 Reliability-Risk Based Maintenance (a) Strategy; (b) Maintenance philosophy scheme [6]

Using this approach a first stage could be reached by RCM using less investment and in a shorter time. Having in mind this simplified way to implement a grouping of RCM distribution system equipment, EPRI presented monitoring and diagnostics options of all equipment containing polymeric insulation between 12 and 46 kV as a single group (Polymer-based: Silicone, EPDM, EVA, Epoxy resin, reinforced fiberglass, etc., used as substation products, e.g. suspension / dead-end insulators, post and line post insulators, transformers bushings, cable terminations, lightning arrestors, equipment and bus bar covers, animal guards, RTV coatings) [26]. This looks a reasonable and useful option because all these assets have the same base material and function, similar ageing factors and mechanisms of degradation and equivalent failure modes, and the data associated with them could be analyzed simultaneously.

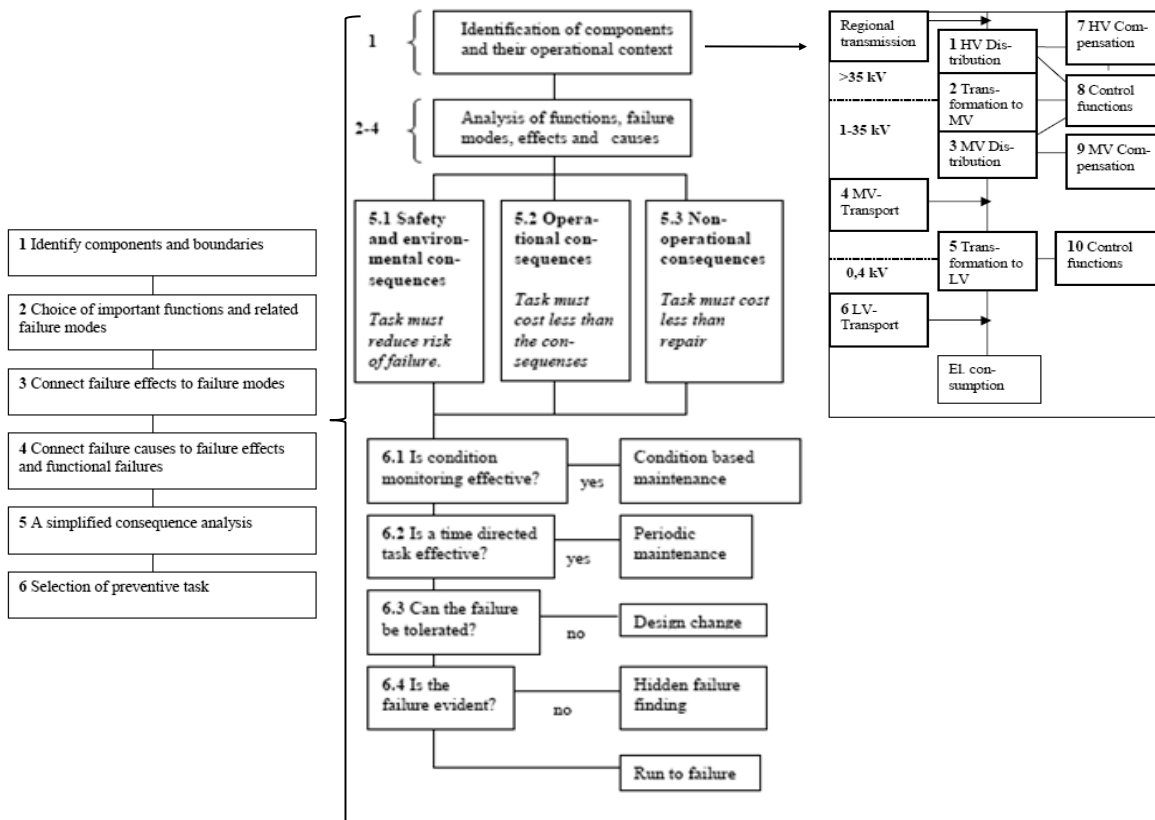


Figure 2.11 Reliability Centre Maintenance (RCM) Simplification - A proposal using asset grouping [25]

2.3.2. Asset Condition Information

Accurate recording of the findings from any action (maintenance activities, tests, replacement, etc) is vital. This is normally one of the most difficult tasks to accomplish. Two important conditions must be precisely described: (i) ‘as found’ and (ii) ‘as left’. The final condition of the asset following maintenance is important but even more relevant is its condition previous to the maintenance actions, because this gives knowledge of how the equipment has performed since the previous maintenance or from its installation, and the degradation trends [13]. Only with reliable condition information can proper planning for asset replacement be properly established.

Electric utilities systems are composed by a large number of individual system components with different characteristics and level of importance. Conventionally, relatively detailed information on each asset would be required in order to make decisions on their monitoring, maintenance and replacement needs. Obviously, this raises an enormous problem because: (i) the amount of information would be economically and

practically infeasible, and (ii) tests and inspections do not have standard for their application and interpretation making them highly dependent on each technician's judgments reducing the uniformity. By using statistical sampling methods these problems are significantly reduced resulting in more accurate evaluations of the overall asset class, and a hierarchical approach to condition assessment would be provided [27, 28]. Figure 2.12 shows the main blocks of information required for a condition based model.

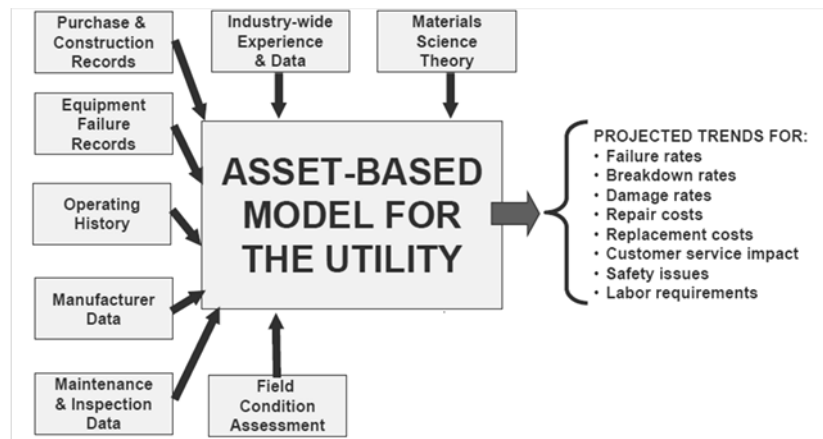


Figure 2.12 Main blocks of information required for an asset condition based model (Source: KEMA)

2.3.3. Asset Degradation Analysis by Health Indices Formulation

Defects are associated with failed or defective equipment or components which affect their operation and reliability well before their end-of-life. If these defects are detected early, during routine inspections, and corrective maintenance actions are taken the life of the assets is not affected. *Long term degradation* is generally less well defined and normally is difficult to determine using routine inspections. It is even more complex to quantify remaining life of an asset or groups of assets or if they are at high risk of generalized failure. Understanding of asset degradation, ageing stress factors, failure processes and modes of degradation/failure is vital to establish assessment or end-of-life criteria. This is also very important to understand the functionality of the asset and the way that the subsystems work together to perform their operation.

Health index is a useful tool for representing the overall condition of a complex component or equipment; this is a way of combining complex condition information to give a single numerical value as a comparative indication of overall condition. The majority of the assets are composed by multiple subsystems each one defined by more

than one mode of degradation and failure. There may be one dominant mode or several independent modes and a critical state of the asset may be considered when several subsystems reach a particular state of ageing which compromises service. Under this condition a combined health index, or single indicator, is defined using a multi-criteria assessment approach, a pragmatic approach, among others [8, 28, 29]. A combined health index captures generalized deterioration of asset subsystems, as well as fatal deterioration of a dominant subsystem and should pursue the critical objectives which are summarized in the Figure 2.13.

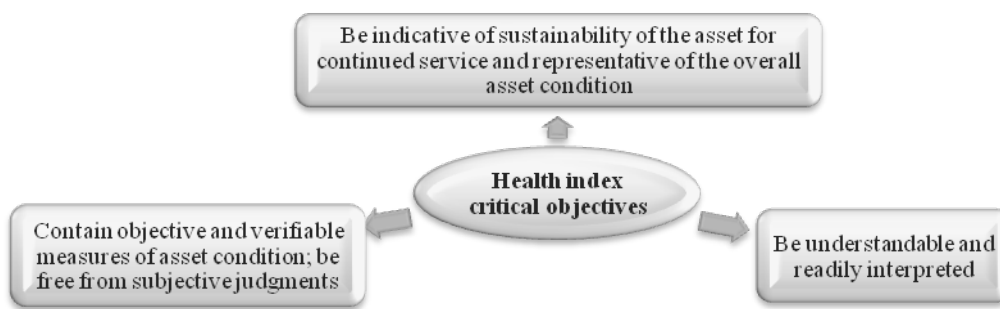


Figure 2.13 Critical objectives of health index

A health index is a way of bringing together all available knowledge and information about a group of assets and using this in a consistent and logical manner helps to define condition and predict future performance. It relies on the knowledge and experience that is available about the assets concerned. It then provides a consistent means of utilizing that information to provide an assessment; it is an aid to engineering judgments to support asset management decisions. The main benefits of developing and implementing health indices are summarized in Figure 2.14.

The more specific condition information that is available the more definitive the health index can be, but normally this means a more costly process. In consequence, an ideal or ‘close to perfect’ health index can be very difficult to define, particularly for distribution assets, and a pragmatic approach using the collection of available data or including only a minimum amount of diagnosis tests can offer the best results. This approach, proposed by EA Technology (UK) [29] is summarized in the Figure 2.15. The goal is to obtain a useful health index to rank assets (proximity to end of life) as quickly and as economically as possible. An initial health index is defined and is improved by ongoing gathering of

information using a consistent and logical method utilizing opportunities such as maintenance or removal of assets from the distribution system or by targeted sampling to obtain results economically [29]. One of the main important aspects is the grouping of assets combining them in relatively large groupings where the essential degradation and failure process are similar for the group so that the critical condition factors are also similar. The relative importance, financial and operational, of the assets must be similar as well.

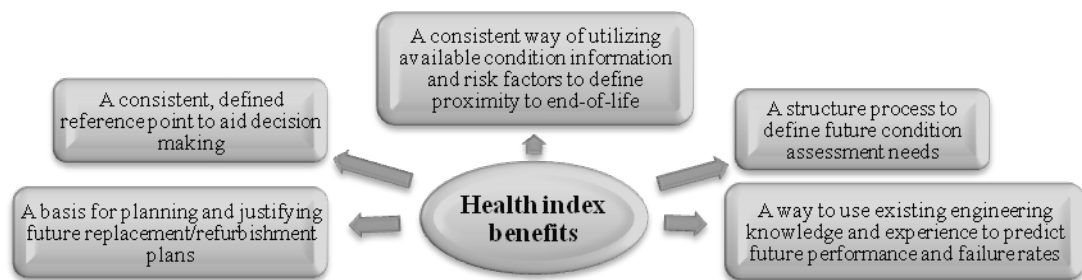


Figure 2.14 Benefits of implementing a health index

To formulate this pragmatic initial health index the most challenging aspect is to take complex condition information, probably recorded in many different ways and convert this into predefined, well specified condition ratings of codes which be turned into simple numerical values for use in an overall health index algorithm. Using HIs the condition of each asset is described by a single numerical value which is factorized to make possible the comparison of assets with incomplete condition information and normalized onto a scale (usually 0 to 10 or 0 to 100), with two conventions: positive mode, i.e. a high value indicates an asset in good condition and a low value poor condition, or negative mode where high number indicates poor condition.

Health indices provide a basis for assessing the overall health of an asset and risk of failure and are, therefore, a key performance indicator on the asset condition. HIs are based on ageing and degradation modes of assets and their subsystems under different environmental and operational conditions.

Using health indices in establishing the investment levels into capital and maintenance activities allows the selection of optimal risk mitigation initiatives for implementation. A key factor in such integration is using the information available to forecast the expected asset failure rates and the corresponding remaining life. This can be done using

demographic, performance and condition information through health index analysis and the effect of different maintenance options can be then analyzed for the optimal extension of the assets.

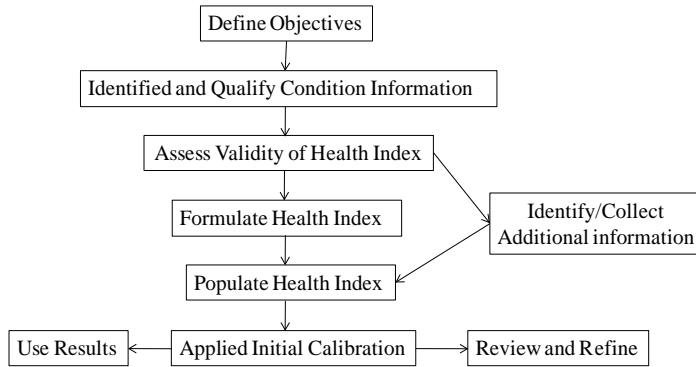


Figure 2.15 Developing a health index using a pragmatic approach

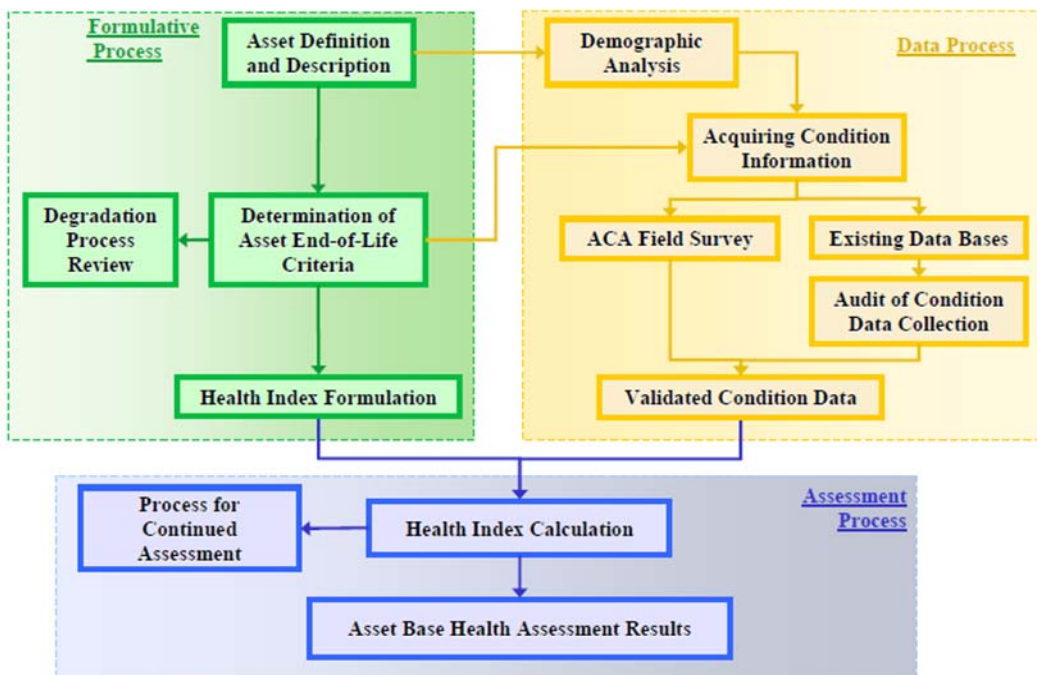


Figure 2.16 Health Index Formulation (Source: Kinectrics)

In [30], the main process and sub-processes required to formulate an asset’s health index are explicitly named as can be observed in the Figure 2.16. The three main processes can be divided into: *Formulative* (knowing the asset, its degradation process and end-of-life criteria to formulate the health index), *Data* (to collect new data and validate the existing

ones to establish the asset condition) and *Assessment* (calculating the asset’s health index and proceeding with the assessment). Because the end-of-life criteria is one fundamental key to formulate the health index, a variety of participants should be involved in its definition, as shown in Figure 2.17 [31]. The most important are: HI knowledge and experience, best maintenance processes, corporate knowledge (key staff) and standards, experts on asset degradation, ageing and end-of-life criteria.

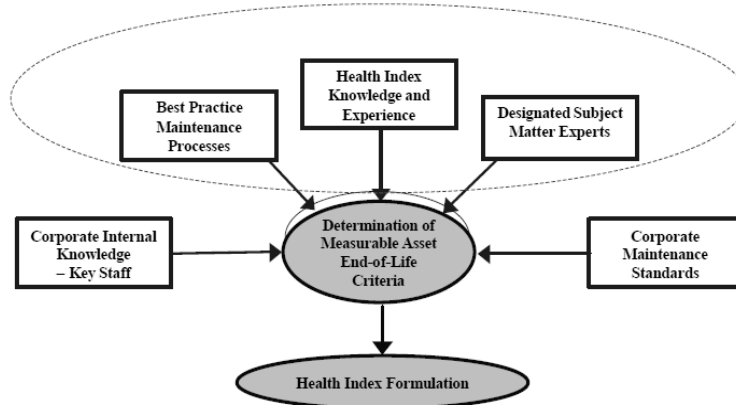


Figure 2.17 Participants involved on the end-of-life criteria definition (Source: Kinectrics)

Appropriate condition or health-degradation factors for an asset must meet the following requirements:

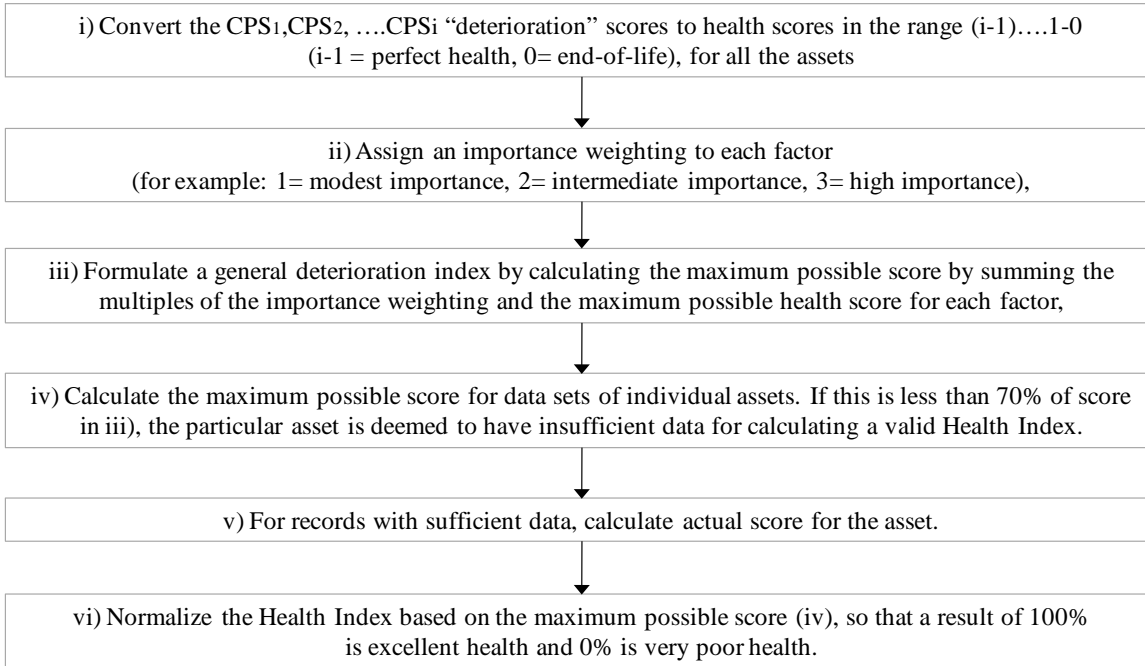
- Selected degradation factors must contribute to the asset's failure.
- Degradation factors must result in irreparable permanent damage (i.e., result in non-renewable degradation).
- All selected degradation factors should have adequate available data in order to arrive at an accurate score.

Table 2.3 shows a classification of condition factors and their relative degree of importance on the ageing process [8, 28]. Each condition factor must be assessed as falling into one of the categories shown.

Table 2.3 Condition factors and their relative degree of importance

Factor Category	Description
No impact	Reflects defects or deterioration measures that have no impact on overall asset health.
Contributing factor	Reflects defects or deterioration measures that range from low to high in importance, but typically in combination with other measures as part of a formulation of generalized deterioration.
Combinatorial factor	Reflects a measure which does not represent asset condition in isolation, but is a critical component in a complex logical and/or mathematical formulation of asset health.
Dominant factor	Reflects the health of dominant subsystems that makes up the asset, and end-of-life based on this single factor represents end-of-life for the entire asset.

It is also relevant to develop a quantified scoring system to appropriately represent the asset health consistent with the philosophical approach used to formulate the condition based Health Index. In general, a uniform scoring system has been adopted through the following steps:



Transforming the previous steps in final equations, using $i=5$, the Health Index Formulation is [31]:

$$HI = \frac{\sum_{m=1}^5 \alpha_m (CPS_m \times WCP_m)}{\sum_{m=1}^5 \alpha_m (CPS_{m,max} \times WCP_m)} \quad (2.1)$$

$$CPS = \frac{\sum_{n=1}^5 \beta_n (CPF_n \times WCPF_n)}{\sum_{n=1}^5 \beta_n (CPF_{n,max} \times WCPF_n)} \times 4 \quad (2.2)$$

Where:

- CPS, Condition Parameter Score
- WCP, Weight of Condition Parameter
- CPF, Condition Parameter Factor
- WCPF, Weight of Condition Parameter Factor

- α_m , data availability coefficient for condition parameter (=1 when data available, =0 when data unavailable)
- β_n , data availability coefficient for condition factor (=1 when data available, =0 when data unavailable).

As can be seen Condition Parameter Scores (CPS), presented in many publications as Condition Ratings (CR), are descriptive indicators of the component under examination. Using them, assets can be graded following their performance or condition. These condition or performance ratings are established as a consequence of visual examinations, test results or any other inspection/observation process, including staff/technician expertise and system knowledge. Usually four or five grades are established but this can be modified if a different scale seems to be more appropriated.

A minimum quota of tests/observations is needed for calculating a valid asset Health Index because it is not reasonable to expect that information will be available on every test criterion. In general, this minimum level is set to 70% of the maximum available score; in other words, test information must be available on criteria that make up 70% of the total maximum index.

Actual asset condition data is then analyzed to ascertain the extent to which valid scores may be calculated using the adopted Health Index. This “sanity check” is used to validate the recommended Health Index formulation and adjustments are made, as appropriate, to ensure the results reflect actual asset condition.

Assignment of the continuum of asset health scores into discrete categories of asset health is needed. Appropriate categories should be established by the utilities for the purpose of helping their programming investment and maintenance activities. Table 2.4 shows a typical classification published on the literature which is adjusted for different equipment (transformers, breakers, etc) both in USA and Europe [19, 28, 29, 32-34].

Cognitive uncertainty associated with the assessment of line condition and failure consequences can best be handled using fuzzy logic. Fuzzy logic was specifically developed to deal with the fuzziness of human concepts such as those embodied in human perception and decision making. In addition, fuzzy logic provides a systematic framework for dealing with linguistic quantifiers such as "*severe, poor, moderate, rusty, fair, very,*

many, few, good, bad, etc." which arise during assessment line condition and failure consequences [9, 35, 36]. Good information about the performance of a group of assets can also be found looking at the HI profiles, as presented in Figure 2.18, where the profile indicates if the family of assets is in good condition with a low stable failure rate or if it is in poor condition with a rapidly increasing failure rate.

Table 2.4 General Health Index categories and descriptions

Health Index	Condition	Description	Probability of Failure (POF)	Equivalent Status on Life Curve	Remaining Life (where supported)	Requirements
85-100	Very Good	Some ageing or deterioration of a limited number of components	Low	First half of mean life expectancy	>15 yrs	Normal inspection and maintenance
70-85	Good	Deterioration of some components	Low but slightly increasing	Second one-third of mean life expectancy	10-15 yrs	Normal inspection and maintenance
50-70	Fair	Noticeable serious deterioration or serious deterioration of specific components	Rapidly increasing but lower than POF at mean age	Final one-third of mean life expectancy	5-10 yrs	Increase diagnostic testing, possible replacement needed before 5 years depending on criticality
30-50	Poor	Noticeable serious deterioration or significant deterioration of a dominant component	Higher than POF at mean age and increasing	First one-third after the mean life expectancy	1-5 yrs	Start planning process to replace, considering risk and consequences of failure
0-30	Very Poor	Extensive serious deterioration or serious deterioration of a dominant component	Very high, more than double the POF at mean age	Second one-third after the mean life expectancy	0-1 yr	At end-of-life, immediately assess risk: replace based on assessment

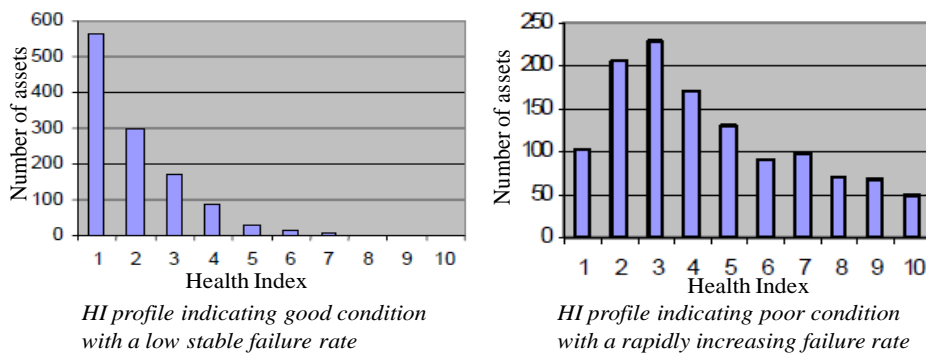


Figure 2.18 Examples of Health Index profiles [9]

In the literature some good examples of how to calculate health indices on different distribution power assets can be found. In [37] a complete study developed on the Toronto Hydro Electrical Systems Limited’s distribution assets is presented. The majority of the HI were found on assets where there were specific tests and specific values of them to point a particular degradation condition (i.e. transformers, circuit breakers, etc).

2.3.4. Typical Asset Life Curves versus Probability of Failure Diagrams

The typical life curves of assets, shown in the Figure 2.19, are fundamentally based on industry knowledge, manufacturer expectations, benchmark failure data and utility specific data [31]. These curves have the following limitations: (i) they present averages, and are not asset specific, (ii) they often present limited failure data, (iii) failure data may be irrelevant and (iv) location, environment, etc may not be considered. In consequence, following these curves to elaborate an asset management plan has many disadvantages.

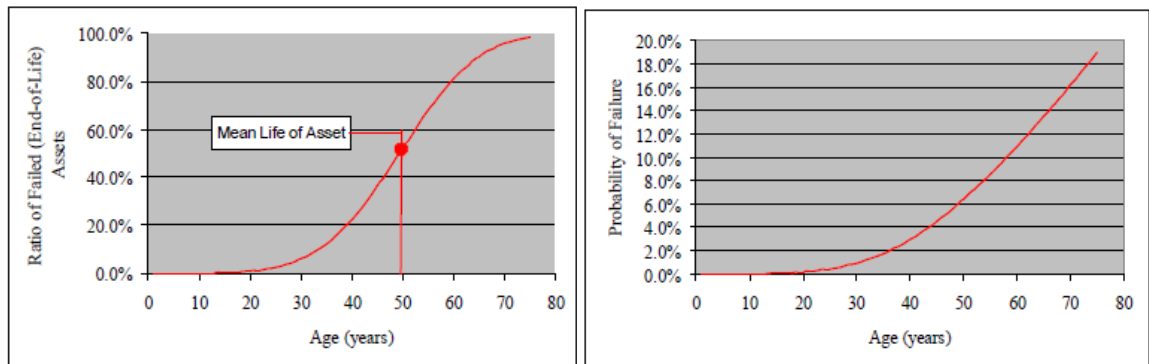


Figure 2.19 Typical assets failure curves [31]

Using failure curves involving asset condition is not an easy task but these include realistic information about the assets considering the differences between ageing processes and degradation factors. Relating condition and failure probability to the effective age of an asset is the main objective and this is based on the scheme presented in the Figure 2.20. Figure 2.21 shows the typical diagrams prepared by Kinectrics, where the Probability of Failure (POF) including stress and condition (strength), is determined. As is shown, Correlating Health Index results to Probability of Failure requires: (i) HI formulation design, (ii) estimation of effective age, (iii) an estimate for the Probability of Failure and (iv) adjustment this with increasing data [30]. Furthermore, values such as Rate of Deterioration, Remaining Life Determinations, Effect of Intervention Options and Asset Class Future Condition should be predicted.

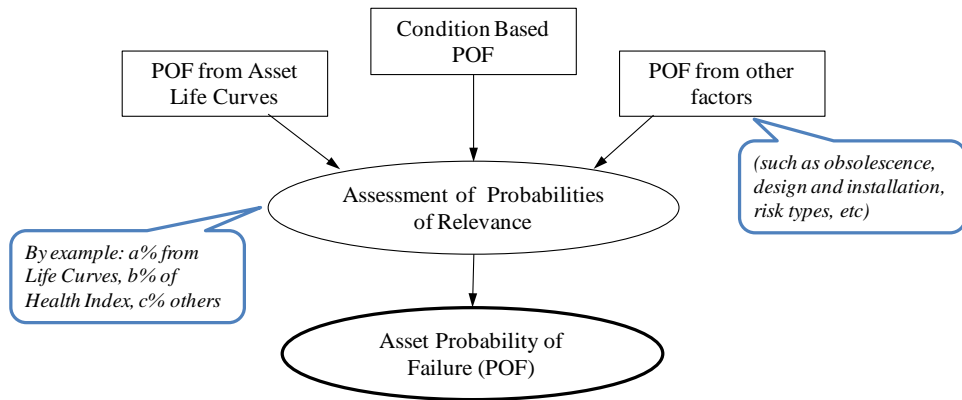


Figure 2.20 Estimation of Probability of Failure (POF) (Source: Kinectrics)

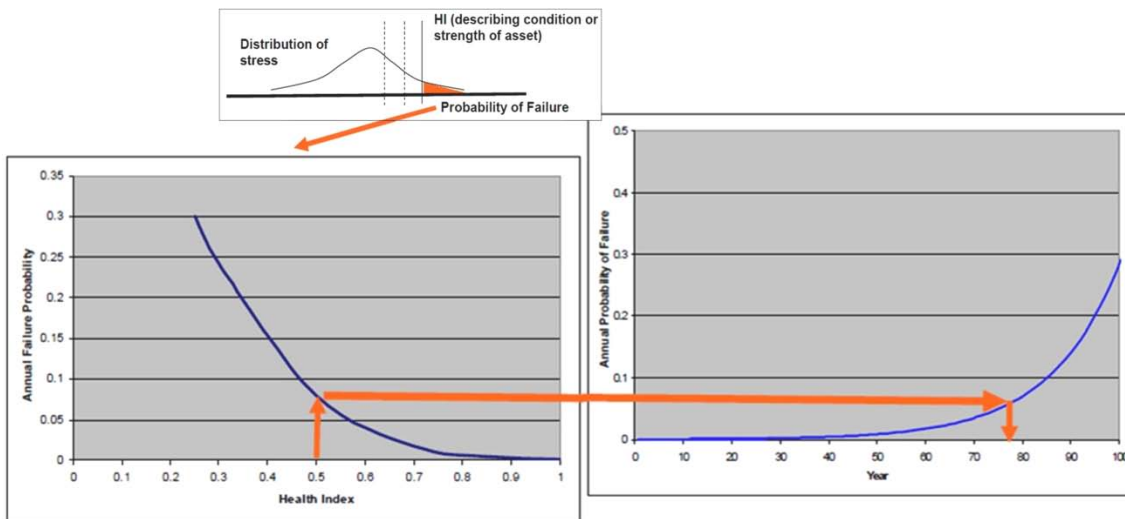


Figure 2.21 Relating Asset Condition and Failure Probability to Effective Age (Source: Kinectrics)

Figure 2.22 presents also this information relating HI, ratio of failed assets and probability of failure, but also includes a colour code with the condition description of the assets.

Looking at this, two different probabilities of failures of an asset can be derived: P_1 , based on the actual age of the asset and the life curve established, and P_2 , based on condition and health index developed. The overall probability of failure depends on how relevant the health index in is predicting the end-of-life and this can be introduced as a weighting factor:

$$P = P_1 + k (P_2 - P_1) ; \quad \text{where } 0 \leq k \leq 1 \quad (2.3)$$

Here, k introduces the relevance of the health index and the two extreme cases are: $k=0$ when health index has no relevance and $k=1$ when health index is the only relevant parameter to indicate probability of failure [19].

EA Technology developed equivalent health index formulation and probability of failure definition with the ones developed by Kinectrics. A description of them is presented with EDF Energy Networks' Asset Management system because it is based on Condition Based Risk Management [33].

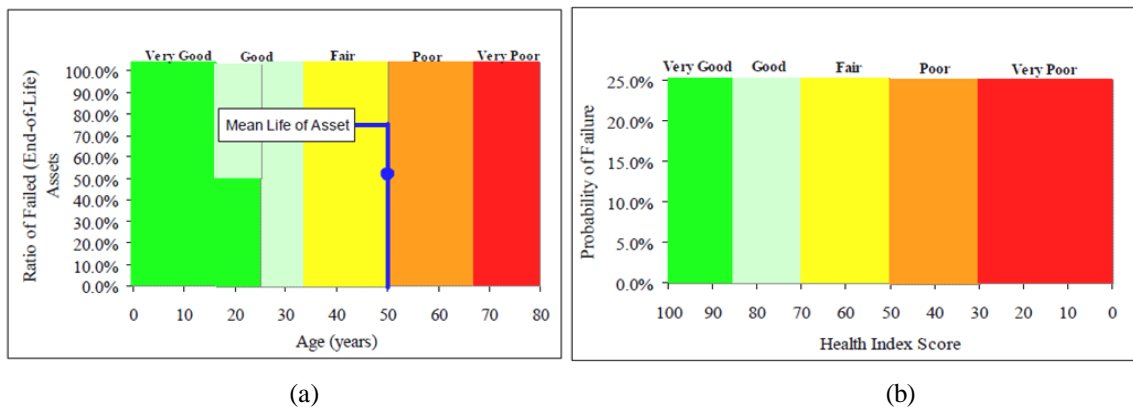


Figure 2.22 Health Index and POF, (a) Scaling categories of health index as reflected on the age curve, (b) Health Index scaling categories and probabilities of failure (Source: Kinectrics)

2.4. EDF Energy Networks' Asset Management

2.4.1. Generalities

Having in mind the inclusion of proper asset management policies for any equipment, the knowledge of what is already implemented at EDF Energy Networks is fundamental. Only some general aspects of the EDF's asset management, which are public domain, will be included, but they provide basic support for any proposal avoiding options that are not aligned with the basic policies of the company.

A summary of the Asset Management scheme at the EDF Energy is presented in Figure 2.23 and Figure 2.24 [33, 38]. It can be observed that the main aspects are based on the BSI PAS 55 recommendations (EDF Energy was certified in 2006). In consequence, all new aspects and policies to be incorporated in the utility procedures should follow the principles reflected in the mentioned standard [2].

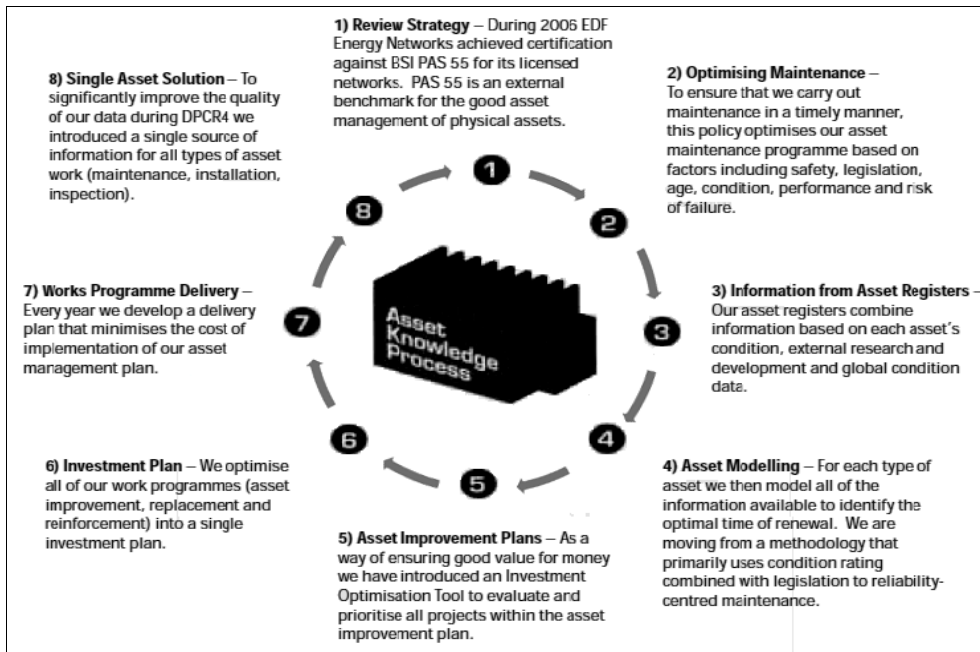


Figure 2.23 EDF Energy’s asset knowledge process (2008) [33,38]

Following the EDF Energy asset management approach, this is necessarily a dynamic policy that can be continuously reviewed, actualized and improved after the information and data collected during inspections, condition monitoring activities, diagnosis tests and maintenance routines are compiled and analyzed. This dynamic cycle between factors is summarized in the Figure 2.24 and along its progress different documents are created to ensure a common and consistent approach [33]. The general philosophy and conception is based on the work developed by EA Technology.

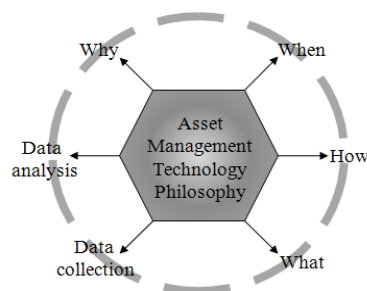


Figure 2.24 Policy Inspection and Maintenance Life Cycle of the EDF Power Networks

EDF Energy established its engineering instructions for maintenance and inspection practices taking into account the best practices and methodology from: Reliability Centre

Maintenance (RCM), Condition Based Maintenance (CBM), Time Based Maintenance (TBM), Failure Mode Effect Analysis (FMEA) and Diagnostic Inspection [33].

The bases of the philosophy are summarized in Figure 2.25 [38] which shows that business essentials and asset condition information are reviewed to formulate an appropriate set of network activities. At the same time, an analysis of existing network performance is used to determine the required level of investment to meet the regulatory Customer Interruptions (CI) and Customer Minutes Lost (CML) targets. This approach ensures that suitable reinforcement schemes are being developed to address increasing demand and meet security of supply standards.

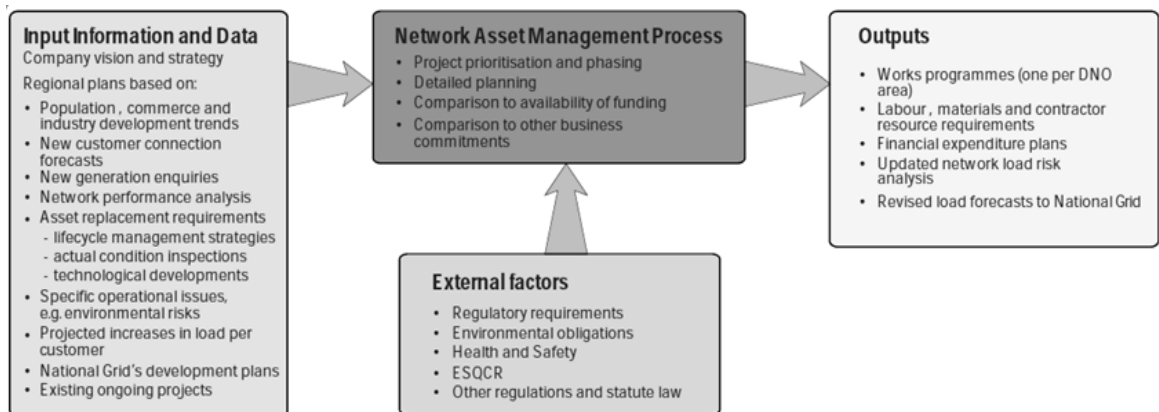


Figure 2.25 Plan Overview of the EDF Energy Networks' Asset Management [38]

Assets are scheduled for removal or replacement based on condition, performance and economic considerations [38]. The management of such asset knowledge is, therefore, a critical element in the development of the investment plan as it generates technical and economic information that is used to develop the asset strategies. Inspection and condition assessments are crucial to our better understanding of asset condition and this process has been bolstered by a significant investment in information technology (IT) systems. This will maximize asset lives while reducing the number of systems that hold critical asset data, thus improving data management and subsequent decision processes.

EDF Energy asset management is supported by Enterprise Asset Management (EAM) solution – Ellipse (developed by AMT-Sybex, which includes in its webpage the EDF Energy's Case Study), to develop a central asset register (including EPN, LPN and SPN),

providing a single source of truth of information relating to all electrical plant and civil structures across distribution networks. Ellipse was chosen due to its proven reputation as a world class EAM. Not only does the solution enable EDF Energy Networks to create detailed and tailored reports in a way that is highly intuitive to support management decision making, it also provides essential information to empower and improve the efficiency of staff right across the enterprise, even out into the field. Through the use of work planning and work dispatch tools, field engineers can now receive accurate instructions for inspection and maintenance duties on their ruggedized hand-held devices via the AMT-SYBEX Mobile Field Working Solution (FDCS). The field engineers can then in turn update central asset records remotely from the field.

Through improved visibility of asset information financial benefits have been realized in ensuring assets to be replaced in the future are not included in the maintenance program. Benefits delivered from implementation of Ellipse include: increased asset utilization, recognized opportunities for cost reduction, mitigation of risk and improved human resource productivity [33, 38].

EDF Energy have implemented AMT-SYBEX Mobile Solutions and Data Transfer Solution (DTS) since 2006, approximately. Using of mobile technology provides a closed loop end to end process from the issue of work to returning it when completed. This reduces the risk of paper records building up, improving the timeliness of data updates. Since 2009 EDF contracted AMT-SYBEX to develop programs to integrate DTS with SAP's IS-U suite (migration tool to change data between old and new information platforms).

Ellipse is defined by its developers as: “A world class Enterprise Asset Management (EAM) system tailored specifically for the utilities, transport and defense industries, providing full asset life cycle management from conception and design, construction, the work management required during the assets' operation and finally the planning for replacement. Ellipse may be implemented as a best of breed solution for Asset and Work Management with standard integration to back office systems such as asset centric Enterprise Resource Planning (ERP), managing all the back office systems such as Oracle and SAP®.

Alternatively it may be implemented as an asset centric ERP, managing all the back office processes such as finance, stores, procurement and human resource management. It does exist fully integrated mobile solutions for Ellipse; delivering process efficiency in the field whilst ensuring accurate and timely data collection. Ellipse has been designed to be integrated with other specialized systems such as GIS, Call Centre, Network Management, Telemetry and SCADA, and automated optimized scheduling and dispatch (Source: <http://www.amt-sybex.com>).

Based on this description, the EDF Energy Asset Management system seems to be open and flexible enough to include the policies and information related with composite insulators installed or to be installed on its networks.

2.4.2. Formulation of EDF’s Health Indices

EDF Power Networks has established a plan using a four-level condition rating system to create its health indices [33] with a scale defined between 0 and 10, being 0 the asset new and close to 10 the end-of-life, as Table 2.5 and Figure 2.25 show.

Inspections, centred on plant equipment, poles and underground cables must have that as an objective if a proper adjusted asset management is proposed.

Table 2.5 Condition rates used to formulate Health Index at EDF Power Networks

Condition Criteria	Condition Rating (CR)	CR Score	Level of degradation / damage / ageing
Asset’s property or characteristic under inspection /test/evaluation or health degradation factors	CR1	0	No measurable or detectable degradation is found. As new.
	CR2	3	Measurable or detectable degradation is found. This is considered normal degradation or ageing and has no significant effect on the probability of failure.
	CR3	7	Significant degradation, considered increased probability of failure in the medium term (during the next maintenance cycle) is detected.
	CR4	10	Serious degradation, considered to significantly increase the current probability of failure, is found.

Having this part of the formulation defined, the health index is calculated by [33]:

$$HI = \frac{\text{Actual scored value}}{\text{Maximum value}} \times 10 \quad ; \text{ scale between 0 and 10 where:} \quad (2.4)$$

$$\text{Actual scored value} = \text{Actual condition rating} \times \text{weighting} \quad (2.5)$$

$$\text{Maximum value} = \text{Maximum condition rating} \times \text{weighting} \quad (2.6)$$

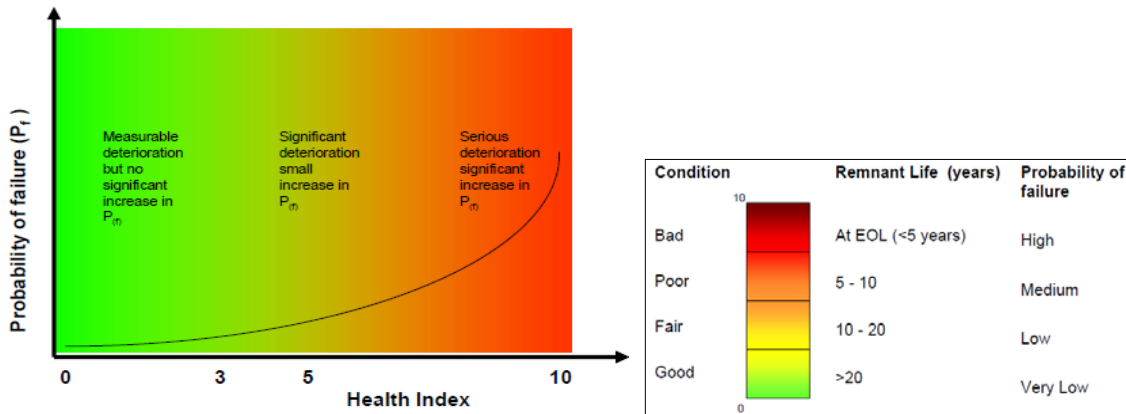


Figure 2.26 Relation Probability of Failure versus Health Index (Source EA Technology)

This procedure is equivalent with the method described in 2.3.3. The difference is established on the final scale chosen, where EDF Energy is using a ranking based on 10 and the general one presented is based over 100. This is only a matter of preferences. In particular for the EDF Energy system it is important to keep only one rating scale for all the assets condition state definition.

After the health index and the probability of failure are established, the optimum time for replacement, which constitutes the financial optimization step, should be determined.

2.5. Distribution Overhead Line Asset Management

The gap in information results from the uniqueness of this asset compared to other asset classes, in that this asset consists of a grouping of overhead line component assets (e.g. conductor, insulators and wood poles) that extend anywhere from 1 km to 100 km.

2.5.1. Overhead Line Health Index Formulation

Literature shows that grouping of the line components is deemed to be the most practical and cost-effective approach for assessing the condition of distribution line sections because end-of-life replacement or refurbishment often occurs on entire sections rather

than on individual components. This approach recognizes that replacement or refurbishment may include some individual components that may not yet have reached their end-of-life. In consequence, the formulation of the health index is based on the process shown in the Figure 2.27.

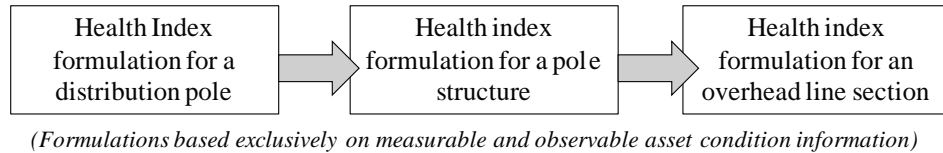


Figure 2.27 Extension of the health index from poles to an overhead line

Typical steps to calculate the overhead line Health Index are [8, 33]:

A) Wood Pole Health Rating

- i) Identify the health index's dominant factors → factors that can independently bring the pole to end-of-life:
 - Strength calculation (outcome of a mathematical formulation of several combinatorial factors).
 - Woodpecker damage.
 - Pole top rot.
- ii) Assign a health rating from 0 to 3:
 - If the factor is below a defined level (for example 70%) would assign a pole a health rating of 0 (end-of-life).
- iii) Overall Health Index calculation:
 - HI is equal to the lowest of the health ratings of the various dominant factors.

B) Subcomponent at each pole structure position Health Rating:

- i) A health rating from 0 to 3 is assigned for the condition of each subcomponent.
- ii) Different weightings are applied to the different components reflecting their relative importance to the overall structure:
 - Dominant Factor: only the wood pole.
 - Combinatorial factor (which can only degrade the overall health index of the structure in comparison with the health rating of the pole): cross arm.

- Contributing factors: insulators, guys and fittings.
- iii) Condition Score for each wood pole structure:
 - The condition score (the product of the condition value and the weighting) for the different components are summed. Maximum score is 51.
- iv) Health index for the wood pole structure is equal to $(\text{total score}/51) \times 100$.

C) Composite score of the inclusive structure scores calculation:

- Types of structures (intermediate, section or terminal) have different weights.
- Structures evaluated as at or near end-of-life are weighted higher for an increased effect on the overall line section.
- Conductor is assessed in a similar way as the section structures, with condition rating from 0 to 3.

D) The Health Index for the line section:

- Composite of the aggregated structure scores and the conductor score, and provides a measure of the level and extent of degradation of the components.
- HI line section (0-100) is a composite of the aggregated structure scores and the conductor score (measure of the level and extent of degradation of the components).

Table 2.6 Different condition criteria, weights and scores for a distribution overhead line’s health index [8]

Condition Criteria	Weighting	Maximum Score
Wood Pole	8	24
Cross Arm	3	9
Insulators	2	6
Guys	2	6
Fittings	2	6

A complete plan for the estimation of overhead line condition is proposed in [39], where the methodology to determine the overhead line condition index is based on the application of fuzzy mathematics. This methodology is based on the condition index of each one of these components: building elements, conductor, protection against lighting

impulse, conductor accessories and line route. Using fuzzy math some human subjective elements can be avoided for the conditioning ranking or score but much more detailed data is required.

2.5.2. Management of Data on Distribution Overhead Line Sections

The data required from distribution overhead lines is normally obtained by:

- Field crews during routine inspections or during other work activities which identify situations that may need further inspection and asset condition assessment;
- Pole testing and regular line patrols capture defects and degradation characteristics on line components, and sections of line that exhibit significant deterioration are noted;
- Performance information indicating poor performance of a feeder or section is noted.

Rather than collecting asset condition information on all distribution line sections, the process noted above is considered to be the most practical and cost effective approach to identify specific distribution overhead line sections that need further assessment and evaluation, and possible refurbishment or replacement. Over time, as more information is acquired, it may be possible to assess the overall health of this asset group.

2.5.3. Challenges of Transmission and Distribution Overhead Line Asset Management

Taking in account all the concepts summarized, some specific challenges of transmission and distribution overhead lines' asset management process can be extracted [31]. They are:

- Not a controlled environment: extrinsic and intrinsic failures will occur.
- No need to perform preventive maintenance (PM) for some assets.
- Hard to estimate Risk/Cost of failures for these utilities.
- Difficult to establish direct impact of Asset Failures on System Performance and Reliability indices.
- History of asset failures is a combination of asset condition and stresses.
- The high number of assets to be managed.

- Incomplete data bases (about assets, failures, replacement, maintenance, etc). This condition is more evident on distribution overhead lines.
- Overhead lines history is still in paper form or in the heads of staff.

2.5.4. Experiences of Life Cycle Cost

Limited examples can be found in the literature with life cycle cost experiences between porcelain and silicone insulators, and all are for transmission lines. One case is summarized in [40] on a 230 kV line in service under severe industrial-coastal pollution in South Arabia. The line initially used porcelain insulators for 15 years and it needed to be washed every two months. After this period, 3.2 km were replaced by silicon insulators. The authors estimated that the insulators will have 25 years of life (30 for porcelain) and they also assumed that they will not need to wash them. Using this premises they found a cost of life 9 times higher for porcelain strings, mainly because of the cost of washing. As a consequence, they found than even replacing the polymer insulators every 2.8 years, the system still be less expensive and it will not have flashovers or any other inconvenience during washing. Two important details must be considered in this study (1) estimated life time equal to 25 years for silicon insulator is not a formal number and experiences in other countries under similar conditions have different values, typically smaller, and (2) previous experiences also show that under extreme pollution condition polymer insulators must be washed.

3. COMPOSITE INSULATOR ASSET MANAGEMENT STRATEGY (AMS)

In this chapter, the fundamentals of asset management concepts included in Chapter 2 are used to make a proposal for the asset management of composite insulators. No difference will be expressed between distribution and transmission networks to be able to use this information independently of that. Even so specific considerations will be included for the distribution overhead lines. Emphasis is given to describe the diagnosis and monitoring techniques currently available, as well as in the methodology for the definition of states of degradation based on visual inspection of the insulators. A general framework is presented for activate alarm levels based on insulation condition determine by visual inspections. A four-state ageing estimator is also proposed to define the actions that must be followed by the utilities and all the data and information that should be collected is also presented.

3.1. Main Objectives of Composite Insulator AMS

Using the general concepts presented on the previous items, the main purposes or goals that can be achieved when a specific Composite Insulators Asset Management Strategy is established are:

- To maintain safety.
- To ensure an acceptable level of reliability:
 - to prevent of unacceptable Customer Interruptions (CI) and Customer Minutes Lost (CML),
 - to prevent widespread systematic equipment failure,
 - to prevent unplanned capital or operational expenditures.
- To optimise insulator renewal.
- To optimise maintenance and inspection:
 - efficiency and cost,
 - key condition indicators are identified and known,
 - new diagnosis techniques to implement,

- failure modes statistics and ageing mechanisms knowledge,
 - differentiating between voltage levels if appropriate.
- To provide information to improve:
 - purchasing specifications,
 - design decisions,
 - construction/installation/replacement records,
 - storage level needs,
 - transporting, storage and installation procedures,
 - new technologies or materials to be under consideration,
 - manufactures' classification.

3.1.1. Main Targets

The main targets of the composite insulators asset management strategy can be listed as:

- Include geographic dependency:
 - natural environment,
 - man-made pollutants,
- Include regimes of inspection:
 - Asset tracking,
 - Timing (c.f. §10.3 EI 10-0002 Inspection and Maintenance Frequency Schedule – EDF Power Network document [41]),
 - Process description (techniques),
 - Data management,
 - Diagnosis techniques,
- Include fault inspection.

3.2. Inspection of Composite Insulators & Diagnostic Condition Assessment Techniques

The inspection of the non ceramic insulators (NCI) is of high importance for the identification of potential risks of failure caused by adverse conditions of their state and to assess their expected end of life. Running this process in a professional manner means that success can be achieved. Selecting the most appropriate field inspection and diagnostic

assessment techniques requires knowledge, comprehension and understanding of the ageing factors, different types and forms of deterioration and damages, and mechanisms and modes of failure. This is also applicable for laboratory testing and diagnostic evaluation. Continuous review of new techniques and monitoring detectors is fundamental for the utilities to improve asset management quality and benefits. Important investigations are conducted around the world which can lead to new commercial applications and, at the same time, many utilities around the world are reporting their evaluations on NCI, which the final diagnosis of which can be useful for other utilities.

3.2.1. Visual Examination

Two different institutes have presented specific definitions and images for the identification of different degradation and damaging process that can be visually identified on non ceramic insulators: the Electric Power Research Institute (EPRI, USA) [42] and (STRI, Sweden) [43]. EPRI's guide also includes a 'risk category' to rank all the phenomena detected, which is an advantage to establish the asset conditioning and management. For its part, the STRI presents two more guides; one with the worldwide used hydrophobicity classification (known as HC using the spraying method) [44] and the other with spreadsheet formats for inspections providing a formal basis for the collection of data from insulators, their environmental service conditions and inspection processes thereof [45]. A third visual guide was found in the literature [46] from the Transmission Department of the Florida Power & Light Co (USA) to help the activities of its own maintenance personnel which include two options: replace or keep in service.

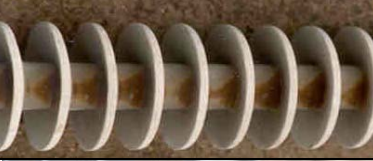
Deterioration

Deterioration is defined as superficial ageing that occurs on the composite insulator as a direct result of exposure to the service environment, electrical stress, mechanical loading and/or careless handling. This ageing is not expected to cause a significant reduction in the insulator's performance and/or lifetime, and does not represent reliability risk. These conditions do not normally require the replacement of these assets. *As specific limits, deterioration does not significantly reduce the thickness of the polymer housing (i.e. by more than 1mm at the sheath) that prevents moisture ingress to the core rod, or reduces the leakage distance by more than about 10%* [26, 43, 46]. The main deterioration processes are presented in the Table 3.1.

Table 3.1 Classification and description of Composite Insulator Deterioration

Deterioration	
<p>Chalking/Whitening - appearance of some filler particles of the housing material forming a powdery or rough surface. This is usually white in color.</p>	
<p>Color changes - change in base color of the housing material of the polymer caused by oxidation, UV attack, weathering, and/or corona discharge activity.</p>	
<p>Cracking - any surface fracture to depths greater than 0.1 mm. Stress cracking breaks weak linkages between polymers (does not break internal polymer strong bonds) when mechanical stresses cause minute cracks in the polymer and they propagate rapidly under harsh environmental conditions.</p>	
<p>Crazing - surface micro-fractures of depths approximately 0.01 mm to 0.1 mm. Crazing is a network of very fine cracks on the surface of a material.</p>	
<p>Fracturing (Aligatoring) - progression of the crazing and cracking whereby surface fractures are deeper than 0.1 mm (Limited to the first and second generation polymer products from the 1970s and 1980s).</p>	
<p>Light Erosion - superficial, irreversible and non-conducting degradation of the material surface that occurs by loss of material increasing roughness, which does not penetrate deeper than 1 mm. This can be uniform or localized.</p>	
<p>Minor Splitting/cutting - separation or opening of the polymer housing, like minor break, tear or crack which can be considered as deterioration.</p>	
<p>Minor debonding – occurring between different components of the insulator that can be considered as deterioration rather than damage.</p>	

Table 3.1 Classification and description of Composite Insulator Deterioration (cont')

<p>Shed undulations – ‘waves’ shape at the rim of the sheds caused either by thermal degradation or inadequate manipulation (during transport or installation).</p>	
<p>Flange Corrosion - metal end-fitting deterioration due to chemical reaction with the environment (rusting).</p>	
<p>Grease Leakage – Escape of grease from shed/sheath or sheath/sheath interface onto the sheath or shed surface.</p>	
<p>Rodent Damage – It is considered as deterioration if the rodents only attack the sheds. If the core is compromised it must be considered as damage.</p>	
<p>Loss of surface hydrophobicity or ability to repel/reject moisture on the surface when wetted. This might have a direct result on the insulator withstand to electrical flashover under wet and polluted conditions.</p>	

Damage

Damage is defined as irreversible changes to the composite insulator that occur as a consequence or progression of pre-existing surface deterioration and/or external influences (careless handling, vandalism, mis-application, lightning, pollution, etc). Damage may be expected to have a negative impact on the insulator’s performance and/or lifetime. Sometimes an insulator is damaged in such a way, or to such a degree, that leaving it in service presents an unacceptable risk and it must be removed [26, 43, 46, 47].

Table 3.2 summarizes the main superficial or irreversible damages that can be detected during visual inspection processes of composites insulators. A highly illustrative photographic exhibition of deterioration, damage and failures on different insulators aged in service is presented in [26, 42-46, 48-50] and constitute a very complete and graphical support for the personnel in charge of the inspection/diagnosis/maintenance activities.

In the Table 3.3 other relevant elements to consider for the ageing analysis are shown. These elements act as degradation accelerators.

Table 3.2 Classification and description of Composite Insulator Damage

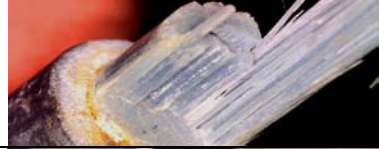
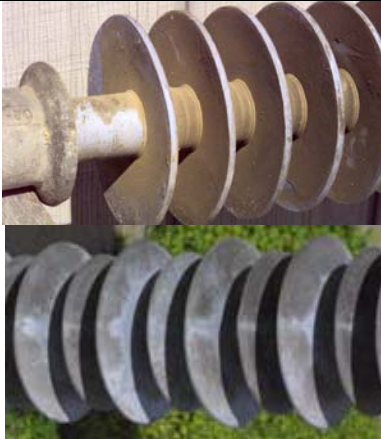
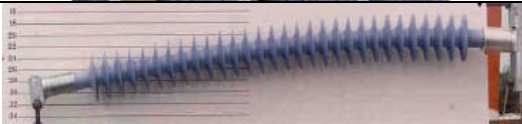
Damages	
<p>Burning/tracking/carbonizing - irreversible degradation by formation of conductive paths starting and developing on the surface of the polymer material, with appearance of carbon paths that cannot be easily removed and are conductive even when dry.</p>	
<p>De-bonding - breakdown of an adhesive material or fusible ingredient intended to create a chemical bond between the fiberglass re-inforced plastic (FRC) core and polymer. This can also be when polymer sheath sections are unclipped from one another.</p>	
<p>Corona cutting - scissioning of the polymer material resulting from exposure to localized high levels of ultra-violet energy associated with the presence of corona discharges.</p>	
<p>De-lamination - in-plane separation of a FRC laminate ply or plies due to adhesive failure. For pultruded FRCs, the separation of two or more layers or plies of reinforcing material.</p>	
<p>Erosion - irreversible and non-conducting degradation of the insulator surface that occurs by significant loss of polymer material, which can initiate the formation of further damages, reducing the thickness at the polymer sheath (i.e. by more than 1mm) that prevents moisture ingress to the core rod. High roughness.</p>	
<p>Exposure of the fiberglass re-inforced plastic (FRC) core - uncovering of the core to the environment caused by damage to the polymer housing such as erosion, tracking, puncture, splitting and/or external influences (careless handling).</p>	

Table 3.2 Classification and description of Composite Insulator Damage (cont')

<p>Fracture - cracks, crazing, or de-lamination, or a combination thereof in a FRC material resulting from physical damage.</p>	
<p>Power arc damage - damage sustained from a high current and temperature on the polymer material, FRC core, and/or metal fittings caused by an electrical flashover.</p>	
<p>Puncture - damage to the polymer material resulting from a disruptive discharge occurring through a solid dielectric (e.g. shed, sheath, core) causing permanent loss of dielectric strength.</p>	
<p>Splitting/cutting - irreversible break, tear, crack or material loss, which reduces the creepage distance (i.e. by more than 10%) or the thickness of the polymer sheath (i.e. by more than 1mm).</p>	
<p>Undermining - The loss of polymer material, resulting in a puncture hole through sheds, usually at the shed/sheath interface and in some cases may expose the FRC core.</p>	
<p>Flashunder – Electrical discharges along the interface rod/housing. Usually occurs when the adhesion between these two layers is damaged by torsion, manufacture problems, damage of the seals, among others.</p>	
<p>Seal degradation – Loss of adhesion or damage of the seal at the metal end-fittings/polymer interface, by peeling, erosion or puncture.</p>	

Note: Similar types of deterioration or aging are not expected to occur with the same severity for third generation (1990's to date) polymer-based products [26].

Table 3.3 Other process to consider for the ageing of composite insulators

Others	
<p>Pollution - Contamination on NCI sheds and/or sheath from marine, agricultural, or industrial sources. Severity effect depends on contamination level.</p>	
<p>Organic growth - polymers can sustain mold, fungi and algae growth. Their presence does not compromise the polymer even do there is evidence that they change the performance of the insulator.</p>	
<p>Apparent creep: Permanent deformation, damaging the fiber-reinforced resin rod, resulting from long-term performance above the damage limit. Torsion: Deflection or twisting about the axis, which causes lines normally parallel to the axis to become helices.</p>	
<p>Excessive protrusion moulding line</p>	
<p>Severe oxidation of end-fittings</p>	

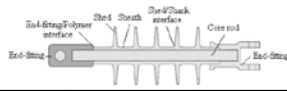
3.2.2. Main Defects and Damage Witnessed

The previous section identified that defects and damage are mainly developed along specific areas of the insulator. The main research groups working on this degradation

classification agree in the regionalization as is presented in Table 3.4 [42, 43, 45, 48] where six main areas are evaluated: (i) end-fittings, (ii) fitting/polymer interface, (iii) sheath or shank, (iv) sheds, (v) shed/shank interface, and (vi) core rod. Knowing this information helps the inspection and monitoring process.

STRI presents a straight forward recommendation: if the core is exposed or any ‘damage’ is growing towards the core, the insulator must be replaced. In the literature was found an American utility using this advice. See Table 3.5 [46].

Table 3.4 Main insulators regions where defects and damages are developed

CONDITION							
		End Fitting	Fitting/Polymer interface	Sheath (Shank)	Shed	Shed/Shank interface	Core Rod
Deterioration	Chalking		✓	✓	✓		
	Colour changes		✓	✓	✓	✓	
	Crazing		✓	✓	✓	✓	
	Flange corrosion	✓					
	Grease leakage					✓	
	Light erosion		✓	✓	✓	✓	
	Minor debonding		✓	✓	✓	✓	
	Minor Splitting/cutting		✓	✓	✓	✓	
Damage	Core exposure	✓	✓	✓		✓	
	Debonding			✓		✓	
	Erosion		✓	✓	✓		
	Peeling		✓				
	Power arc damage	✓	✓	✓	✓		
	Puncture		✓	✓	✓	✓	
	Splitting/Cutting/Punctures		✓	✓	✓	✓	
	Tracking/Carbonizing		✓	✓	✓		
	End fitting/polymer seal degradation ⁽³⁾		✓				
Mechanical Failure	Non-brittle fracture						✓
	Brittle fracture						✓
Others	Loss of hydrophobicity		✓	✓	✓	✓	

Using the information published by EPRI, Table 3.6 is prepared. EPRI had established a four-level maintenance priority rating: A, B, C and D, where A is ‘as new’ and D means ‘severely damaged’. Each level of the rating has a maintenance action to take as summarized in Table 3.7 [42, 48, 51].

An alternative visual inspection guide is given in [52] and presented in Figure 3.1. The main difference with the previous proposals (STRI and EPRI) is the consideration of extensive mold growth as a reason to prepare to stop. Others consider washing as an appropriate option.

Table 3.5 Conditions to replace or not a polymer insulator using visual inspection

CONDITIONS WHICH DO NOT REQUIRE REPLACEMENT
<ul style="list-style-type: none"> • Chalking • Grease leakage • Accumulation of dirt • Accumulation of mould • Hydrophobicity reduction • Mechanical damage to a few sheds • Low fault current arc damage • Arc damage to corona ring • Minor corrosion of end fittings • De-bonding of sheds • Crazeing
CONDITIONS WHICH REQUIRE REPLACEMENT
<ul style="list-style-type: none"> • Damage to the fibreglass rod • Exposed fibreglass rod • High fault current flashover on suspension insulators • Severe corrosion of end fittings • Alligatoring • Hardware seal failure • Significant erosion of surface material • Puncture of sheath • Overloaded polymer post

Table 3.6 Conditions and its extension along the insulators

	CONDITION	A	B	C	D
Sheds	Splits and Punctures		Localized to sheds	Progressing towards or close to sheath. Puncture through shed.	
	Torn or Damaged		Tear is across shed	Tear has progressed or is progressing to the sheath	
	Gunshot Damage		Damage to sheds only	Bullets lodged in sheds	
Sheath	Exposed Rod (Electrical Activity)				Exposed rod
	Exposed Rod (Mishandling)				Exposed rod
	Unclipped Sections				Exposed rod between: end fitting/ sheath sections or between sheath
	Splits			Silicone gel present; rod not exposed	Exposure of rod
	Gunshot Damage			Sheath damaged, rod not exposed	Exposed rod. Bullets on sheath
Sheds and Sheath	Whitening	White powder or film on surface			
	Tracking				Conductive path along surface
	Animal Damage	Minor shed damage	Shed damage only	Sheath damage, rod not exposed	Rod exposed
	Undermining			Sheath damage, rod not exposed	Rod exposed
	Cracking		Only sheds cracked	Sheath and sheds cracked	Sheath cracked and moisture penetration possible
	Alligatoring	Superficial, material is not brittle	Significant depth	Severe embrittlement	
	Erosions		Shallow surface erosion	Deep surface erosion	Excessive surface erosion
	Contamination	Varying levels of contamination (washing can be needed)			
	Crazing	Shallow surface fractures			
	Fungus or Mold Growth	Fungus or mold accumulation (Concern in contaminated environments. Continued research is underway, specific situations may require special actions)			
	Insect Activity	Webs, nests, or cocoons present	Excessive webs, nests, cocoons (Consider removal or washing)		
	Hydrophobicity (SIR)	Localized loss of hydrophobicity	Complete loss of hydrophobicity		
	Silicone Grease on Surf.	Grease on sheds and/or sheath	Sheds and/or sheath are split		
Corona Rings	Flashover Damage		Damaged but no AN/RI complaints	Damaged with AN/RI complaints	Serious damage
	Incorrect Position			Backwards or incorrect position	
	Loose Ring			Corona ring is loose	
	Gunshot Damage		Damaged, no AN/RI complaints	Damaged with AN/RI complaints	
	Flashover Damage			End fitting damaged by flash-over, rod not exposed	End fitting damaged by flashover, rod exposed
End Fittings	Degraded Seal		Degraded end fitting seal	Significant degraded end fitting seal	
	Corrosion		Corrosion and rust accumulation of end fitting		

Table 3.7 Insulator condition and maintenance priority rating (by EPRI)

MAINTENANCE PRIORITY RATING	DEFINITION	DETERIORATION OR DAMAGE	ACTION
A	Good or like new.	-	No action required.
B	Low degree of damage, wear, decay.	Any degradation process developing far from the shank or do not grow towards it.	Monitor for future damage.
C	Moderate degree of damage, wear, decay.	Any degradation/damage process growing close to the shank or moving towards it.	Consider replacement.
D	High degree of damage, wear, decay.	Any kind/size/source of damage where the core rod is exposed; flashover damage; seals damage.	Remove polymer insulator from service.

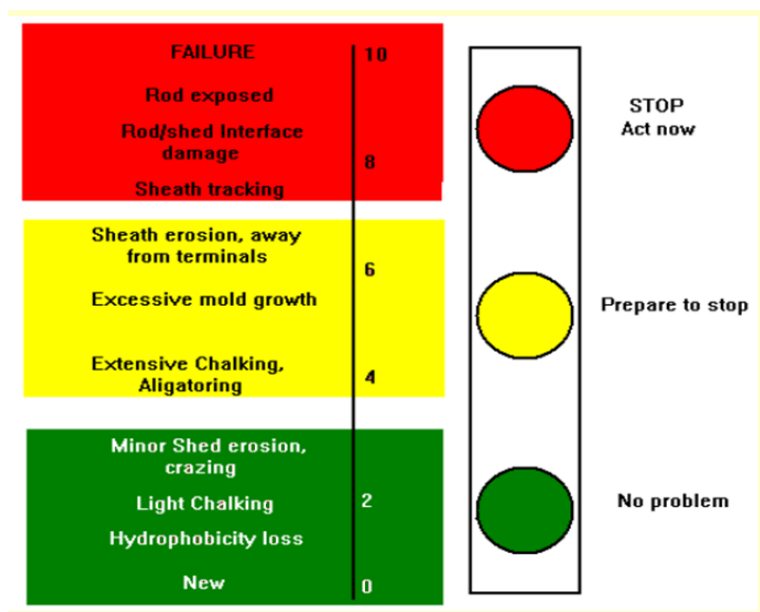


Figure 3.1 Gorur's Visual Inspection Guide

3.2.3. Main Diagnostic Techniques

In order to get good results during monitoring/inspection/diagnosis process, the examiners should be familiar with the design and the materials, as well as the typical failure modes of the insulator type. At the same time, knowledge of service conditions is fundamental to establish good conclusions and define actions.

A brief description of some techniques is presented in this report. Electric tests such as withstand and flashover voltage, lightning or switching impulses, partial discharges, radio interference voltage (under dry or wet conditions) are not included because they are fully described by international standards (ANSI-IEEE or IEC).

Visual Inspections

For polymer insulators (and for any other non ceramic component like bushings, terminations, arresters, coatings, coverings, etc.), visual inspection can help to detect five main ageing processes: (1) many types of material surface deterioration and damage; (2) hydrophobic condition; (3) surface pollution (e.g. cement, salt, etc.), etc. that may lead to future corona discharges and/or dry band arcs activity, (4) damage of the seals and (5) exposure of the FRC core. The main instruments used are: binoculars (10 X magnification max, unless gyrostabilized: 10X – 20X), spotting scope (20X – 60X, tripod mounted), high-powered video camera with stabilization and high magnification. To get reliable results, the inspector should be positioned close to the insulator, i.e. preferably climb a tower (magnifying mirrors mounted on bars or sticks to see the back sides can be used), or use a bucket truck or helicopter [26, 47, 48, 53]. Hydrophobicity classification is widely through using the Guide STRI 1-92, see Figure 3.2 [44]. Improvement for its use in the field [54] and interpretation using digital image processing or neural networks of the different states have been presented in the literature [55-57]. This guide was incorporated to the IEC Technical Specification, IEC TS 62073 (First edition, 2003): “Guidance on the measurement of wettability of insulator surfaces” [58, 59].

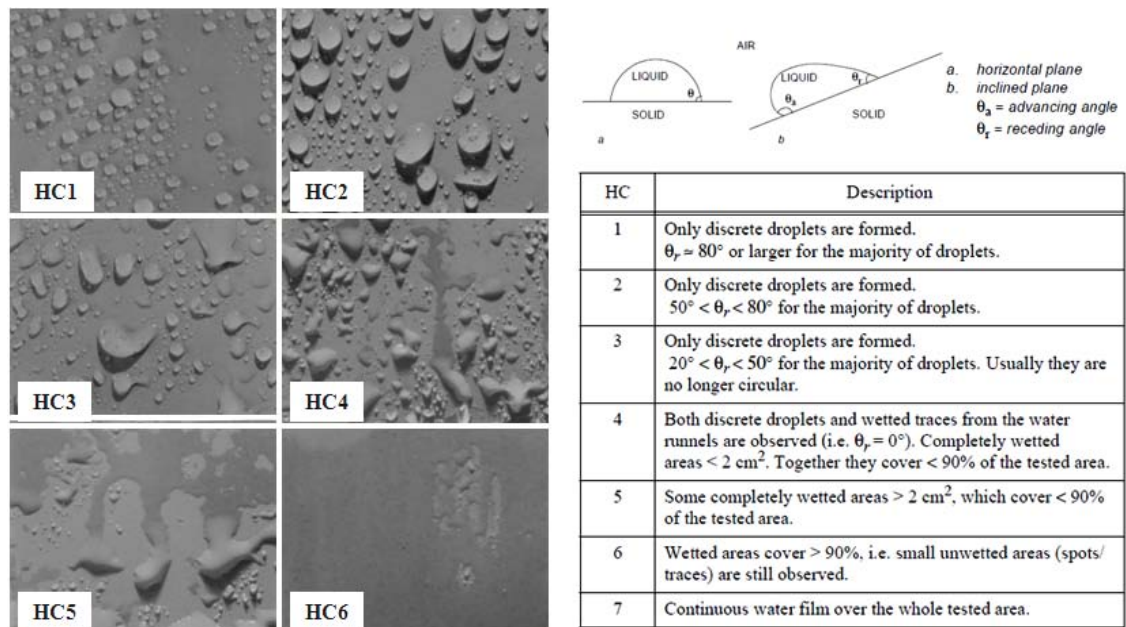


Figure 3.2 Hydrophobicity classification following the STRI Guide 1-92

There is a recommendation to improve the view over insulators in the horizontal orientation (line post or end-fittings) for their visual inspection [52] by managing the position of the patrol members doing the procedure walking under the post. See Figure 3.3.

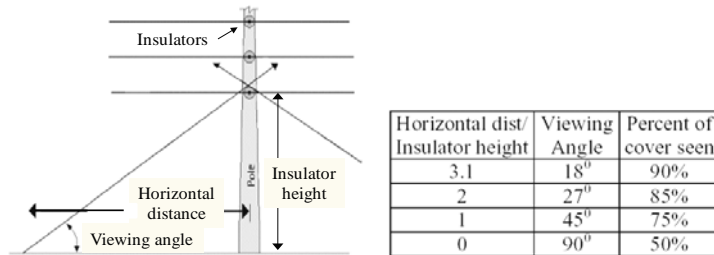


Figure 3.3 Patrol Position to maximize the overall view of the insulators [51]

IR Thermography

Thermal scans can detect temperature variations (See Figure 3.4 [60]). Degradation of materials under electric fields is, in many cases, associated with heat generation and it may help to detect evidence of: (1) internal moisture ingress; (2) large FRC core voids and cracks; (3) polymer and FRC surface tracking, and (4) localized electrical surface discharging, etc [26, 48]. Any heat rise on a polymer insulator in the absence of visual or ultraviolet emission indicates an ongoing “flashunder” process between weathershed and FRC [61]. Appearance of elevated temperature spots, resulting from current flow in the interface between housing material and FRC rod, were found to be suitable for detecting punctures, cracks and tracking damages. The major disadvantage is that temperature increase induced is usually quite small and makes the technique sensitive to environmental measurement conditions and interpretation of IR results may be affected by strong winds, dew, and rain temperature distribution (for example from sun radiation, and rapid temperature changes). It was therefore suggested that best results could be obtained if measurements were performed at night [62]. This test requires infrared (IR) cameras (normally, portable field hand-held units).

UV Light or Discharge Detection

Corona will appear when the local electric field exceeds a critical value $E_{critical} = 24-30$ kV/cm. Since corona phenomena depend on the *electrical field value*, it may occur in low voltages as well.

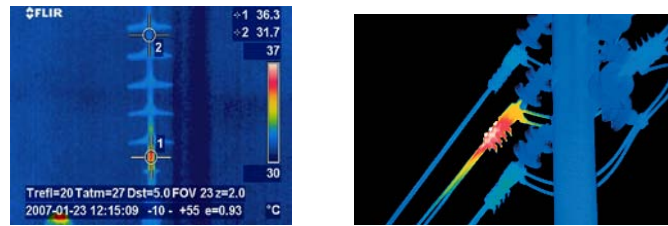


Figure 3.4 IR Thermography on polymer insulators [60,61]

Ultraviolet (UV) light typically arises where electrical discharging occurs and so damaging discharges can be identified at early stages. Light amplification equipment can be used to detect presence of surface discharge activity on insulators. At night, discharges may be seen directly by the naked eye (depending on distance) or by using standard night vision equipment. However, most of the photons emitted from discharges have energies corresponding to wavelengths in the region 300-400 nm (outside the region of standard night vision units and the human eye). The detection limit can be enhanced significantly by utilizing UV-A sensitive equipment using optical filters. The main inconvenience is that solar radiation is several orders of magnitude stronger than the signal from the discharge and the measurements have to be performed during night to avoid it.

However, there are more expensive instruments able to detect discharge activity during the daytime developed using two main approaches: (1) Using the fact that corona occurs close to the peak of power voltage, to separate light emitted by corona discharges from light radiated by the sun; two images are recorded, one with and one without corona, using an UV image intensified video camera synchronized to the power voltage. After some image processing, the result is an image of the corona discharge on the surface of the object under test [60, 63]; (2) avoiding interference from sun radiation by detecting radiation in the 240-280 nm region (UV solar blind band) where the intensity of light emitted by corona is much weaker than in the 300-400 nm region, but there is also less background radiation from the sun (because it is blocked by the atmosphere) [64]. For polymer insulators discharge detection using a day-time UV light sensitive camera may help to detect evidence of: (1) internal moisture ingress; (2) large FRC core voids and cracks; (3) polymer and FRC surface tracking, and (4) localized electrical discharging which are often indications of the beginning of erosion damage or cuts in the housing material, etc.

There are portable field hand-held units to use in the field and in laboratories and there are two main commercial cameras on the market which integrate IR and UV detection; they are Corocam and Daycor. Some images can be seen in the Figure 3.5 [60].



Figure 3.5 Corona discharges detected on polymer insulators using IR and UV integration [60]

X-raying

X-ray imaging may help detect internal damage or structural changes that could be detrimental [26] to their service performance and life expectancy. The portable field hand-held X-ray unit and lab X-ray equipment may help to detect evidence of: (1) polymer / FRC de-bonding, and (2) large FRC core voids, de-laminations, cracks and other mechanical damage to FRC matrix that can be very difficult or impossible to visualize by the naked eye. There are both portable and laboratory based equipment and the images are better analyzed using digital imaging filters (i.e. Laplacian and Gaussian) [26, 65-67]. Pattern recognition can also be utilized [68].

Recently, 3D industrial computed tomography has used digitally processed images and neural networks [69]. Figure 3.6 shows the X-ray test performed on a high density polyethylene (HDPE) pin insulator where an internal defect was detected; dissection of the sample verified this [67]. Figure 3.7 shows the X-rays of suspension insulators with defects at the interface core/housing [70].

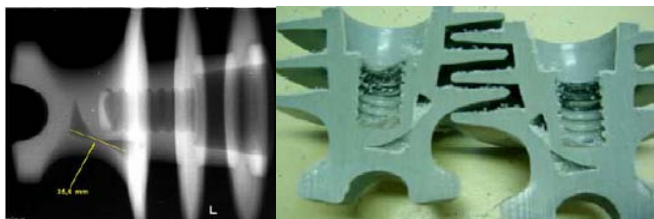


Figure 3.6 Defects on HDPE insulators detected using X-rays [67]

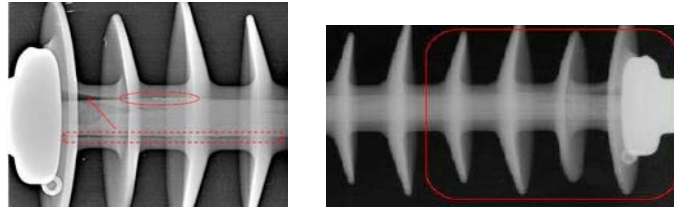


Figure 3.7 Defects on polymer suspension insulators detected using X-rays [70]

Electrical Field Profile Measurement

E-field measurement may provide an indication of internally damaged polymer insulators when the measurements deviate from the expected voltage or E-field profile. This method may help to detect evidence of: (1) internal moisture ingress; (2) polymer and FRC surface tracking; (3) polymer / FRC de-bonding for insulators and bushings; (4) large FRC core voids, de-laminations, cracks and other mechanical damage to FRC matrix. Figure 3.8 shows an example of electric field distribution in a 33 kV insulator with no defects and with voids at the interface between the core/housing interface [71]; Figure 3.9 shows the changes to the electric field distribution when the sample has defects, and Figure 3.10 represents the FEM simulation of a 40 kV sample under dry and wet conditions [72]. This technique is not widely used for distribution equipment. There are portable hand-held probes or laboratory cell designed to detect E-field [26, 73].

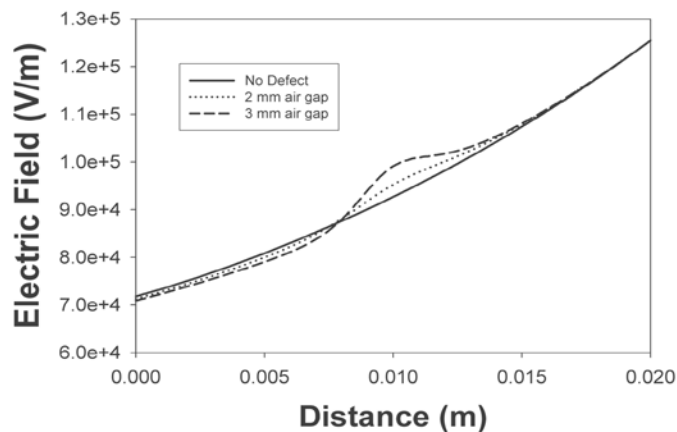


Figure 3.8 FEM Simulation of E field distribution in a 33 kV polymer insulator with no defects and with voids at the fibre glass core/polymer interface (calculations 0.01 mm away from the insulator surface) [70]

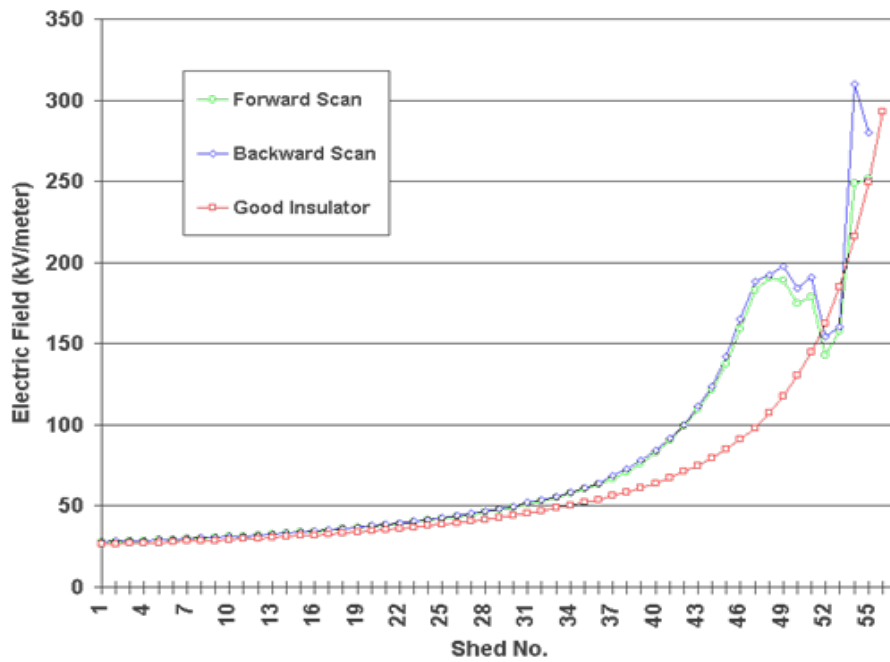


Figure 3.9 Electric field distribution (in laboratory) of a healthy and a defective insulator removed from service having a 42 cm long visible defect at the HV end (Source: www.positronpower.com)

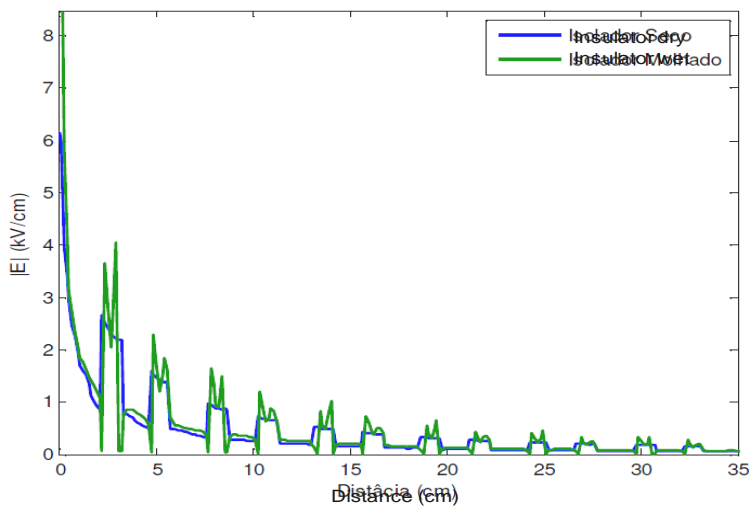


Figure 3.10 E-field distribution (FEM simulation) along a 40 kV insulator under dry and wet condition [71]

Leakage Current

EPRI published data on some current sensors that can be linked with the Advanced Distribution Automation (ADA), concept for a fully controllable and flexible distribution system, and can be used for monitoring an assets' condition [74].

Utilities in Brazil have been doing significant studies collecting leakage current data from their overhead lines with polymer insulators; Coelba Grupo Neoenergia (Companhia de

Electricidade da Bahia) started developing an electromechanical sensor [75] and nowadays, Celpe (Companhia Energética de Pernambuco member of Coelba) developed an electronic sensor (see Figure 3.11.a) which sends radio frequency signals to a concentrator port and sends alarm messages to a portable device when a threshold is reached [76]. The sensors are used mainly on 69 kV lines with EPDM insulators in a coastal region. The sensor can be installed with the line in operation and the results were confirmed by laboratory testing of the insulators after their removal. They determined that leakage current magnitude can give information about when the insulators should be washed (level of pollution).

Figure 3.11.b shows the EPRI prototype which senses continuously and sends blocks of key information. It sends alarms when the conditions indicate that washing is needed or there is a risk of flashover occurrence.

Figure 3.12 illustrates some examples of leakage current patterns and their harmonic content. Full analysis of the leakage current signals along specific extension of time offers good information about the degradation processes that are occurring on the insulators surface and the relation of it with the environmental conditions and pollution [77-80].

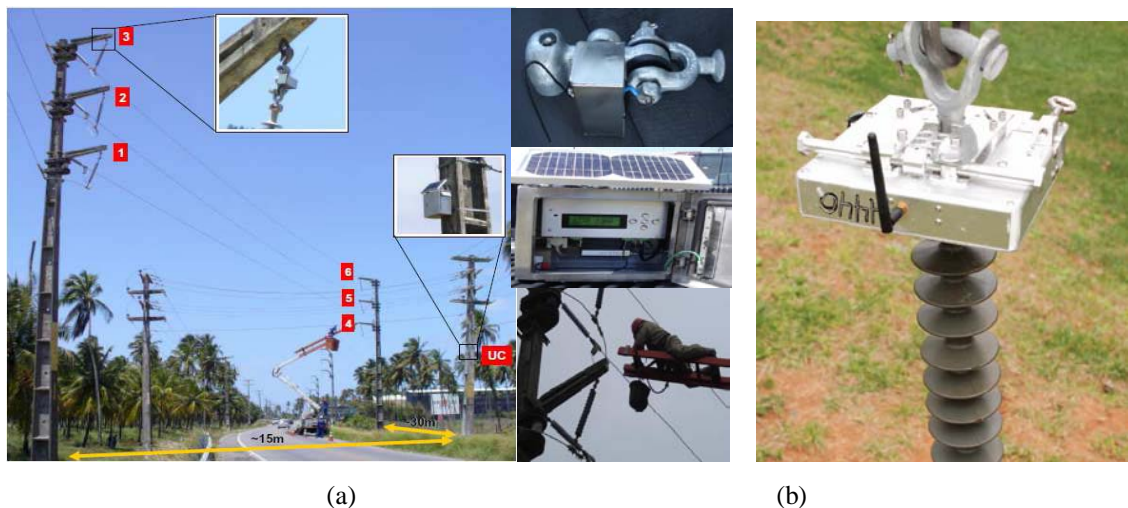


Figure 3.11 Leakage current sensors installed by (a) Celpe, Brazil, to monitor leakage current over a peak threshold on 69 kV EPDM insulators; (b) EPRI prototype, USA.

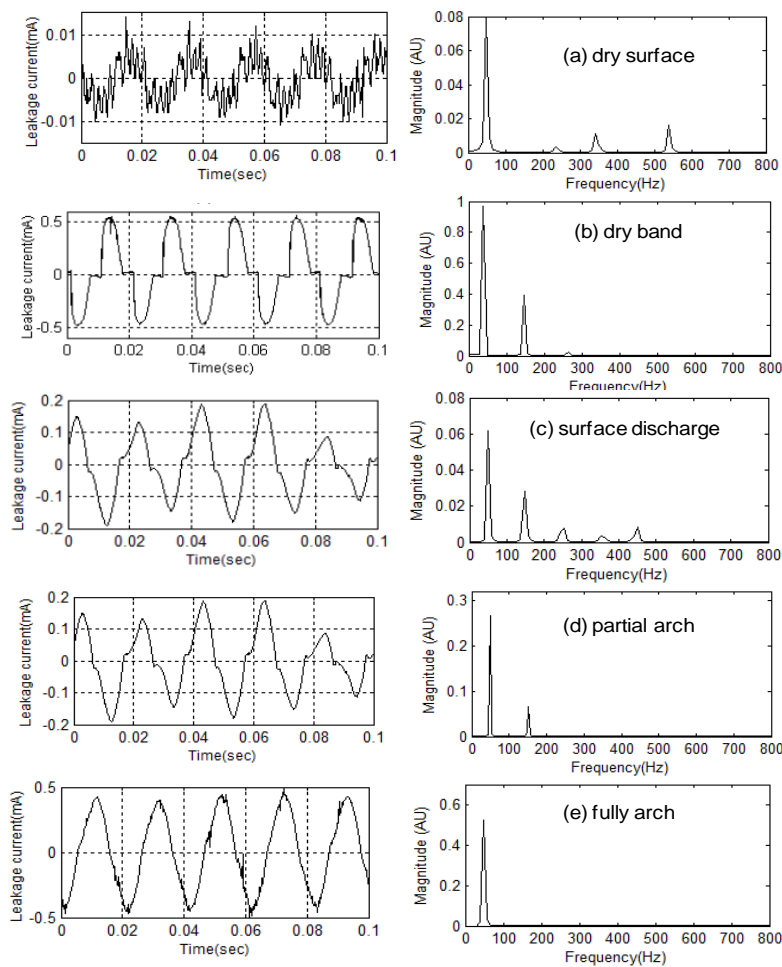


Figure 3.12 Leakage current patterns [79]

Resistance Measurements

High Voltage AC resistance measurement may indicate internal damage of polymer insulators by measuring a drop in resistance value under high voltage conditions. This could reveal the following situations: (1) internal moisture ingress; (2) polymer and FRC surface tracking; (3) polymer/FRC debonding, and (4) large core voids, delaminations, cracks and other mechanical damage to FRC matrix. There are HV ohm-meters, portable field hand-held units designed for insulators, or this can be done in the laboratory [26].

A technique using low voltage DC surface resistance (approximately 2 kV) measurement, under wet conditions, has been proposed to evaluate the condition of insulators along with a methodology and physical equations/approximations to predict the flashover voltage, including or not the effect of weathering [81-84]. This method can provide: (1) an indication of aging of housing material and (2) a more sensitive indicator of true

contamination severity on insulators than provided by conventional ESDD (equivalent salt deposit density) measurements. The values found in some specific experiments are shown in the Table 3.8. The limitation of the method is that values of resistance found using this method are specific for the insulators tested. The values depend on geometrical parameters or design of the housings.

Table 3.8 Minimum DC surface resistance with different polymer housings, pollution and hydrophobicity [80,83]

Insulator	Remarks	HC (STRI)	Min. Surface Resistance
New Silicone	Stored outdoors	1	>500 k Ω /cm)
Aged Silicone (no failure)	Heavy black dirt on surface	1-2	111 k Ω /cm
Aged EPDM 1 (flushed over)	Heavily chalked	7	11 k Ω /cm
Aged EPDM2 (no failure)	Heavily chalked	7	44 k Ω /cm
New Porcelain	Post insulator	7	44 k Ω /cm

Ultrasound Laboratory Measurements

Ultrasonic inspection is a non-destructive diagnostic method where beams of high frequency sound waves are introduced into materials for the detection of surface and sub-surface flaws and damage. The sound waves travel through the material with some loss of energy due to attenuation and are reflected at interfaces. Some methods are: Ultrasonic Through Transmission, Ultrasonic Pulse-Echo, and Ultrasonic Resonance Test. Ultrasound measurements may help to detect evidence of: (1) internal severe damage caused by tracking and burning; (2) polymer / FRC de-bonding; (3) large FRC core voids, cracks, discontinuities, delaminations, and other mechanical damage to the FRC matrix [26, 47]. There are some applications of this technique to monitor distribution systems [85].

Vibrational or Frequency Response Measurement

Vibrational or frequency response technique using a Laser Doppler Vibrometer/ Velocimeter device may help detect the dominant resonant frequency indicating internal damage of insulators. This technique can usually help to detect evidence of: (1) polymer/ FRC debonding, and (2) large FRC core voids, cracks, delaminations, and other mechanical damage to FRC matrix. There are portable field hand-held units or laboratory equipment [86].

Radio and TV Interference Detection

This is a diagnostic technique that can be useful in detecting electrical discharging on mostly externally damaged insulators. While this damage may mostly identify electrical damage, it could also possibly indicate some latent mechanical damage [50].

Acoustic Emission Detection & Measurement

Laboratory based acoustic emission (AE) testing and measurements conducted while under mechanical load to detect cracking and fiber breakage, and may help to detect evidence of: (1) polymer / FRC debonding, and (2) large FRC core voids, delaminations, cracks and other mechanical damage to the FRC matrix [26, 87].

Laser-induced Fluorescence (LIF) Spectroscopy

This technique has been proposed for remote detection of biological contamination on polymer surfaces (60 m range). Using a laser pulse the molecules or atoms on the surface are first excited. When the molecules or atoms relax from a higher to a lower energy state they emit light and this is recorded. This spectrum depends strongly on the characteristics of the surface and is, in fact, a fingerprint of the surface condition. The emitted light will partly have the same wavelength as the incoming radiation, but some emitted light will consist of photons with longer wavelengths (i.e. chlorophyll fluoresce strongly at 685 nm when excited at shorter wavelengths, it has been shown that algae can easily be detected). The method is based on component analysis of the obtained spectra (mathematical post processing), allowing for automatic differentiation of spectra from regions with and without the biofilms [88, 89]. Figure 3.13 shows spectrums obtained using this technique on insulators under clean and polluted with algae [47].

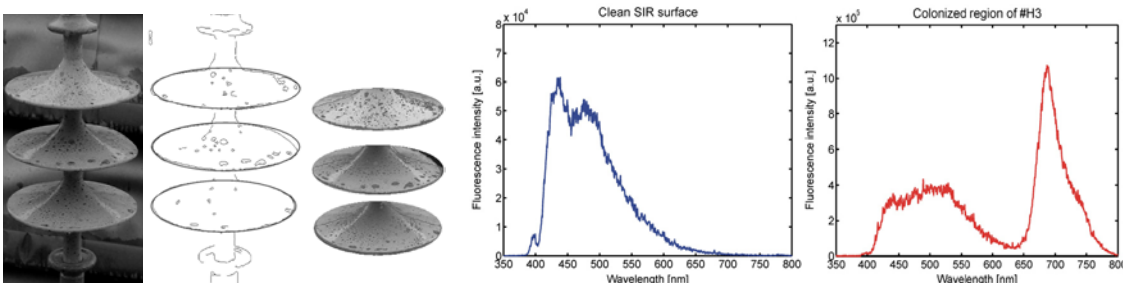


Figure 3.13 Spectrums using laser-induced fluorescence on clean and polluted insulators (biofilms) [46]

Near-field Microwave Non-destructive Testing (Recently proposed)

The ability of microwaves to penetrate deeply inside dielectric materials was successfully used to detect defects on MV polymer insulators. Microwave techniques are based on transmitting a microwave signal into a dielectric structure and using the magnitude and/or phase information of the transmitted and/or the reflected signal to either create a two dimensional image of an object, get line scans or get a single point measurement [71]. As the microwave signal reaches the specimen a reflection occurs, dictated by the dielectric properties of the material in front of the waveguide. The presence of defects changes the dielectric properties of the region within the sensing region and that causes a different reflection to occur. See Figure 3.14. Microwave nondestructive inspection techniques can detect minute thickness variations in dielectric layers as well as slight dielectric property variations in stratified dielectric composites mainly because: (1) When delamination occurs, this may be considered as an additional new thin layer of material in an insulator; (2) microwave signals can penetrate inside low-loss dielectric materials and interact with their inner structure without suffering from high attenuation; and (3) microwaves are also sensitive to changes associated with boundary interfaces, which makes them useful to detect thickness variation [71, 90]. The developers indicate that no special operator skills, in the fields of microwaves or signal interpretation, are needed for successful defect detection, the required microwave power is in low milliwatt range, and such a system may be battery operated and portable. The results are obtained in real-time, and the technique is neither a source of electromagnetic noise pollution (interference), nor sensitive to external electromagnetic sources of interference [71].

Fourier Transform Infrared Spectroscopy (FTIR)

This technique provides structural information and compound identification, evaluating molecular structure based on specific frequencies associated with internal vibrations of groups of atoms in molecules using a beam of light in the infrared region to excite the material and analyzing the frequencies absorbed. Each material has a fingerprint IR spectrum and each change in its molecular structure can be observed. Depolymerization and oxidation (carbonyl groups) can be detected [91-93]. FTIR has been a widely used test for the analysis of polymeric insulators fundamentally to detect the rate of oxidation suffered by the surface.

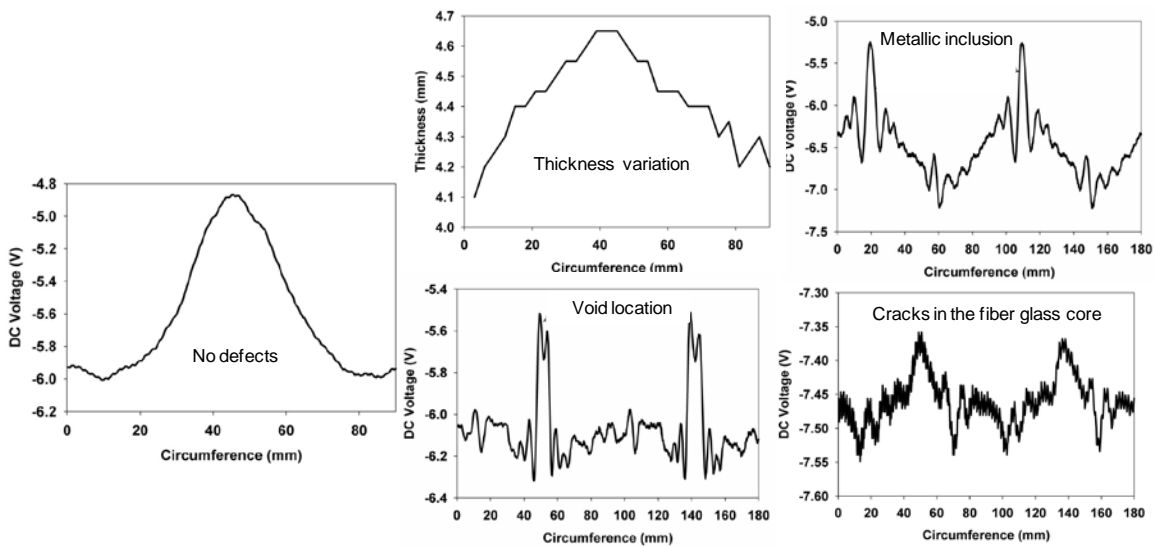


Figure 3.14 Evaluation of 33 kV insulators; cases: no defects, thickness variation, presence of a void, metallic inclusion and cracks on the core using a microwaves sensor (near 24GHz) [70]

In reference [94] the application of this technique in the field is presented (see Figure 3.15). Sampling of the insulators can be done with the line in service or not. At present, FTIR is the only reported physicochemical test where samples are taken in a nondestructive manner in the field and has been used to generate geographic clusters with insulators with similar conditions of degradation [93, 95, 96].

In the case of EPDM a peak due to hydrocarbon bonds (C-H bend) in the polymer appears at wavenumber 1460 cm^{-1} and a broad band due to carbonyl (C=O) occurs in the range 1710 cm^{-1} to 1785 cm^{-1} . As the surface oxidizes, the amplitude of the carbonyl peak increases relative to the hydrocarbon peak. Three different indices have been defined: (1) oxidation index initially defined as the ratio of the carbonyl peak to the hydrocarbon peak and more recently it was redefined as the ratio of the area under the spectrum of the carbonyl band to the area under the spectrum of the hydrocarbon band; (2) A high value of the ratio of ester (wavenumber 1734 cm^{-1}) to ketone peaks (wavenumber of 1717 cm^{-1}) indicates degradation is primarily due to UV whilst a low value of the ratio indicates thermal degradation, and (3) chalking index defined as the ratio of the ATH peak (wavenumber 1020 cm^{-1}) to the polymer peak (CH stretch - wavenumber 2918 cm^{-1}), or an alternative definition of this index has also been suggested using the ATH band at 3520 cm^{-1} to give an index with lower scatter [93, 97, 98].

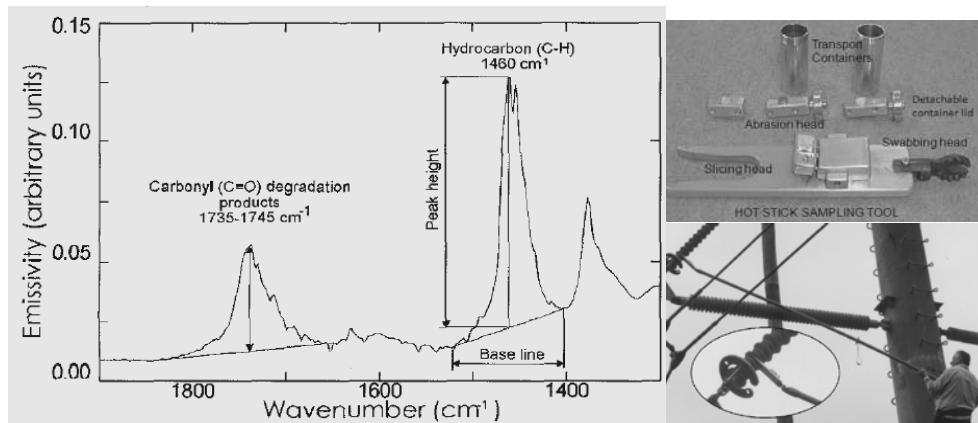


Figure 3.15 Typical FTIR emission spectrum obtained from field-aged EPDM using the swabbing technique; detail of the tool to do the sampling [92,94,95]

Figure 3.16 shows an example of virgin and aged silicon rubber FTIR spectrums. Unaged SR has the following chemical bonds: C–H bonds in CH₃ groups at 2960 cm⁻¹, Si–CH₃ bonds (side chains) at 1270–1255 cm⁻¹ and Si–O–Si bonds (silicone backbones) at 1100–1000 cm⁻¹. UV radiation decreases all these absorptions. The spectrum of aged SR also shows that the hydrophilic OH groups at 3700–3200 cm⁻¹ and C=O bonds at 1740 cm⁻¹ appeared after corona discharge and the ratio of Si–CH₃ and Si–O–Si decreased after corona discharges. The auto-oxidation reactions usually happen on the polymeric surface in the presence of oxygen which forms hydrophilic groups (OH) as by-products of ageing, instead of hydrophobic CH₃ groups on the surface of corona-aged SR.

Using oxidation ratio values to diagnose NCI aged in service, clusters were found based on geographical locations and environmental conditions differences [94].

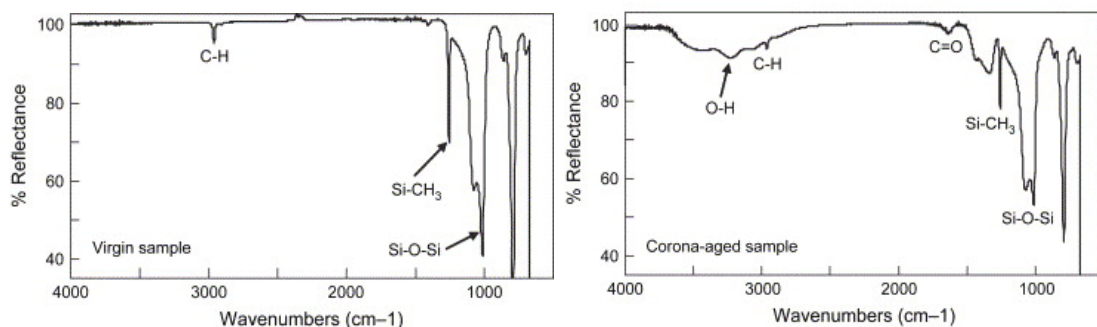


Figure 3.16 FTIR spectrum of unaged and aged (by corona discharges) silicon rubber [94,95]

Other Commonly Used Physicochemical Diagnosis Tests

Some of the main physicochemical tests techniques used to evaluate composite insulators are briefly summarized in the Table 3.9 [88, 89, 92, 99, 100].

Table 3.9 Main physicochemical techniques used to diagnose composite insulators

TECHNIQUE	ASPECT DETECTED ON SURFACE
Raman Spectroscopy (RS)	Used to study surfaces in a similar way to FTIR for weaker frequencies of resonance or highly absorbing materials. A laser excites the polymer, usually in the visible region of the spectrum.
Scanning Electron Microscopy (SEM)	Gives high level information about surface topography, oxide growth and failure analysis. SEM enables qualitative three dimensional imaging of surfaces using a bombardment of the surface by electrons which generate secondary electrons. Erosion, pollution, microcracks, etc can be observed.
Energy dispersive X-ray (EDX)	Chemical elements in a material emit characteristic X-rays, so they can be identified. This technique is normally attached to SEM and evaluates the secondary electrons liberated by it. Chemical elements and their concentrations are detected.
Atomic Force Microscopy (AFM)	AFM measures the topography and morphology of surfaces on the atomic scale which allows a quantitative evaluation of surface roughness.
Gas Chromatography/ Mass Spectroscopy (GC/MS)	Detects molecular weight distribution [101]. GC is used to separate compounds through their different volatilities. The identification of these compounds is done using MS where the molecule dissociates into smaller fragments each one depending on its molecular structure. Aged samples have a larger concentration of low molecular weight (LMW) siloxane species than new samples. Surfaces exposed to UV generated more LMW species.
Thermogravimetric Analysis (TGA)	Weight percentage of polymer/filler. Continuously monitors the weight of a sample during isothermal or dynamic temperature scans over the range from 30° to 1000°C in an air, nitrogen, oxygen, or specialty atmosphere. Applications: thermal stability, compositional analysis, filler content, sample preparation, comparative analysis, specification testing and product analysis. Aged samples present loss of siloxane matrix by depolymerization. Siloxane matrix decomposition is done under oxygen presence and fillers can act as catalysis in silicone rubbers.
Differential Scanning Calorimetry (DSC)	For examining polymers to check their composition, presence of impurities and plasticizers by examining thermogram peaks. The method can show up possible polymer degradation (oxidation) by the lowering of the expected melting point, T _m , for example. T _m depends on the molecular weight of the polymer, so lower grades will have lower melting points than expected. DSC can also be used to study other chemical reactions. The technique is widely used across a range of applications, both as a routine quality test and as a research tool. DSC can be less effective to evaluate some changes on silicones.
X-ray Photoelectron Spectroscopy (XPS, or known by Electron Spectroscopy for Chemical Analysis – ESCA)	Analytical technique that measures the energies of photoelectrons emitted from atoms of a sample when it is irradiated with low energy X-rays. It can detect all elements except hydrogen and helium. It gives information about chemical structure, bonding energy and elements distribution. It can discriminate different oxidation states. It can detect fracture surfaces.
Secondary ion Mass Spectroscopy (SIMS)	Samples are bombarded either by ions or atoms and the secondary ions emitted from the surface during this process are detected and analyzed. Static SIMS is used to analyze surfaces and dynamic SIMS erodes the surface and is used for depth profiling like aged surfaces.

Monitoring Test Stations

The performance of insulation systems in regions of saline contamination is a concern for electric utilities in coastal regions. The failure of different assets due to pollution is responsible for a large proportion of power outages, disrupting the supply and causing degradation in quality of electricity. To study the problem of contamination in insulating systems, different monitoring stations recording leakage current simultaneously with a record of climatic conditions, allows an assessment of performance insulators of the different systems in use by the utilities. These stations can be owned by utilities and manufacturers or even can be shared by utilities/manufacturers. Some of the most representative monitoring stations and associated works can be found in [102-105]. Some examples are given in Figure 3.17. These test stations help with the evaluation of new material formulations, designs, etc, under specific environmental conditions and condition services.

A list of new technologies under development for composite insulators evaluation and monitoring are presented in [47, 100, 106].



Figure 3.17 Test Stations of Insulators [101-104]

To date the selection of the most suitable condition monitoring techniques for a utility or industrial plant has been undertaken mainly by internal subjective expertise, vendors of instrumentation or as a result of the references of suitable behaviour in a similar enterprise. In the literature a formalization for this kind of decision was found in [107]. This proposes a model for the selection of the most suitable condition monitoring technique where different criteria, indicators, and utility functions are defined; different alternatives are proposed depending on the technological level of the condition monitoring program. The model applies the analytic hierarchy process to obtain a ranking of alternatives. Owing to the special characteristics of the decision, discrete probability distributions are defined and

the final ranking is computed by applying the Monte Carlo method and a sensitivity analysis is done after this.

3.2.4. Diagnostic and Monitoring Techniques at EDF Energy Networks

In [33] a list of the condition monitoring techniques that will be used by the company is reported. From this, combined with visual inspection, three options can be used to support the evaluation of composite insulators: thermography, ultrasonic discharge monitors (fixed and handheld) and insulation resistance.

3.2.5. Quality Control of Composite Insulators

To ensure the service life of polymeric insulators, the quality of the product coming from the factory, must be guaranteed. The IEEE Working Group 101 identifies a minimum set of activities required to have quality control of composite insulators [108]. These are shown in the Figure 3.18. To this list other important actions must be take in account: (1) collect the experience inside the company, (2) keep updated the know-how in reference with new materials, design, standards, testing and monitoring technologies, and (3) improve the data collection and keep updated the data base of the assets. In parallel, important specific documents must be collected. The main ones indicated by the IEEE Working group are summarized in the Figure 3.19.

- What Is Needed in a Quality Plan?*
- Identifying critical design parameters.
 - Qualifying ‘new’ suppliers.
 - Evaluating current suppliers.
 - Establishing internal specifications.
 - Monitoring standards compliance (audits).
 - Understanding installation requirements.
 - Establishing end-of-life criteria.
 - Ensuring safety of line workers.
 - Communicating and training.
 - *All aspects defined by the company plan.*

Figure 3.18 Aspects to be covered by a plan to ensure quality [108]

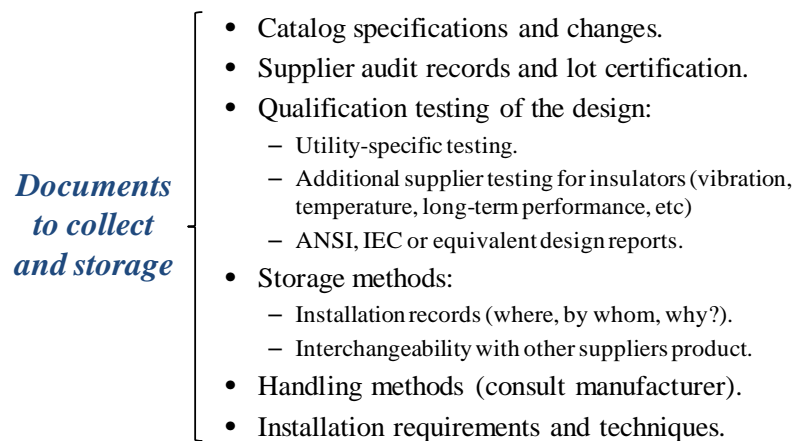


Figure 3.19 Documents to collect and to keep in the insulators data base

3.3. Composite Insulator Maintenance Procedures

Polymer insulators are currently installed and no maintenance processes are generally expected to be performed. Nevertheless, under severe or highly severe pollution conditions washing is a recommended practice. Similarly, under severe biofilms or insect activity, washing can be a solution if the performance of the asset is compromised [51]. IEEE developed a standard for insulators' cleaning (IEEE-PES, "Guide for Cleaning Insulators" vol. IEEE Std 957™-2005, [109]), which covers ceramic and composites for transmission and distribution installations. This guide includes the different methods that can be used to clean the insulators under energized and de-energized conditions, and the best industry practices safe operation in live-line washing and technical considerations for energized cleaning with water. Additionally, this also includes a list of the most critical pollutants that can affect the insulators performance.

It is important to take in consideration that no washing procedure can be done on polymer insulators without the confirmation of the manufacturer.

[110] reports washing in the laboratory of 69kV EPDM insulators recovered from a coastal distribution line highly polluted by salt. Using only pressurised water, the leakage current magnitude reduction was 40% and using in addition hand wiping the reduction was more than 70%. Additionally, the leakage current was initially almost resistive and after cleaning started to present recovery of a significant capacitive behavior. An important reduction of the dry band arc activity also resulted.

In [111] washing of insulators on energized distribution lines (between 15 and 69 kV) using a robot is summarized. They developed a device with an injector gun mounted on a robot installed at the end of a non isolated telescopic boom, which in turn is on a tanker with a capacity of 7,500 liters of water. The robot can swivel 300° on its own axis. The gun and robot are remotely controlled through a radio system and must be positioned at a distance of recommended security from the live energized point of the installation to be washed (1.5 m for 15 kV to 2.8 m for 69 kV lines). The procedure is safe, fast, and only requires two patrol workers, one to manage the truck and other to manage the robot (see Figure 3.20). In [112] high flow compressors instead of high pressure were successfully tested to execute dry cleaning with no water needed, to make a more ecological method.



Figure 3.20 Robot developed to wash insulators. View of the truck and patrol members [110]

3.3.1. Scheduling at Cleaning

Insulators should be washed prior to the time of reaching the critical contamination level. This point can be estimated from the following [109]:

- Past experience on periods between flashovers or pole fires.
- Allowable equivalent salt-deposited density (ESDD, obtained from de-energized test insulators or from energized insulators).
- High degree of scintillation during high humid weather conditions.
- Complaints of radio/television interference (when no damage is involved).
- Proximity and exposure to the pollution sources.
- Type of contaminant, and its rate of build-up on the insulator.
- Weather conditions (danger of flashover and pole fires is great after a long, dry period, either in winter or summer, followed by a light drizzle or fog condition).

- Sensor insulators that indicate contamination level (to be used for areas of consistent contamination levels or worst-case areas).

3.3.2. Pollution Identification

Knowledge of pollution compounds and levels surrounding polymer insulators can be evaluated as: (1) contaminants that affect the operation and (2) contaminants which accelerated the ageing process of the insulators. Outdoor insulators are subject to surface dirt deposits to some degree in all operating areas. Most commonly encountered contaminants have little effect on insulator performance and degradation as long as the surface is dry. Humidity (fog, mist, or light rain) usually creates conditions that produce a conducting film on the dirty insulator surface, without washing the impurities from the surface.

A number of types of contaminants have been identified as sources of surface deposits on insulators affecting insulator performance [113]. These contaminants are distinguished primarily by the source of the impurities. Local agricultural, industrial, and geographic conditions determine which are present in the atmosphere. The various types of contaminants identified are: salt, sea brine, cement/lime, dust, bird excrement, chemicals (fertilizers, insecticides, etc), smog (automobile emissions), aircraft emissions, cooling tower effluents, desert soil/sand, volcanic ash, smoke, organic biofilms (i.e. mold, algae, fungi, lichen), and ice/snow, and the mix and rates of deposit of these contaminants determines the characteristics of the mixture. More than one of these contaminants may be deposited on a group of insulators at a particular location and their identification is vital. Ordinarily, wind and rain provide sufficient washing action to remove most of the common deposits but areas with long periods of dry seasons can accumulate unmanageable amount of pollutant that cannot be properly washed when the first rains of the wet season arrives.

3.4. Main Proposals for Polymer Insulator Asset Management

Significant work has been done on the diagnosis of composite insulation, failure records databases, identification of new material formulations, new designs, etc for transmission overhead lines. The main surveys for the failures have been done by EPRI since 1997 and the last update was published in 2009 (the last survey with open access is from 2005), but this database only include voltages over 69 kV. Under this voltage, companies have not

been keeping information about the failures suffered by composites (as for many other distribution assets as well) which represents an important limitation for the asset management program. EPRI results provide the industry with fundamental information for making better decisions regarding the selection, application, and maintenance of polymer insulators—and ultimately extending polymer insulator life expectancy and avoiding outages from premature failures [113].

The asset management of polymer insulators has not been presented in the literature as an independent asset. This is grouped as a constituent element of the overhead lines, as presented in 2.5.

3.4.1. Framework to Develop Condition Diagnosis of Polymer Insulators Using Visual Inspections

Using the information collected from different authors and institutes about the different degradation and damaging phenomena involved on composite insulators, a detailed ageing stages' diagram or framework was organized and presented in the Figure 3.21. Four final states of aging depending on the results obtained by visual inspection of the insulators were identified. Each of these stages activates a specific alarm level which defines a set of actions to perform, as it is shown in the Figure 3.22.

The four levels of ageing define: (1) 'no alarm' stage, where the asset can be defined 'as new'; (2) yellow alarm, when the asset presents damage growing in a direction or areas where the core is not compromised; (3) orange alarm, when damage is growing towards the core, and (4) red alarm when the core is exposed in any way, area, or extension. An extra stage was introduced to classify all those conditions that can be named as "inconclusive". This is presented in the right side of the Figure 3.21. At this stage additional diagnostic tests or analysis are needed to establish the real condition of these assets. In this case it will be fundamental to consider operational conditions of the power system as well.

Once an alarm is activated there are three main actions to take: (1) follow your original monitoring/maintenance plan if there is a yellow condition; (2) replace the asset during the next maintenance work if the alarm is orange, or (3) replace immediately because the asset operation is running under imminent risk of failure.

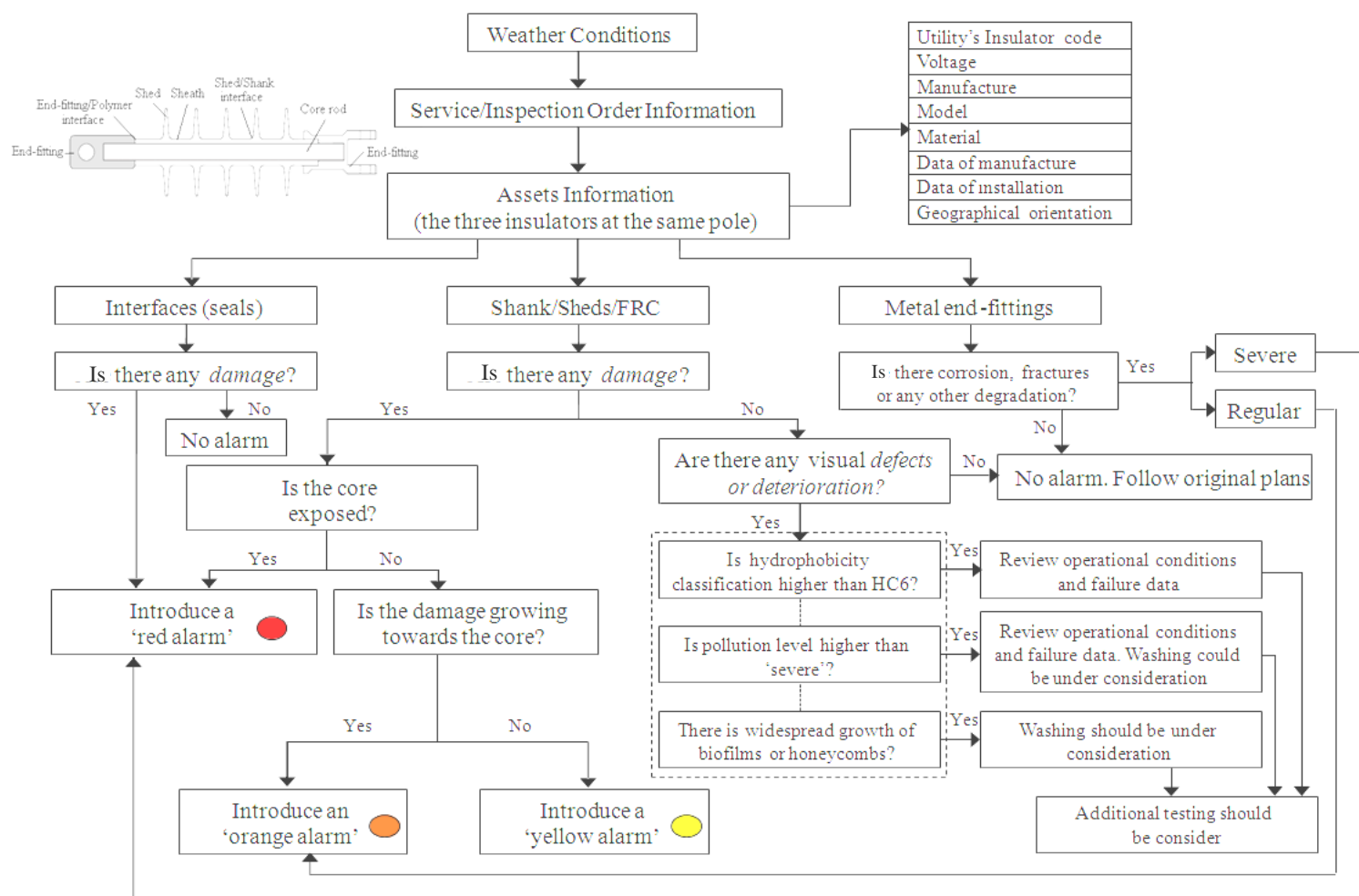


Figure 3.21 Framework to develop the condition diagnosis of polymer insulators using visual inspection supported by non expensive equipments

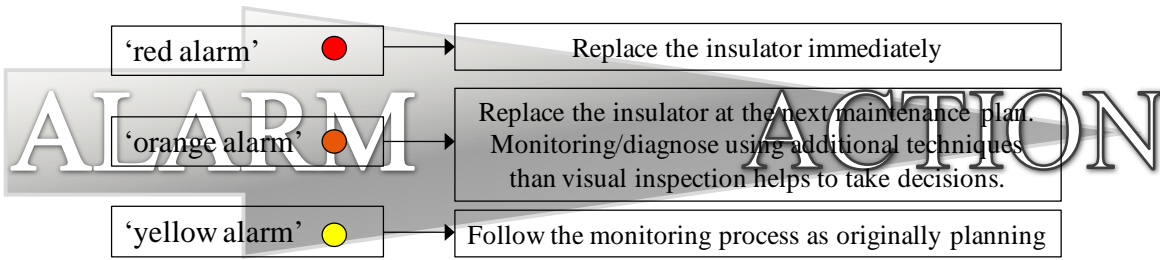


Figure 3.22 Action to be taken when an alarm is triggered after a monitoring process is concluded

An ageing estimator encompassing a risk of failure is presented in Figure 3.23 (explained and published in [114]). In this, also four states are defined and some of the main ageing processes involved in each of them are listed.

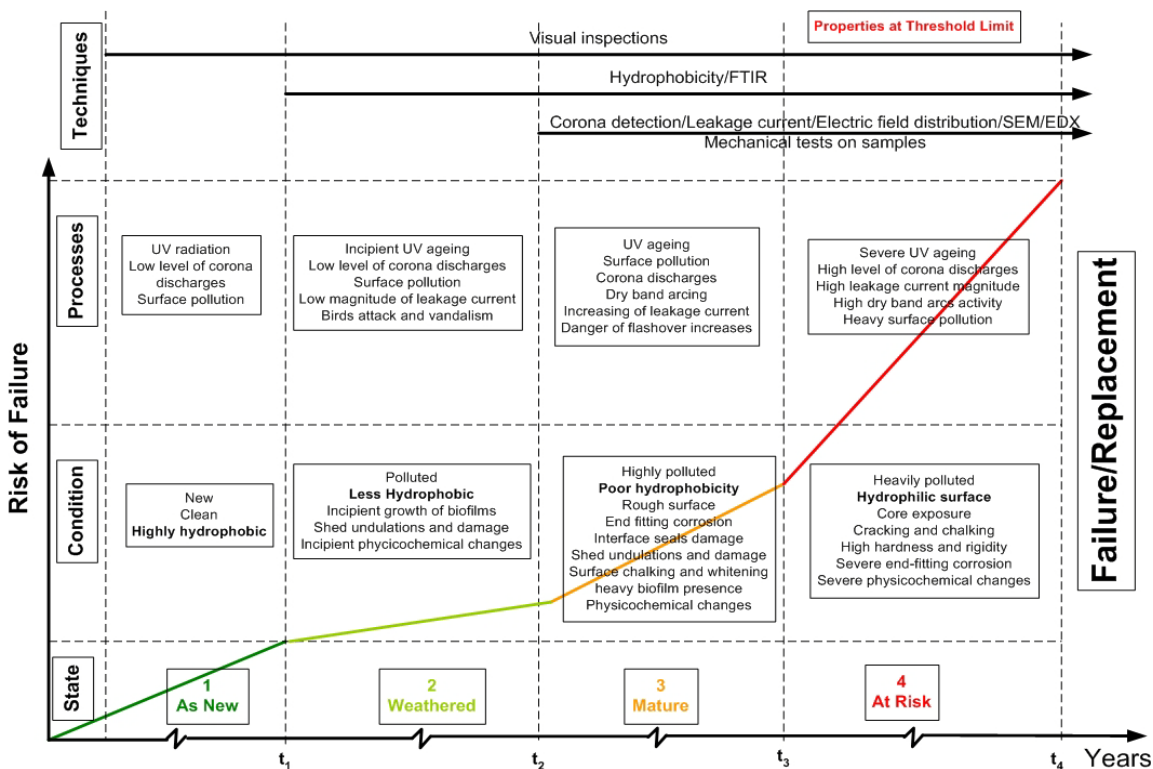


Figure 3.23. General ageing state estimator of composite insulators. Different conditions and processes. (A. Tzimas, E. Da Silva, S. Rowland [114])

3.4.2. A Supporting Matrix to Select Diagnostic or Monitoring Techniques

For the purpose of providing a support in the selection of a diagnostic technique a table was developed (see Table 3.10) analyzing the information previously presented in 3.2.3 and previous experiences where the main techniques are classified and ranked according to:

- Level of difficulty to interpret the results.
- Training needed to perform the test.
- Information relevance to establish the condition of the assets.
- Option to perform it in laboratory, in service or both.
- Destructive or not destructive: full assets or small samples.
- List of references or previous publications where the techniques were used in laboratory or in service.

This is important to highlight that visual inspections (using inexpensive equipment) of the insulators constitute the most important diagnosis and monitoring method for composite insulators and this should be supported by other techniques. In service, the most common monitoring options are, for (1) transmission: IR cameras, daylight UV cameras and electric field distribution; for (2) distribution: IR cameras and radio interference detectors.

Table 3.10 Classification of the Diagnosis Techniques Normally Used to Study Composite Insulators

TECHNIQUES	Interpretation	Requires training	Information Relevance	Applied in		Samples		References/Publications	
	Easy → Difficult	Low → High	Low → High	Service	Lab	Full	Dissected	Service	Lab
Visual Inspection (naked eye, binoculars, digital cameras)	✓	✓	✓	✓	✓	✓	✓	[43, 45, 51]	[43, 45, 51]
IR Cameras (Temperature)	✓	✓	✓	✓	✓	✓			[60, 115]
UV Cameras (Corona discharges light amplification)	✓	✓	✓	✓	✓	✓		[116, 117]	[60, 115]
Electric Field Distribution	✓	✓	✓	✓	✓	✓		[118]	[119]
Hydrophobicity	✓	✓	✓	✓	✓	✓	✓	[44, 54, 120, 121]	[44, 122]
Portable X-Ray	✓	✓	✓	✓	✓	✓	✓	[67]	[65, 67-69]
HVAC Resistance	✓	✓	✓	✓	✓	✓			[26]
DC Resistance	✓	✓	✓		✓	✓			[81-84]
Electrical tests (dry and/or wet): <ul style="list-style-type: none"> • Leakage current • Withstand voltage and Flashover volt • Transient volt • Pollution level classification • PD (Partial Discharges), RIV (Radio Interference Voltage) • Low voltage surface resistance • Surface Voltage Decay • Dielectric impedance 	✓ ✓ ✓ ✓ ✓ ✓ ✓	✓ ✓ ✓ ✓ ✓ ✓ ✓	✓ ✓ ✓ ✓ ✓ ✓ ✓		✓ ✓ ✓ ✓ ✓ ✓ ✓	✓ ✓ ✓ ✓ ✓ ✓ ✓	✓ ✓ ✓ ✓ ✓ ✓ ✓	[76]	[21, 81-84, 96, 123-132]
Acoustic Emission	✓	✓	✓	✓	✓	✓			[26, 87]
Near-field Microwave Non-destructive Testing	✓	✓	✓	✓	✓	✓			[71, 90]
Laser-induced fluorescence spectroscopy	✓	✓	✓		✓	✓			[47, 88, 89]
Physicochemical tests: <ul style="list-style-type: none"> • FTIR, RS (Fourier Transform Infrared and Raman Spectroscopy) • SEM (Scanning Electron Microscopy) • EDX (Energy Dispersive X-ray) • XPS (X-rays Photoelectron Microscopy) • GC/MS (Gas Chromatography/Mass Spectroscopy) • GPC (Gel Permeation Chromatography) • TGA (Thermogravimetric Analysis) • LIFS (Laser-induced fluorescence Spectroscopy) 	✓ ✓ ✓ ✓ ✓ ✓ ✓	✓ ✓ ✓ ✓ ✓ ✓ ✓	✓ ✓ ✓ ✓ ✓ ✓ ✓	✓	✓ ✓ ✓ ✓ ✓ ✓ ✓	✓ ✓ ✓ ✓ ✓ ✓ ✓	✓ ✓ ✓ ✓ ✓ ✓ ✓	[96, 98, 133]	[91, 93, 95, 97, 134-141]

3.4.3. A Proposal for Composite Insulators Health Index Formulation (First Step using only Visual Inspection Information)

As indicated above (item 2.4.2), Condition Ratings (CR) are descriptive indications of the asset under examination and they enable the grading of the insulators according to their performance or condition. Four grades are described following the four degrees established by EPRI (named A, B, C and D), the STRI guide, Gorur's semaphore and the previous HI used by EDF Energy Networks.

Using the information presented in 3.2.1 and 3.2.2 a four-grade condition rating approximation is proposed in the Table 3.11 for the ranking of the polymer insulators aged in service, only using the results of the visual inspections.

Table 3.11 Composite Insulators' Condition Rating (CR)

Condition determine by visual inspection	Condition Rating (CR)	CR Score	Level of degradation / damage / ageing
Sheds	CR1	0	No measurable or detectable degradation is found. As new.
	CR2	3	Deterioration: Chalking, Colour changes, Crazing, Light erosion, Minor debonding, Minor Splitting/cutting. Complete loss of hydrophobicity. Damage by animals far from the core.
	CR3	7	Deterioration/Damage transition: medium Erosion, incipient Splitting/Cutting, incipient Tracking/Carbonizing. Severe tears. Damage is not growing towards the core. Damage by animals close to the core.
	CR4	10	Damage: Power arc damage, Puncture, severe Erosion, severe Tracking and carbonizing. Damage growing toward the core.
Shank/Core	CR1	0	No measurable or detectable degradation is found. As new.
	CR2	3	Deterioration: Chalking, Colour changes, Crazing, Light erosion, Minor debonding, Minor Splitting/cutting. Complete loss of hydrophobicity.
	CR3	7	Damage: Erosion, Power arc damage, Puncture, Splitting/Cutting/Punctures, Tracking/Carbonizing but the rod is not exposed even though the damage is growing towards the core. Damage by animals with no exposure of the rod.
	CR4	10	Severe Damage where the rod is exposed, including by gun shot. Undermining. Brittle fracture. Damage by animals with exposure of the rod. Unclipped Sections with rod exposure. Flashunder evidence.
Shed/Shank interface	CR1	0	No measurable or detectable degradation is found. As new.
	CR2	3	Deterioration: Chalking, Colour changes, Crazing, Light erosion, Minor debonding, Minor Splitting/cutting, Grease leakage. Complete loss of hydrophobicity.
	CR3	7	Severe deterioration processes. Corona cutting.
	CR4	10	Damage with exposure of the rod: severe Erosion, Power arc damage, Puncture, Splitting/Cutting/Punctures, Tracking/Carbonizing
Seals (Polymer /end-fittings interface)	CR1	0	No measurable or detectable degradation is found. As new.
	CR2	3	Incipient corrosion of the area close to the seals.
	CR3	7	Deterioration of the seals where penetration of humidity looks non feasible. Degradation of the seal.
	CR4	10	Damage of the seals where penetration of humidity is unavoidable. Severe damage.
End-fittings	CR1	0	As new.
	CR2	3	Normal degradation. Flange corrosion.
	CR3	7	Flange corrosion.
	CR4	10	Power arc damage. Severe corrosion where the fitting strength is compromised.

It is very important to highlight again the distinction established by EPRI (which is the only numerical one that can be found in the literature) between ‘deterioration’ or ‘damage’, where: “*deterioration does not significantly reduce the thickness of the polymer housing (i.e. by more than 1mm at the sheath) that prevents moisture ingress to the core rod, or reduces the leakage distance by more than about 10%*”.

The condition rating scores used are based on those used in the EDF Energy Network [33] and are included considering only “empirical perception”. The cause of this is basically the absence of data about the polymer insulators used in the EDF Energy Network (or any other source). The final table to use for the health index is shown in the Table 3.12. Proper calculation of the HI can be only made after data has been collected. It can be observed that the damage at the sheds and end-fittings are classified with a lower weighting than any damage involving the core or seals.

Table 3.12 CR Scores Weighting Empirical Proposal

Insulator Condition Criteria	Condition Ratings (CR)	CR Scores	Weighting	Maximum value (CR4 score x Weighting)	Actual Condition Ratings (CR _i)	Actual Score Value (CR _i x Weighting)
Sheds	CR ₁	0	2	30		
	CR ₂	3				
	CR ₃	7				
	CR ₄	10				
Shank/Core	CR ₁	0	4	40		
	CR ₂	3				
	CR ₃	7				
	CR ₄	10				
Shed/Shank interface	CR ₁	0	4	40		
	CR ₂	3				
	CR ₃	7				
	CR ₄	10				
Seals (Polymer /end-fittings interface)	CR ₁	0	4	40		
	CR ₂	3				
	CR ₃	7				
	CR ₄	10				
End-fittings	CR ₁	0	2	20		
	CR ₂	3				
	CR ₃	7				
	CR ₄	10				
				160	Totals =	Σ
Health Index = Weighting value/Maximum value x 10 = Σ/160x10						

Different studies made by power distribution utilities in different countries (such as USA, UK and Australia), present condition diagnosis results and rating for overhead lines. None of them have results for composite insulators. On the contrary, all highlight the lack of data about their failures.

3.4.4. General Overview of Data Base Inputs at Different Operational Stages

Figure 3.24 shows the main information that must be collected during the process of the composite insulator management. Along an asset life time different fundamental information must be stored in a well designed data base and the success of the whole process is linked with this.

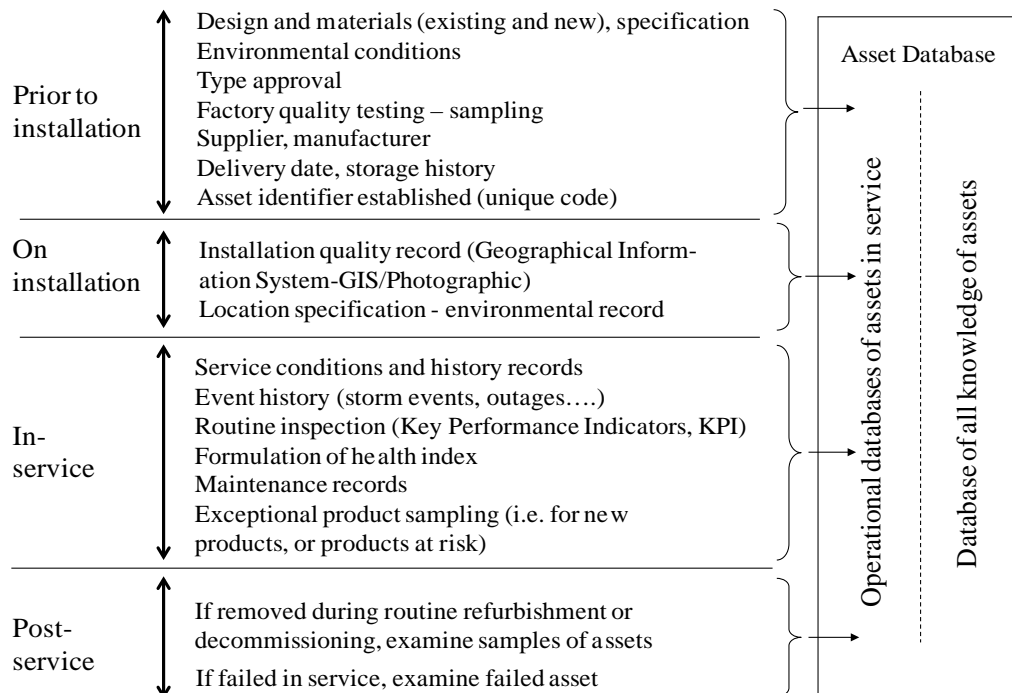


Figure 3.24 Composite Insulators Asset Database Information

3.4.5. Fundamental Documents and Knowledge to Recover and Archive

Success of any management plan is based on how well documented the whole process is and how well the data bases are filled and updated. In this area, utilities must spend a lot of effort and resources during the initial stages of the asset management plan.

Management of polymer insulators requires updating fundamental information continually. For the new insulators the most important topics to be covered are: (1) what it is necessary to know about new technologies, material formulations, new standards and guides and benchmarks; (2) knowledge about new test protocols and guides; (3) environmental condition changes and pollution quantification; (4) needs of new technical specifications; (5) classification of new and old manufacturers, and (6) new handling, storage and maintenance recommendations. For the insulators in service it is important to

review (1) new monitoring tests and diagnostic technologies that can be easily incorporated, (2) accessible data from other utilities’ experience, and (3) confirm if there is any change in the environmental conditions surrounding assets in service. These steps, related with the updating of the knowledge, are summarized in the Figure 3.25.

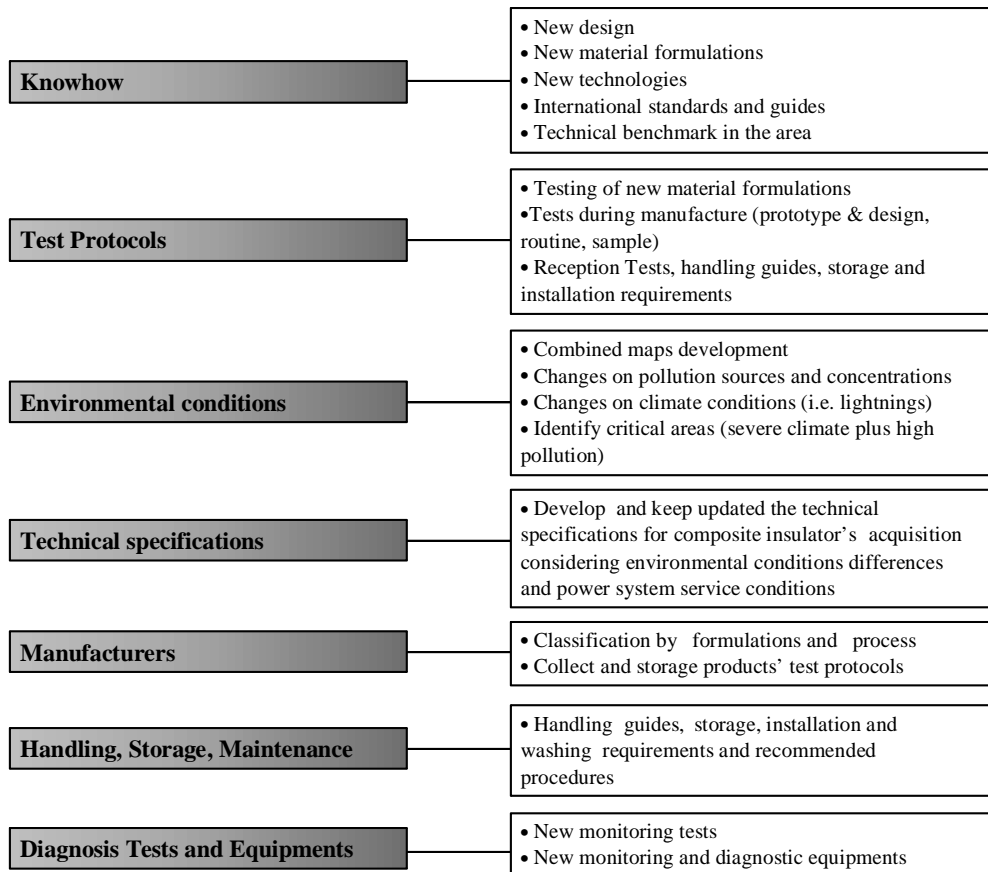


Figure 3.25 General Steps to Cover and Information to keep Updated

Over many years companies have been keeping fundamental information about assets performance and quality in the memory of their work force. Nowadays this must be changed and there are many procedures, instruments and equipments that can help in this task. New technologies can be initially rejected by patrol members; in consequence, the involvement of them and their education is fundamental. Inappropriate storage of information, documents and data will influence negatively the asset management of the insulators. For the EDF case, the Ellipse system must be adapted and used to incorporate distribution infrastructure components or assets, and different IT resources must be also implemented for this level, as handheld storage units.

3.5. EDF Energy Networks: Conditions to be Considered During AMS Development

EDF Energy serves the areas shown in Figure 3.26. The South East network covers an area of 8,200 sq km containing 12,900 km of overhead lines. The East of England network covers an area of 20,300 sq km containing 34,700 km of overhead lines [142]. The main lines of EPN (East of England Power Network) and SPN (South East of England Power Network) operate at 132 kV, 33 kV and 11 kV. LPN (London Networks) is mostly underground with less than 50 km of overhead lines (132 kV).

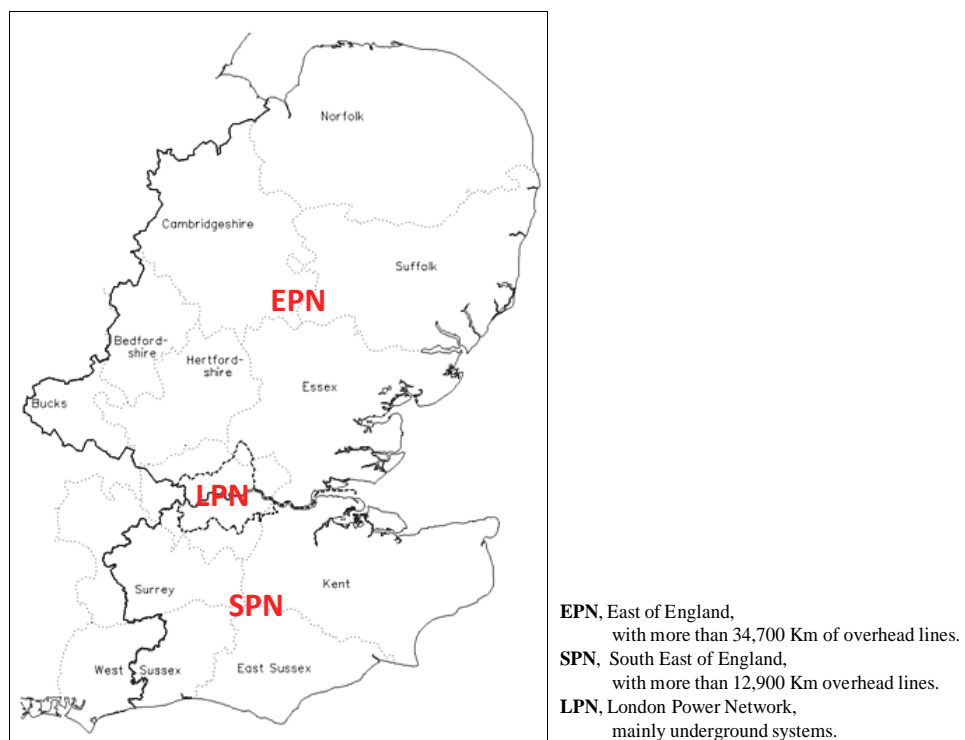


Figure 3.26 Regions in which EDF Energy Networks operates

3.5.1. Main Pollutants and Contamination Sources in EDF areas

In Table 3.13, the main topics relating to the pollution sources covering the EDF Energy served areas which affect outdoor insulators, especially the acid rain components (compounds of carbon, ammonium, sulphur, and nitrogen combined with water vapours), or the ones increasing its conductivity, are summarized. Some definitions are included.

The information related to pollution in the UK was extracted from different official web pages of institutions, organizations and public offices, etc. The UK has numerous monitoring stations and different organizations are working to collect data concerning

contaminant sources and air conditions [143-154]. The European Pollutant Release and Transfer Register (<http://prtr.ec.europa.eu/PollutantReleases.aspx>) presents the location of the main sources of the most relevant pollutants released to the atmosphere in Europe (last update in 2008). All this information is needed to prepare aggregated maps to locate the most critical areas.

In the following paragraphs a brief description of the main contaminants is included to make the subsequent identification of the sources that surround the assets in a specific geographical location easier.

Table 3.13 Main Pollution Sources of Elements Affecting Polymer Insulator Surface

<i>Carbon Dioxide (CO₂)</i>
CO ₂ is created by both natural and man-made sources. Our bodies, animals and plants create CO ₂ continually. Man-made processes are increasing CO ₂ levels. When any carbon-based fuel (such as wood, coal, petroleum, or natural gas) is burned in the presence of oxygen, carbon dioxide will be emitted. CO ₂ levels are also increased when we deplete tree habitats for new developments.
<i>Ozone (O₃)</i>
Ground-level ozone (bad ozone) is caused by the release of volatile organic compounds (VOC) from vehicles, solvents, paint and industry and nitrogen dioxides (NO ₂) from vehicle emissions and industry into the air. When these chemicals are released into the air they react with sunlight and heat to create ozone. Consequently, as temperatures rise, ozone levels rise as well. This is: $\text{VOC} + \text{NO}_2 + \text{heat} + \text{sunlight} = \text{ozone (O}_3\text{)}$ This also means that levels are higher in the summer. Whereas NO ₂ helps form ozone, nitrogen oxide (NO), a pollutant primarily emitted from motor vehicles, contributes to the destruction of O ₃ . Therefore, areas with high NO emissions, such as urban centres, have lower concentrations of O ₃ than rural areas. The highest levels tend to be found in rural areas downwind of urban or industrial areas.
<i>Nitrogen Dioxide (NO₂)</i>
Nitric oxide (NO) is produced during high temperature burning of fuel (e.g. road vehicles, heaters and cookers). When this mixes with air, NO ₂ is formed. Levels are highest in urban areas as it is mainly a traffic-related pollutant. In the presence of sunlight, NO ₂ also reacts with other pollutants, such as VOCs, to form bad ozone. NO ₂ is primarily the result of gases from motor vehicle exhaust and stationary fuel combustion sources like electric utilities and industrial boilers. It can also be produced from gas stoves and heaters. In addition, nitrogen oxides contribute to the formation of acid rain. NO _x , when in the presence of water vapour in the atmosphere, partially converts into nitric acid, HNO ₃ . Nitric acid and sulphuric acid combine to create acid rain.
<i>Sulphur Dioxide (SO₂)</i>
Roughly one-third of atmospheric sulphur compounds come from human-made sources. Of this one-third, 70% of annual SO ₂ emissions come from electric power plants that burn coal. Burning fossil fuels such as oil, converting wood pulp to paper, and smelting copper, zinc, lead and incineration of refuse are also contributors to SO ₂ formation. Natural sources of SO ₂ include volcanoes and hot springs. Generally, the highest concentration of SO ₂ is found near large industrial sources and power plants.
<i>Particulate Matter (PM₁₀ and PM_{2.5})</i>
The principal source of PM is road traffic emissions; particularly from diesel vehicles (traffic-related pollutant). This means that levels are highest in urban areas. Industrial combustion plants and public power generation, commercial and residential combustion, and some non-combustion processes also emit PM. Natural sources (such as volcanic ash, salt from ocean spray, forest fires, and dust from fields) only produce a small percentage of fine PM. PM is categorized according to its size in micrometers. PM ₁₀ refers to particles under 10 µm, sometimes called the 'coarse fraction'. PM _{2.5} refers to particles under 2.5 µm, sometimes called the 'fine fraction'. PM greater than 2.5 micrometers in diameter is usually the result of smoke and dust from industry and agricultural production, while particles less than 2.5 generally come from combustion of fossil fuels.

Table 3.13 (Cont') Main Pollution Sources of Elements Affecting Polymer Insulator Surface

<i>Lead (Pb)</i>
As much of the airborne emission of lead originates from road traffic, concentrations are decreasing with most cars running on unleaded and lead replacement petrol. Other sources of lead pollutants include waste incineration and metal processing.
<i>Carbon Monoxide (CO)</i>
CO is created when the carbon in fuel is not burned completely. Most fuels we use, such as natural gas, are made out of molecules containing carbon. When there is not enough oxygen present during combustion to form carbon dioxide (CO ₂), CO is the result. CO can come from appliances fuelled by natural gas, liquid petroleum, oil, and kerosene. Approximately 60% of nationwide CO emissions come from automobiles generating over 90% of urban CO pollution. The remainder comes primarily from industrial processes and fuel combustion in sources such as boilers and incinerators, from electricity production, and from natural sources such as wild fires. In the UK levels are generally low, well below the targets set by the Government.
<i>Volatile Organic Compounds (VOCs)</i>
While VOCs can be emitted from natural sources, many are man-made, created by industrial processes. VOCs include chemicals such as benzene, toluene, and methyl chloroform. Chlorofluorocarbons (CFCs), Hydrofluorocarbons (HFCs), and Perchloroethylene (the principle dry cleaning solvent) are VOCs that are greenhouse gases. VOCs are released from burning fuel, solvents, paints, and glues. VOCs can combine with nitrogen oxides to help form ozone. The main sources of atmospheric benzene are petrol vehicles, distillation, refining and evaporation of petrol from vehicles. The main source of 1,3-Butadiene is also principally from road traffic, in the combustion process of petrol and diesel vehicles. An additional source is from industrial processes such as synthetic rubber manufacture.
<i>Toxic Organic Micro-Pollutants (TOMPs)</i> <i>PAHs (Polycyclic Aromatic Hydrocarbons), PCBs (Polychlorinated Biphenyls), Dioxins, Furans</i>
Produced by the incomplete combustion of fuels, road transport and industrial plant are the largest source. Open burning is a major source in the UK and comparatively large amounts are released on and around bonfire night. Tobacco smoke is also a source. Dioxins are a class of chemical contaminants that are formed during combustion processes such as waste incineration, forest fires, and backyard trash burning, as well as during some industrial processes such as paper pulp bleaching and herbicide manufacturing. Chlorinated dioxins are released into the air in emissions from municipal solid waste, industrial incinerators, exhaust from vehicles powered with leaded and unleaded gasoline and diesel fuel, emissions from oil- or coal-fired power plants, cigarette smoke and, manufacture and use of various chlorinated pesticides and herbicides. The larger particles will be deposited close to the emission source, while very small particles may be transported longer distances.
<i>Mercury (Transition metal)</i>
Natural sources such as volcanoes are responsible for approximately half of atmospheric mercury emissions. The human-generated half is generated by stationary combustion, of which coal-fired power plants are the largest aggregate source. This includes power plants fuelled with gas where the mercury has not been removed, from non-ferrous metal production, typically smelters, cement production, waste disposal, including municipal and hazardous waste, crematoria, and sewage sludge incineration, caustic soda production, pig iron and steel production, mercury production, mainly for batteries and other minor ones.
<i>Selenium</i>
The majority of man-made sources of release into the environment are mainly from the glass manufacturing industry and coal combustion. The major man-made source of release of selenium in the UK is glass production. Coal combustion in power stations is also a source of selenium emissions although this has declined due to lower levels of coal use. Trace amounts are emitted by the combustion of petroleum-based fuels.
<i>Metal Vanadium</i>
It is released from the combustion of residual fuel oil from industrial sites such as refineries. It is a naturally occurring element and therefore present in rocks, soils and natural waters to varying extents. Major man-made sources of emissions are the combustion of fuel oils - liquid fuels (by example, power stations). Emissions from refineries are particularly important due to the high consumption of refinery fuel oil and residues. Emissions of vanadium may be high in the vicinity of large plants producing steel alloys.

As it was mentioned, reactive compounds of nitrogen are a source of acid rain which affects the polymer surface. The main compounds are: nitrate ion (NO₃⁻), nitric acid (HNO₃), nitrogen dioxide (NO₂), nitrous acid (HNO₂) and nitric oxide (NO). The major

source of nitrogen compounds in the environment is now the increasing use of fertilizers to enhance crop yields.

The evolution of contaminants in the UK is a very dynamic phenomenon and many pollutant sources were reduced as a consequence of climate change conscience policies, as presented in Figure 3.27 (This can be found in different published environmental reports [145, 150-154]). In consequence, two things should be considered. Firstly, contaminant type and amount must be frequently updated. Secondly, new assets will be under lower emissions of acid rain but assets with years in service have been under the effect of rain with lower pH (acids) and other contaminants probably with higher concentrations. This is an important consideration for diagnosis.

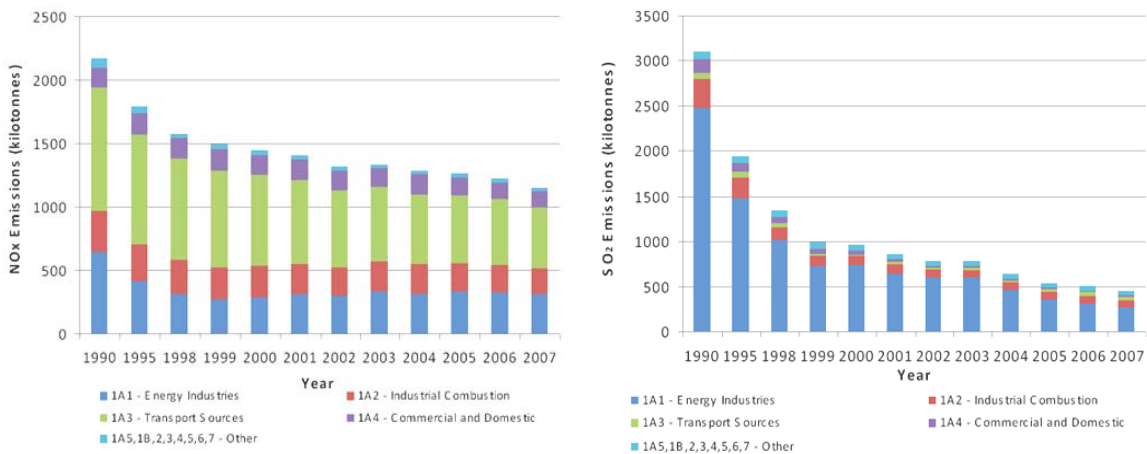


Figure 3.27 Reduction of NO_x and SO_x in England over recent decades

Knowledge of pollution sources means knowledge of economic activities (manufacturing processes, industries, agriculture, etc), generation power plant type, and density of road traffic, amongst others and this is fundamental to establish good emission maps. Changes in the economic activities surrounding a system directly imply that changes can occur to the type and amount of contaminants.

At the same time, is also important to remember that synergy exists between pollutants and environmental conditions. These must be observed individually but so also must the interactions between them: acid rain requires humidity (rain) and UV radiation, wind will move the pollutants to different directions, high humidity and fertilizers can produce organic pollution, lightning produces nitric acid in the atmosphere, etc.

It could be also important to emphasize that the level of salty pollution coming from the sea is not information that can be easily found. In consequence, utilities should undertake some measurements to determine the value of deposited salt on their outdoor insulators used in different equipment or components.

Additionally to the polymer surface degradation, it must be considered that metal end-fittings can be attacked by corrosion. The main sources of aggressive components, mixed with humidity, in the environment which need to be considered during overhead lines inspections [155] are shown in the Table 3.14.

Table 3.14 Main contaminants which activate metal corrosion

Fossil Fuel Gen Plant	Pulp & Paper Industries	Road salts	Live Stock Yard
Swamps	Bleaching Plants	Ocean Spray	Pipelines
Tidal Areas	Metal/ Steel Production	Road Crossings (Auto emissions)	Large Welding/ Fabrication Facilities
Refineries	PVC plants	Smog	Aluminum and Alumina Plants
Sewage Treatment Plants	Subways	Pickling (Acid Bath) Industries	Mining Operations
Chemical Industries	Fertilizers (Agricultural)	Semiconductor industries	Landfills

3.5.2. Pollution in EDF Energy Networks

The following maps (Figure 3.28 and Figure 3.29) will be used as the base for the final analysis of the pollution over the EPN and SPN areas. Information of the main local pollutants can be prepared aggregating the information showed in these maps. Other important pollutant emissions maps can be found in [154, 156].

It is important to understand the meaning of the unit: t/1x1km which is tonnes in a 1 x 1 km area. Pollution maps can be presented on grids with different dimensions. The models are used to extrapolate the pollution monitoring data considering the influence of particle dispersion. When bigger grids are used, local pollutant concentrations are not detected.

Figure 3.30 shows the main sources of NO_x and SO_x surrounding the EDF Energy overhead lines. This information can be accessed at the European Pollutant Release and Transfer Register (<http://prtr.ec.europa.eu/MapSearch.aspx>).

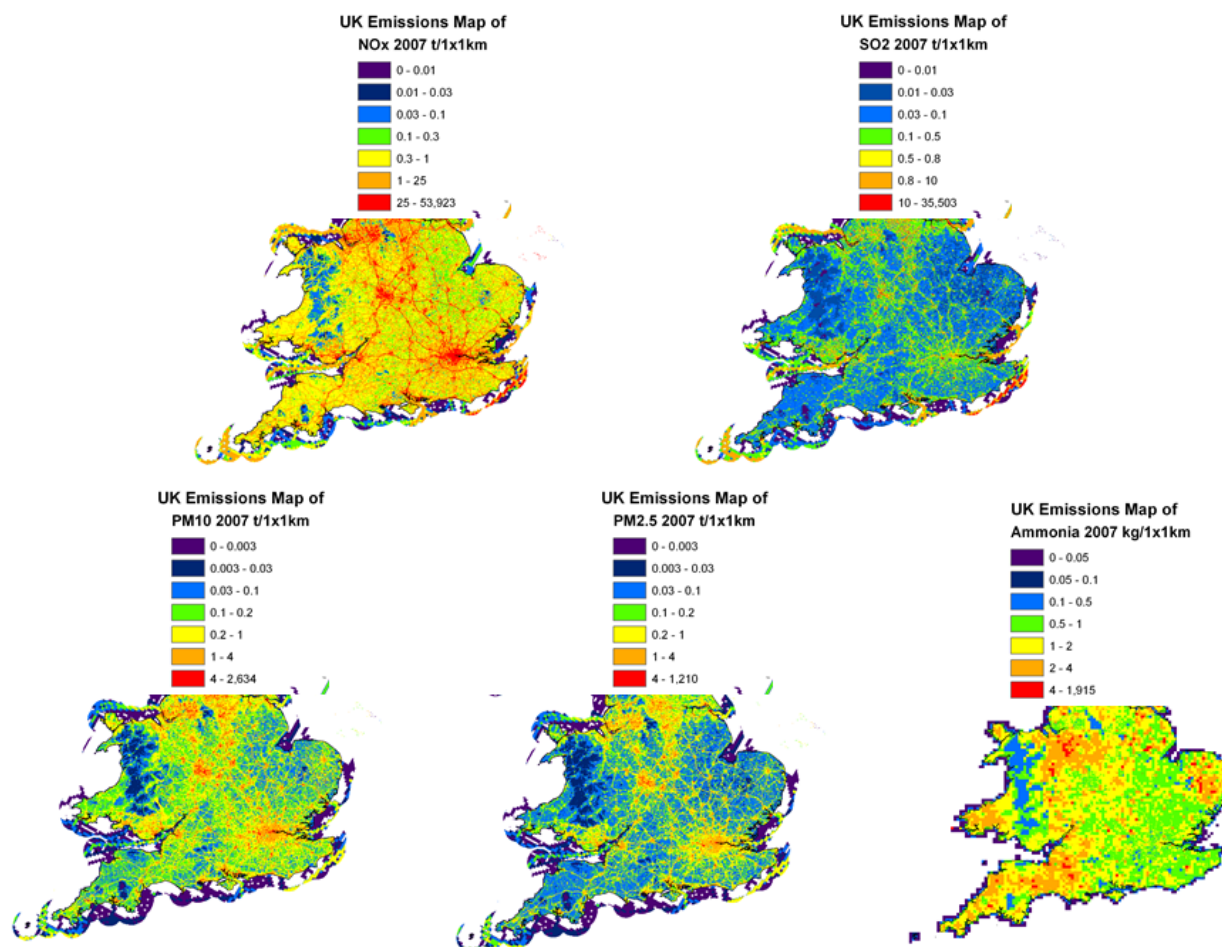


Figure 3.28. Main pollutants emissions (2007 maps) over the EDF Energy served areas [157]

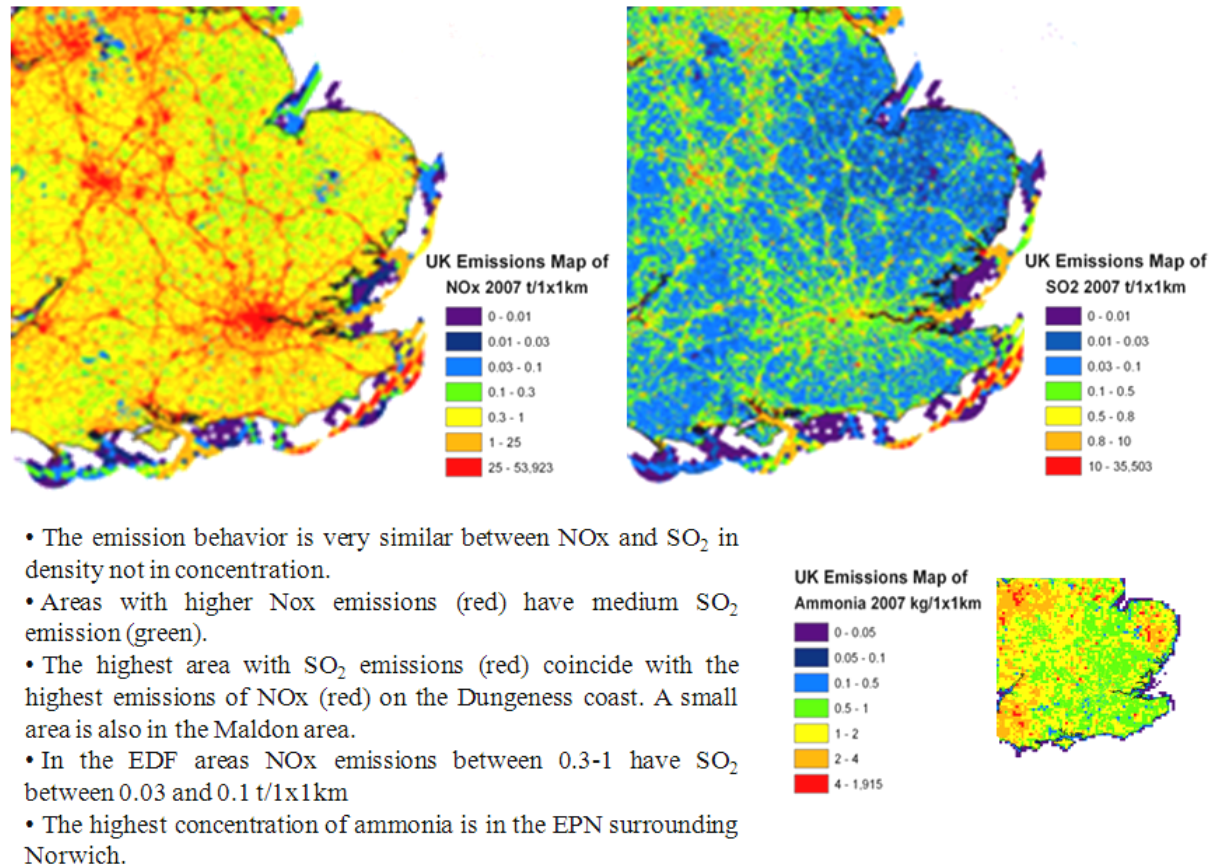


Figure 3.29. Aggregated information with the three main contaminant components of acid rain (2007) over EDF served areas

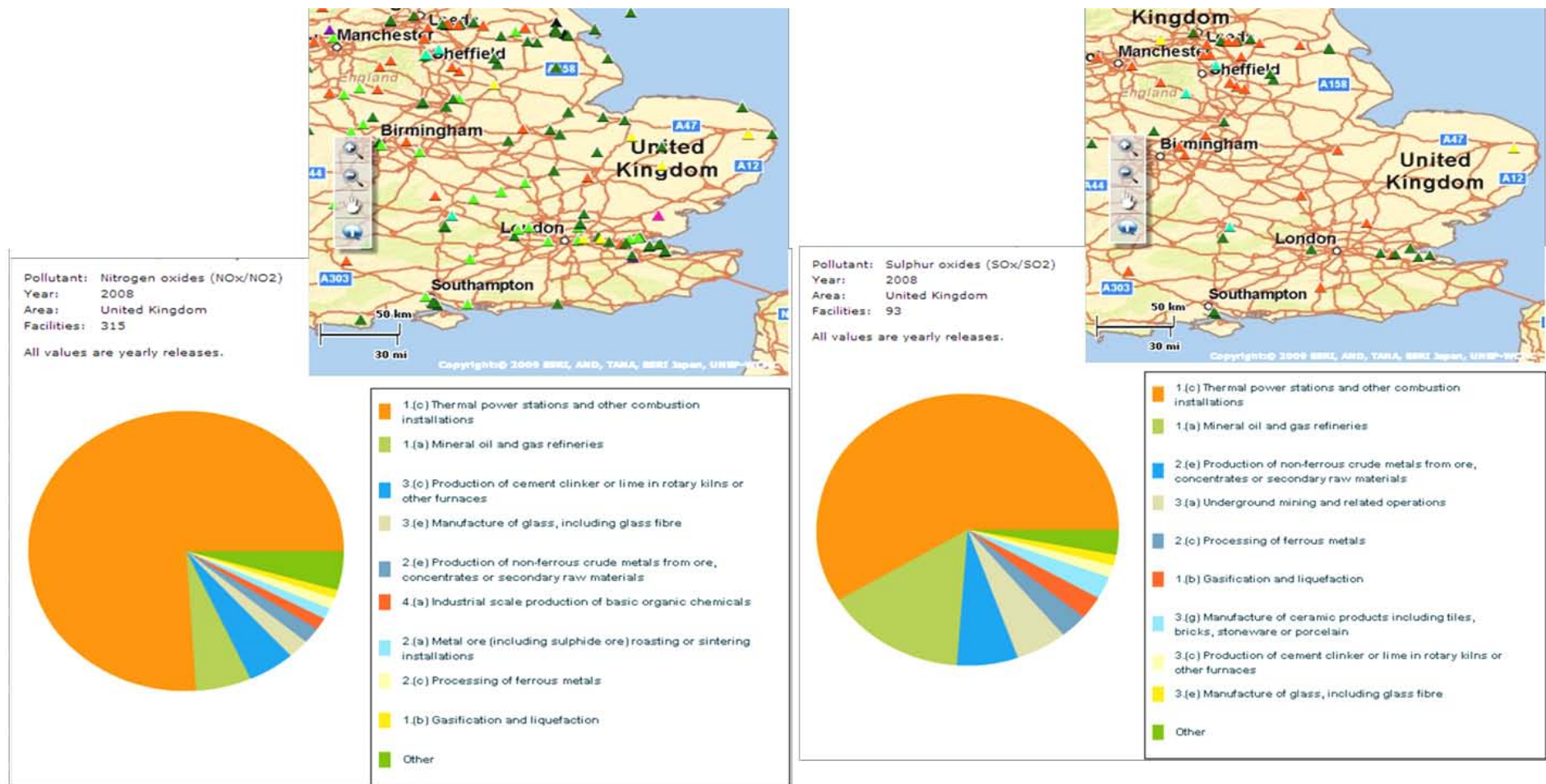


Figure 3.30 Main sources of NOx and SOx (2008) surrounding EDF Energy Networks (source: European Pollutant Release and Transfer Register)

3.6. Fault Statistics from of the EDF Energy System

Failure data collected during the periods 2006-07, 2007-08, 2008-09 from the EPN (East of England Power Network) and SPN (South East of England Power Network) was evaluated. The interruptions were quantified taking in account the direct cause identified by the company. LPN (London Networks) is not considered because is mostly underground.

Different tables were extracted from the data: weather conditions, human errors, ageing or corrosion and, trees, animals and possible sources of pollution (Table 3.15 to Table 3.23). These may be used to infer which faults can be directly related to environmental conditions or human causes, for example. Some of this information will be useful to identify, by qualitative extrapolations, additional sources of pollution that can introduce stress on the insulators, for example: trees and farm animals can be source of organic pollution, birds can deposit residues, lightning with heavy rain, airborne deposits with windborne material could be associated with acid rain, etc. The EDF Energy data does not record which equipment presents a fault when the interruption occurs by a specific cause.

Table 3.15 Failures caused by known weather conditions

	Total	Snow, ice, sleet and blizzard	Wind and gale (including windborne material)	Wind and gale (excluding windborne material)	Rain	Solar heat	Lightning
132kV EPN	5	0	1	0	0	0	4
33 kV EPN	32	3	12	0	0	0	17
11 kV EPN	921	47	677	0	17	1	179
132 kV SPN	2	0	1	1	0	0	0
33 kV SPN	31	3	1	11	1	0	15
11 kV SPN	713	32	28	344	52	1	256
Total	1704 (100%)	85 (4.9%)	720 (42%)	356 (21%)	70 (4%)	2 (0.1%)	471 (28%)

Table 3.16 Failures by 100 Km of 11 kV lines by weather conditions

	Km	Wind and gale (including windborne material)	Wind and gale (excluding windborne material)	Lightning
11 kV EPN	19,197	39.73	0.00	10.50
11 kV SPN	5,745	1.64	20.19	15.02

Failures caused by lightning presents a high ratio. This may be caused by the high lightning density and magnitude around the South coast of England. This value has been also detected by EDF Energy and actions must be taken [38].

Table 3.16 shows the density of fault by 100 km of overhead lines caused by weather conditions (classified as wind and gale with and without windborne material and lightning). This indicates that SPN is suffering a higher level of interruptions than EPN.

Table 3.17 Failures caused by human error

	Total	Faulty installation or construction by EDF Energy staff	Faulty Installation or Construction by Contractors	Faulty manufacturing, design, assembly or materials	Inadequate or faulty maintenance
132kV EPN	0	0	0	0	0
33 kV EPN	2	1	0	0	1
11 kV EPN	55	24	9	1	21
132 kV SPN	0	0	0	0	0
33 kV SPN	0	0	0	0	0
11 kV SPN	4	0	0	1	3
Total	61	25	9	2	25

Table 3.18 Failures caused by ageing or corrosion

	Total	Deterioration due to ageing or wear (excluding corrosion)	Corrosion due to atmosphere / environment	Corrosion
132kV EPN	4	4	0	0
33 kV EPN	32	32	0	0
11 kV EPN	951	932	19	0
132 kV SPN	2	2	0	0
33 kV SPN	9	8	0	1
11 kV SPN	291	279	0	12
Total	1289	1257	19	13

Table 3.19 Failures per 100 Km of 11 kV lines by ageing or wear

	Km	Deterioration due to ageing or wear (excluding corrosion)
11 kV EPN	19,197	4.85
11 kV SPN	5,745	4.86

Table 3.20 Failures caused by trees, animals and possible sources of pollution

	Total	Growing Trees	Farm and domestic animals	Growing or falling live trees (not felled)	Falling dead trees (not felled)	Birds (includ. swans and geese)	Vermin, wild animals and insects	Fire not due to faults	Airborne deposits (excluding windborne material)
132kV EPN	0	0	0	0	0	0	0	0	0
33 kV EPN	39	9	0	17	2	11	0	0	0
11 kV EPN	1396	590	6	581	87	132	61	7	8
132 kV SPN	1	0	0	1	0	0	0	0	0
33 kV SPN	20	0	0	18	0	2	0	0	0
11 kV SPN	478	0	5	416	0	57	74	0	2
Total	1934	599	11	1033	89	202	135	7	10

Table 3.21 Failures per 100 Km of 11 kV lines caused by trees and animals

	Km	Growing Trees Growing or falling live trees (not felled) Falling dead trees (not felled)	Birds (including swans and geese) Vermin, wild animals and insects
11 kV EPN	19,197	6.55	1.01
11 kV SPN	5,745	7.24	2.28

Table 3.22 Number of interruptions by voltage levels and networks

Network	Area (km ²)	Voltage (kV)	Overhead Lines (km)	Interruptions	Density Interruption/100 km
EPN	20,300	132	5,545	12	0.21
		33	3,479	119	3.40
		11	19,197	3,819	19.89
		Total ₁	28,221	3,950	11.30
SPN	8,200	132	1,161	8	0.69
		33	1,313	78	5.94
		11	5,745	2,369	41.24
		Total ₂	8,219	2,455	19.10
			Total	6,405	

Table 3.22 shows the overall number of interruptions by voltage level and density per 100 km of overhead lines. This indicates that SPN is suffering a higher level of interruptions than EPN.

Table 3.23 Number of failure with unknown reason or cause reported

	Unknown Cause of Failure*
11 kV EPN	3255
11 kV SPN	1047
Total failures	4302

*The proportion is 10 times higher than for the 33 kV circuits.

From the tables, the following can be extracted:

- In the group of interruptions identified as ‘ageing or corrosion’ there were 97.5% by ageing and 2.5% by corrosion and more than 17.6 % higher per km of line in EPN overhead lines than in SPN ones. In particular, 96.3% of the ‘ageing’ failures happened in the 11 kV systems. Time in service is one of the most important parameters to define this point but it is not included in the failure data base.
- Interruptions identified as ‘weather conditions’ are more than 58.8 % higher per km of line in EPN overhead lines than in SPN ones. This may be due to many factors: weather conditions, time in service, coastal location, more pollution, etc.
- Interruptions identified as ‘human errors’ are more than 5.33 times (81.1% per km of line) higher in EPN overhead lines than in SPN ones. This could indicate that deterioration due to ageing or wear is higher than in SPN but the time in service of the assets is required to confirm this but is not available.
- Interruptions identified as ‘caused by trees, animals and possible sources of pollution’ are more than 6.3% higher per km of line in EPN overhead lines than in SPN ones. This could be caused by the environmental conditions inland in the EPN. SPN is dominated by coastal and close-to-coast areas with fewer trees.

In an additional step, the information must be disaggregated on the maps in conjunction with the lines routes and the main interruption locations. In a second step the environmental conditions and pollution must be integrated.

The link between the interruptions and the environmental/pollutions conditions will be an approximation taking in accounts that:

- The time in service of equipment in the overhead lines is unknown for these voltage levels.
- The data collected from the overhead lines’ faults is a global value and it is not specifically for polymer insulators.
- The maps do not include salty pollution coming from the sea. Areas around the coast will be considered as a separate environment. The effect of wind on pollution emissions is also difficult to infer because it is a multifactor phenomena.

3.7. Important Environmental Information and maps of the EDF Energy System

3.7.1. Solar Irradiation in the UK

In Figure 3.31 solar irradiation over the UK is presented. As can be seen from the map, the area served by EDF Energy has a horizontal irradiation of 980 - 1020 kWh/m² and between 1000 and 1200 kWh/m² when the irradiation has an inclination angle of 30° to the horizontal. Considering this, SPN receives more solar irradiation than EPN. The incidence angle of the radiation and the orientation of the assets toward the sun should also be considered.

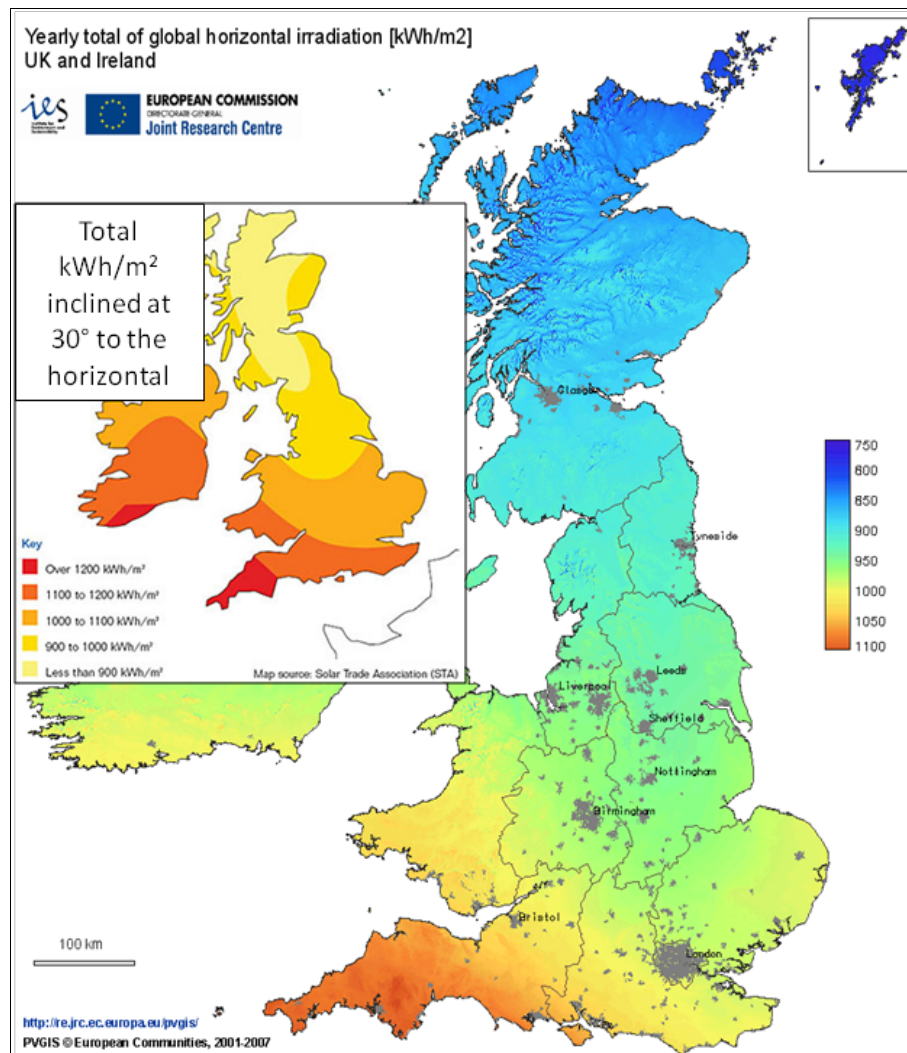


Figure 3.31 Solar irradiation over the UK [158-161]

3.7.2. Wind maps

Two different maps are included having different information about the wind in the UK.

Figure 3.32 shows the annual mean wind speed with information about the direction of the wind coming from the ocean or sea; Figure 3.33 presents the maximum speed. The EDF Energy networks area has annual mean wind speed range between 5 and 7 m/s and some small corridors over the SPN with 7-8 m/s.

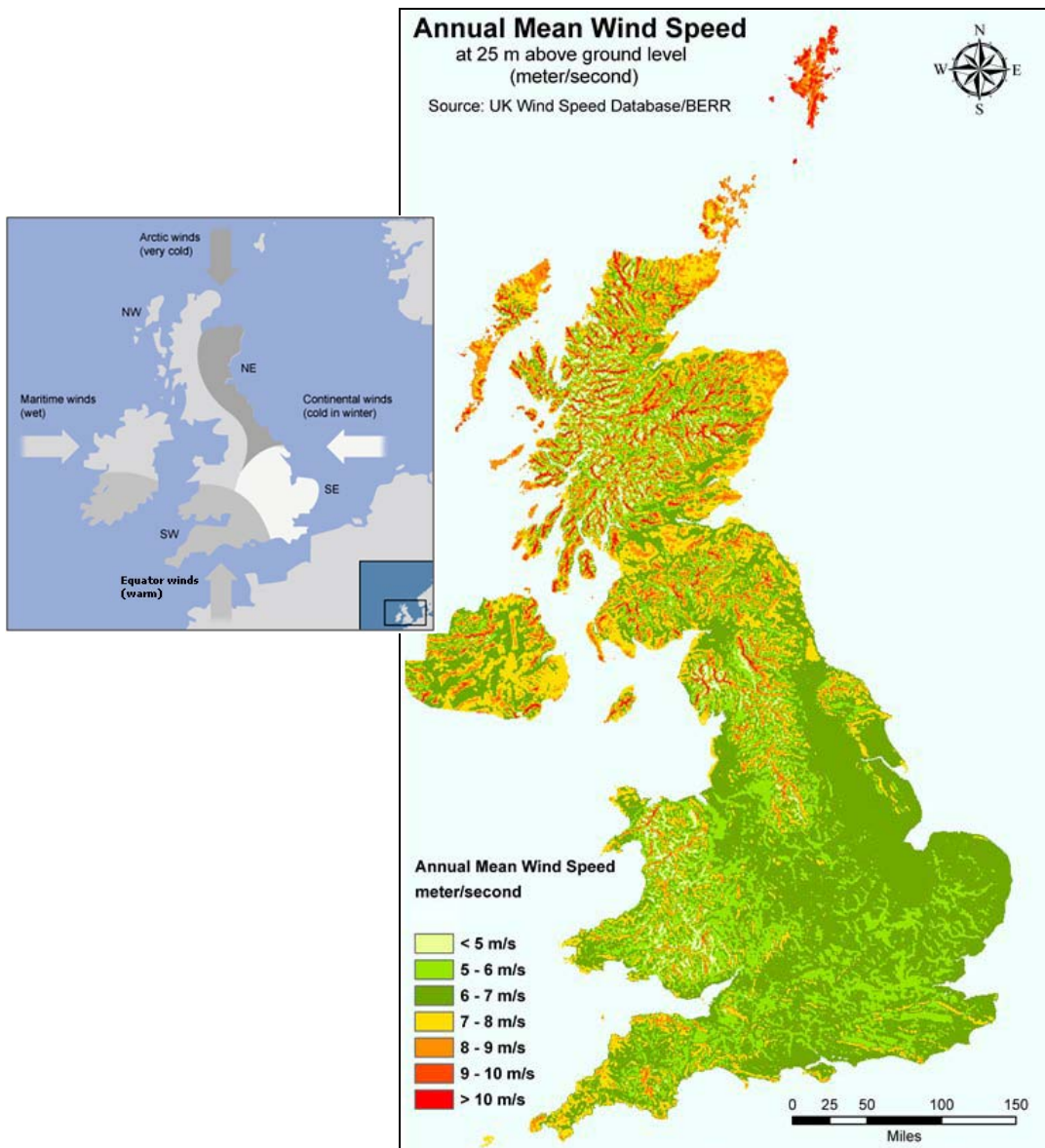


Figure 3.32 Annual mean wind speed and influence introduced by the maritime, equator, continental and artic winds

[162, 163]

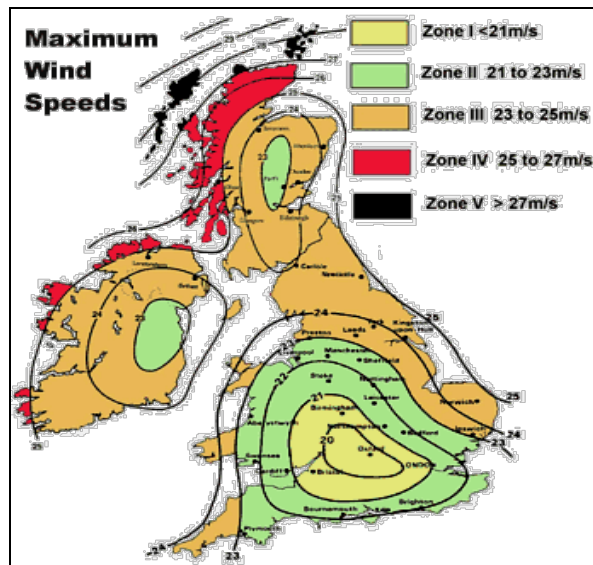


Figure 3.33 UK maximum wind speeds [163]

3.7.3. Rain map

The average annual rainfall is presented as a first approximation in Figure 3.34. Additional maps with the seasonal changes are not included at this time. It can be observed that SPN area has more annual average rain than the EPN.

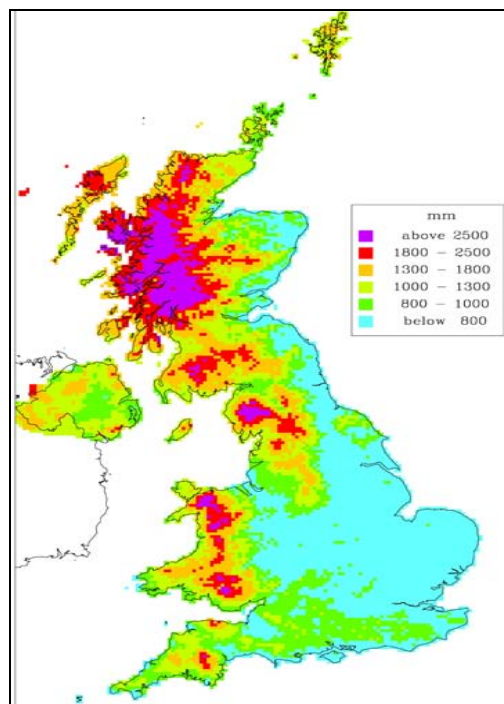


Figure 3.34 Rain Annual Average

3.7.4. Some considerations using this preliminary data taken from the environmental maps

When the environmental conditions are considered with the emission concentrations some interesting details can be found:

The SPN area, in particular the Dungeness coastal region, has:

- High concentration of NO_x.
- High concentration of SO₂.
- Low/medium rain → humidity.
- High levels of salt.
- Low wind.
- High concentration of copper, vanadium, nickel, benzene and medium level of dioxins (chlorides).
- The simultaneous concentration of the emissions is higher than in other areas.

In consequence, a high degree of corrosion on metal end fittings, and damage of the seals (interface polymer/end-fitting) by erosion is a consequence of severe acid rain and salty pollution acting synergistically. Figure 3.35 shows the level of NH₄⁺ ion associated with acid rain, is high.

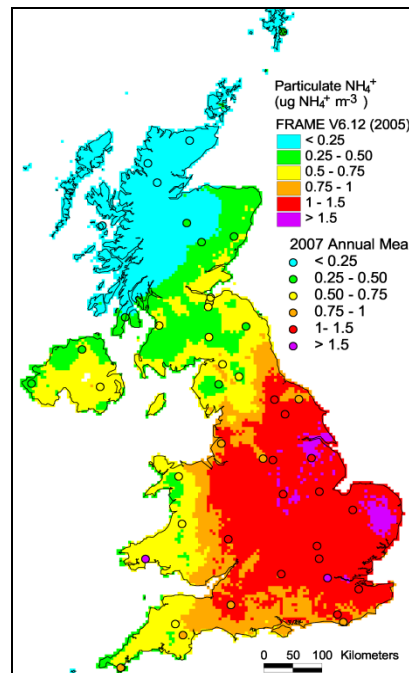


Figure 3.35. Concentration of NH₄⁺ over UK (Source: Defra)

The same situation is happening in the EPN system surrounding Norwich. In this case the concentration of NH_4^+ is higher but the salt level is lower.

Insulators from Circuit I, II and IV (Introduced in Chapter 5) are located in less aggressive areas with a medium level of concentration emissions. Circuit I and II also could receive salty depositions.

Finally, it is important to mention that the whole area surrounding London presents high concentration of all type of pollutant emission. Salt deposition is likely to be low but acid rain can have a very low pH producing a very acid rain.

UK Climate Projections from DEFRA (<http://ukclimateprojections.defra.gov.uk/>) collects the data from multiple national and international institutions to extrapolate environmental conditions in the country.

3.8. A Proposal for Future Work on Insulator Asset Management

Figure 3.36 summarizes the main steps to be followed by utilities to start and continuously improve the asset management of polymer insulators based on condition and risk of failure, focused on distribution overhead lines where a lack of recorded information is one of the main obstacles.

Figure 3.37 shows the main steps suggested to prepare the asset management proposal for polymer insulators installed on distribution aerial lines. Figure 3.38 presents some important indices that can be established to give the proper weighting of each condition in the final monitoring and replacement plan, putting emphasis on environmental conditions and criticality of the circuits.

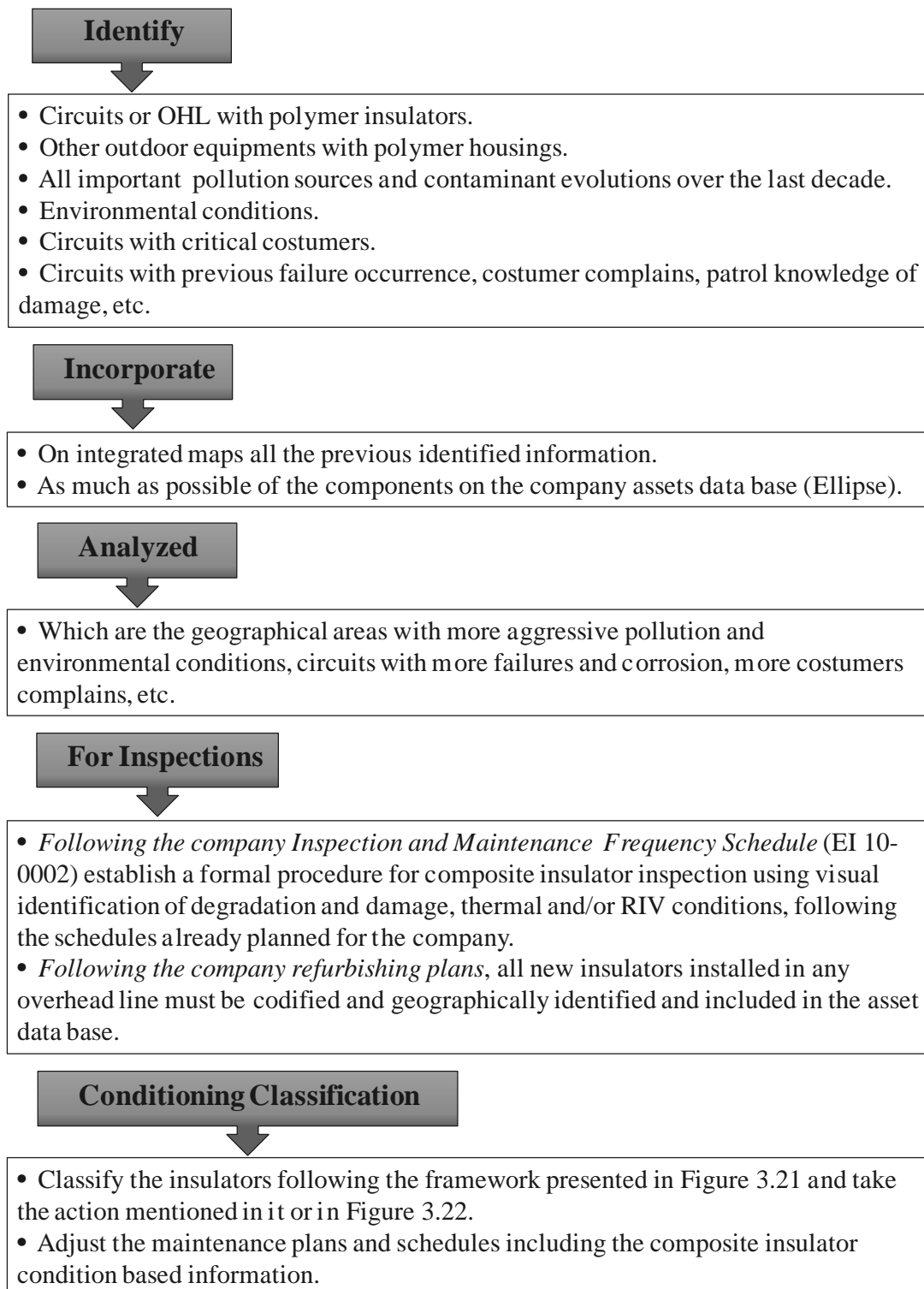


Figure 3.36 Future Work Plan Overview for Insulator Asset Management (Proposal)

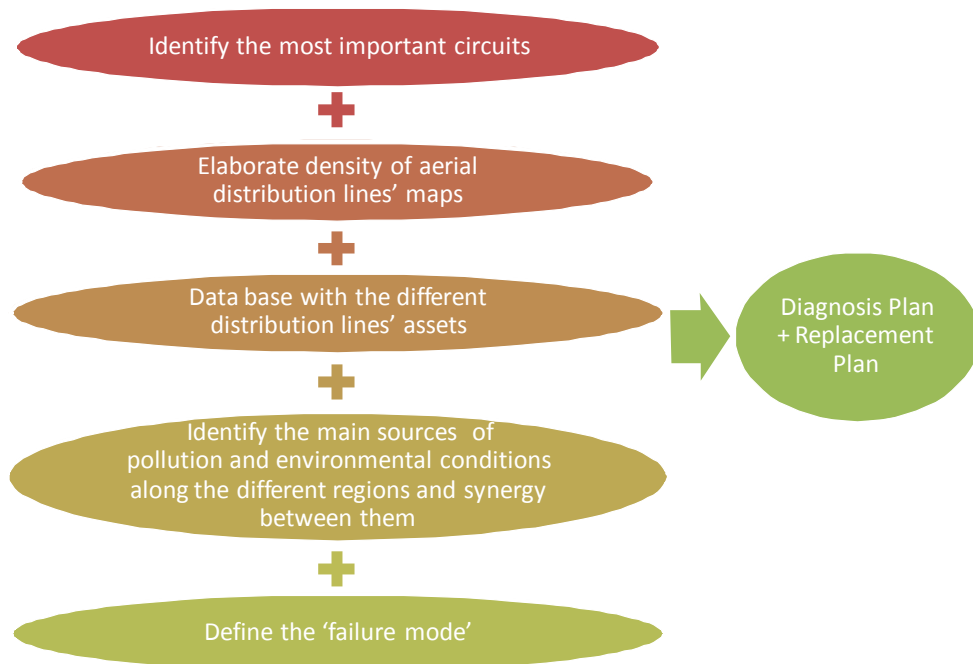


Figure 3.37 Steps to elaborate an Asset Management Plan for composite insulators used on Distribution Aerial Lines

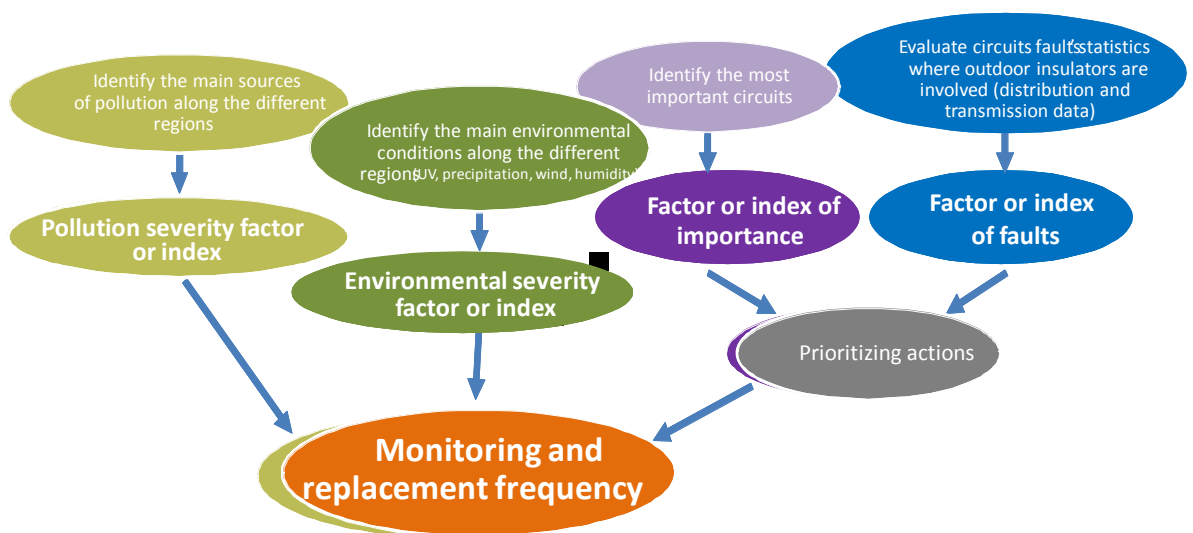


Figure 3.38 Different aspects and factors to consider when planning monitoring frequency and replacement plans

4. COMPOSITE INSULATORS AGED UNDER MULTISTRESS FACTORS

4.1. Introduction

In this chapter, the main concepts related to ageing processes or degradation phenomena of polymer insulators are presented. The main stress factors and the most accepted ageing mechanisms, valid for almost any polymer, are summarized. Particular phenomena valid for Ethylene Propylene Diene Monomer (EPDM) or/and Silicon Rubber (SIR, in particular Polydimethylsiloxane, PDMS) are subsequently included. Two different stages were initially presented in 1996 to describe the ageing of composite insulators [1] and the flashover mechanism was well described since 1995 in [164, 165].

4.2. Ageing Processes of Composite Insulators

Composite insulators' overall performance are the consequence of different factors acting from the beginning of their design and manufacturing process until its removal or failure. Figure 4.1 shows the main list of factors which influence non ceramic insulator behaviour and its degradation along its time in service. All these factors acting synergistically activate physiochemical, mechanical and thermal reactions causing a progressive degradation or an accelerated ageing of the insulators.



Figure 4.1 Main factors influencing composite insulators performance

4.2.1. Composite insulators' ageing processes activated under multistress

The polymer ageing phenomenon is an interrelated and interdependent complex process and the inclusion of all of the sub-processes and links between them is practically an impossible task. Two important facts must be considered when ageing of outdoor polymer insulators is evaluated. First, ageing of many polymers, in particular EPDM and SIR is not a basic 'cumulative process'; this is for two main reasons: (i) hydrophobicity is one of the most important conditions that can be degraded but it can be recovered with the migration to the surface of low molecular weight (LMW) groups, and (ii) depolymerization occurs during ageing but new bonds can be created under certain thermal conditions [166]. Second, they are installed outdoors so being exposed to different environmental and climatic conditions which are continuously changing.

Different reactions are activated during the degradation of composite insulators under natural or artificial conditions (Figure 4.2). All together, including their particular sub-reactions, will be acting synergistically to produce the final state of the material.

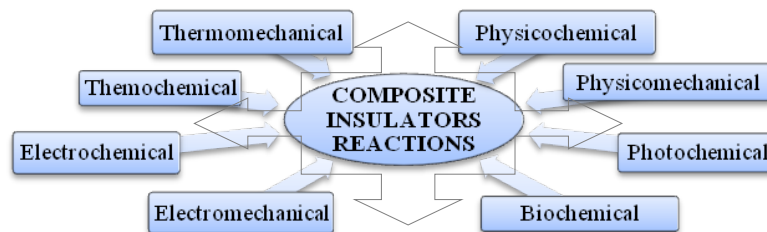


Figure 4.2 Reaction acting synergistically on composite insulators

In general, when the surface is deteriorated the degradation of the electrical characteristics of an insulator may have been caused by an increase in the passage of leakage current between its terminals. This increase is due mainly to the degree of contamination by pollutants that change the electrical resistivity of the surface and humidity. These contaminants may be deposits of dust, inert conductive minerals, such as carbon and metal oxides, and solutions of water and salt, which lead to behaviour similar to a highly variable and nonlinear resistor, and, in many cases, instabilities in the presence of electric fields. Ultimately this leakage current causes heat, products from electrolysis, and corona discharges.

The main processes of transport and deposition of materials on the insulators surfaces are caused by gravitational forces, electrostatic attraction of charged particles, migration of particles of high permittivity in regions with high electric field divergence, evaporation of solutions or suspension and their imprisonment by aerodynamic action. The latter are related to the geometric shape, size, density of particles and also the intensity of the airflow. The insulator causes the airflow to divide, forming stagnation points where the particles can be trapped. The removal of these particles is aided, in most cases, by the washing with water from natural rain or artificial washing [166].

As was previously mentioned, the insulator surface degrades under electric stress acting synergistically with organic and inorganic pollution and humidity. When the electric field parallel to the surface exceeds certain critical value (4.5 kV/cm [48]), the process of electric discharges starts. This is followed by the formation of electrical tracking, which propagates along the electric field direction and this can be finally followed by dielectric breakdown or flashover. The main stages of this process can be summarized as: (1) wetting and contamination of the surface, forming a conductive layer with low surface resistance; (2) flow of leakage current on the surface with high heat dissipation and non-uniform loss of the conductive solution layer, favouring the formation of dry bands; (3) interruption of leakage current flow due to the presence of dry band; (4) raising the temperature by surface discharges or dry band arcs, causing the formation of residues generated by gradual erosion, (5) the spread of a track of carbon residue, and eventually (6) occurrence of flashover [164-166].

Looking at the process in more detail, an overview of the multifactor stress effects on a polymer at two different condition levels, early stage and late stage, was presented [1]. It is relevant to mention that many efforts have been done to understand the late stage of degradation but few researches have been focusing on the early stage. It is important to notice that this first stage introduces specific conditions for the subsequent ageing processes which occur during the later one (Figure 4.3). More recently, a simplified scheme of a ‘very early stage’ of composite insulators ageing was proposed (Figure 4.4) [167]. The main difference between the proposals is the inclusion of the hydrodynamic process involved on the increase of the leakage current.

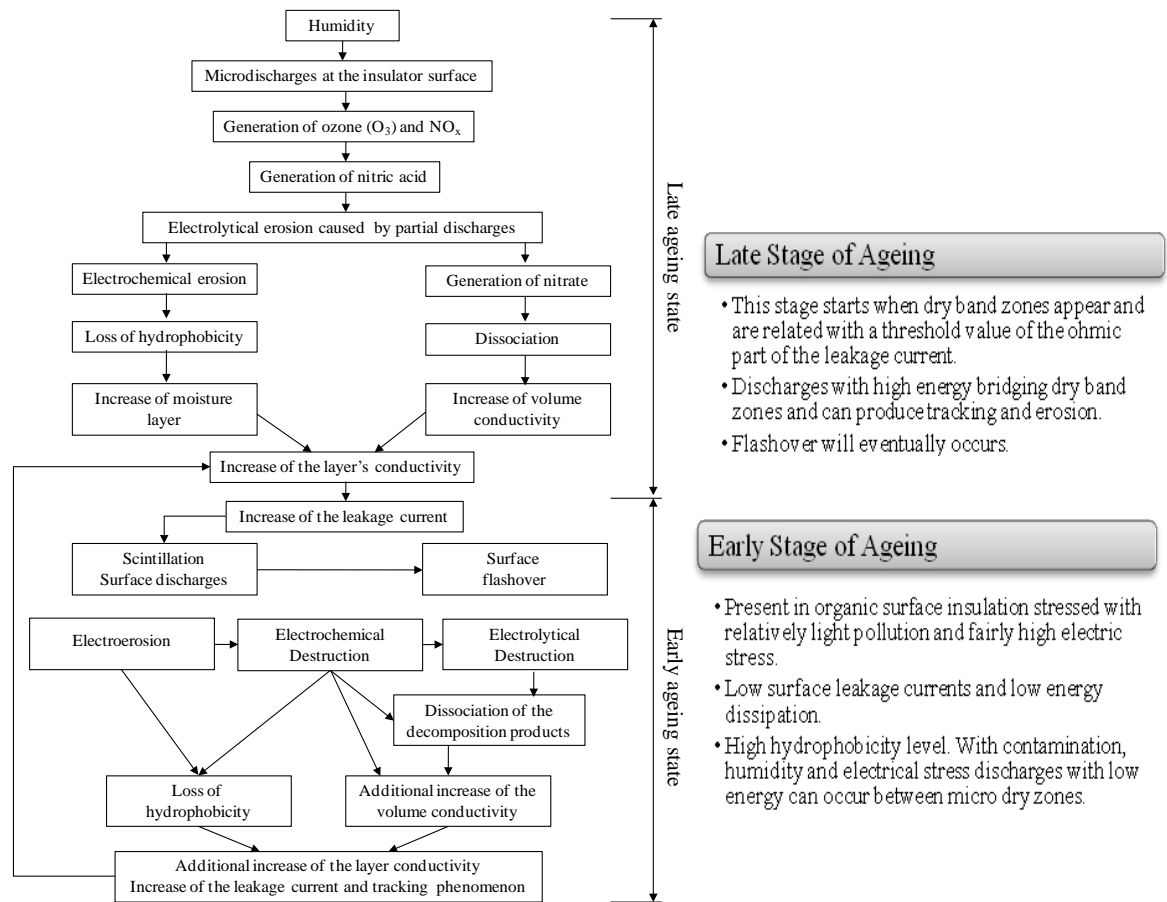


Figure 4.3 Two stages to describe outdoor polymer's surface ageing mechanisms [1]

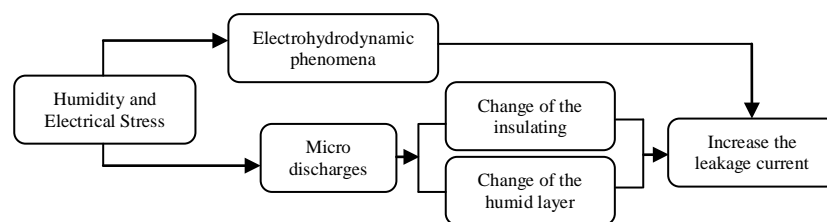


Figure 4.4 Very early ageing stage: electrohydrodynamic is added in parallel with the two processes generate by microdischarges [167]

4.2.2. Rate of Bond Breaking

The ageing of the polymer surface is controlled by breaking bonds or chain scission (which is the breaking of molecular bonds within the backbone of a polymer due to chemical or thermal attack that divides the polymer chains into smaller segments, with a resulting loss in physical properties in its chemical structure). In consequence,

understanding this particular topic is relevant to understand the whole process. Looking at explanations for ageing and breaking of insulation (micro-cracks propagation), a relationship is needed to define the bond breaking and chain scission in polymers [168, 169]. These processes are influenced by the electric field, mechanical stress, and chemistry, accentuated by temperature. The bonds involved in this may be the weak Van der Waals inter-molecular bonds or the stronger intra-molecular chemical bonds. In either case the breaking process will be a statistical one requiring the chance to concentrate thermal energy on a bond in order to rupture it. The rate of bond breaking can be expressed as:

$$K_b = \omega \exp[-(U_b \pm u_c \pm \gamma_{bm} \sigma_m - \gamma_{be} \varepsilon E^2) / kT] \quad 4.1$$

where U_b represents intrinsic structure or necessary energy to break the bond, $\pm u_c$ chemical modification of the bond energy (influence of compounds on bond energy), σ_m represents mechanical stress, γ_{bm} and γ_{be} are factors for mechanical and electrical modifications (the factor γ_{bm} takes account of any local enhancement of the field E but more importantly represents the effective volume change). εE^2 is the electrical stress and T is the temperature. $\omega \sim kT/h$ is the so-called attempt frequency which is about $6 \times 10^{12} \text{ s}^{-1}$.

There is always a finite chance that, by thermal activation (or probably radiation too), a broken bond will be repaired and the structure regain its original form. For this to occur, activation energy, U_r , again modified by the stress εE^2 will be required.

The rate of bond repair can then be expressed as $K_r = \omega \exp[-(U_r + \gamma_r \varepsilon E^2)/kT]$, where, γ_r is equivalent to γ_b above and can be expressed as $\gamma_r = \lambda_r / (N - n)$. The differential equation determining the concentration of broken bonds n is then: $dn/dt = K_b (N - n) - K_r n$.

If it is convenient to consider the proportion of broken bonds $b = n/N$, in which case previous equation can be expressed as $dn/dt = K_b (1 - b) - K_r b$. Assuming that $b = 0$ at $t = 0$, this equation may be integrated to give b as a function of time for various values of field E . So then, it is easy to conclude that ageing is a multistress effect where all factors act synergistically or interdependently. Formal quantification of the stress factors is vital for a valid calculation of the rate value estimation.

It is important to mention that different ageing processes are activated at different values of temperatures which are not reflected in the equation 4.1. This equation only shows a unique inverse relation with temperature and not the particular or individual effect of it on sub-processes activated by mechanical or electrical stresses, among others.

4.2.3. Influence of Ultraviolet Radiation on Insulators' Surfaces

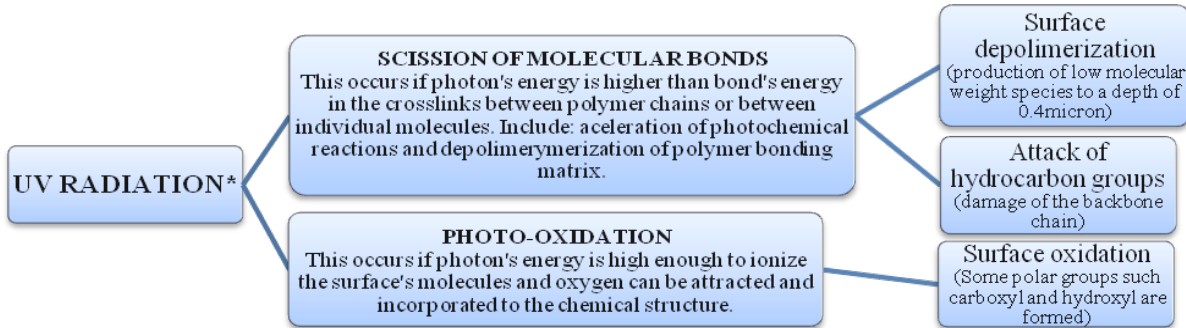
Photodegradation is usually initiated by solar UV radiation and oxygen, and is accelerated by pollutants, water and heat [170]. Initiation usually consists of a complex sequence of reactions. Theoretically, many polymers should not absorb near-UV light. But impurities, on surface or in the bulk, change this.

Approximately 43% solar radiation is in the infrared region and this does little to most polymer surfaces apart from heating them; around 52% of solar radiation is in the visible region and may heat the surface and can also start photochemical reactions. The last 5% of the radiation is in the ultraviolet region (400 to 290 nm) which excites the polymer chains. UV radiation has enough energy to break the C-H bond and form alkyl radicals. During their exposure to UV irradiation photo-initiated reactions lead to the formation of free radicals or excite impurities to also generate free radicals, oxygen-containing products chain-scission and cross-linking. The main products of this photo-degradation are hydroperoxides and carbonyl-containing compounds [170, 171].

The photochemical effect of UV radiation is responsible for most of the damaging effects of sunlight. The absorption of UV radiation results in mechanical and chemical degradation of a polymer structure which can affect its dielectric and weathering properties. Two direct consequences are the reduction of the arc resistance and mechanical strength.

The rate at which degradation occurs depends upon the intensity and wavelength of the radiation. These factors vary with season, time of day, elevation and latitude. Acceleration of the effects occurs in the presence of moisture on the surface. The main visual effects include: crazing, checking or cracking, and discoloration. Loss of hydrophobicity (reductions in contact angle implies introduction of functional groups), increasing the leakage current and reduction of the flashover voltage are the main consequences. Under

ultraviolet radiation two main physicochemical processes are activated: scission of molecular bonds and photo-oxidation (Figure 4.5).



*All the processes are enhanced under high temperature and humidity

Figure 4.5 Main processes activated by UV radiation on polymer's surface

Chemical Reactions Involved in Polymer's UV Oxidation

Oxidation generally involves a free radical chain reaction. Some of the main steps in this chemical process are shown in Figure 4.6. Oxygen reacts with radicals formed during the initial step (reaction*) leading to new chain reactions. The decomposition of hydroperoxides by heat or UV light (reaction**) causes formation of alkoxy and hydroxy radicals leading to chain branching.

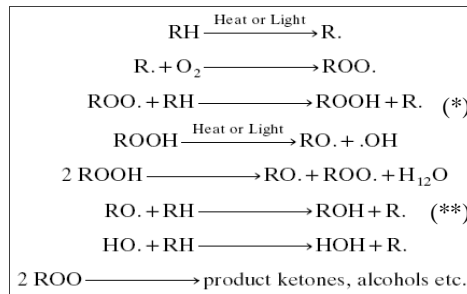


Figure 4.6 Chemical oxidation reactions [170]

4.2.4. Main Effects of Corona Discharges on the Insulators' Surface

In Table 4.1 some characteristics of corona discharge emissions and dry band arcs are listed. Looking at values such as temperature, photon energy and frequency it is possible to infer that the magnitude of local energy released during these phenomena is high enough to damage the polymer surface [172].

Corona discharges (CD) are the start point of many important processes involved in the insulators' surface degradation. Releasing a high quantity of energy, the presence of oxygen, electric field distortion, etc. are only few factors involved during CD activity. Discoloration, chalking, cracking, erosion and roughness are some visual consequences. In the Figure 4.7 some CD effects are presented.

Table 4.1 Properties of dry band arc and corona discharges [172]

Property	Dry Band Arc	Corona
Wave length (nm)	590 ~ 800 300 ~ 500	300 ~ 500
Pulse number (/cycle)	1 ~ 2	1000 ~ 1500
Pulse width (ms/cycle)	1 ~ 5	$10 \times 10^{-3} \sim 30 \times 10^{-3}$
Charge/pulse (μC /pulse)	5 ~ 20	$5 \times 10^{-6} \sim 20 \times 10^{-6}$
Cumulative/sec (μC /cycle)	10 ~ 50	$5 \times 10^{-3} \sim 30 \times 10^{-3}$
Photon energy (eV)	2.1 ~ 1.6 4.2 ~ 2.5	4.2 ~ 2.5
Temperature ($^{\circ}\text{K}$)	1200	800

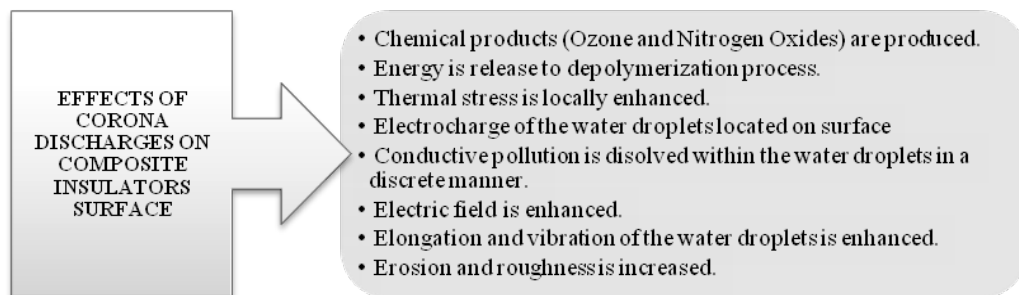


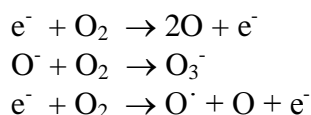
Figure 4.7 Consequences of corona discharges on polymer surface

Degradation influences the electrical and mechanical performance of insulators. Looking at the partial discharge process some additional phenomena are induced as shown in Figure 4.8. It is important to remark that there are additional sub-processes or reactions activated during each step which are not included in Figure 4.8. For example, leakage current increases ohmic heating and wetting, diffusion of low molecular weight molecules component to the surface reduces the loss of hydrophobicity, etc.

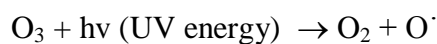
Insulators in service are under intermittent surface discharges (corona and dry band arcs) in a quasi-stable intermittent state which changes surface resistance when water is evaporated. Discharges are not continuous because electric field and current density are changing and they determine the type of discharge. Under low current density, glow and

'silent' discharges occur. If current density and voltage increase, corona discharge will be the consequence, leading to spark or flashover discharge [173].

Ozone is generated under 'silent' discharges (under flashover or arcs with high energy, O₃ is not generated because is thermally destroyed). The mechanism can be simplified by:



Under UV radiation effect ozone is photolyzed, producing as oxygen molecule plus an excited oxygen atom:



It can react with the water located on surface forming two hydroxyl radicals per O[·]:



Hydroxyl radicals have one of the highest oxidation potentials (2.80V) and will react very strongly with the polymer, causing fission of C-C, C-H, C=O bonds and others [173]. Without moisture, the process never reaches sufficient magnitudes to produce damage. If water polluted is present, the process is more severe.

Thermal energy released during arc discharges can accelerate the ageing process, or on the contrary can enhance the recovery of water repellence capacity helping the migration of low molecular weight components. It is important to mention that under corona discharges alone the temperature would never reach the threshold of 200 – 300 °C required to initiate thermal degradation [174].

Corona discharges induce less surface damage (manifested in the form of cracking, >50µm in depth; crazing shallow cracks, <5µm in depth, and deposition of filler powder due to polymerization of the surface layers) in EPDM than in SIR, if the formulation (fillers) are the right ones [175]. Under corona discharges EPDM roughness can be reduced at the beginning and subsequently it can start to increase [174].

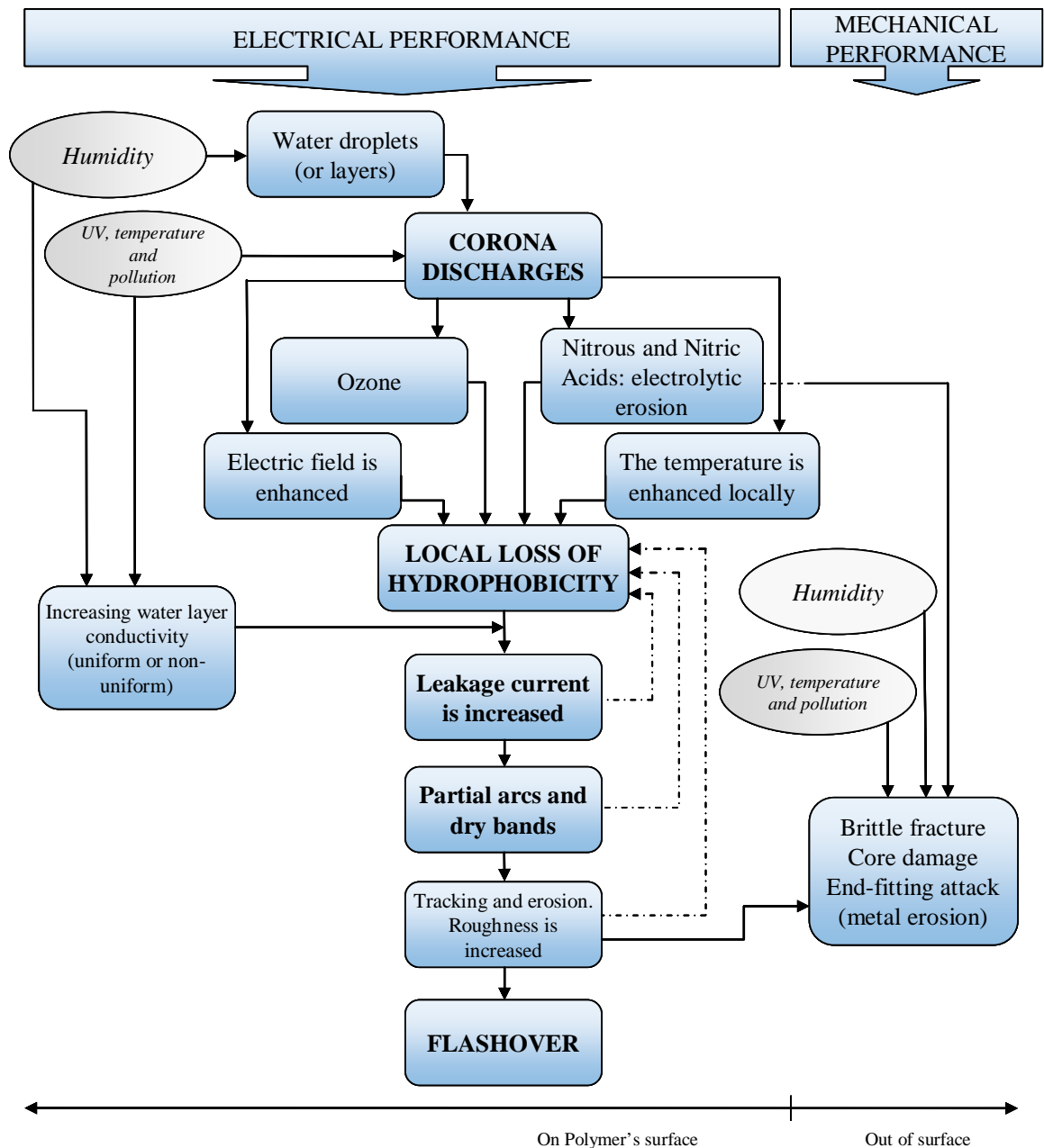
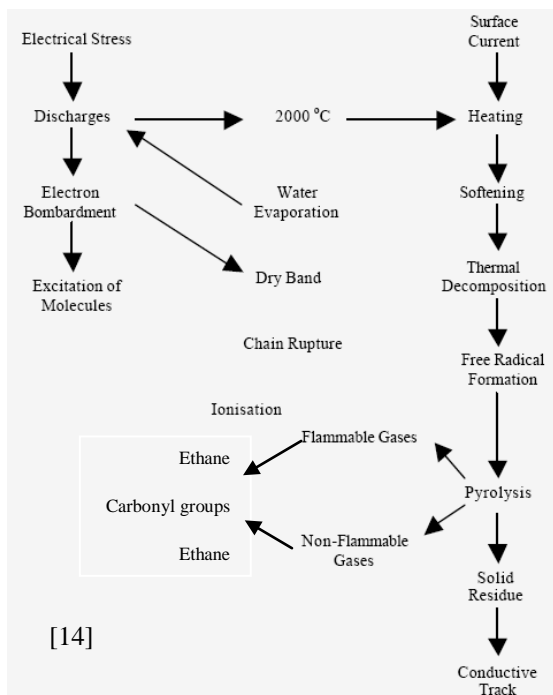


Figure 4.8 Some important processes associated/connected with corona discharges on polymer surfaces

4.2.5. Surface Tracking

Surface tracking is a severe degradation process observed on polymeric insulators working in hostile environments with high aggressive pollution levels, humidity and UV radiation. In Figure 4.9, a tracking process is summarized [176-179]. Information about the severity of tracking phenomena can be extracted by analyzing leakage current waveform (magnitude, pulses frequencies and transitions). See Figure 4.9.



Main Characteristics of the Process

- Tracking is basically a carbonaceous process.
- Once tracking occurs, the surface loses its electrical insulation property.
- Leakage along the surface occurs as a result of surface contamination and moisture, may result in dry-band arcing and carbonization of polymer and hence conduction along the carbonized path.
- High local temperature is involved (~500 °C).
- It is usually progressive, eventually linking one electrode to another and causing complete breakdown along the carbonized track.
- Begins with the creation of low intensity discharge activity. The discharge arises from formation of dry bands and subsequent interruption of leakage current flowing in the layer of ionized water flowing over the surface of the insulator.
- The form of the current flow across the surface changes in terms of its magnitude and frequency content according to the discharge activity on the surface.

Surface Tracking vs Leakage Current (LC) Stages

- **Leakage current domain 1:** When materials are new, their surface is particularly hydrophobic. Surface LC is restricted and the insulators have an excellent pollution performance exhibiting high surface resistance.
- **Leakage current domain 2:** Slow build-up of pollution and cyclic wetting allows the surface LC to increase, which in turn may produce a temporary or more permanent loss of hydrophobicity. Dry band arcing in domain 2 may be responsible for surface erosion since relatively stable arc roots are able to inject significant energy into the material.
- **Leakage current domain 3:** As LC increases, the roots become increasingly mobile and because flash-over is then more likely, the ability to inject significant energy into localized regions is lost.

It is a mixed process of:

- discharge inception,
- carbon formation,
- carbon path propagation under the influence of an electrolyte,
- applied voltage,
- type of electrode,
- location of discharge,
- energy of discharge,
- molecular composition of material.

It is the result of two main contributors [14]:

- Pure thermal decomposition with eventual Pyrolysis.
- Polymer damage by electron bombardment.

Surface Tracking effects on Hydrophobicity and viceversa

- Dry band arcs causes scission of long polymer chains producing short chains.
- Small silanols are formed when silicone bonds are attached hydrolytically.
- These are water soluble and the cyclic species are more volatile.
- One permanent change is done: reduction in quantity of low molecular weight polymer chains on material surface.
- This produces that dry band arced zone presents a reduction in the contact angle.
- The contact angle starts to increase after certain time when low molecular weight contents start diffusing. The original values are not longer reached.
- **Tracking time is longer if contact angle is higher.**

Figure 4.9 Main concepts and processes associated with surface tracking

4.2.6. Ageing by Biofilms

All organic materials have properties to support the growth of biological microorganisms attached to them. They grow by colonizing the surface in the form of biofilms. This results in the presence of microorganisms (algae, lichens and fungi), water and nutritional elements. The latter normally come from the material itself. In Figure 4.10 and Figure 4.11 the main microorganisms, their characteristics and consequences are summarized [180].

ALGAE	FUNGI	LICHEN
<ul style="list-style-type: none"> • Simple plants. • Make photosynthesis to produce its food. • Multiply under favorable temperature, humidity and water. • Six categories have been identified. • Are sprayed through water, wind and animal movement. 	<ul style="list-style-type: none"> • Multicultural organisms composed of long, thread-like filaments. • Absorb nutrients for surrounding environment using enzymes to make transformations in the substrate to absorb them. • Growing on large areas on surface and inside of polymer. 	<ul style="list-style-type: none"> • Combine algae and fungi living together; fungal filaments+ algae cells living from them. • Can grow in almost all surfaces only need enough sun illumination. • Algae cells produce the nutrients that the fungi requires to live. • Normally, growth slowly.
Main consequences of biofilms on polymer surfaces ageing (figure 4.11)		
<ul style="list-style-type: none"> • <i>Fouling</i>: can interfere with the properties of the surface creating a ‘false state’; masking hydrophobicity or increasing surface conductivity. With organic pollution, contact angle in a sessile droplet looks higher. • <i>Degradation of leaching components</i>: all compounds can be used by the biofilm as nutrients; consumption of plasticizers increase embrittlement and loss of mechanical stability. • <i>Corrosion</i>: biofilms increase PH, redox potential, concentration of oxygen and salts. Some reactions are initiated by free radicals and extra cellular enzymes generated by fungal metabolism accelerating surface damage. • <i>Hydration</i>: biofilms consist of lot of water and it can penetrate the material and the conductivity of surface is increased by electrolytes. • <i>Discoloration (and bad odors)</i>. 		

Figure 4.10 Main microorganisms in biofilms and consequences of them on polymer surface ageing

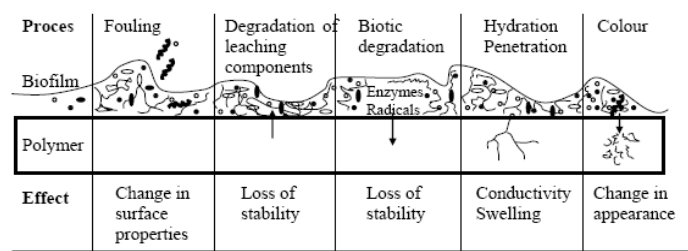


Figure 4.11 Undesirable effects of biofilms [180]

4.3. Ageing of EPDM and SIR Insulators

4.3.1. Degradation and Ageing Process of EPDM Distribution Insulators

Surface properties of polymer insulators may be altered significantly with age when they are exposed to different environmental conditions and pollution, even when the stress caused by the electric field is under the corona discharge activity threshold, which is the

typical service condition of medium voltage or distribution insulators. This effect is particularly noticeable for EPDM which, unlike silicone rubber or polydimethylsiloxane, does not typically remain hydrophobic for any length of time, becoming hydrophilic after ~2 to ~8 years in service [93].

UV Radiation Stress on EPDM

Pure EPDM should not, in principle, be degraded by UV, as it is not absorbed by C-C or C-H bonds, and hence cannot cause direct cleavage of the polymer backbone or saturated diene cross-links but, in service, real compounds of EPDM are degraded by UV. Oxidation of EPDM can be briefly summarized as:

- UV is absorbed by impurities present at the time of manufacture (carbonyl, peroxides and catalyst residues), which degrade to produce free radicals.
- Free radicals attack the polymer backbone and cause bond scission, introducing impurities. When the free oxygen required for their reaction is not readily available (as in the bulk), free radicals can initiate cross-linking between the polymer chains.
- Chain scission produces surface cracking. Polymer is lost exposing the underlying filler material, creating a chalky appearance, and increasing surface wettability (loss of hydrophobicity making the material hydrophilic).
- Thermal or photo oxidation starts with the production of hydroperoxides and at later stages unsaturated and saturated carboxylic acids, ketones and alcohols are formed. Independent of the presence of environmental pollutants brittle fracture is caused by the nitric acid formed through corona discharges.
- Roughness and hardness are increased.

Chemical Degradation of EPDM caused by Acids

Some natural processes and many human activities, mainly the use of coal and heavy oil fuels and industrial pollution, create atmosphere pollutants. Of concern are mainly oxides like sulphur and nitro oxides (SO_x and NO_x), than can react with oxygen upon exposure to UV and then dissolve into rain producing acid rain. The main components of this consist of positive and negative ions, such as SO_4^{2-} , NO_3^- , NH_4^+ , Cl^- , Ca_2^+ , K^+ , Mg^{2+} and Na^+ . The former two ions increase the acidity (low pH) and the last four inorganic salts influence the conductivity [181]. Acid rain can lead to the erosion of the polymer and make the

material surface rough, and high levels of conductivity increase the leakage current, discharge heat and dry band arcing. This means that the whole ageing process will be accelerated along with the disruption of the chemical structure and the formation of hydrophilic areas and microdefects.

Specifically for EPDM, its backbone is quite stable under sulphur acids; however, studies using 20% H₂SO₄ show that this acid attacks the double bonds (C=C) [182] and substantial chemical degradation is produced upon exposure to acids [98, 183]. The degradation initiates at the crosslinks with coagent domains and proceeds via de-crosslinking through hydrolysis of the cured site. EPDM cured by peroxide (typically used to process composite insulators) results in oxygenated species on the surface which combine upon prolonged exposure. The extent of surface degradation is found to be sufficiently strong to affect the bulk properties.

Chalking, cracking, discoloration, roughness and loss of hydrophobicity can be observed when an EPDM surface is losing its properties and at the same time a reduced rate of water repellence recovery in EPDM can be possible after discharge activity and when low molecular weight compounds are present (e.g. alumina trihydrate). This recovery process is less than seen in silicone.

4.3.2. Degradation Processes Particular to PDMS / SIR

Chemical Degradation of SIR caused by Acids

The main processes that occur when silicone rubber is attacked by acids can be listed as follows:

- Inorganic fillers in silicone rubber are used to improve the mechanical properties, tracking resistance, and contamination performance of the rubber material but, fillers are hydrophilic and suffer more from acid rain than the base polymer material.
- ATH filler in the surface layer can be easily dissolved into the acid rain by electrolytic dissociation. At the same time, the increasing tracking and discharge heat in the dry band arcing due to acid rain will cause an increase of the loss of ATH [181].

- The loss and wear of ATH (particle size is 0.5 to 10 μm) will leave micro pores and defects of the same size on the insulator surface.
- The base silicone rubber material in the surface layer also is degraded by acid rain. PDMS is mainly composed of methyl groups and chains of alternating silicon and oxygen atoms and the Si-O bond has high bond energy.
- The weakly linking bonds in the molecular structure of silicone rubber, such as the C-H bond in methyl groups CH_3 , are easily degraded in acid rain. Acid rain can attack and dissociate the weak bonds of silicone rubber. In service, the increase in discharge heat during dry band arcing will lead to the formation of erosion pits in which ignition occurs and the resulting flaming accelerates the degradation of silicone rubber material, and decomposes the methyl group to yield active terminals and free radicals to initiate the chain dissociation reaction.
- The degradation of the base silicone rubber material will result in a low density area and micro defects on the insulator surface.
- Due to the loss of ATH filler on ageing by acid rain, the insulator surface gets damaged and becomes rough. The concentration of hydrophobic methyl groups decreases in the surface layer. Some active terminal radicals and free radicals as well as a residual remain on surface.
- The hydrophobicity of the aged insulator decreases.
- Weight loss is caused by the loss of ATH filler and degradation of the base polymer, which also leads to the decrease of contact angle.

Influence of Aluminium Hydroxide Tracking in PDMS

HTV silicon rubber filled with ATH shows a better performance than that with fumed silica filler. The silicone rubber with ATH filler can enhance its resistance to the discharge heat from dry band arcing because ATH has a higher thermal conductivity than the base silicone rubber, and the thermal decomposition of ATH will decrease the discharge heat and has a self-cleaning effect. The concentration and the particle size of ATH filler particles also affect the contamination performance of silicone rubber. ATH, as discussed before, is dissolved into the acid rain and starts, in consequence, an ageing cycle.

Tracking phenomena in PDMS vs. Type of Electric Stress

One of the most important points of tracking in PDMS is that during the process the concentration of carbon released by silicone is extremely low (1% of the total solid residue weight). The reason for this is that silicone polymers can make carbon atoms leave the material as CO or CO₂ under the presence of oxygen. Even if the amount of oxygen is low or in its absence, carbon can be bound to Si atoms [178].

Some conclusions in the literature related with tracking phenomena on PDMS are:

- SIR is ideal for AC voltage applications. Under DC voltages SIR may fail due to tracking. Conductivity increases under DC irrespective of the polarity of voltage but the time to fail is less in negative polarity [176, 177].
- The magnitude of leakage current is less in AC than in DC, and is higher under negative DC.
- The energy involved in DC tracking is higher than the energy involved in AC.

PDMS's Recovery of Hydrophobicity

Loss and recovery of hydrophobicity has been studied for many different groups, and some specific processes or phenomena involved have been established. From the information presented in the literature, the main ideas related with it are listed here.

The main mechanisms proposed for hydrophobicity recovery are [184]: (1) Reorientation of polar groups from the surface to the bulk phase or reorientation of non-polar groups from the bulk to the surface, (2) Diffusion of LMW silicone fluid from the bulk to the surface, and (3) Condensation of the surface hydroxyl groups.

They can be briefly described by:

- A thin wettable, brittle silica-like phase is formed after partial discharges on PDMS, which could prevent the reorientation of the polymer chains. Figure 4.12.
- Diffusion of unoxidized LMW silicone fluid through the silica-like layer (mechanism b). This process might be facilitated by cracks in the silica-like layer; a mild oxidation condition produces uncracked surfaces, with only a few of the polymer side groups oxidized.

- Since no crosslinking occurs, the chains in the network could reorient (mechanism a). Mechanically deformed specimens after partial discharges recover at a faster rate than the comparable untouched specimens. Presence of cracks in the thin silica-like layer allows the migration of the LMW silicone fluid to the surface.
- Diffusion-controlled migration plays a more important role in the recovery process than the reorientation of the newly formed polar species from the surface toward the bulk. Recovery is due to the reorientation of the polymeric chains (mechanism a) and diffusion of the LMW PDMS chains (mechanism b).
- Hydrophobic recovery is due to burial of polar groups into the bulk (mechanism a) accompanied by the condensation of surface silanols and consequent cross-linking in the contact angle-probed layer (mechanism c).
- Formation of relatively short fragments by the scission of long polymer chains occurs before diffusion of the LMW species to the surface, and that is responsible for hydrophobic recovery.
- There is a widespread belief that fluid migration from the bulk to the surface is a key mechanism on the effect of preexisting fluid in the bulk on the restructuring of the oxidized silicone elastomer: the uppermost surface of the elastomer is converted to a silica-like layer when exposed to electrical discharge. In the zone beneath the silica layer, significant chain scission occurs producing the LMW species. These LMW species eventually migrate to the surface through the porous or cracked silica-like layer, and thus the surface regains its hydrophobicity. Free fluid, present in the network, undoubtedly aids the recovery process [138].

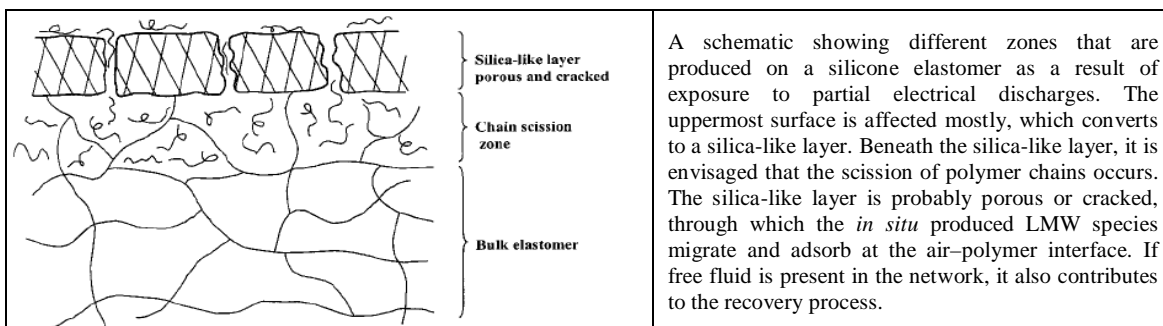


Figure 4.12 Damage on SIR surface under partial discharges and hydrophobicity recovery [184]

Temperature has big influence in the recovery process by diffusion [185] (random migration of LMW species to the surface), drift (force applied to a given special species in the presence of a background species, for example, crosslinked rubber), temperature dependence (diffusion coefficient and mobility are affected by temperature), transition (thermodynamic transitions, glass transition and crystallization), time-temperature equivalence (applicable to any temperature dependant mechanism) and reorientation of polar groups (under corona discharges, oxide groups can attract water but still can have higher surface energy than the surrounding methyl group, if corona stops they will be reorientate).

4.3.3. Surface Degradation of SIR under UV Stress. Comparison with EPDM.

The main differences in the degradation processes of EPDM and SIR under ultraviolet radiation are presented in the Table 4.2.

Table 4.2 Differences in the ageing process under UV stress on EPDM and SIR

<i>Differences under UV radiation</i>		
	<i>EPDM</i>	<i>SIR</i>
<i>Main phenomena triggered</i>	Chain scission reactions followed by the generation of free radicals and oxygen-containing groups	Cross-linking reactions
<i>Hydrophobicity</i>	Highly degraded. Decrease more than 6 times the magnitude lost by SIR and very fast. After time remain constant because the number of broken chains suffers saturation.	Less degraded. High binding energy of (SiO) _x functional groups prevents chain scissions.
<i>Surface resistivity</i>	Significant decrease. The generation of free radicals and polar groups through scission of side-chains causes a precipitous loss of surface resistivity	Increase gradually with time. The oxidized layer formed on surface is assumed to act like silica, a very high resistivity material
<i>Oxidative products</i>	Increase. Highly oxidized carbon groups of C=O, O=C-O.	Increase. Formation of the inorganic silica-like structure of Si bound with three to four oxygen atoms.
<i>Surface damage</i>	Severe chalking and cracking. Significant amount of loose filler on the surface.	No significant changes. Slight amounts of loose filler are on the surface.
<i>Generation of free radicals and oxygen groups</i>	Can be induced	Can be induced
<i>C and O content changes</i>	C decrease ~20%, O increase ~ 30%	C and O remain almost constant
Differences are strongly determined by the structural parameters of the polymer matrix such as free volume and chain flexibility		
The energy for C-C bonds rotation is 14 kJ/mol. The damaged side chain is continuously exposed to photo oxidation.		The energy for rotation about siloxane bonds in PDMS, is almost zero. The damage side chain is protected by non-ionic groups.
EPDM can present better resistance to UV stress if appropriate quality of compounds, fillers and formulations are introduced (but not better than SIR).		

5. EPDM MV INSULATORS AGED UNDER NATURAL SERVICE CONDITIONS

5.1. Introduction

Surface properties of polymer insulators may be altered significantly with age when they are exposed to different environmental conditions and pollution, even when the stress cause by the electric field is under the corona discharge activity threshold. This effect is particularly noticeable for EPDM which, unlike SiR, does not typically remain hydrophobic for any length of time, becoming hydrophilic after ~2 to ~8 years in service [93].

5.1.1. Experience of EPDM Insulators Aged in Service around the World

Many investigations have been focused on the understanding of transmission composite insulators ageing, but this has not been the case with their application on distribution systems. Information about them aged in-service is scarce.

In the literature, diagnosis of 33 kV EPDM insulators under tropical conditions after approximately five years in service was reported [186]. Three different pollution conditions were evaluated: (i) industrial; very heavy with a high amount of cement, (ii) marine; very heavy exposure to sea spray and (iii) agricultural; light pollution with frequent rain and wind. Service temperature was ~23/35 °C and relative humidity ~65/99 %. Samples' surfaces were deteriorated at all locations, showing signs of discoloration and chalking, although less intensely under condition (iii). Under condition (ii) weak tree-like erosion paths appeared after two months in service and became severe after a year. After two years the material was completely white. UV radiation was inferred as the main cause because the discoloration is higher in the areas directly exposed to solar radiation. The insulator under condition (i) had a partly solidified cement layer not easily removable and surface discoloration was less severe. It is possible that this layer acted as protection against UV radiation. No significant differences were found when the insulators were or were not under electric stress, except for the signs of tracking erosion on the surface. After

twelve months the surface lost its hydrophobicity and after two years was completely hydrophilic.

A second evaluation of 33 kV EPDM insulators is presented in [135]. In this work three samples aged in service (#1, four years in service, #2, ten years in service without failure, and #3, ten years in service with failure-flashover) were compared against a new one. The nominal composition of the rubber was 55% ethylene, 42% propylene and 3% diene-monomer and reinforced with ceramic particles in a proportion of 44 wt %. The aged insulators were recovered from a system located in an industrial and agricultural region, where the temperature ranges between $-4\text{ }^{\circ}\text{C}$ in winter to $+40\text{ }^{\circ}\text{C}$ in summer. Autumn months are very foggy, with relative humidity between 75% and 80%. Yearly average rainfall is about 1025 mm. An extensive physical and morphological analysis is reported showing, in general for the samples in service, that oxygen trapped on the polymer surface leads to the deterioration of mechanical and electrical properties and an increase of the hydrophobicity index (HI). Then, oxidation of the surface of the EPDM housing can be produced by a coupled mechanism involving temperature during the sunny days in summer, corona and ultra violet radiation. FTIR revealed the appearance of the characteristic peaks at 2950, 1650, 1465 and 1380 cm^{-1} related to C-H, C=C and -CH₂-bonding. Changes shown by spectrums were minimum when the bulk of the materials were evaluated, but indicated a slight degree of oxidation. Authors concluded that the small response in the IR patterns almost rules out the possibility of bulk oxidation of the sample, and could be related to a surface oxidation effect, where the oxygen content decreases towards the inner matrix according to a diffusion gradient. With it, even if the layer in the surface could have a considerable degree of oxidation, the bulk contribution is lower. Additionally, the measured hydrophobicity, HI values, in insulators before washing were larger than the measured ones after washing; owing to the deposition of organic dust (from grain processing factories), on the surface of the sheds during the outdoor service. They observed that the hydrophobicity level is very similar between aged samples and only the aged-failed insulator is more hydrophilic close to the damaged zone.

An interesting novelty of this work is the study of $\tan(\delta)$ spectra and dynamic shear modulus as a function of temperature. As a summary of the results and analysis of these evaluations, the following conclusions are presented:

- A reduction in the height of the $\tan(\delta)$ maximum in outdoor aged samples is related to a decrease in the volume fraction of crystallites in the matrix. In addition, the shift in melting temperature (T_M) towards lower temperatures indicates that the size of the crystallites has decreased during outdoor ageing. In summary, outdoor ageing in the active transmission lines causes a decrease in both volume fraction and size of the crystallites in EPDM. The decrease in the dynamic elastic shear modulus, G' for samples removed prior to failure is in agreement with a smaller volume fraction of crystallites.
- Results for in-service failed samples show an important difference. The measured values of G' for in-service failed samples are significantly higher than for non-failed samples. These high values could be related to the promotion into the matrix of inclusions harder than the polymer matrix, during the appearance of the dry-band arcing phenomenon prior to the electrical breakdown. It is well known and reported that dry-band arcing and electrical breakdown phenomena promote the appearance of both amorphous and graphite carbon. These carbon agglomerates, depending of their concentration, could operate as inclusions that harden the matrix, also making it more brittle. In fact, dry-band arcing is a spatially random phenomenon which damages a localized zone of the shed. This area is wider than the zone flashed by the electrical breakdown. The promotion of carbon agglomerates and the consequent deterioration of the surface is in agreement with the results from hydrophobicity tests which indicate an irreversible damage of the surface close to the damaged zone.

Substantial differences in roughness of a new and a degraded (in-service) 69 kV EPDM insulator was reported [134]. Roughness values of $\sim 0.4\text{-}0.9\ \mu\text{m}$ and $\sim 0.9\text{-}4.9\ \mu\text{m}$, respectively, were found.

A number of papers present the capacity of EPDM to recover part of its hydrophobicity. This depends substantially on material compounding. An important dependence between temperature and low molecular weight (LMW) fluid mobility (hydrophobicity recovery) was shown in a 46 kV EPDM insulator after six years in service [187]. At high temperature LMW content can migrate. Extremely high temperatures help the mobility but

also can force the decomposition of alumina trihydrate (ATH) helping recovery of hydrophobicity.

One evaluation of one suspension and one tension 88 kV EPDM insulator degraded under natural conditions in a test station was reported in [188]. Samples were placed in a coastal subtropical region over three years. The temperature was $\sim 34/8$ °C, average annual precipitation ~ 1140 mm and vegetation was protecting the area from sea wind. The main visual degradation symptoms after three years in service were: chalking, colour changes, light erosion, splitting and corrosion. These, and also the magnitude of leakage current, were more severe on the suspension insulator compared with the tension insulator ($\sim 25\%$).

There are many countries in Latin American, in particular Brazil, Argentina, Venezuela and Colombia, using polymer insulators in transmission and distribution power systems. EPDM insulators were particularly installed in many lines during the nineties up to 150 kV. Different experiences have been occurring and some failures occur; mainly under very aggressive or saline environments. A study of annual changes during the first seven years in service of EPDM 115 kV insulators, aged under coastal conditions, with a tropical climate and average temperature of 30°C, showed an increased tendency of flashover occurrence after ~ 12 years in service [189]. In [190] the inspection and diagnosis of 132 kV insulators is reported. After only ten years in service, 65 % of the insulators (160 units) had to be replaced. They were in service under very aggressive pollution and consequently experienced high corona activity. One recent work published by Brazilian utilities and laboratories [139] shows experience with 138 kV EPDM insulators recovered from their overhead lines and comparing them with new samples. The insulators were under different pollution conditions (low, medium, heavy and ultra heavy, following the IEC 60815 standard classification) and exposed to a range of service periods. In their experience over 11 years of insulators under heavy and ultra heavy pollution and coastal/tropical weather with high temperatures (21-40°C), wet summers with strong rains and dry winters and, the life expectancy could be ~ 15 years. After examination of insulators exposed to low and medium pollution, tropical weather (17-25°C, two seasons, strong rains, $\sim 1,300$ mm annually) for 15 years, their results are indicative that the life time will be shorter than the expected 25/30 years. The methodology was proposed and used in [189]. None of the insulators under study exhibited structural damage.

5.2. Diagnosis of MV EPDM Insulators Degraded In Service

This part of the chapter is presented following the structure described in Figure 5.1.

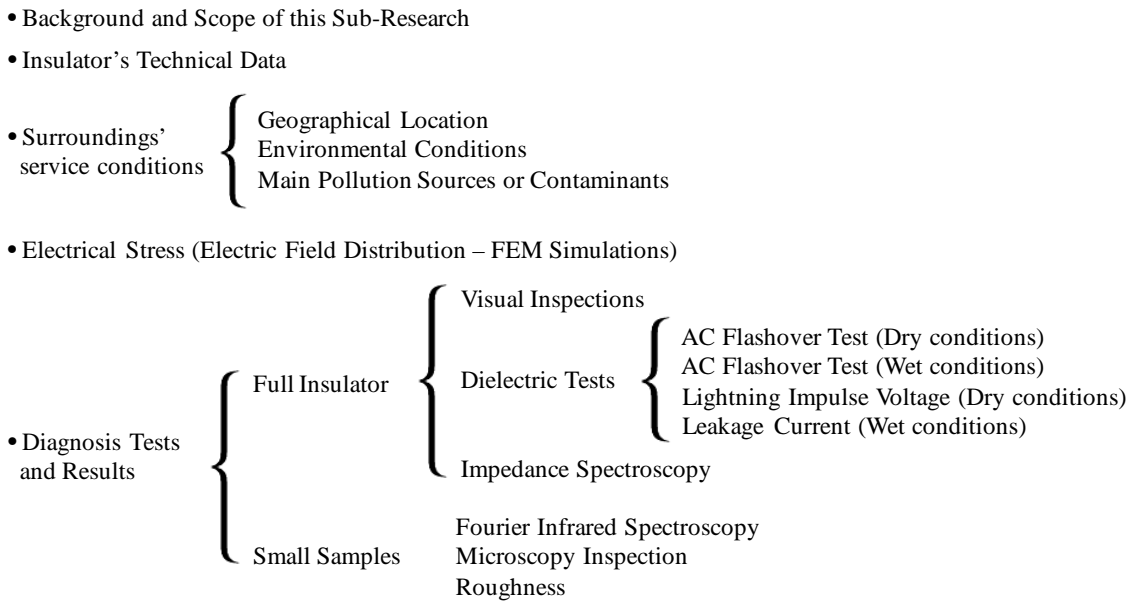


Figure 5.1 Structure of the 11 kV insulators diagnosis results presentation

5.2.1. Background and Scope of this Sub Research

The utility which owns the distribution lines where these insulators have been in service, given its condition based asset management, is carrying out a plan to monitor and diagnose their main equipment. The efforts were centred on transformers, circuit breakers, cables and poles (considering the insulators as an attached element to observe when an inspection is done by patrols) and there was no recorded information on the performance and condition of the EPDM insulators installed in its 11 kV overhead lines. Nowadays, there is an urgent need to increase awareness of the specifications, materials, design, degradation process, stress factors, installation and storage, diagnosis and monitoring methods of polymeric insulators to start the process of tracking the actual state of them in service. Furthermore, installation is scheduled to take place of EPDM insulators on 33 kV overhead lines in the short term.

Having this in mind, a testing plan was organized and adjusted following the maintenance plans, availability and limitations of the utility, to recover insulators from different circuits, environmental conditions and times in service. In reference to this last

requirement, there is an important limitation because there is no record of when the insulators were installed.

The main purpose of this study was to diagnose 11 kV insulators and analyze the service conditions and stress factors acting on them.

5.2.2. Insulators' Technical Data

One new sample and all the samples recovered from the 11 kV overhead lines of the EDF Power Networks (3 samples each from 4 circuits = 12 insulators) are from the same manufacturer. Using the information presented in the supplier brochure, the samples have the characteristics presented in Table 5.1 and 5.2. The dimensions were confirmed on the recovered insulators.

Table 5.1. Characteristics of the Insulators under Study (Source: www.wt-henley.com)

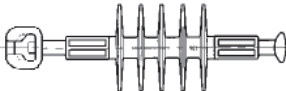
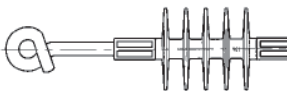
Characteristic	Type A	Type B
Design type		
Manufacturer / Type	Henley / 56145-06	Henley / 56145-09
Housing material	EPDM	EPDM
Voltage rating (kV)	15	15
Shed diameter (mm)	99	99
Creepage (mm)	465	465
Taught String (mm)	179	179
Impulse Flashover (Dry) (kVp)	130	130
Impulse Withstand (Dry) (kVp)	125	125
AC Flashover (Dry) (kV)	95	95
AC 1 min Withstand (Dry) (kV)	85	85
AC Flashover (Wet) (kV)	65	65
AC 1 min Withstand (Wet) (kV)	55	55
Mechanical load (kN)	70	70
End fitting	16 ball – 16B socket	16 ball – 15/81 open hook

Table 5.2 Insulators qualification tests and used standards (Source: www.wt-henley.com)

Product Qualification	
Test on Polymer Insulators	IEC 1109
Electrical Qualification	IEC 60383
Environmental Testing	IEC 1109 Annex C
Creepage Distance Ratios	IEC 815
Thermal Endurance	IEC 60216
Metalwork Protective Coating	BS EN ISO 1461

5.2.3. Service Conditions

Geographical Location

EPDM dead-end insulators in service in different 11 kV overhead circuits were recovered from four different geographical areas located at the South of England, as is presented in the Table 5.3 and Figure 5.2. The areas were selected by the EDF Power Network mainly using the options given by its own maintenance activities plans.

The time in service of the insulators is not a well defined parameter. It was confirmed by patrol members that they do not keep any records of the time in which the insulators were installed; the time is less than ten and more than five years ago and it might be six or seven years. This condition is the same for all 11 kV insulators that have been installed in the system. In consequence, the value was estimated taking in account the manufacturing date placed on the assets and information provided by the more experienced patrol members.

Table 5.3 Geographical location and estimated time in service

Circuit	Location	Estimated years in service
I	Centred on 51° 27' North, 0° 58' East. Lower Stoke, Rochester, Medway.	7
II	Centred on 51° 27' North, 0° 58' East. Lower Stoke, Rochester, Medway.	7
III	Centred on 50° 55' North, 0° 58' East. Britannia, Dungeness.	6
IV	Centred on 51° 1' North, 0° 7' East. Horam Primary area at East Sussex.	7

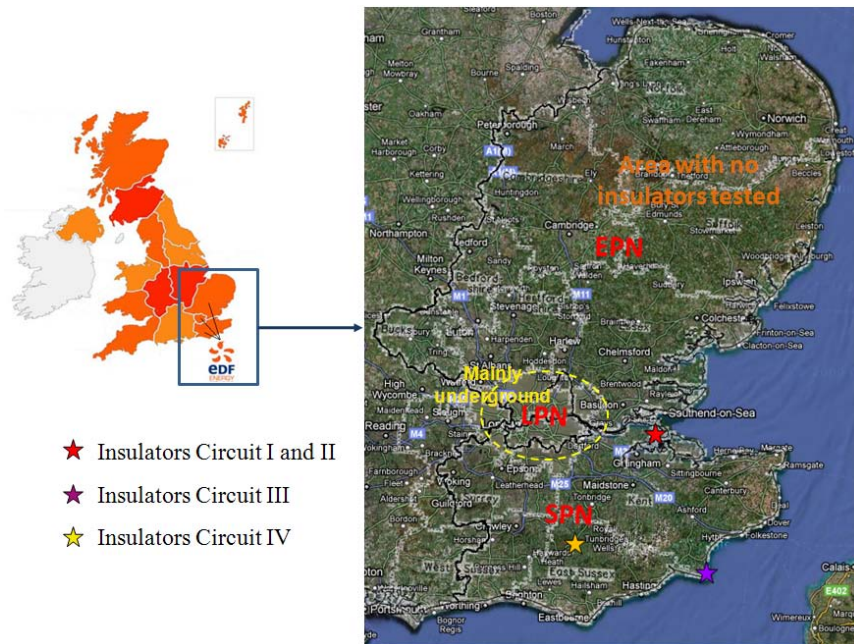


Figure 5.2 Geographical location of the three areas where insulators were recovered

Additional details of the geographical areas are shown in the Figure 5.3 to Figure 5.6.



Figure 5.3 Satellite view showing the surrounding area including two power plants (The distance between the Recovery Area and each plant is approximately 3 km)



Figure 5.4 Satellite view of the installation location where insulators from Circuit I and II were recovered

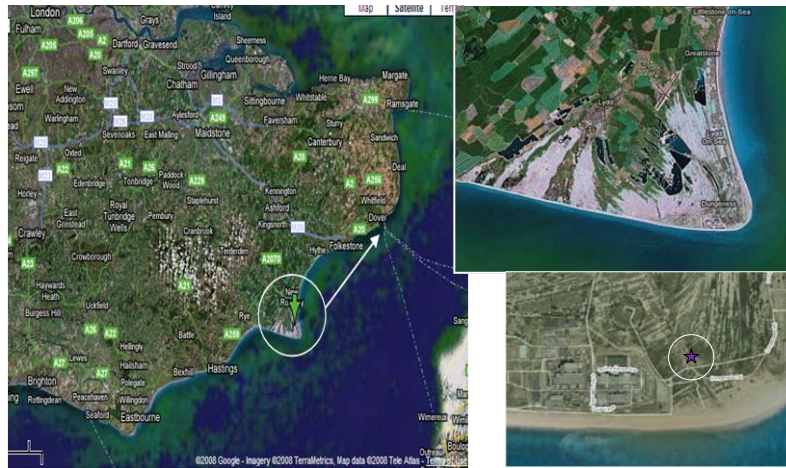


Figure 5.5 Satellite view of the installation location where insulators from Circuit III were recovered



Figure 5.6 Satellite view of the installation location where insulators from Circuit IV were recovered

Geographical Orientation

The geographical orientation determines the angle of the solar radiation over the insulators and as a result the amount of the UV radiation received by the different areas along the surface. Figure 5.7 shows the conditions in which each group of insulators were in service.

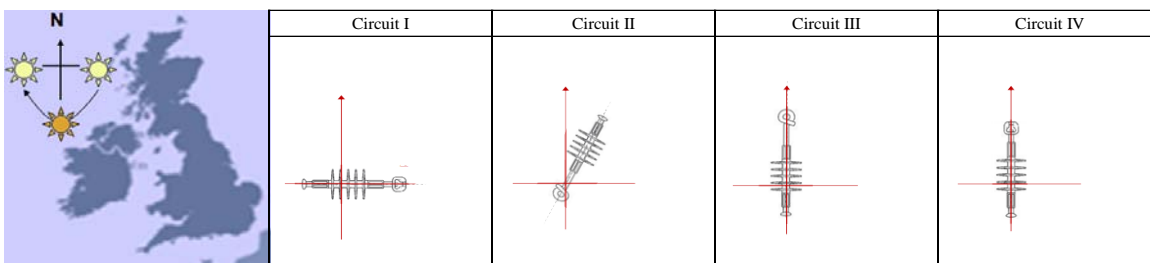


Figure 5.7 Insulators' geographical orientation connected in tension (horizontal, dead-end)

In general, the horizontal orientation of the insulators causes:

- The upper (sky-facing) part of the sheds to be more exposed to UV radiation than the bottom part.
- Higher exposure to fertilizers at the bottom part of sheds and core and the upper part of them to acid rain and salty dust.
- The pollution to be more easily removed by rain from the upper part and washed to the bottom part.
- The drying process to occur first on the sky-facing part of the insulator sheds and core.
- The mechanical effects to be tension and gravity. The first acts in opposite horizontal direction and the second one vertically. The gravity effect can be omitted because its magnitude is very small compared to tension stress.

Environmental Conditions

Statistics of 30 years data were used to obtain the following summary of the climate presented in Table 5.4. The data was extracted from the Met Office UK [143].

Table 5.4 Main Environmental Conditions

	Circuit	Spring	Summer	Autumn	Winter	Annual
Temperature Max (°C)	I, II	13 - 14.2	20.9 - 22.2	14.4 - 15.5	7.4 - 7.8	14 - 15.1 13.6 - 13.9
	III, IV	11.4 - 12	19.1 - 20.1			
Temperature Min (°C)	I, II	4.8 - 8.2	11.3 - 13.6	7.2 - 11.2	1.8 - 2.3 2.4 - 7	6.5 - 10
	III, IV					
Temp Aver (°C)	I - IV	8.8 - 10.3	16 - 17.7	10.7 - 13	4.5 - 8.7	5 - 8.7
Days of air frost	I - IV	0 - 8	-	-	1 - 25	2 - 39
Sunshine (h)	I - IV	461 - 569	591 - 796	321 - 393	175 - 217	1541 - 1885
Rainfall (mm)	I, II	99 - 150	107 - 160	122 - 180	101 - 160 161 - 200	466 - 640 641 - 740
	III, IV			211 - 260		
Days of rain (≥0.2mm)	I - IV	36 - 40	28 - 33	37 - 41	41 - 45	144 - 160
Days of rain (≥1mm)	I, II, IV	26 - 29	26 - 35	26 - 30	28 - 32 33 - 35	103 - 115
	III			31 - 33		
Days of thunder	I, II	3.6 - 4.4	7 - 8	2.7 - 4	0.8 - 1 1.1 - 1.3	14 - 18
	III, IV		9			

*Temperature Record = 38.5 °C in 2003.

The most important values are [191]:

- Temperature: the average daily highest varies from 20°C on the coast to 22°C inland. The minimum average ranges from 2°C to 0.5°C or less inland.

- Wind: thermal gradients produce local land and sea breezes along coastal regions. Annual average speed: 7-8 m/s.
- Rainfall: in summer it is showery, falling over short periods, and is normally more intense than in winter. In winter the rainfall is more frontal and falls over longer periods.
- Density of lightning is low but there is a slight upward trend.
- UV: maximum intensities are $\sim 3000 \text{ J/cm}^2$ (June and July) and the annual average is $\sim 1000 \text{ J/cm}^2$.
- The sun is in the South, travelling East to West during the day. The upper part of the sheds is more exposed to the sun (UV) than the bottom part and the internal-facing shed surfaces in the lower half of the insulators are exposed to relatively low intensities of solar radiation.

Main Pollution Sources or Contaminants

Looking at Figure 5.3 and Figure 5.4, the area surrounding Circuits I and II is located between farms, near to two power stations, close to an estuary and to the coast (sea/river). Circuit I is located in the middle of farmland and Circuit II is on the border of a farm and a small residential area. There are two power stations:

- Kingsnorth (1940 MW). It is a dual plant and can operate with coal and oil. 10% of coal can be replaced by biomass.
- Grain (1380 MW). This plant uses oil.

In consequence, emissions to the atmosphere (mainly SO_x and NO_x), are liberated and can be dispersed by wind. These elements combined with humidity forming acid rain. Other evident pollution sources are fertilizers, salty dust and sand, and Circuit II is beside a residential area and a small parking car area is located under the insulators.

The Circuit III location in the Dungeness area is a well defined area for electrical designs requirements. Previously the National Grid Test Station was located there and the main characteristics are reported in various papers. The main conditions are summarized in Table 5.5 [102, 192].

Circuit IV recovered insulators were in service in a farmland area composed of crops and high vegetation (trees) in one side and with livestock production on the other side. In consequence, the main pollutants are fertilizers; CO₂ and biofilm grows were detected.

Table 5.5 Dungeness National Grid Test Station main conditions (Circuit III conditions)

Parameter		Value
Location		SE UK coast
Climate		Temperate
Temperature range, C		-1 to +32
Max rain (in 10 min), mm		4
Environment		Marine
Pollution severity (Cigre/IEC method) mm/cm ²	Ave ESDD, 50% value	0.15
	Max ESDD, 2% value	0.05
Pollution level (IEC 60815)		IV

In the previous paragraphs the empirical identification of the main pollutants was presented. Using the maps included in the Chapter 2 additional information is extracted. Looking at them, a strip of the coastline in front of the Dungeness area presents the highest concentration levels of NO_x and SO_x. Additionally, main sources of Nitrogen oxides and Sulphur oxides are located close to location of Circuit I and II. These are: thermal power plant, mineral oil and gas refinery, basic organic chemicals industries, gasification and liquefaction, among others. In this case, the contaminants can be moved by wind to other areas.

Ranking the four areas shows that the Circuit III insulators are under more aggressive pollution conditions (acid rain + salty humidity + dust + sand), followed by the insulators recovered from Circuits I and II, while insulators Circuit IV are affected by less severe conditions of pollution but one conducive to develop biofilms. As a consequence of the horizontal orientation, a higher exposure to fertilizers on the bottom part of sheds, and more acid rain and salty dust on the upward facing surfaces might be expected. Pollution is removed by rain from the upper part and it is washed to the bottom.

Connection Conditions

Figure 5.8 to Figure 5.11 present the main electrical connection conditions of each group of insulators recovered. The connections define the electric field distribution along the insulators. Looking at the images it can be seen where the potential and ground terminals are connected and the presence or not of conductor bridges. A schematic summary is presented in the Table 5.6.



Figure 5.8 Detail of the connections of Circuit I recovered insulators



Figure 5.9 Circuit II insulators connection detail

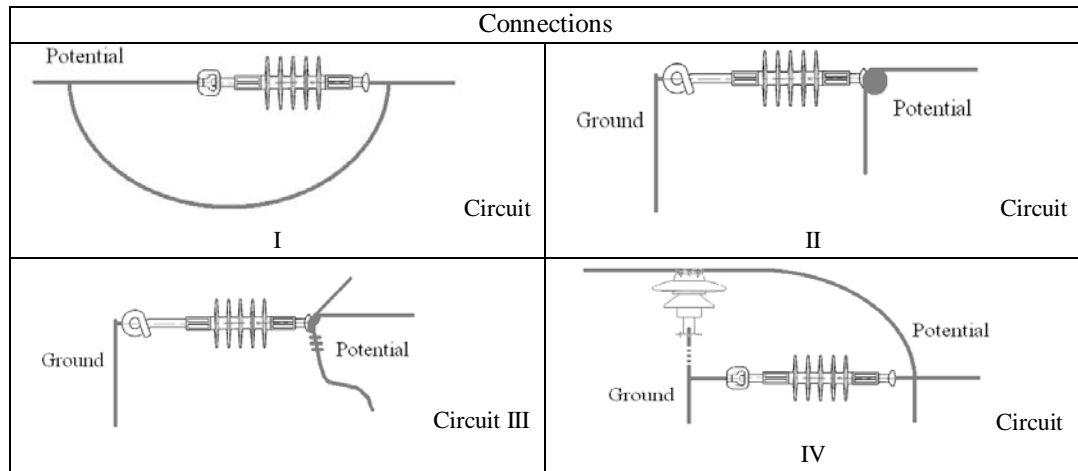


Figure 5.10 Detail of the connections of Circuit III recovered insulators



Figure 5.11 Detail of the connections of Circuit IV recovered insulators

Table 5.6 Potential and ground connections of each circuit



Observation: All circuits have the influence of the ground plane of the land.

5.2.4. Electric Field Distribution

Because the aging of medium voltage insulators (according to the most recent studies, less than 130 kV) are not affected by electric field strengths if the critical point to induce corona discharges activity (0.45 kV/mm) is not reached, the aim of this part of the study is to determine the maximum values under which each of the circuits recovered operates.

The electric field distribution on overhead lines insulators depends on many factors such as: design of insulators, distance between poles, and distance to other circuits, disposition, environmental conditions, corona ring presence and design.

The electric field distribution can be directly obtained from the electric potential distribution by determining its gradient [193]. In electrostatic field problems it is presented as:

$$E = -\nabla V \tag{5.1}$$

From Maxwell's equation:

$$\nabla E = \nabla(-\nabla V) = \rho/\varepsilon = \rho/(\varepsilon_0\varepsilon_r) \tag{5.2}$$

Where ρ is the resistivity in Ω/m , ε is the material dielectric constant, ε_r is the material's relative dielectric constant and ε_0 is the dielectric constant of free space ($\varepsilon_0 = 8.854 \times 10^{-12}$ F/m). Poisson's equation is obtained when the expression 5.2 is placed in 5.1.

$$\varepsilon \cdot \nabla(\nabla V) = -\rho \quad 5.3$$

Without space charge, $\rho = 0$, Laplace's equation is finally derived from Poisson's equation:

$$\varepsilon \cdot \nabla(\nabla V) = 0 \quad 5.4$$

Finite element method software was used [193] to find the solution for Laplace's differential equations taking in account that the composite insulation material has an isotropic permittivity distribution ($\varepsilon = \varepsilon_x = \varepsilon_y$), and assuming the domain under consideration does not contain any surface or space charges. Two dimensional function in Cartesian coordinates system is considered as an approximation to three-dimensional situation.

Table 5.6 shows different connections. Circuit II and Circuit III have an equivalent arrangement. These three configurations were used to evaluate the static electric field intensity along the insulators. The simulation was done neglecting the mutual coupling between phases and the potential used was 6,500 V (phase-ground voltage) and in two dimensions. The relative permittivity used was $\varepsilon_{\text{polymer}} = 3.6$ and $\varepsilon_{\text{porcelain}} = 6$.

Specific points of interest are: (1) interfaces between end fitting / polymer housing and core surface between sheds using lines a and b; (2) tip of the sheds at the top and bottom using lines c and d, and (3) shed surface on lines e and f.

Circuit I

Figure 5.12 to Figure 5.14 show the electric field distribution along the Circuit I insulators. The first detail that can be observed is the effect introduced by the metal bridge at the top. If the bridge is removed the line is in an open condition. As a consequence of these connections the electric field intensity is low and the electric field distribution is not symmetrical.

The highest fields are located at the HV end fitting / polymer housing interfaces and are 2500 and 6000 V/m (or 0.025 and 0.06 kV/cm) at the top interface and bottom interface,

respectively. The electric field is 650 V/m maximum at the sheds' tips located at the top and between 2500-3500 V/m at the bottom. Reviewing the maximum intensity along the shed's surface, the value is close to 2500 V/m located at the shed/core interface at the bottom.

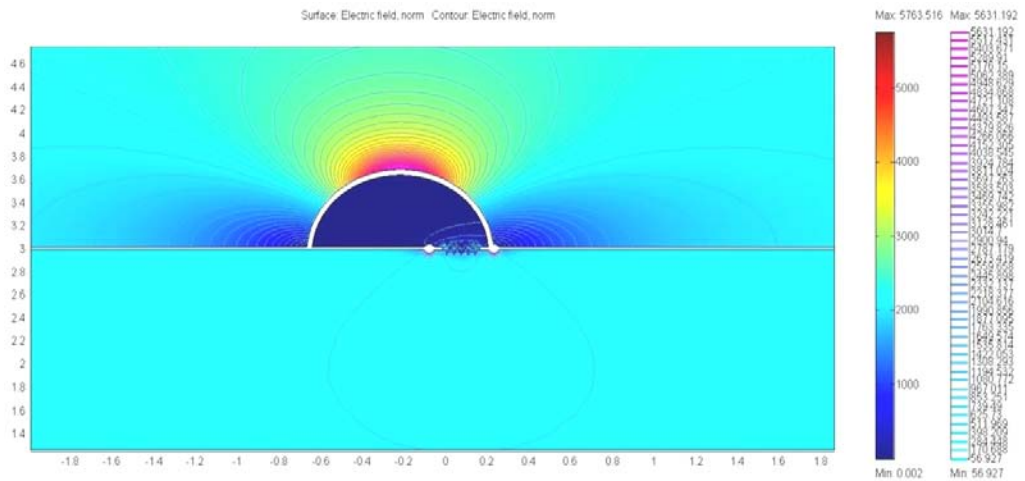


Figure 5.12 Electric field distribution along the insulators under Circuit I connection

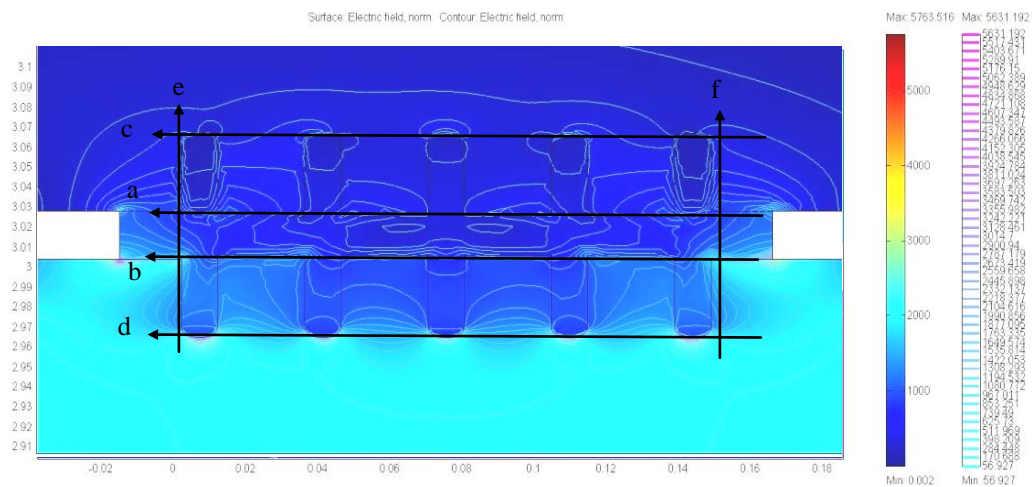


Figure 5.13 Close up of electric field distribution along Circuit I' insulators. Lines a to f show where the figures 5.15 (a to f) were determined

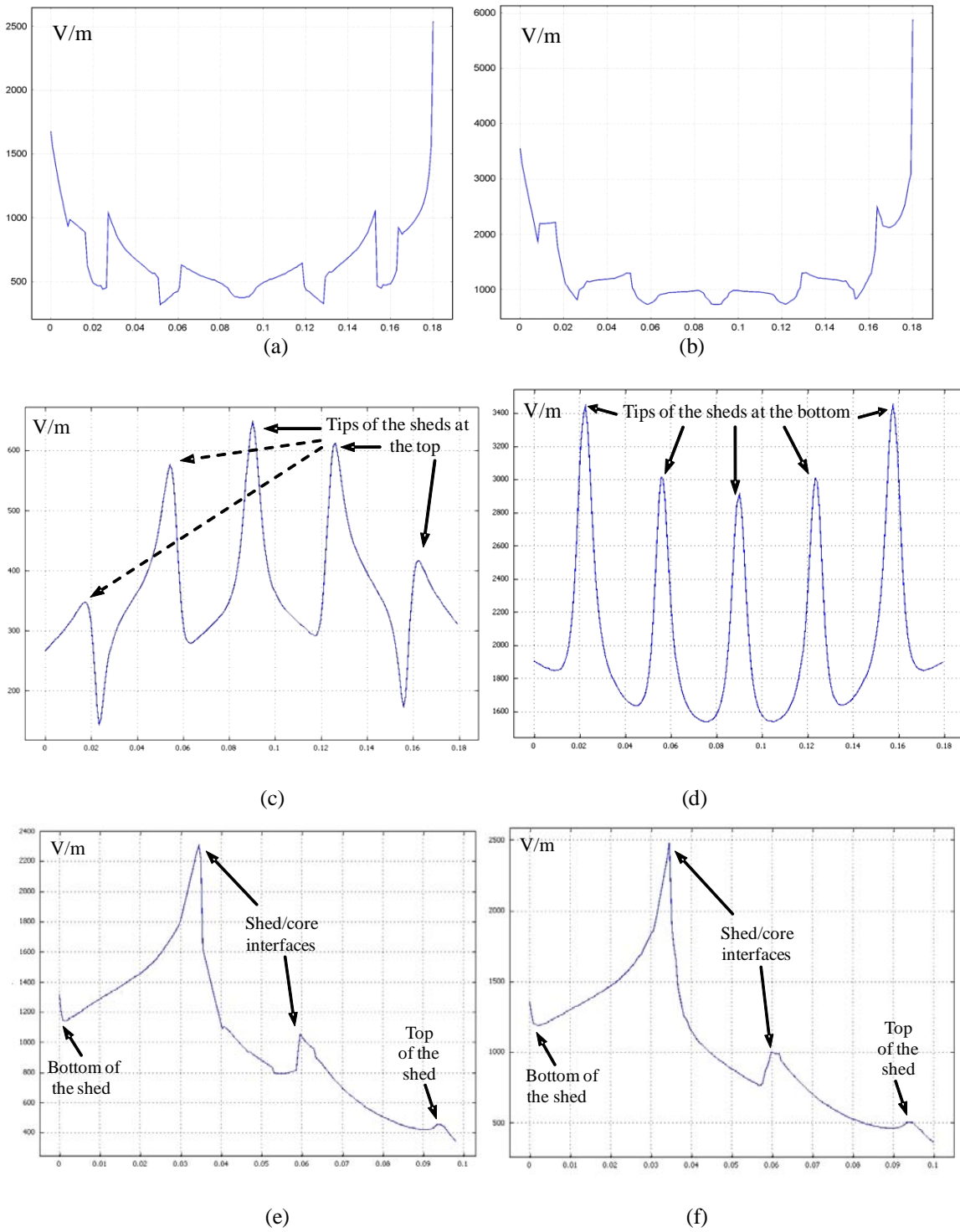


Figure 5.14 Electric field along Circuit I's insulators, V/m versus position (cm). Line at: (a) top part of the core, (b) bottom part of the core, (c) between upper sheds' tips, (d) between bottom sheds' tips, (e) Shed 1 surface, (f) Shed 5 surface (See a-f locations in the Figure 5.13)

Circuit II and Circuit III

Figure 5.15 to Figure 5.17 show the electric field distribution along the Circuit II and Circuit III insulators. As a consequence of this connection the electric field distribution is highly symmetrical between the top and the bottom part of the insulators. The maximum intensity of electric field is located at the end fitting/polymer housing interface at the high potential side (right), its magnitude reaches 160×10^3 V/m. Along the surface of the core the field reaches 40×10^3 V/m and over the tip of the sheds the value does not exceed 30×10^3 V/m. At the shed/core interface the electric field intensity has a maximum of 80×10^3 V/m.

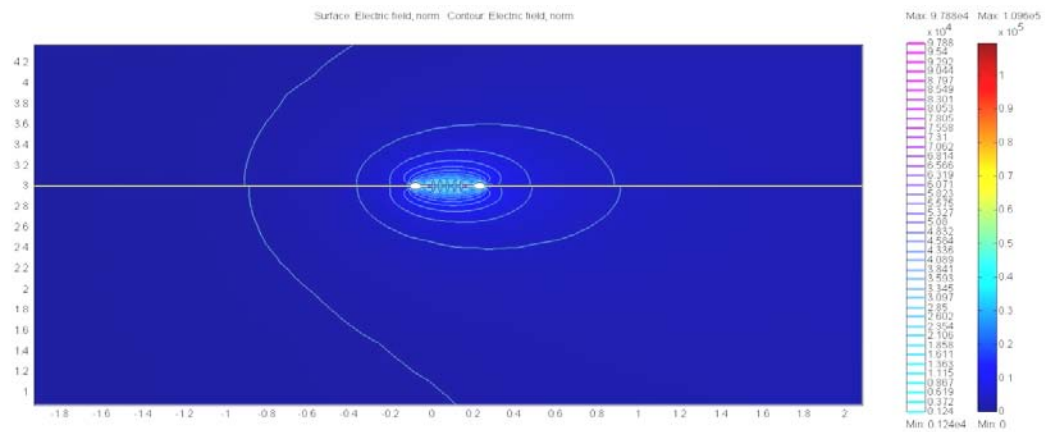


Figure 5.15 Electric field distribution along the insulators under Circuit II and Circuit III connection

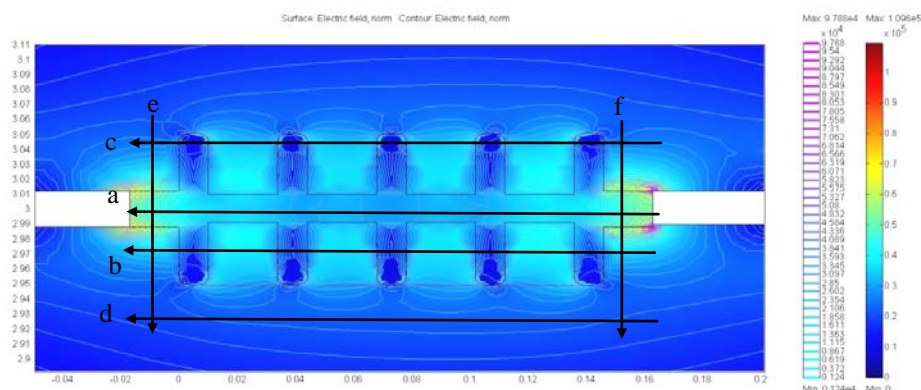


Figure 5.16 Close up of electric field distribution along Circuit II and Circuit III's insulators. Lines a to f show where the Figure 5.17 (a to f) were determined

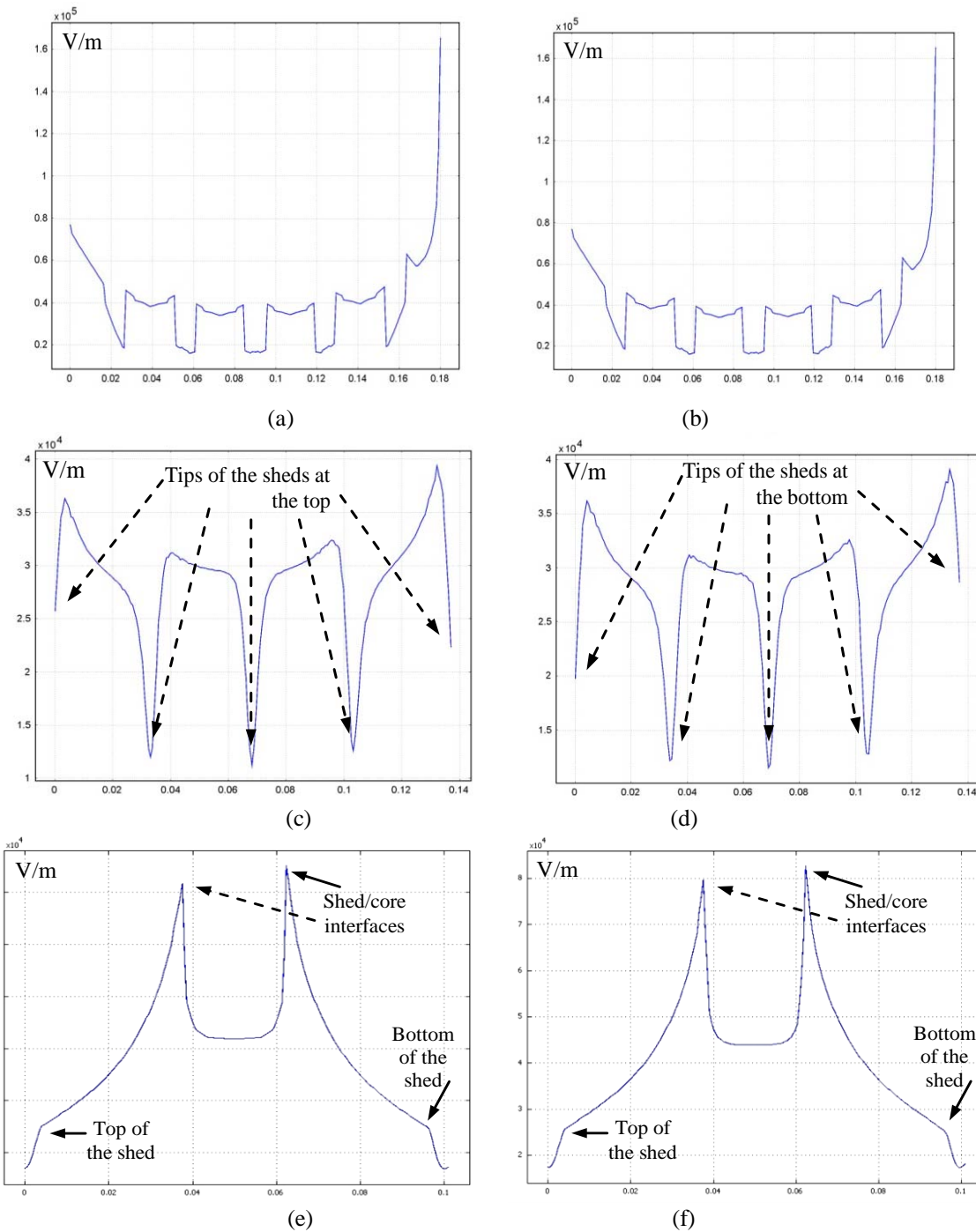


Figure 5.17 Electric field along Circuit II and II's insulators, V/m versus position: Line at: (a) upper part of the core, (b) bottom part of the core, (c) between upper sheds' tips, (d) between bottoms sheds' tips, (e) Shed 1 surface, (f) Shed 5 surface (See a-f locations in the Figure 5.16)

Circuit IV

Figure 5.18 to Figure 5.21 show the electric field distribution along the Circuit IV insulators. In this connection the porcelain insulator, which is supporting the conductor bridge, influences the electric field distribution. As can be observed in Figure 5.21 a and b, there is no difference between the side connected to ground with the HV side, but the magnitude of the electric field is different between the bottom and the top side of the insulator; 84×10^3 V/m and 110×10^3 V/m, respectively. This is caused by the presence of the conductor which is acting as a ‘voltage regulator’ between terminals at the top, as can be observed in Figure 5.20 where the potential distribution is presented. This homogenization effect can be seen in Figure 5.21c where all the shed’s tips have the same intensity of field (15×10^3 V/m) and it is lost over the tips of the sheds at the bottom part of the insulators (between 16×10^3 and 21×10^3 V/m), see Figure 5.21d. The maximum value of field at the interface shed/core reaches 70×10^3 V/m. The maximum electric field in this configuration is over the porcelain insulator, specifically at the point of contact with the conductor ($>305 \times 10^3$ V/m), and it is a consequence of its higher permittivity and the simulated geometry.

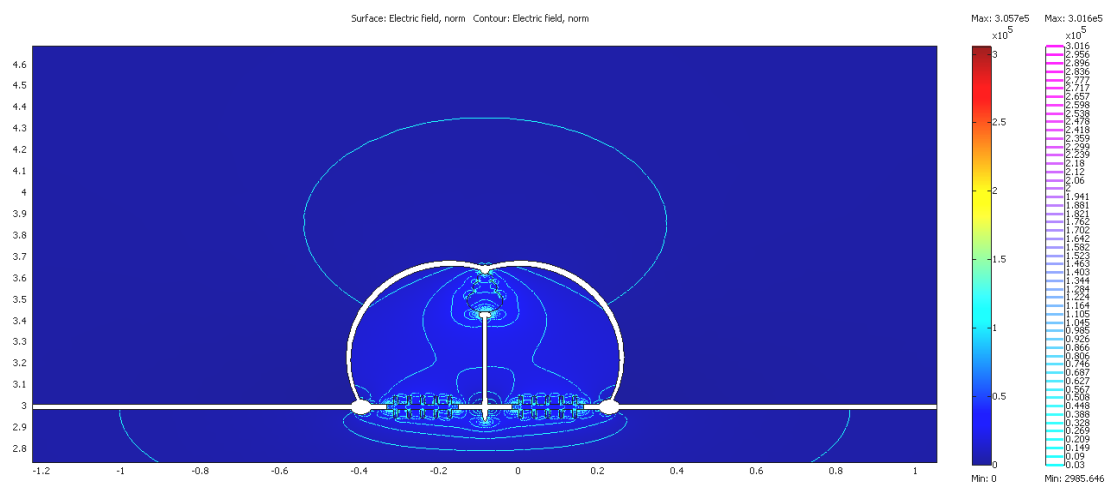


Figure 5.18 Electric field distribution along the insulators under Circuit IV arrangement

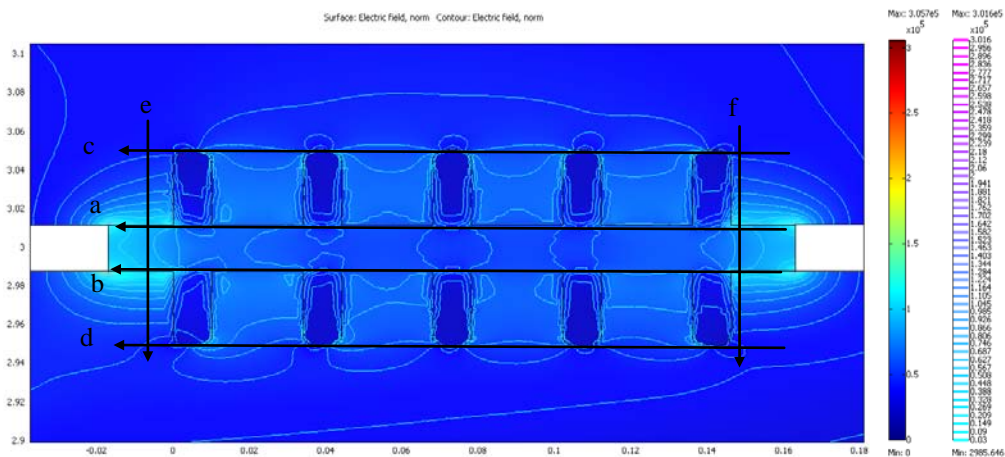


Figure 5.19 Close up of electric field distribution along Circuit II and Circuit III's insulators. Lines a to f show where the Figure 5.21 (a to f) were determined

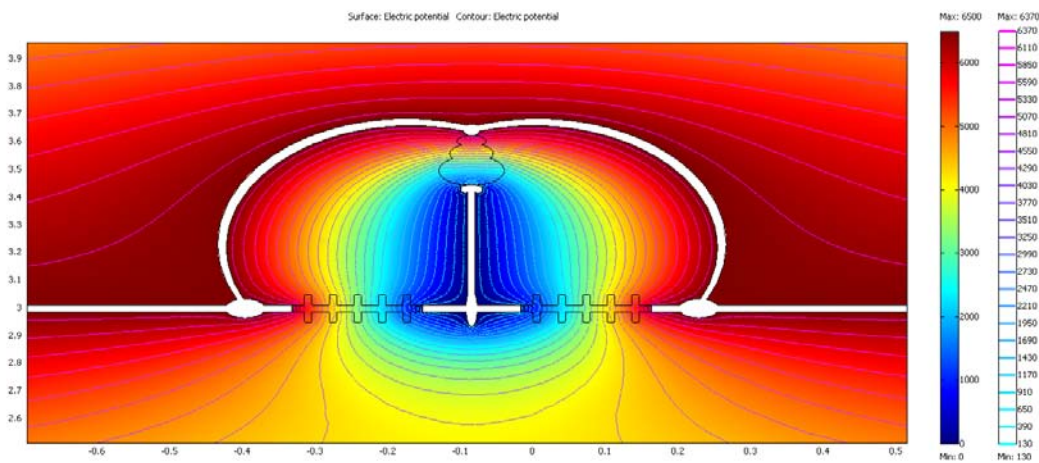


Figure 5.20 Electric potential distribution along the insulators of Circuit IV (Volts)

Summary

Electric field FEM simulation and analysis, under dry and clean conditions, show that none of the insulators under study is under significant electric stress which is the expected result for MV insulators. Between simulated cases the higher intensity of electric field was found surrounding the potential electrode of Circuit II and III's insulators.

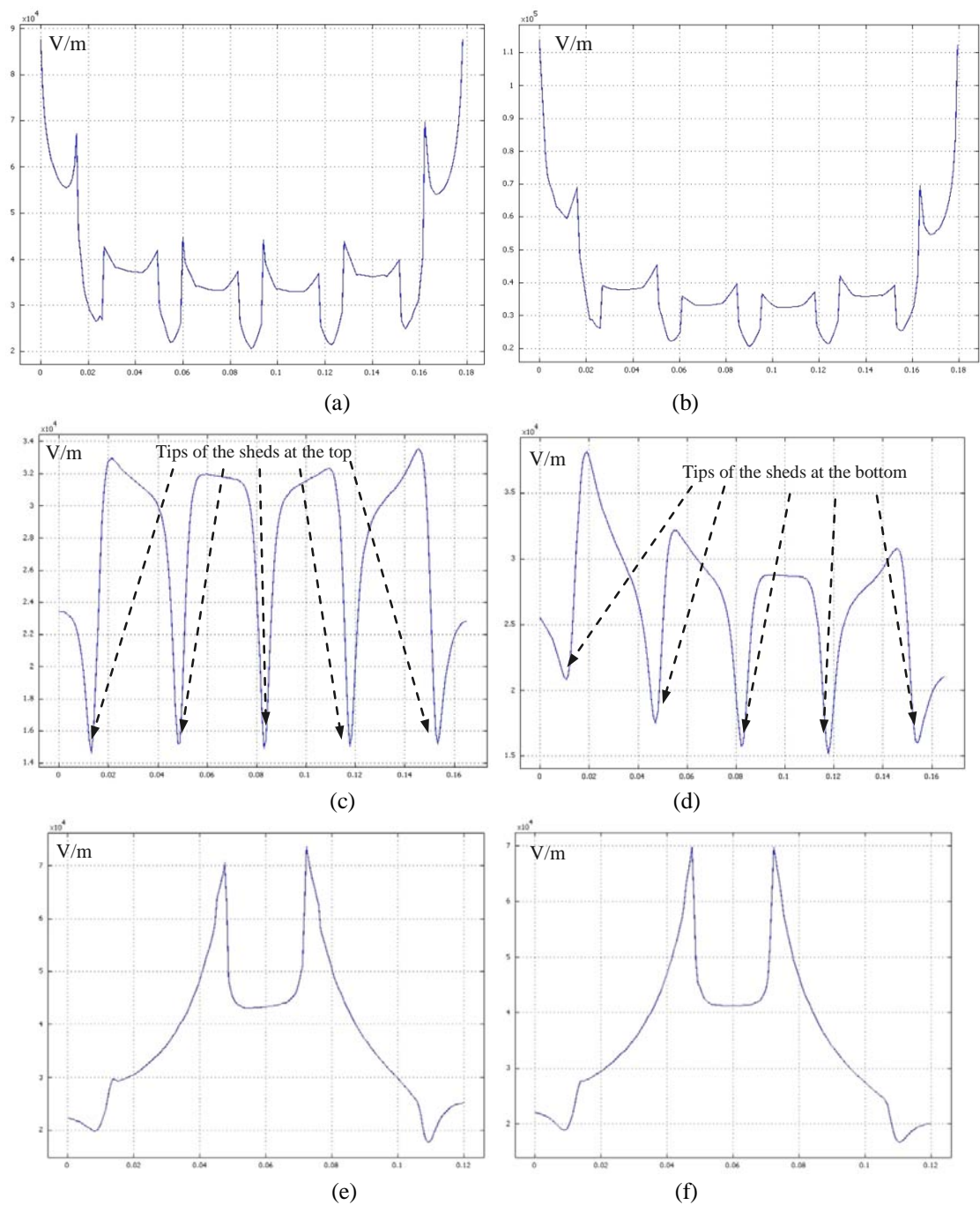


Figure 5.21 Electric field along Circuit I's insulators, V/m versus position: Line at: (a) upper part of the core, (b) bottom part of the core, (c) between upper sheds' tips, (d) between bottom sheds' tips, (e) Shed 1 surface, (f) Shed 5 surface (See a-f locations in the Figure 5.19)

5.3. Diagnostic Tests and Results for Complete Insulators

5.3.1. Visual Inspections

One new sample, having the same manufacture year than the ones recovered from the system, was used for comparison purposes. Its hydrophobicity classification is HC2-HC3 (See Figure 5.22). All insulators are described using the identification of different surfaces shown in Figure 5.23.



Figure 5.22 Hydrophobicity condition of a new similar EPDM insulator

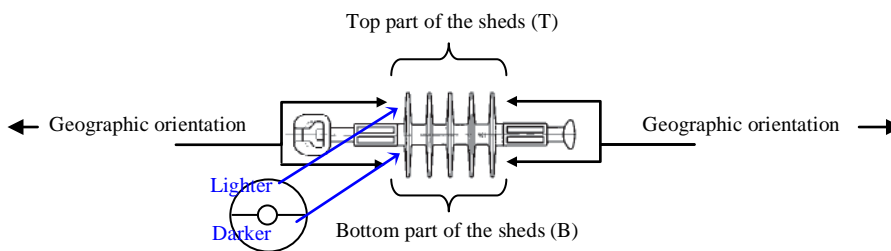


Figure 5.23 Insulators' areas definition

Circuit I

No mechanical damage or metal end fitting corrosion was observed. A small defect: a void without sealant was detected at the polymer/socket type end fitting interface of the insulator (Figure 5.24). This appears to be a manufacturing defect.



Figure 5.24 Void in the interface polymer/socket end fitting

The external borders of the sheds (rims) are very non-uniformly polluted on the bottom side of the insulators. Dark circles around the sheds, near to the core, were detected. These

circles are darker on the South face of the sheds. See Figure 5.25(a). The opposite faces of the sheds present spots, see Figure 5.25(b). They might be organic pollution or fertilizers. The insulators present discoloration, looking whiter than new material (See Figure 5.25).

The hydrophobicity classification of the three insulators of Circuit I was HC7 (Figure 5.26). One hundred per cent of the insulator's surface after spraying is totally wet at the recovery moment and during the first two months after their removal from the system. The drying occurs first on the lighter regions of the sheds (Figure 5.27). High roughness is observed on almost the totality of all insulators surfaces (Figure 5.28). It looks more severe on the side of the sheds facing at the sea. No evidence of corona activity, dry band arcs or flashover, mechanical damage or corrosion was detected.

Two months after the recovery some changes were detected and the darkness half of the sheds, both sides, starting to recover their hydrophobicity (Figure 5.29).

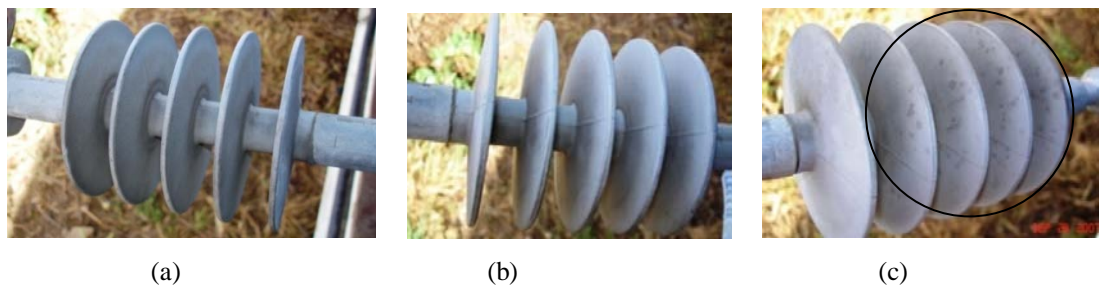


Figure 5.25 View of the (a) East face, (b) West face, and (c) Spots on North face



Figure 5.26 View of the Circuit I insulators after spraying to see hydrophobicity classification. Both sides have the same condition (HC7)



Figure 5.27 Drying differences between darker and lighter areas, the lighter side dried first



Figure 5.28 High roughness on the surface of an insulator



Figure 5.29 Some hydrophobicity was recovered after four months in only one of the insulators

Circuit II

Lighter and darker polluted areas are identified (Figure 5.30). Some sheds (3) closer to the South/West terminal have deformations in the shed (like waves, see Figure 5.31). All the samples are hydrophilic (Figure 5.32(a)). A small area on one shed of one insulator with some hydrophobic level was detected (Figure 5.32(b)).



Figure 5.30 Lighter and darker areas are identified

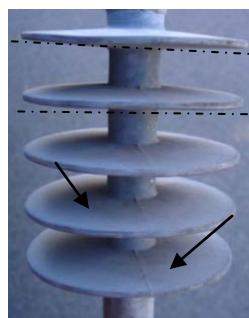


Figure 5.31 Undulation in some sheds (South-West facing sheds)

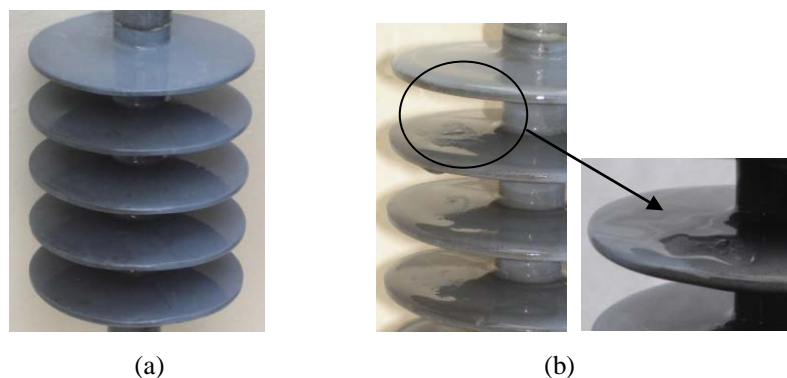


Figure 5.32 Hydrophobicity, (a) Classification equal to HC7, (b) a small hydrophobic area is detected

Local pollution levels were identified (Figure 5.33). Equivalent to Circuit I, the external borders of the sheds (rims) have very non-uniform pollution at on bottom side of the insulators (Figure 5.33(c)).

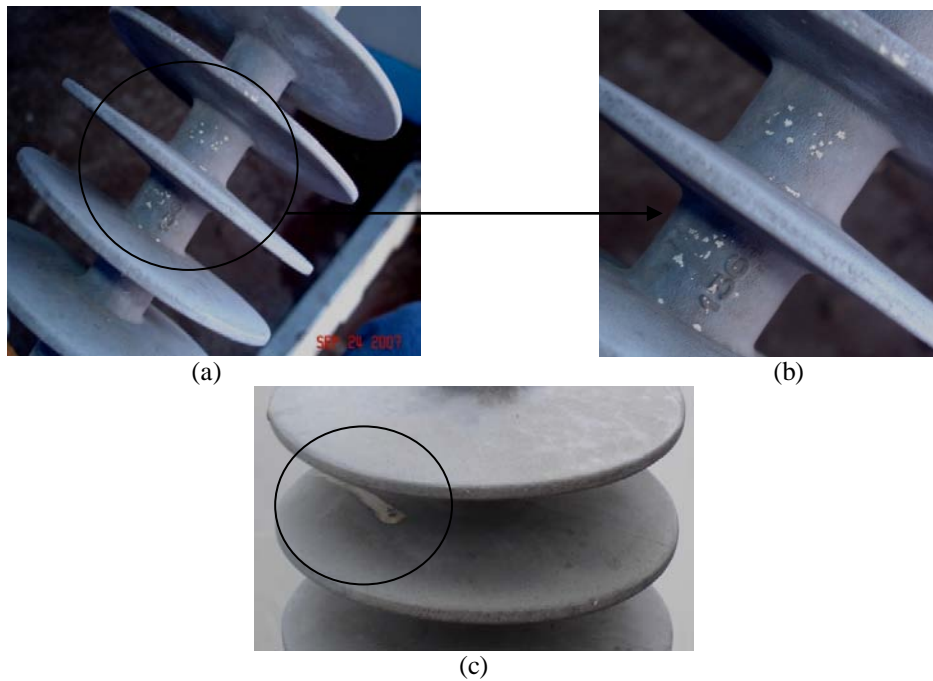


Figure 5.33 Pollution on the core on the red phase insulator bottom side and on the rims, (b) Close-up of the area, (c) Pollution on the second shed of the red phase insulator

Evidence of flashover was found in one insulator (See Figure 5.34). Two marks are located on the polymer / end fitting (North-East direction or R face) interface. No dry band arcs or corona activity can be visually identified. No corrosion in the end fittings was detected. No mechanical damage was observed.

No important changes, as found on Circuit I insulators, such as hydrophobicity recovery were found on Circuit II insulators surface.

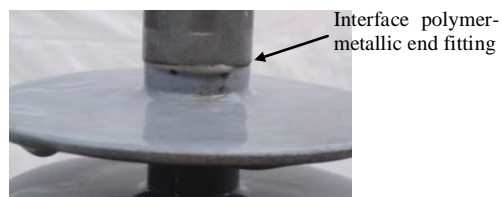


Figure 5.34 Possible evidence of flashover at the South-West facing end fitting

Circuit III

Pollution on this group of insulators differs from the one detected on the previous two groups; contaminant is ochre and sand-like. The deposition is also higher on the bottom side (See Figure 5.35). The hydrophobicity classification is HC7; all insulators are completely hydrophilic (Figure 5.35(b)).

Surface roughness seems less severe than in the previous insulators' groups and few sheds present undulation (Figure 5.36). A high level of corrosion and pollutant deposition (which cannot be removed) is on all the end-fittings covering the whole surface of them (Figure 5.36). Severe and dangerous erosion levels are observed on the seals covering the interface polymer housing/end-fitting compromising their function blocking against moisture ingress (See Figure 5.37). Pollution is deposited in such a way that there is cleaner ring around the rim (See Figure 5.38).

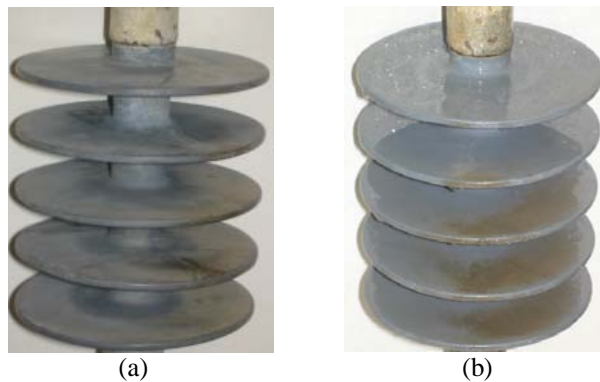


Figure 5.35 Ochre, sand-like contaminant at the bottom of the sheds; (a) dry conditions, (b) wet conditions



Figure 5.36 Undulations detected in some sheds close to the South side terminal; high level of corrosion on metal end-fittings



Figure 5.37 Severe erosion is detected in the interface polymer/end-fitting seals



Figure 5.38 Local pollution in one of the sheds. Contaminant deposition detail, a less polluted ring is surrounding the rim of the sheds

Circuit IV

The presence of biofilms on these insulators' surfaces is obvious as can be seen in Figure 5.39. Two insulators have a green layer of biofilm (Figure 5.39(a)) and over the other there are dark spots (Figure 5.39(b)). One of the insulators with a green layer also has bird droppings. Biofilms are mainly growing on ground facing part of the sheds and on the ground facing part of the core (See Figure 5.39 and Figure 5.40). Other pollutants are also present mainly on those surfaces.



Figure 5.39 Organic pollution deposition; (a) green biofilm layers and bird droppings, (b) darker spots

Insulators' surface is completely hydrophilic (See Figure 5.41) and the biofilms get easily wet when are sprayed.

Three additional things were also found: (1) there are some areas of the core between sheds where some kind of pollutant (similar to spider web) is retaining cow hairs on it (See Figure 5.42(a)); (2) there is a manufacturing misalignment between the metal of one end-fitting and the polymer housing which means mechanical forces are acting inappropriately and electric field enhancement will result (Figure 5.42(b)), and (3) the material quality of socket type end-fittings is different compared to the ones used on Circuit I insulators.

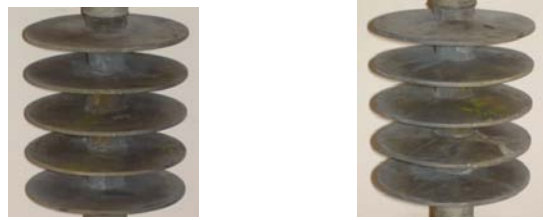


Figure 5.40 Biofilms on the sheds and core combined with other contaminants



Figure 5.41 Hydrophilic surfaces. Biofilms get completely wet



Figure 5.42 (a) Cow hairs on spider webs; (b) misalignment between metal end-fitting and polymer



Figure 5.43 Differences between end-fittings (a) Circuit IV; (b) Circuit I

Summary

Table 5.7 shows the main details detected during the visual inspections.

Table 5.7 Summary of the main visual conditions, deterioration and damage detected

Circuit I	Circuit II	Circuit III	Circuit IV
<ul style="list-style-type: none"> • Loss of hydrophobicity (HC7). A continuous water layer can be observed. • Non-uniform surface conditions. West face also presents dark rings around the core. • High level of roughness and higher pollution at the rim of the sheds. • Metal end fittings are not corroded. • The silicone seals look in good condition. No erosion detected. • High roughness - high pollution dispersed heterogeneously at the upper part and medium roughness – high pollution at the bottom. 	<ul style="list-style-type: none"> • High level of roughness and spots of pollution. • Loss of hydrophobicity (HC7). A continuous water layer can be observed. • End fittings are not corroded. • The silicone seals look in good condition. • No erosion is detected. • Some local contaminants can be observed. They can't be removed by washing. • High roughness - pollution dispersed almost homogeneously but different type on the upper and bottom part. 	<ul style="list-style-type: none"> • Loss of hydrophobicity (HC7). A continuous water layer can be observed. • Severe erosion and damage of the seals (mainly at the ground end fitting). • Metal end fittings (ground side) present high level of corrosion. • Shed undulations. • High level of salty sand pollution. • High roughness - high pollution dispersed heterogeneously on the ground facing side and medium roughness – high pollution at the upper part. 	<ul style="list-style-type: none"> • Loss of hydrophobicity (HC7). • Metal end fittings do not present any sign of corrosion. • The silicone seals look in good condition and no erosion is detected. • High level of roughness and spots of solid pollution. • Organic contaminant can be observed on the sheds on the bottom part of the insulators. • High roughness - pollution dispersed almost homogeneously but different type at the upper and lower surface.
<ul style="list-style-type: none"> • Through the day the direction solar irradiation is travelling along the longitude of the insulators, from the ball to the socket end fittings. The upper part of the sheds is more exposed to the solar influence than their bottom part. • Each insulator can be divided in four different polluted areas: East (or North East) face, West (or South West) face, bottom and top of the sheds. The severe polluted area is observed on the bottom of the insulators and the higher discoloration is observed on the upper part caused by higher exposure to UV radiation. • There are two manufacturer defects: defective seal in one Circuit I insulator, and misalignment between metal end fitting and polymer housing in one Circuit IV insulator. Both conditions affect the final performance. 			

STRI Visual Guide and Hydrophobicity Guide Application

As it was mentioned, the STRI Guide, 5, 2003 [43], ‘Guide for Visual Identification of Deterioration & Damage on Suspension Composite Insulators’ presents a very good list and images of the main ageing that can be directly observed mainly on transmission insulators. Following this deterioration and damage list, the items that can occur on distribution insulators were selected and shown on Table 5.8, in which is also included items from [44, 46].

Medium voltage insulator deterioration is mainly associated with stress factors generated by environmental conditions such as UV radiation, temperature, wind, fog, rain, pollution (for example, acid rain) and mechanical effects. Electrical stress is not a determinant factor because the electric field intensity is not high enough to produce discharges or dry band

arcs, and all the subsequent phenomena created by them. In consequence, all phenomena associated with high electric fields can be normally neglected.

Subsequently, on this last list, the ageing signs that were found on the EDF Energy 11 kV EPDM insulators have been marked.

Table 5.8. Insulators diagnosis using visual inspection (STRI Guides 1 and 5 [43, 44, 194, 195])

		STRI Guide 5 (2003) Visual ageing/failure process identification						MV Insulators	
		End Fitting	Fitting/Polymer interface	Sheath (Shank)	Shed	Shed/Shank interface	Core Rod	Distribution insulators can have	Recovered EDF 11 kV insulators have:
	Deterioration or damage								(4)
Deterioration	Chalking		✓	✓	✓			✓	
	Colour changes		✓	✓	✓	✓		✓	✓
	Crazing		✓	✓	✓	✓		✓	✓
	Flange corrosion	✓						✓	✓
	Grease leakage					✓			
	Light erosion		✓	✓	✓	✓		✓	✓
	Minor debonding		✓	✓	✓	✓			
	Minor Splitting/cutting		✓	✓	✓	✓		✓	
Damage	Core exposure	✓	✓	✓		✓		✓	
	Debonding			✓		✓			
	Erosion		✓	✓	✓			✓	
	Peeling		✓					✓	
	Power arc damage	✓	✓	✓	✓				
	Puncture		✓	✓	✓	✓		✓(non-electrical)	
	Splitting/Cutting		✓	✓	✓	✓		✓	
Tracking/Carbonizing		✓	✓	✓					
Mechanical Failure	Non-brittle fracture						✓	✓	
	Brittle fracture						✓		
Others ⁽¹⁾	Loss of hydrophobicity ⁽²⁾							✓	✓
	End fitting/polymer seal degradation ⁽³⁾							✓	✓

⁽¹⁾ Not included in the STRI Guide 5 but include in the STRI Guide 1.

⁽²⁾ Deterioration.

⁽³⁾ Failure [46].

⁽⁴⁾ Three manufacturing defects.

5.3.2. Dielectric Tests

Electric tests were conducted on the new sample and on all recovered insulators. Circuit assembly and procedures followed were adjusted as described in the IEC Standard 60-1 (High-Voltage Test Techniques - Part 1: General definitions and test requirements), and IEC Standard 60383-2 Insulators for Overhead Lines with a Nominal Voltage above 1,000 V - Part 2: Insulator strings and insulator sets for a.c. systems - Definitions, Test Methods and Acceptance Criteria). The tests performed were:

- AC 50 Hz flashover under dry conditions.
- AC 50 Hz flashover under wet conditions.
- Positive impulse voltage under wet conditions (1.2/50 μ seg)
- Leakage current under wet conditions.

General circuit arrangements are omitted since they are very well known. Figure 5.44 shows the final insulator arrangement to perform the electrical tests the results of which are summarized in Table 5.9. Values between brackets are the percentage obtained in reference with the values given in the insulators technical catalog (See Table 5.1). Values are the average between the three insulators recovered from each circuit.



Figure 5.44 Insulator arrangement for dielectric tests

Table 5.9 Dielectric Tests Results

Insulator	AC Flashover (Dry) (kV)	AC Flashover (Wet) (kV)	1.2/50 μ sec (Positive; wet) (kV)
New	95.8 (100%)	66.0 (100%)	133.6 (100%)
Circuit I	95.6 (100%)	43.2 (65%)	134.2 (100%)
Circuit II	78.6 (82%)	34.9 (47%)	127.5 (95%)
Circuit III	89.0 (93%)	59.8 (91%)	136.9 (100%)
Circuit IV	93.3 (97%)	37.4 (57%)	129.2 (97%)

Table 5.10 shows the magnitude, phase and main harmonics of leakage current. All values were estimated using the oscilloscope’s mathematic options. Only the insulators with the highest magnitude of leakage current of each circuit are reported here. Variations in the leakage current can be present as a consequence of changes of the water rate as a function of size of the samples.

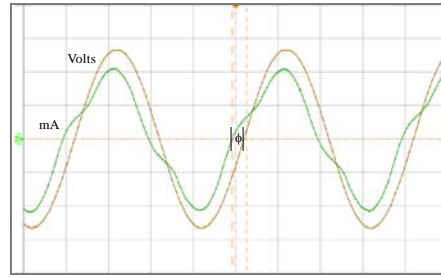


Figure 5.45 Example of the voltage (brown) and leakage current (green) waveforms taken (New insulator under wet conditions), Scales: V = 0.5 kV/div ($V_{\text{test}} \approx 1.8$ kV); I = 95 μ A/div

Table 5.10 Properties of leakage current under wet conditions

Insulator	$I_{\text{Resistive}}^{(2)}$ (mA)	Phase ($^{\circ}$)	3 rd harmonic ⁽³⁾	5 th harmonic ⁽³⁾
New	0.17	-27.0	0.82	0.69
Circuit I	1.94	-18.0	0.41	0.14
Circuit II	8.69	-2.2	0.34	0.26
Circuit III	5.34	-2.7	0.58	0.62
Circuit IV	3.84	-4.5	0.59	0.60

⁽¹⁾ At 1.8 kV approximately; ⁽²⁾ $I_{\text{Resistive}} = I_{\text{Total}} \cdot \cos(\text{Phase})$, $I_{\text{Total}} = \text{magnitude measured}$;

⁽³⁾ Proportion of harmonic to fundamental component.

Looking at the results it can be observed that under wet conditions all insulators present good impulse voltage performance but significant reduction of their properties under AC voltages. Circuit II insulators have the worst behaviour losing ~53% of the original flashover withstand voltage under wet conditions (but it is still ~5.5 times higher than the system's line-ground voltage) and ~20 % under dry conditions. Circuit III insulators present the best results losing less than 10% of the AC flashover voltage under dry and wet conditions. Circuit I insulators keep their properties under dry conditions and have a reduction of 35% under wet conditions.

Observing the leakage current behaviour, insulators of Circuit I have the lower active or resistive leakage current magnitude. It can be seen that insulators of Circuit II to IV have the leakage current in phase with the voltage and distortion and tends to be close to sinusoidal. This is caused by a continuous water layer on the insulator surface which shows a mainly resistive behaviour with minor local discharges. The new sample and the Circuit I insulators show capacitive and non-sinusoidal behaviour. This distortion is eliminated when the voltage is reduced. This is indicative of electrical discharges on the surface and it can be confirmed by the magnitude of the 3rd harmonics in both cases.

Leakage current behaviour is similar between insulators recovered from the same circuit except for those collected from Circuit II in which one of the three samples (pole R) presents approximately 10% more current magnitude than the other two (poles B and W). It can be also mentioned that high values of leakage current on Circuit III insulators could be caused by the high level of salty pollution and corrosion deposited on the end fittings which can be dissolved by the artificial rain increasing water conductivity running over the samples.

5.3.3. Dielectric Impedance

A summary of this technique is included here because its application is novel and does not follow the standardized type of samples and methodology. In this study, full insulators were tested under wet and dry conditions. Polymer insulator studies are focused on their performance under wet conditions considering that hydrophobicity loss will be reflected in dielectric characteristics such as leakage current, corona discharge activity, dry band arcs, withstand voltage, etc. This is even more relevant when pollution is also included.

Polymers' surfaces are relatively dynamic in comparison to porcelain and glass. Polymer molecules have much greater freedom for rearrangement in the bulk or at the surface. The relaxation time for a polymer surface to establish equilibrium with a new environment varies dramatically between different polymers and within a generic polymer system such as silicones [196].

Electrical characterization of materials, including polymers, has been performed using dielectric spectroscopy in which the impedance (Z) spectra give details about the dielectric dispersion of the complex permittivity of the material with frequency. Changes in a dielectric can be detected by evaluating the changes in its polarization and conduction phenomena (or dielectric mechanism) at different frequencies [197]. The dielectric properties of the polymers are due to electronic, ionic, molecular and interfacial polarization and are related with the physicochemical structure of the material [197, 198].

Studying of the relaxation processes of materials, nowadays between millihertz to terahertz, offers invaluable information about new materials' properties and diagnosis of degraded materials [127, 196, 199]. Traditionally, dielectric spectroscopy has been used to evaluate molecular motion or relaxation times in material samples, looking at the

phenomena as a process occurring in the bulk. Some applications using this technique to study material surface properties can also be found in the literature [200, 201]. Even though dielectric spectroscopy is particularly sensitive to small changes in the system and is non-destructive, it is normally applied on small specimens and not on whole pieces or complete equipment.

The applied AC voltage and the resultant AC current are measured and the complex impedance calculated ($Z^* = V/I$) at different frequencies. To obtain a response, electrodes are placed in contact with the sample and a sinusoidal voltage applied. This produces sample polarization and current circulation which has the same frequency but different phase and amplitude (Figure 5.46). By measuring the complex impedance and separating the real and imaginary terms, Z' and Z'' may be calculated and plotted (or its equivalent complex admittance, $Y^*=Y'+jY''$). These results then allow the permittivity (ϵ'), loss factor (ϵ''), dissipation factor (ϵ'' / ϵ') and ionic mobility ($\sigma = \epsilon_0\omega\epsilon''$) to be calculated when the geometry of the sample is regular (for example, discs, where area and thickness are known and the electric field is uniform). When the geometry is non-regular the values which can be determined are: impedance Z (complex value, Z' and Z'') and admittance Y (with Y' and Y''). These parameters relate to the dielectric measurement of materials giving information on molecular structure and dipole alignment [200, 201]. By studying the response of a system over a range of frequencies it is possible to analyze reaction mechanisms and material characteristics. Complex impedance can be presented on a Cole-Cole diagram by plotting the imaginary part (Z'') on the vertical axis and the real part (Z') on the horizontal axis with frequency as an independent parameter (Figure 5.47). A material that has a single relaxation frequency (known as Debye relaxation) will appear as a semicircle with its centre lying on the horizontal axis and the peak of the loss factor occurring at a relaxation time constant equal to τ^{-1} [with $\tau=1/(2\pi f_r)$ where f_r = relaxation frequency].

Parallel, series and combinations of RC circuit models can be used to describe the system behaviour. Phenomenologically, resistances represent the dissipative component of the dielectric response, while capacitances describe the storage component. A single RC parallel circuit is often an adequate model of polarization by charge migration where the resistance represents the overall loss and one capacitor can model the overall ability to

store charge by all polarization mechanisms [202]. Complex relaxation phenomena require more complex models. If regular geometries are used, the complex dielectric constant ($\epsilon^* = \epsilon' + j\epsilon''$) can also be calculated [203].



Figure 5.46 Impedance or admittance estimation

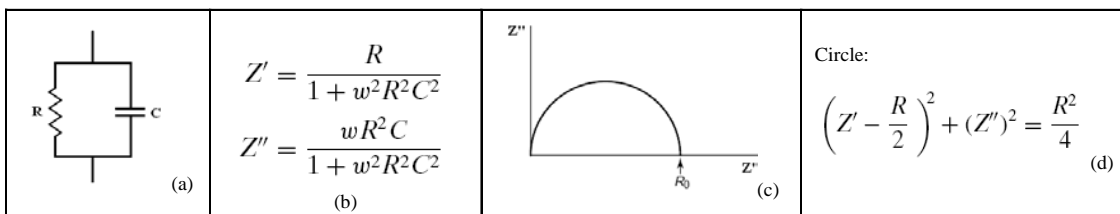


Figure 5.47 (a) Insulator’s RC parallel model; (b) Active and reactive components of the impedance; (c) Z' versus Z'' diagram (Cole-Cole plot); (d) Circle equation of the circle showed in (c)

In Figure 5.48 more complex Cole-Cole behaviours are shown. As is observed that while is relatively easy to collect data with this technique, their interpretation and analysis is not a straightforward task. The ‘tail’ observed is usually caused by interfaces, electrodes reactions like diffusion or parasitic couplings [203-205]. This behavior is typically detected when surfaces are studied (such as coated substrates, concrete surface degradation, enamel of teeth, biomaterial behaviors, open circuit potential electrodes).

Dielectric spectroscopy has proven to be a useful tool for studying the structure and the dynamics of polymers used as electrical insulation. Their dielectric properties are due to electronic, ionic, molecular and interfacial polarization and movement, associated with their physical and chemical structure [199, 202]. This technique has also been successfully used to diagnose polymer cables, transformers and, more recently, bushings and different measurement techniques have been implemented [207].

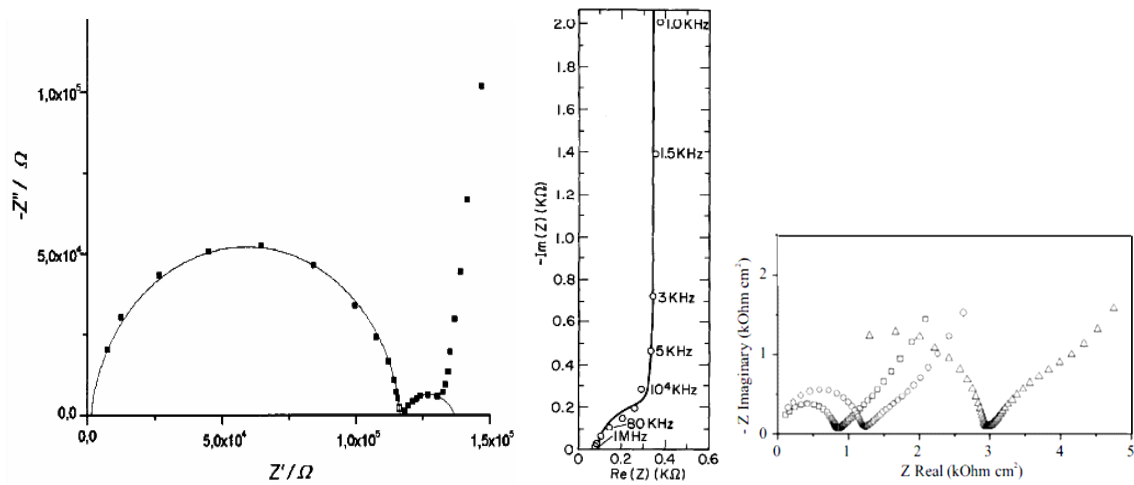


Figure 5.48 Cole-Cole plots of more complex dielectric behaviours [205, 206]

The main purpose of this test is to present a preliminary study of the feasibility of dielectric impedance testing to evaluate the surface condition of MV composite insulators aged under natural service conditions. Using different graphical representations initial results were evaluated to determine which one offers greatest sensitivity to small differences measured under dry and wet conditions (Z_{module} , reactance, dissipation factor and Cole-Cole plots were published in [208]).

Figure 5.49 shows the experimental arrangement used to test the samples. 15 kV was applied to the samples using an amplifier (Trek 20/20C) with a signal generator. Under dry conditions, eighteen frequencies, between 5 Hz and 25 kHz, were used and ten, between 5 Hz and 20 kHz, were applied under wet conditions. At frequencies higher than 25 kHz the supply cannot provide the value of the voltage required and at frequencies lower than 5 Hz the magnitude of the current is too small to be measured accurately. At frequencies above a few hundred kHz the parasitic impedances can also become important [198].

Detail in Figure 5.49 shows how insulators were connected, collecting leakage current. Magnitude and phase of voltage and current signals were measured at each frequency using an oscilloscope with megazoom and phase calculation option. Parasitic capacitances were avoided keeping prudent distances between the insulator and any object surrounding it. All changes in the system were minimized to reduce differences. Additionally, samples New and Circuit I-III were tested the same day. Circuit IV was unavoidably tested at a different time.

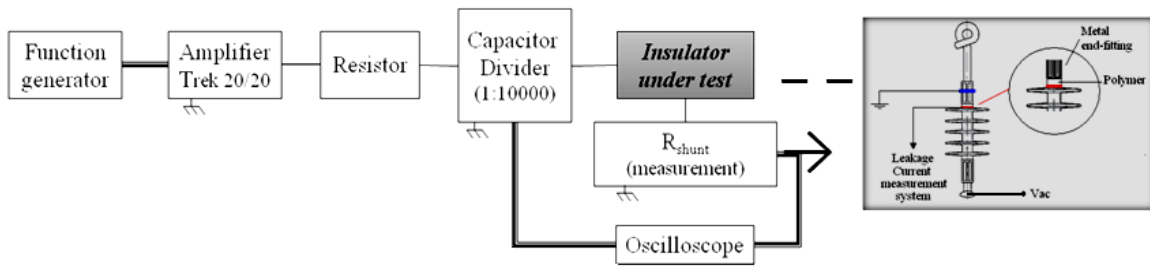


Figure 5.49 Impedance spectroscopy test system and sample connections

Experimental Procedure

An overview of the test regime is as follows:

- Leakage current and voltage waveforms were measured under dry and wet conditions.
- Voltage was applied over a range of frequencies. The values of frequency used under dry conditions were: 5, 10, 25, 50, 100, 150, 200, 250, 500 Hz, and 1, 1.5, 2, 2.5, 5, 10, 15, 20, 25 kHz. The values used under wet conditions were: 25, 50, 100, 250, 500 Hz, and 1, 2.5, 5, 10, 15, 20 kHz.
- Voltage was increased from zero to 1.8 kV.
- To test under wet conditions, tap water was sprayed on each insulator following the IEC-60060 recommendations: conductivity $<100 \Omega\cdot\text{m}$, pre-conditioning for 15 min and 3 ± 0.3 mm/min on vertical and horizontal water spray components.
- The insulators were changed carefully between tests, avoiding any alteration in the connections or system arrangement.

Results and Analysis

Different options to represent graphically the results were evaluated. Only a small representative group of them are presented here to show the feasibility of this technique to detect changes in the surface of polymeric insulators under dry test conditions, which constitutes the main goal of this test.

a) Total Impedance

Figure 5.50 and Figure 5.51 show the total impedance (module) of the new and aged insulators under dry and wet conditions, respectively.

For the new insulator an excellent fit to a power-law is found ($R^2_{\text{dry}} = 0.97$ and $R^2_{\text{wet}} = 0.98$) with a negative index ($\text{Index}_{\text{dry}} = -0.84$ and $\text{Index}_{\text{wet}} = -0.79$) indicates that the impedance is capacitive [127] as is expected for insulating materials. Comparing this with a simplified parallel model of dielectric materials (R in parallel with C), capacitive reactance module [$|X_c| = |-j \cdot 1/(\omega \cdot C)|$] tends to be reduced when frequency is increased and vice versa.

The total impedance value under dry conditions does not show significant differences between insulators. Only at 5 Hz does total impedance show slight differences but no substantial information can be extracted from this presentation of the results.

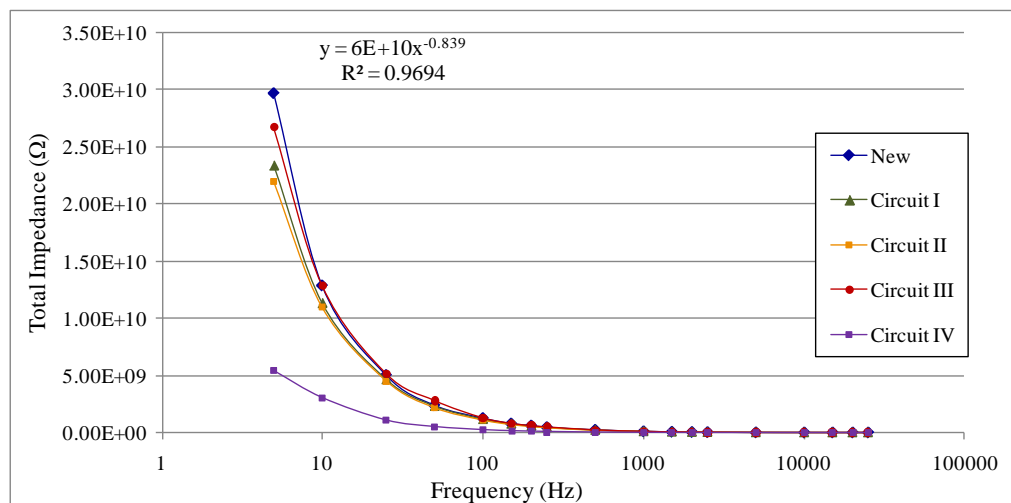


Figure 5.50 Total impedance under dry conditions

Under this frequency current magnitude is small and many factors could influence the measurement. This can be improved using an amplifier circuit but this solution will introduce other inconveniences that will be discussed later.

Under wet conditions Circuit I and Circuit II insulators present similar magnitude and 33.3% of reduction is observed between them and the unaged sample. Circuit III and IV

total impedance is more than two orders of magnitude smaller than the new sample and its capacitive behaviour is almost lost.

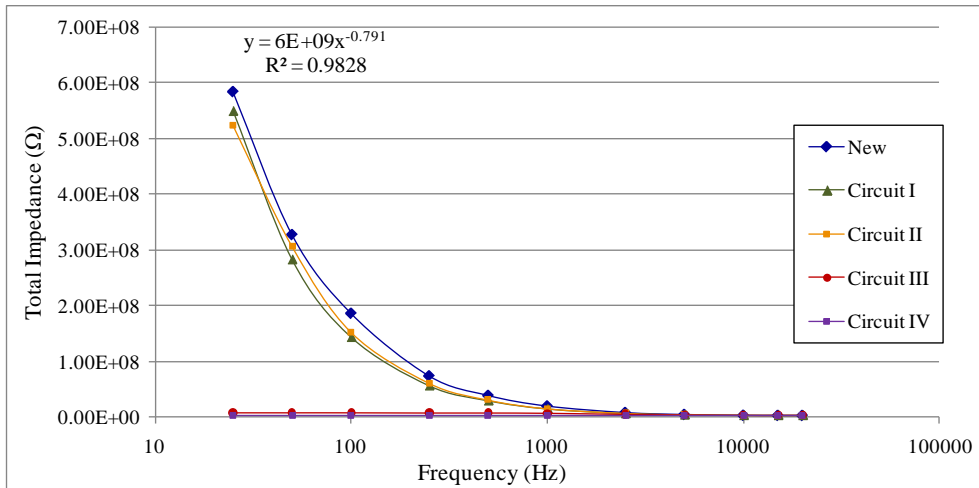
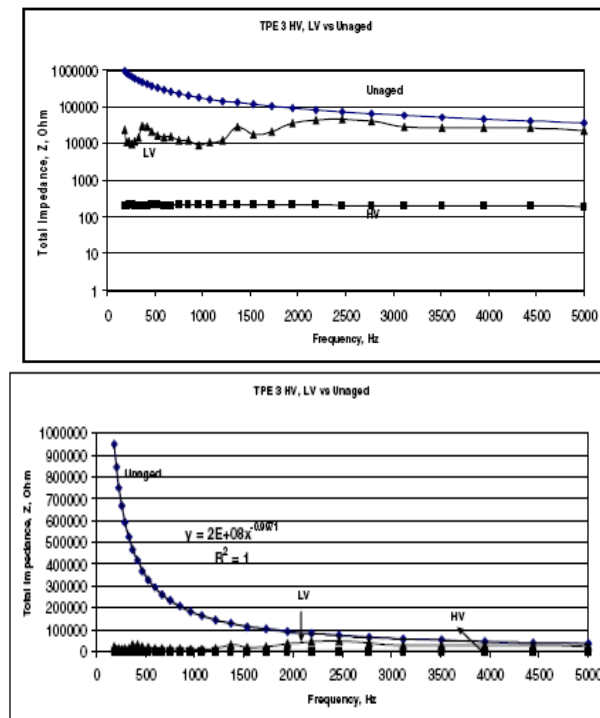


Figure 5.51 Total impedance under wet conditions

As described previously, insulators recovered from Circuit I and II were in service under similar environmental conditions but under different electric stress intensities and UV incident angle. Looking at these results Circuit III and IV insulators lost almost completely their impedance under wet conditions and higher leakage current circulates over them. These two groups of samples were under similar UV radiation than the other two but their pollution condition is very different. Circuit III was under severe salty pollution (a condition that does not allow biofilms to grow) and Circuit IV insulators developed organic pollution. This topic will be seen with more details during microscopy analysis.

In [127] values of total impedance versus frequency of one 28 kV thermoplastic elastomeric insulator, new and after degradation in a multistress chamber (UV, temperature, voltage and acid rain) are presented. They used an Autolab/PGSTAT30 impedance analyzer to evaluate samples cut from the insulator. The values presented by them are shown in Figure 5.52.



(LV and HV are measurements at the lower and higher voltage side of the sample)

Figure 5.52 Total impedance of 28 kV thermoplastic insulator, new and aged in laboratory

Figure 5.50 and Figure 5.51 to make an easier analysis with reference [127], two new views can be observed. As can be seen in Figure 5.53 and Figure 5.54 the dielectric behaviour is similar between cases and looking at frequencies less than 2.5 kHz differences between all the samples under wet conditions which allows ranking the samples from best to worst: new, Circuit I and II, Circuit III and Circuit IV.

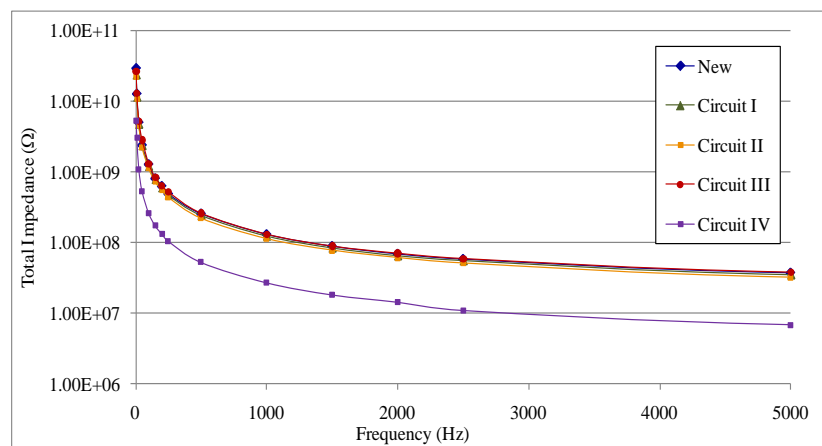


Figure 5.53 Total impedance under dry conditions using lineal axes

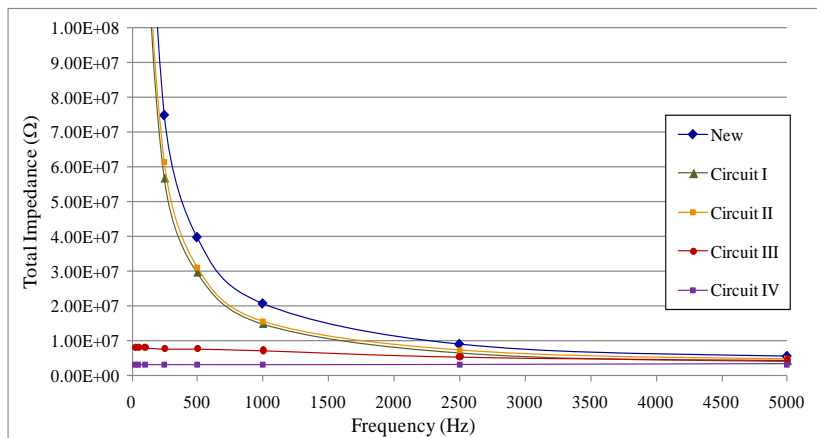


Figure 5.54 Total impedance under wet conditions using lineal axes

b) Cole-Cole Plots using Reactance versus Resistance

As in the previous case, only some cases are included. Having in mind the major objective of finding a technique that can identify degradation or ageing levels on polymer insulator surfaces under dry conditions, all the examples included here are plots under dry conditions.

The Cole-Cole representation is based on imaginary versus real impedance plots, often referred to as Nyquist plots [8]. Figure 5.55 and Figure 5.56 presents Cole-Cole plots for the insulators under test. It is evident that the aged samples response requires a more complex representation than a semicircle offered by a parallel RC model or Debye relaxation. Only some cases are included here to show the results in the form of Cole-Cole plots and evaluate them as an option to compare full samples of insulators.

Looking at the literature, similar behaviour can be found in [203, 204] and third or fourth order circuits are used to represent it. Such behaviour is often observed in many systems presenting interfacial layers [196]. Low frequency relaxation observed is often correlated with interfacial phenomena, as observed in systems with contact layers or metal-coated thin films [196]. This behaviour could be related to different external factors surrounding the circuit system and also the electrodes and connections used. It could be good practice to shield the insulator with an Aluminum tube to reduce interference [207]. Different publications fit the behaviour to a semicircle for high frequencies; followed by a tail for

low frequencies values, but normally all points can be fit using general linear regression. Having in mind that capacitive-resistive behaviour of dielectrics follows semicircle or partial semicircles, a general linear representation should not be used.

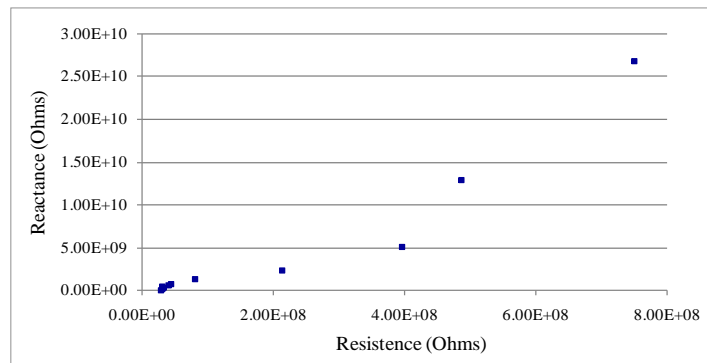


Figure 5.55 Cole-Cole Plots (Impedance: Reactance versus Resistance) of new insulator

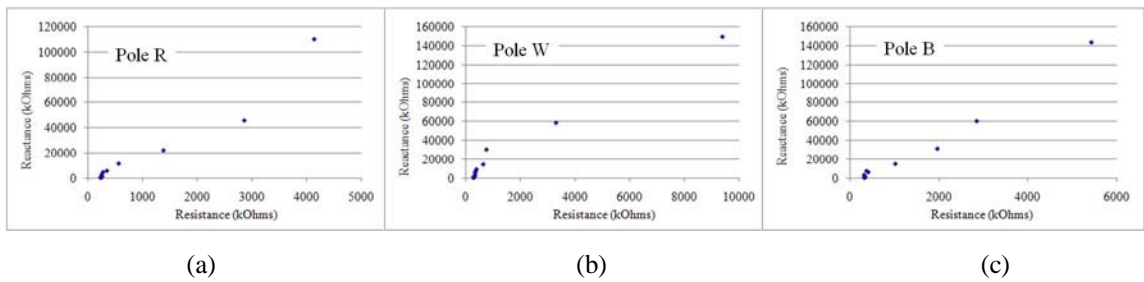


Figure 5.56 Cole-Cole Plots (Impedance: Reactance versus Resistance) of the three insulators recovered on location II (poles R, W and B)

c) Cole-Cole Plots using Susceptance versus Admittance

In Figure 5.57 the difference between dry and wet of new insulator can be seen.

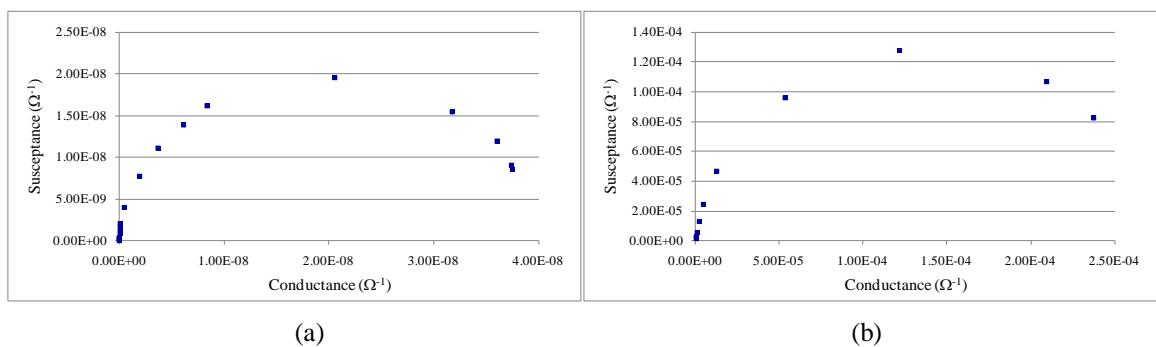


Figure 5.57 Cole-Cole Plots (Admittance: susceptance versus conductance) of new insulator, (a) Dry, (b) Wet conditions

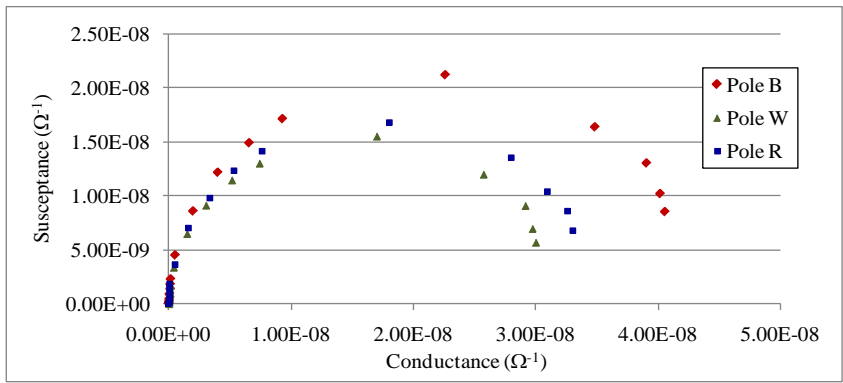


Figure 5.58 Cole-Cole Plot (Admittance: susceptance versus conductance) of three insulators, poles R, W and B, recovered from location II (named Circuit II insulators) under dry conditions

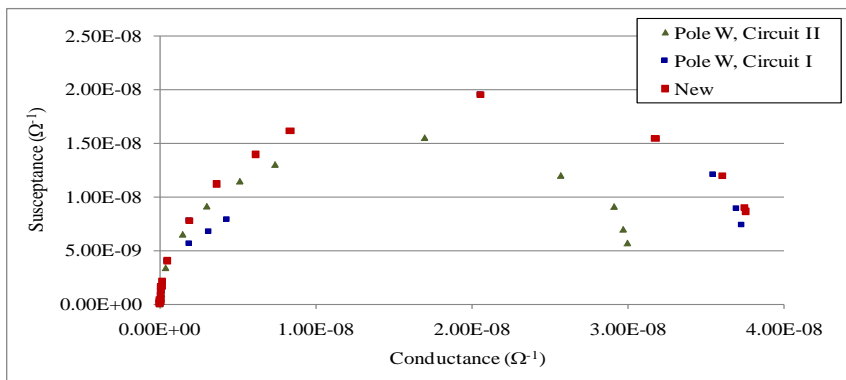


Figure 5.59 Cole-Cole Plots (Admittance: susceptance versus conductance) of insulators recovered from Circuit I, Circuit II and their comparison with new insulator under dry conditions

It is noticeable that with Cole-Cole plots, aged samples under dry conditions show variations in comparison with the new sample that cannot be observed looking at the impedance module (Z_{total}) or even dissipation factor values. This could mean that Cole-Cole plots might be a very good representation of the measured complex impedance to detect changes on insulator surface under dry conditions that other evaluations cannot match.

d) Model Regressions

References in the literature present numerical methods to find circuit model parameters [204, 209, 210]. In particular, [205, 211-213] were used as a base to make a regression program (Matlab) using a complex nonlinear least square fittings, and subsequently confirm its results with examples published in these references. A graphical fitting approach was also applied to review some of the parameter found [205].

To have a starting point of the values for the models, values of C and R were obtained testing the insulators with a Schering Bridge (AC 50Hz). Values are shown in Table 5.11. As can be observed, two different measures were performed: (1) using the connection describe in Figure 5.49, and (2) using the typical connection collecting the total current to ground. With this the influence of the connection is demonstrated.

Table 5.11 Values of capacitance and resistance using Schering Bridge

Insulator	Type of measurement	C (F)	tan δ	R (Ω)
New	Total ⁽¹⁾	2.15E-12	4.00E-03	5.92E+06
	Only sup ⁽²⁾	1.30E-12	4.00E-03	9.79E+06
Circuit I	Total	2.18E-12	2.00E-03	2.92E+06
	Only sup	1.39E-12	2.00E-03	4.58E+06
Circuit II	Total	2.19E-12	6.00E-03	8.72E+06
	Only sup	1.35E-12	7.00E-03	1.65E+07
Circuit III	Total	2.12E-12	9.00E-03	1.35E+07
	Only sup	1.39E-12	1.20E-02	2.75E+07
Circuit IV	Total	2.13E-12	7.00E-03	1.05E+07
	Only sup	1.30E-12	8.00E-03	1.96E+07

⁽¹⁾Total includes volumetric current; ⁽²⁾Only surface current.

 Table 5.12 Values of the parameter R [Ω], C [F], obtained from the dielectric spectroscopy test

	Model: R and C in series		Model: R and C in parallel		Model: R2 in series with R1//C1		
	R1	C1	R1'	C1'	R1	C1	R2
New Dry I	1.25E+08	1.35E-12	6.75E+07	1.35E-08	7.57E+07	1.35E-08	7.19E+03
New Wet I	2.14E+07	1.07E-11	2.98E+05	1.03E-07	3.24E+05	1.04E-07	7.67E+02
Circuit I Dry	8.56E+07	1.39E-12	1.63E+07	1.39E-07	2.20E+07	1.39E-07	6.82E+02
Circuit II Dry	1.03E+08	1.19E-12	4.66E+07	1.87E-07	4.71E+09	1.87E-07	4.97E+02
Circuit III Dry	9.75E+07	1.14E-12	4.75E+07	1.14E-07	4.75E+07	1.14E-07	8.87E-09
Circuit IV Dry	5.83E+06	5.58E-12	3.31E+08	5.59E-08	1.22E+09	5.59E-08	5.65E+02
Insulator BII Dry	6.98E+07	1.45E-12	4.41E+07	1.45E-07	1.83E+08	1.45E-07	6.79E+02
Insulator RII Dry	1.51E+08	1.10E-12	7.68E+06	1.10E-07	8.43E+06	1.10E-07	7.90E+02
Insulator WII Dry	9.01E+07	1.10E-12	5.90E+07	1.10E-07	2.53E+08	1.10E-07	8.78E+02
Insulator BIV Dry	2.27E+06	5.72E-12	6.66E+12	5.72E-08	6.74E+02	2.78E-08	9.71E+02
Insulator RIV Dry	1.14E+07	5.75E-12	4.02E+11	5.40E-08	2.52E+19	5.40E-08	3.75E+02
Insulator WIV Dry	3.74E+06	5.39E-12	1.08E+08	5.65E-08	1.94E+08	5.65E-08	1.03E+03

Comparing the values of C obtained using the Schering Bridge with the ones found by regression they are almost identical with the ones found using the model with C and R in series, except for the Circuit IV values. They have a proportion of 1:5. Two things can be noticed: (1) Circuit IV was tested few months after the others; and (2) Circuit IV insulators seem to be different to the others including the end fitting quality. It could be indicative of any change in manufacturing formulation (even though with the Schering Bridge value at

50 Hz is equivalent with the other samples) or caused by the biofilm growth (even though this can be more reflected by R). Additional testing is required.

Although there is very good agreement between the measures and the regression of the three models presented (additional model with R2 in series with R1//C1 was also found but the correlation was not as good as the others shown in Table 5.12), the model analyzed here is C in series with R because of its simplicity to make the comparison between samples. The main reason of this is that the values of C are almost the same between samples (except Circuit IV, as it was mentioned) making it possible to review only the value of R.

e) Dielectric Impedance of Two New Insulators made using Different Formulations

This additional test was performed on two 33 kV new silicon rubber insulators of which the original material formulation characterization is well known and the geometrical design and dimensions are exactly the same. The main difference between these two materials is conductivity. Looking at the Figure 5.60 the difference between the resistance behaviour is evident for frequencies lower than 250 Hz. The highest rate of resistance increment occurs between 25-50 Hz for the material A and between 100-250 Hz for insulator with material B. Above 250 Hz both materials behave in a similar way. This result allows the inference that dielectric impedance could be used to detect changes in the polymer formulation.

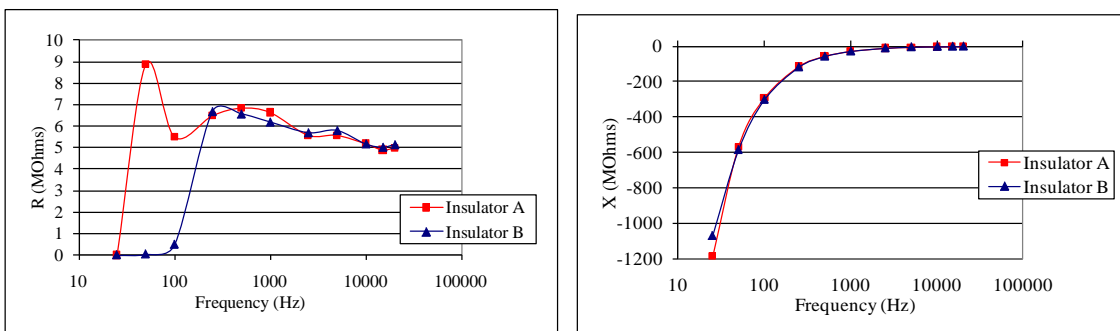


Figure 5.60 Resistance and Reactance versus frequency of two identical new insulators with two different formulations

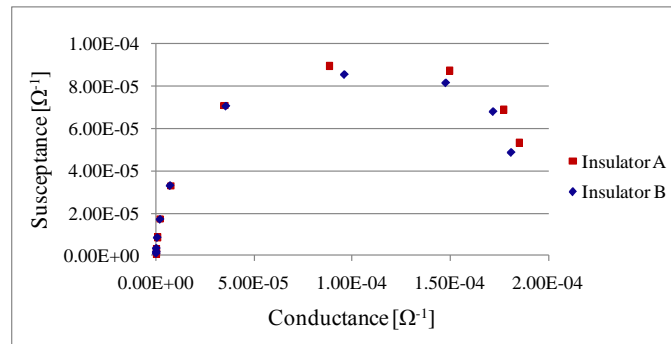


Figure 5.61 Cole-Cole of two identical new insulators with two different formulations

5.4. Diagnostic Tests and Results from Small Samples from Insulators

The previous tests done on full samples do not offer information about specific differences on local conditions observed along insulators' surfaces. Figure 5.62 shows the areas with asymmetrical conditions along the insulators where small samples were cut to perform: (1) Fourier Infrared spectrums, microscopy, roughness and static contact angle analysis.

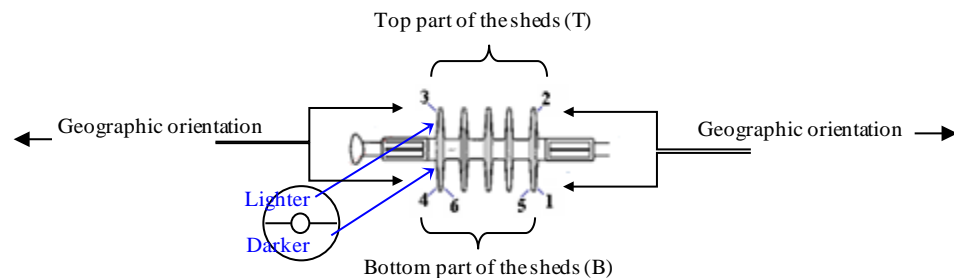


Figure 5.62 Areas for the asymmetrical conditions study

Specific three letters nomenclature is established for each position numbered 1 to 6 keeping a full description of the sample, as follows: X Y W, where X is I, II, III or IV, which is the Roman number circuit identification; Y is dark (bottom) or light (top) side of the insulator, and W is the geographical orientation side faced by each specimen (See Figure 5.7).

5.4.1. Infrared Spectroscopy (FTIR) Spectrums Analysis

Analysis of the FTIR spectrums confirms that the degradation process of the insulators under study is highly non-uniform, changing rotationally and longitudinally. The highest

reduction of intensities at 2919 and 2849 cm^{-1} (CH_2 asymmetric stretch and CH_2 symmetric stretch, respectively) [5] occurred on the darker (lower) part of the Circuit I insulators and on the lighter (upper) part of the Circuit II to Circuit IV insulators. This reduction is higher than 50% (Figure 5.63). Thus, ageing decomposed a significant group of methyl bonds on the UV exposed surface of the upper part of the sheds and it is possible that acids are acting in a more severe way on the bottom part of the Circuit I insulators than UV radiation on the upper part.

Looking at the reduction average at 2849 and 2920 cm^{-1} of each insulator, Circuit II samples present a lower loss of CH_2 bonds. This might explain the lower magnitude of leakage current and might be caused by less direct solar radiation and less exposure to salty pollution. At 970 cm^{-1} (out of plane CH bend) [95] the reduction is not significant in any evaluated zone of any of group of insulators.

EPDM surfaces react with moisture, and the alumina filler is reduced to form hydroxyl bonds [95] that can be detected with peaks at 3370-3620 cm^{-1} . Changes were found higher than 50% in these bands at the darker region of Circuit II insulators and in the lighter part of Circuit I samples.

The alumina fillers ($\text{Al}_2\text{O}_3 \cdot 3\text{H}_2\text{O}$) in the 1015 cm^{-1} band significantly increase on the whole group of insulators. For Circuit I insulators, an approximate 80% increase is seen on the darker side with higher variation at the East face (~100%) and 160% on the lighter side of both faces. Insulators of Circuit II present an increase of 150% on the darker faces and on the lighter South West face and only 80% of variation on the North East face. Circuit III insulators present different values at the each face of the bottom and at the upper part, with the higher increment on the West face of the darker part (~100%) and on the East face of the lighter part (~160%). Variations on Circuit IV are more uniform between area; the lighter one facing North the one with smaller increment (~40%), and the darker one facing South the one with the highest (~140%).

This provides evidence that the insulators' surfaces are covered by inert material originating from the filler (the concentration of aluminium is high) and this may be the major cause for the surface becoming hydrophilic [136]. Biofilm presence on Circuit IV insulators does not introduce any particular changes on FTIR spectrums.

These main changes to the FTIR spectrums suggest that the oxidation and ageing of the insulator surfaces is a non-uniform process and will be due to a combination of the environmental conditions acting synergistically. Sun radiation incidence, pollution type and amount, natural washing (rain and wind conditions) are changing locally and their combination is highly non-uniform. Additional physicochemical tests can give further information to explain this particular condition.

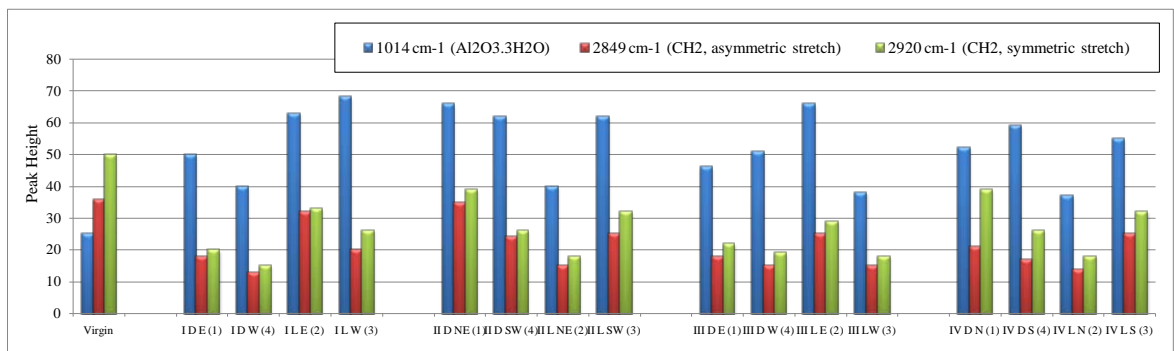


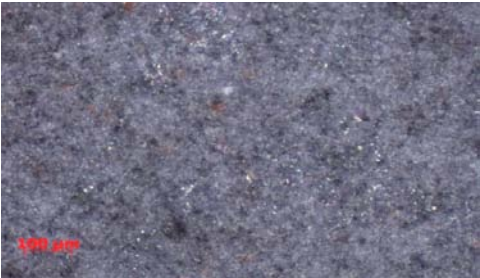
Figure 5.63 Changes in hydrocarbons groups and in alumina fillers along the insulators

5.4.2. Surface Microscopy, Roughness and Static Contact Angles

Optical Microscopy and Roughness Estimation

Microscopy images were taken from samples. These were the same samples used to determine the FTIR spectrums. In this study, 3D parameters are obtained by averaging 2D parameters recorded on different profile layers using the best automatic adjustment given by the microscope. The surface measurement software includes calculation of roughness parameters. 2D parameters are set by international standards [214]. The following values were directly determined:

- Average roughness R_a , is the arithmetic average of all departures of the roughness profile from the centre line within the evaluation length l_m ,
- Average roughness R_q is the geometric average of all departures of the roughness profile from the centre line within the evaluation length l_m ,
- Total height of profile or maximum roughness depth R_t (peak to valley height) is the vertical distance between the highest peak and the lowest valley of the roughness profile from the centre line within the evaluation length l_m .



Nomenclature:
X Y W
X: Circuit Roman number identification (I-IV)
Y: Dark (bottom) or light (top) side of the insulator
W: which geographical side is facing

Figure 5.64 New insulator surface detail



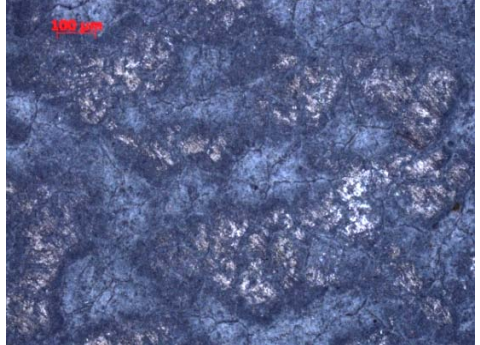
ID E



ID W



IL E



IL W

Figure 5.65 Surface of Circuit I insulator samples

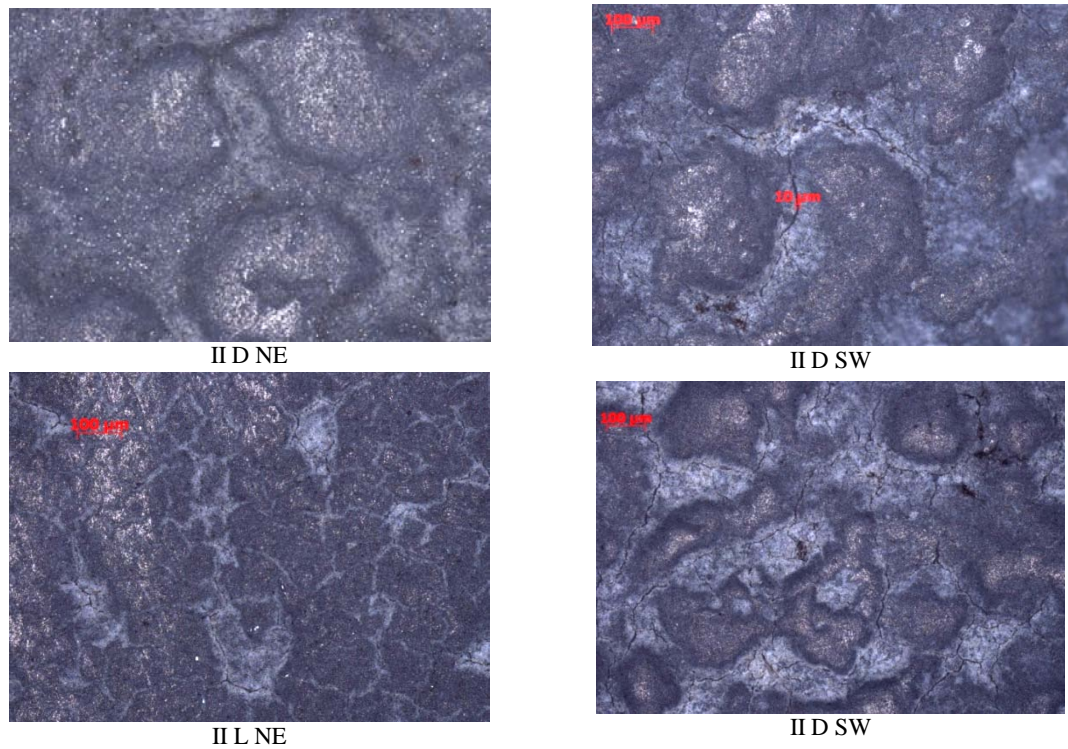


Figure 5.66 Surface of Circuit II insulator samples

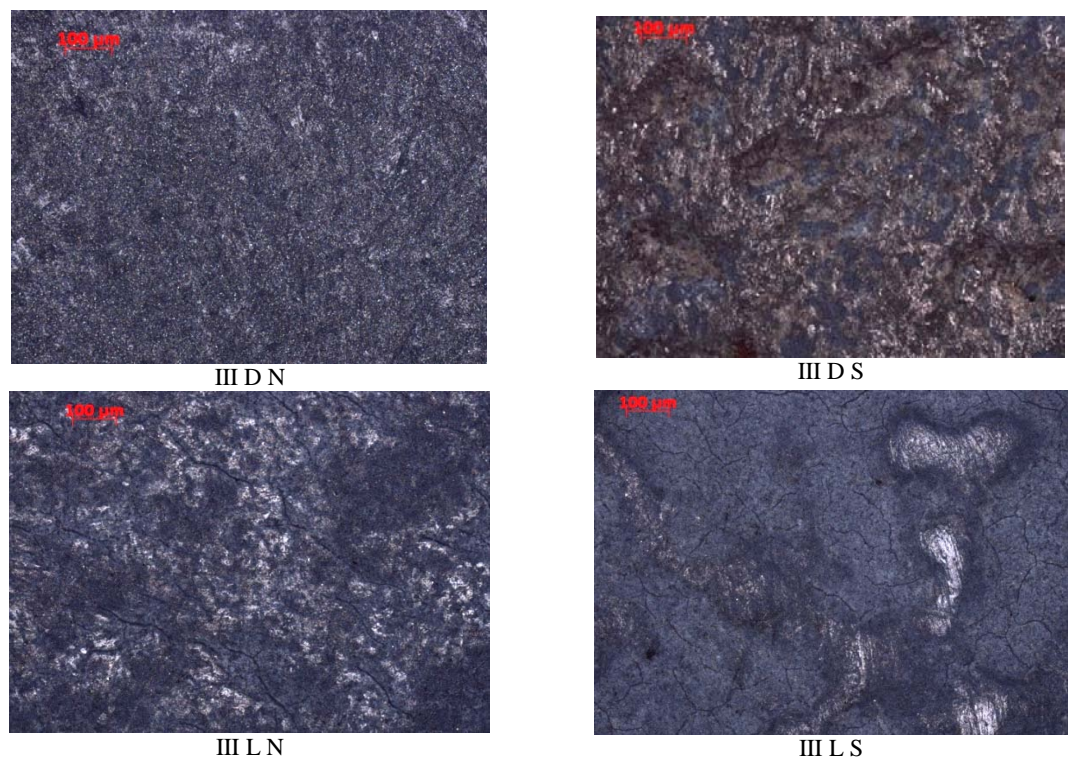


Figure 5.67 Surface of Circuit III insulator samples

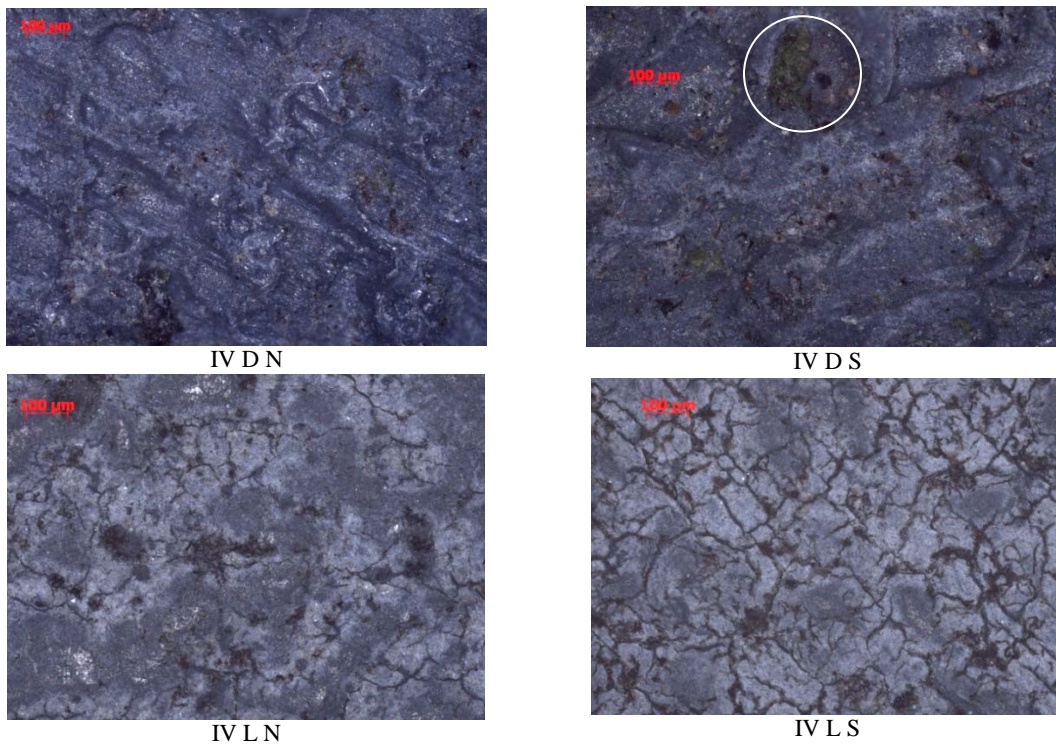


Figure 5.68 Surface of Circuit IV insulator samples

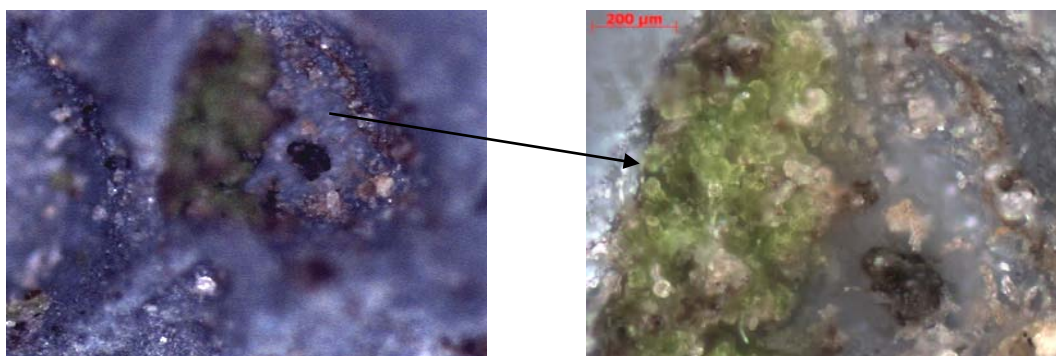


Figure 5.69 Close up of the circled area in the Figure 5.68, IV D S sample

Figure 5.70 to Figure 5.72 show the most important values used to define the surface profile of the samples: roughness arithmetic average, R_a , depth of greatest valleys (V_h) and peaks (P_h) and total height of profile ($T_h = P_h + V_h$).

The main information that can be extracted is: (1) roughness on new material is smaller than on aged samples; (2) changes on darker areas are higher than on lighter ones; (3) highest values are on Circuit IV insulators' darker side and the maximum is on the sample facing South increasing approximately 280% over new condition; and (4) the insulator samples with smaller changes are on Circuit I, followed by very similar behavior between Circuit II and III, and Circuit IV with the biggest changes.

Looking at the Figure 5.71(a) and Figure 5.71(b) differences between darker and lighter, and also under geographical orientation influence, can be easier visualized in more detail: (1) as was previously mentioned, darker areas have higher roughness than lighter; (2) at the same time, all samples facing South, South-West and East present the highest roughness, excepting Circuit I samples, (3) those facing North, North-East and West have values very similar between Circuit I, II and III samples independently of whether they are in lighter or darker areas, and samples collected from Circuit IV darker parts have the highest values independently of which side they are facing.

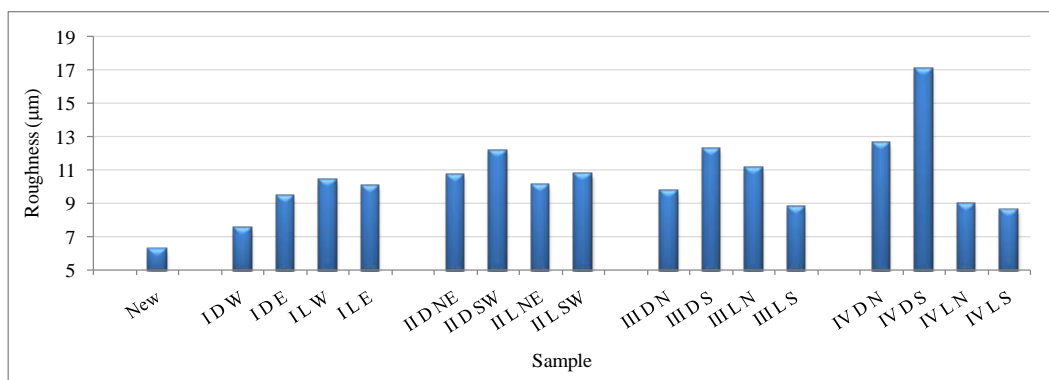
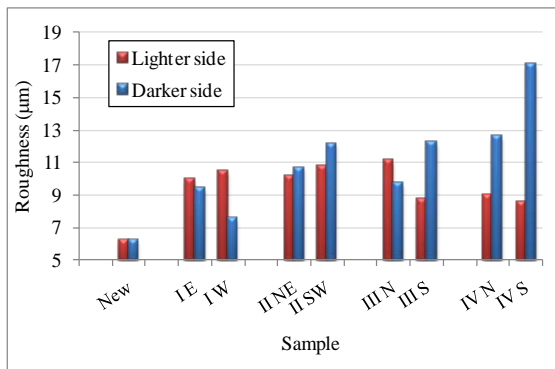
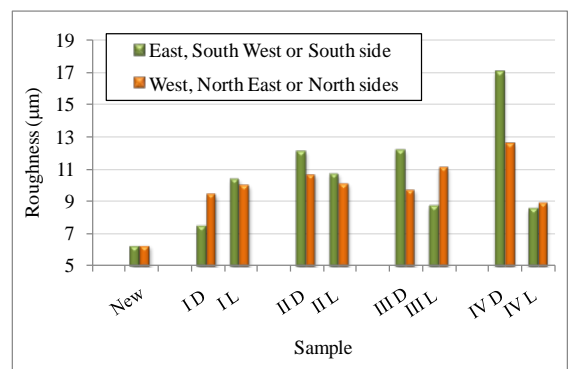


Figure 5.70 Roughness arithmetic mean, Ra [µm]



(a)



(b)

Figure 5.71 Roughness arithmetic mean focusing the differences between (a) lighter-top and darker bottom side of the insulators; (b) geographical orientation

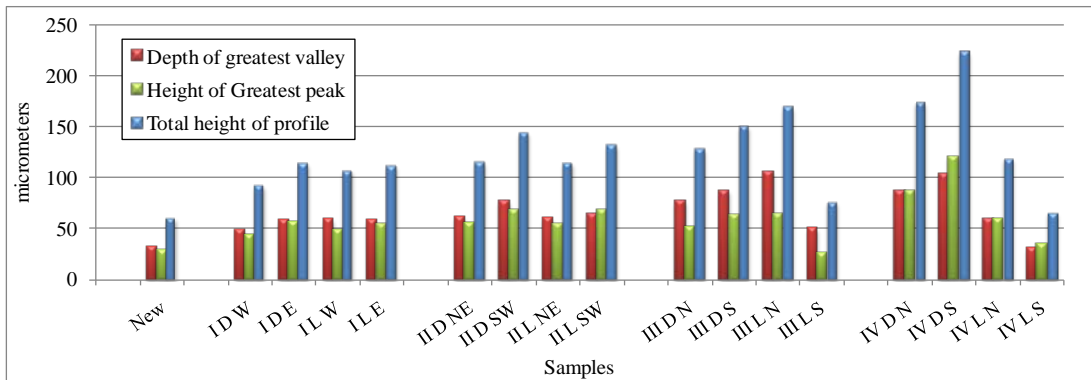


Figure 5.72 Profile: depth of greatest valleys (V_h) and peaks (P_h) and total height of profile ($T_h = P_h + V_h$)

Figure 5.72 shows the greatest valleys (V_h) and peaks (P_h), and total height of profile ($T_h = P_h + V_h$). Circuit IV also has the highest heights on the profile and the greatest peaks, although the valleys are similar to the other samples. This could be a consequence of biofilm presence, as can be observed in the Figure 5.69.

Static Contact Angle (Sessile Drop Method)

The equilibrium or static contact angle θ_s , was measured using a sessile drop of distilled water placed on the sample. The drop volume was about 10 μ l and the software used was the ImageJ. The results are shown on Figure 5.73.

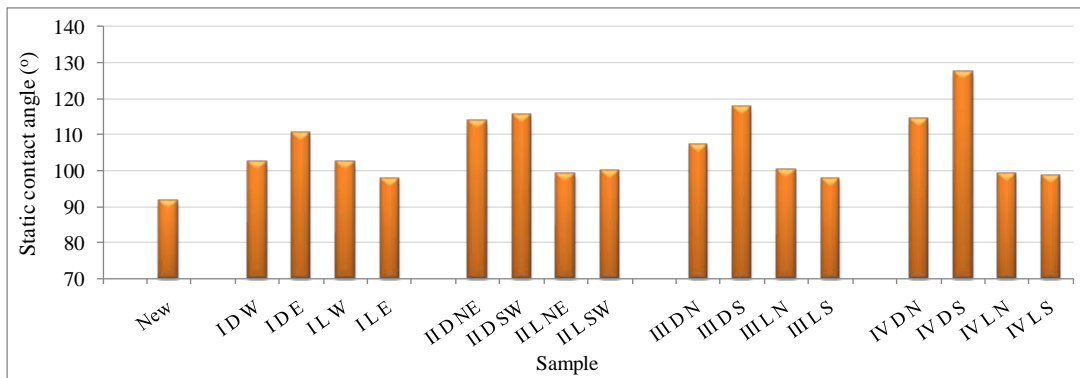


Figure 5.73 Static contact angle, SCA (sessile drop method)

The main information that can be extracted is: (1) static contact angle (SCA) on new material is smaller than on aged samples; (2) changes on darker areas are higher than on lighter ones; (3) the highest values are on Circuit IV insulators’ darker side and the maximum is on the sample facing South increasing 40% over the new condition; (4) lighter samples tend to have a similar value of static contact angle which is approximately

10% higher than new, and (5) the insulator's samples with smaller changes are on Circuit I, followed by very similar behavior between Circuit II and III, and Circuit IV with the biggest changes.

Static Contact Angle / Roughness Relation

In order to assess surface roughness effects on static contact angles, Figure 5.74 shows all the data obtained for the whole group of samples evaluated. A linear relation between both properties is found with correlation of 0.71 a gradient equal to 3.35.

Looking closely at the points, a difference between data located on darker areas versus data found on lighter areas is clear following different linear tendencies, as can be observed on Figure 5.75. Higher scatter is presented in measures collected from samples on lighter regions, having correlation equal to $R^2 = 0.75$ and a gradient equal to 1.91. Much better correlation, equal to 0.9, is observed in values obtained for darker areas and a gradient of 3.1.

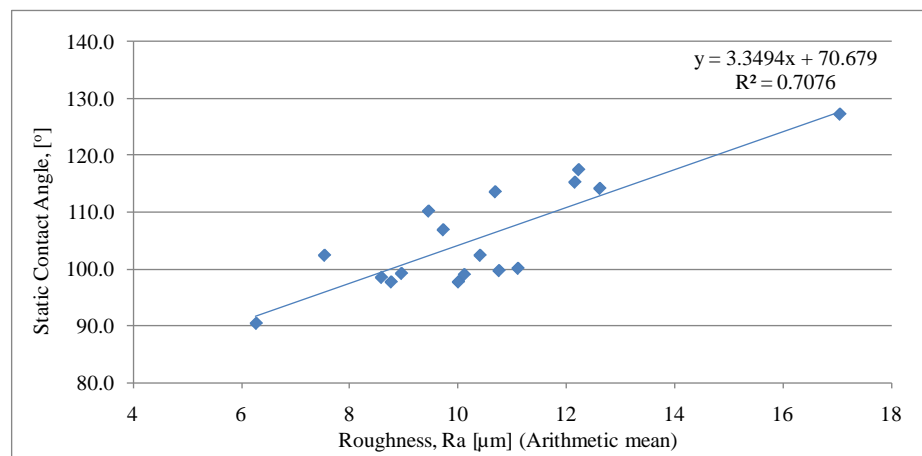


Figure 5.74 Static contact angle variation versus surface roughness

This shows that is possible to obtain a relation between roughness and static contact angle taking into account the different ageing factors acting on the polymer surface. Changes on the gradient could indicate that roughness-static contact angle relationship depends on which is the dominant stress during the ageing process.

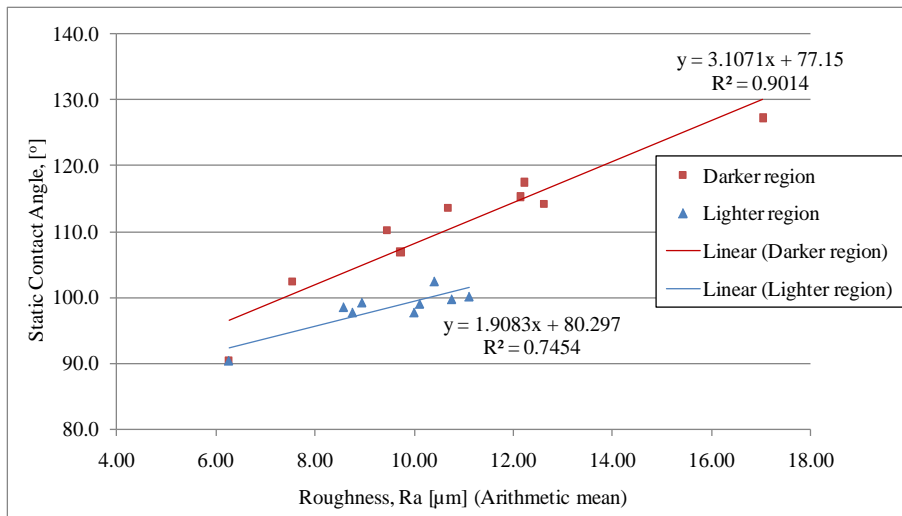


Figure 5.75 Static contact angle variation versus surface roughness considering sky-facing and ground-facing surfaces

Considering the results shown in Figure 5.75 it is important to notice two different conditions: (1) the range of variation strongly differs between data collected from samples on darker areas ($\Delta Ra_{\text{darker}} = \sim 11\mu\text{m}$ and $\Delta SCA_{\text{darker}} = \sim 40^\circ$) and the ones collected from the lighter ($\Delta Ra_{\text{lighter}} = \sim 5\mu\text{m}$ and $\Delta SCA_{\text{lighter}} = \sim 10^\circ$), and (2) the gradient is 60% higher in the first case as well. It can be inferred that all insulators are similarly degraded by UV radiation and pollution is naturally washed before high deposition takes place. Under this condition, changes in roughness tend to be uniform and similar between samples. On the contrary, at the bottom, the amount of pollution attached to the surface determines the final result of roughness degree and different kinds of contaminants produce different surface profiles.

A lineal relationship between static contact angle and roughness for silicon rubber specimens degraded in laboratory was presented in [215] having lower values of roughness and higher contact angles. In [216] an inverse power relationship between roughness and HC hydrophobicity classification was proposed for transmission insulators removed from service.

Variation of static contact angle along sheds (close to the core, middle and close to the rim) was also measured (Figure 5.76). Differences between the darker and lighter sides, and geographical orientation influence were established.

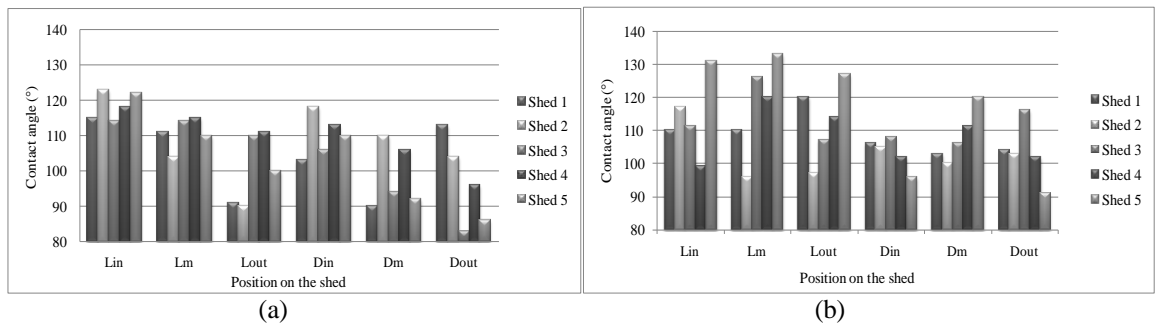


Figure 5.76 Static contact angle values, insulator Circuit I, (a) surface facing North, (b) surface facing South

5.4.3. Ranking of Insulators Condition. Summary

With the aim of ranking the degradation between the four groups of insulators and having in mind the conditions presented in the Table 5.13 and the full reports [217-219], a qualitative scale can be made to show which groups of insulators lost more/less qualities or properties. These valuations are showed in the Table 5.3.

Table 5.13 Severity of service condition, loss of properties and degradation level

	Circuit I	Circuit II	Circuit III	Circuit IV
Time in service	✓✓	✓✓	✓✓	✓✓
Electric field		✓	✓	✓
UV radiation intensity	✓✓	✓✓	✓✓✓	✓✓✓
Loss of Hydrophobicity	✓✓✓✓	✓✓✓✓	✓✓✓✓	✓✓✓✓
Deposited pollution	✓✓	✓✓✓	✓✓✓✓	✓✓✓
Organic pollution	✓	✓✓		✓✓✓
Colour changes	✓✓✓	✓✓✓	✓✓	✓✓✓
Roughness increment	✓✓✓	✓✓✓	✓✓	✓✓✓
Shed undulations	✓	✓✓	✓✓	✓✓
Hydrocarbons Groups/ broken bonds	✓✓✓✓	✓✓✓	✓✓✓✓	✓✓✓✓
Loss of alumina fillers	✓✓✓✓	✓✓✓	✓✓✓✓	✓✓✓✓
Damage of seals			✓✓✓✓	
Metal end fitting corrosion			✓✓✓✓	
Loss of Dielectric Performance:				
AC Flashover (Dry, kV)		✓✓	✓	
AC Flashover (Wet, kV)	✓✓	✓✓✓✓	✓	✓✓✓
Impulse 1.2/50 (µsec)				
Leakage Current Magnitude (mA)	✓	✓✓	✓✓✓	✓✓✓✓
Voltage/Current Phase (°)	✓	✓✓✓✓	✓✓✓✓	✓✓✓

Less: ✓..... More: ✓✓✓✓✓; Better: ✓..... Worst: ✓✓✓✓✓.

As an example of how to use the aging state estimator proposed on chapter 3, insulators from Circuit II and IV are compared on Figure 5.77.

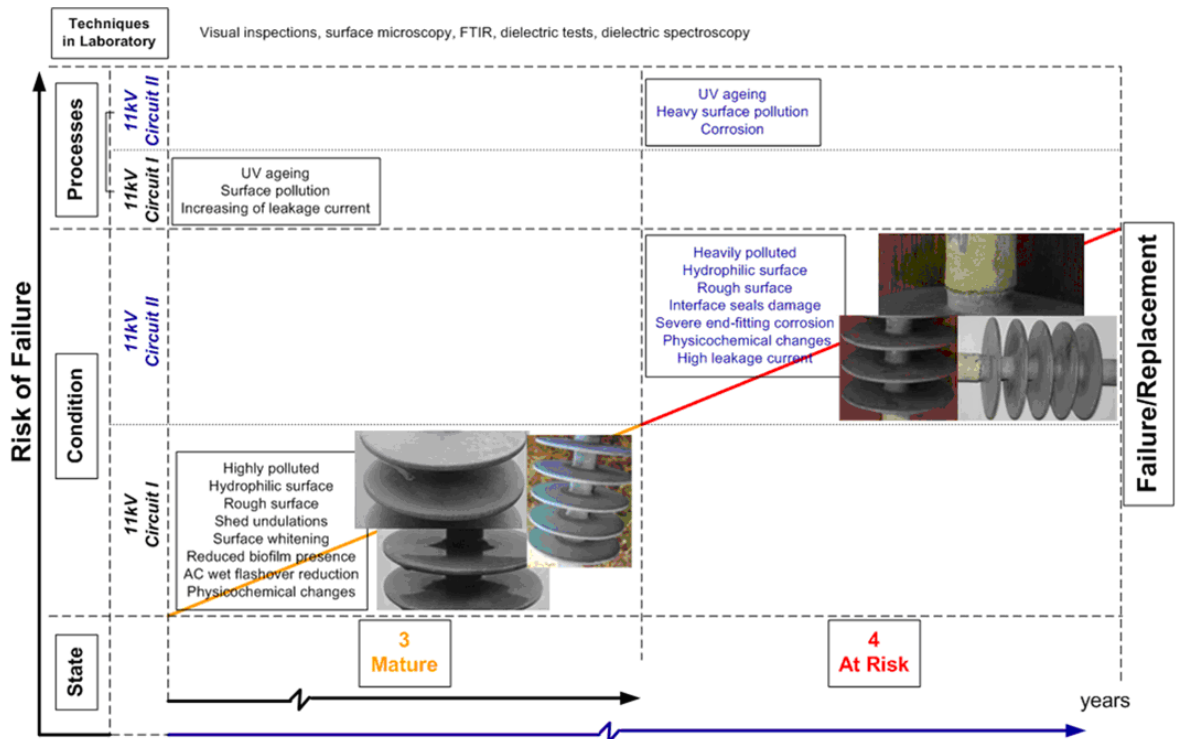


Figure 5.77 Circuit II and Circuit IV insulators ranking using the state estimator proposed on chapter 3

6. DROPLETS ON POLYMERIC SURFACES UNDER THE INFLUENCE OF ELECTRICAL FIELD

6.1. Introduction

When a water droplet is placed on a polymer insulator surface under electric potential stress, the local electric field (\vec{E}) distribution changes along and degrading phenomena start (electrothermal, electrochemical, physicochemical, etc.). Distortion and different movements take place under the influence of Coulomb forces and Maxwell stress. These two processes (distortion of \vec{E} and droplet's movements), are interdependent and interactional, and its modelling and explanation is a very complex matter. At the same time, when two or more water droplets are located on a polymer surface the whole process is enhanced which makes a formal description more complicated.

One relevant fact in water droplet electrohydrodynamic behaviour's studies is that no systematic test procedures are applied. In consequence, investigations have been done under many different conditions such as conditions such as electrode configurations, materials formulations, environments, water conductivities, etc. introducing important difficulties when results are going to be compared.

The main objectives of this chapter are: (1) to summarize the most relevant results published on electrohydrodynamic behaviour of single and multiple droplets placed on insulation surfaces, and (2) to describe how electrohydrodynamics are linked with the early degradation stage of insulation surfaces. This chapter is organized with the following structure: a brief presentation of the types of electrodes frequently used and study of the hydrodynamic behaviour of one or multiple water droplets under electric field with no emphasis on subsequent phenomena generated. Electric field, corona discharges, leakage current and flashover process will be presented individually with their most important processes associated.

The purpose of this structure is to establish the main characteristics of each part of the process (even so all of them are linked, interrelated and interdependent), with the idea of identifying the most important mechanisms related with the ageing process of outdoor insulator’s surface under specific parameters or stress conditions presented in the literature. It has to be taken in to account that degradation processes of composite insulators under electric field action are fundamentally related with water droplets’ presence and dynamic, and the understanding of all phenomena involved is crucial.

6.2. Main Factors Influencing Water Droplets Behaviour

Figure 6.1 shows the main factors involved in the electrohydrodynamic’s behaviour of water droplets located on a material surface submitted to an electric stress.

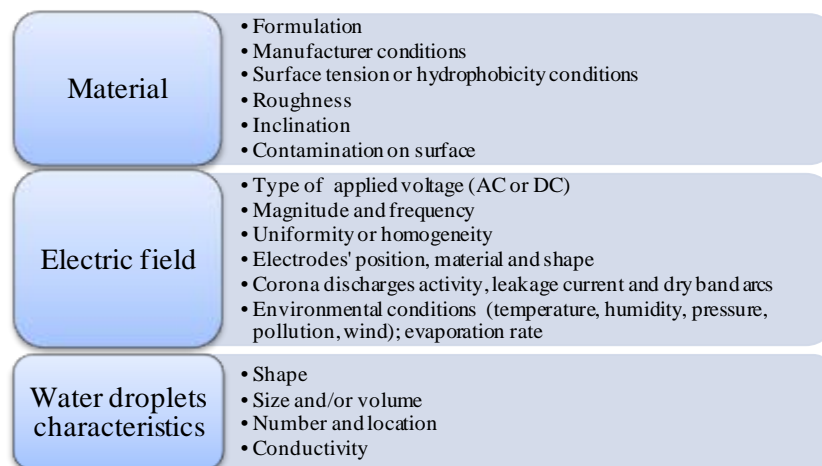


Figure 6.1 Factors influencing the behaviour of water droplets on polymer surfaces under electric field stress

6.2.1. Similarities between Free droplet vs. Droplets on Hydrophobic Surfaces under Electric AC Field

The phenomenon of free droplets under electric field has been well documented in the literature and it is a good start point to understand the whole process. The shape of a water droplet and its mechanical stability are influenced by the electric field at critical field strength, depending on radius and surface tension. The free droplet instability threshold value is defined by: $\bar{E}_{cr} = C \cdot [\gamma / (\epsilon_o \cdot r)]^{1/2}$, where C is a constant, γ is the surface tension and r the droplet radius [220, 221]. The value of C is in the range of 0.4-0.5 (Taylor, one of the pioneers in the area, estimated C as 0.461 in his theoretical calculation; some studies use 0.454 [222]) and γ_{water} is $0.073 \text{ N}\cdot\text{m}^{-1}$.

At this critical value, the droplet starts to eject water filaments from its vertices [223]. These filaments are highly charged small droplets that reduce the mass and electric charge of the original one. Looking for a relation between \bar{E}_{cr} and volume of the droplet it is obvious that it decreases as $V^{-1/6}$ (because it decreases as $r^{-1/2}$). Only one paper was found where the authors did not find a clear relation between small or big droplets [224].

Different investigations agreed that electrohydrodynamic effects on a droplet located on hydrophobic surfaces with electric field tangential to the surface is quantitatively the same such as for a free droplet [220, 223]. If the surface is less hydrophobic, the assumption starts to be erroneous. In this case, the balance of forces near the triple point differs too much from that of a free droplet. Some additional considerations should be taken in account to use the value of \bar{E}_{cr} previously defined. These are: (1) the theory assumes that the droplet is uncharged and (2) that is spherical before it disintegrates. In consequence, the value of \bar{E}_{cr} decreases when the conductivity of the droplet increases and when the shape starts to be less rounded.

The shape of a water droplet is influenced by the electric field basically because water is polar and elongates and contracts following the direction of it. Droplets become unstable and disintegrate into smaller droplets when the amount of surface charge on them is high enough [225]. The total surface charge, of spherical droplets at the point of instability was defined as:

$$V = Q / a_0 = (16 a_0 T)^{1/2} \quad (6.1)$$

where: V is the potential in volts, Q is charge in Coulombs, a_0 is the surface area of the droplet in cm^2 , and T is the surface tension in c.g.s. units ($\text{dyn/cm} = (\text{g} \cdot \text{cm/s}^2)/\text{cm}$). This is known as the Rayleigh's criteria instability. Rayleigh described a water droplet becoming unstable when the liquid starts to be thrown out in fine jets.

6.2.2. Taylor Cone, Taylor Cone Jet and Corona Discharges

In 1964, Sir Taylor [222] verified previous work on water droplets under electric field and that they will distort and disintegrate following Rayleigh's criteria. Tests performed by Taylor shown that droplets elongate under an electric field and cone shape with angles of $\sim 49.3^\circ$, are produced before fine jets of conical apex or tips are ejected (See Figure 6.2).

Taylor also showed that a droplet becomes unstable when the length (reached by elongation) is 1.9 times its equatorial diameter.

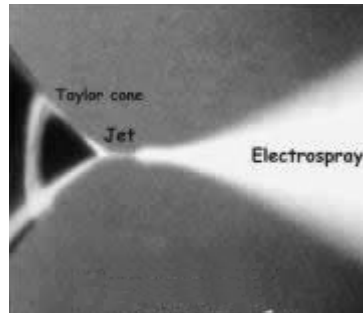


Figure 6.2 Taylor cone jet

6.2.3. Electric Field on Material Surfaces with Water Droplet Presence

The electrohydrodynamic behaviour of water droplets causes field intensification, water droplet distortion, local corona discharges and reduction of the distance between water droplets, enhancing further the electric field. This feedback in the phenomenon causes more distortion and finally the surface's wetting is caused, water channels coalesce and flashover can occur.

Important facts around the electric field (\vec{E}) distribution on a material surface with water droplets present (that will be explained in the chapter) are summarized in Figure 6.3.

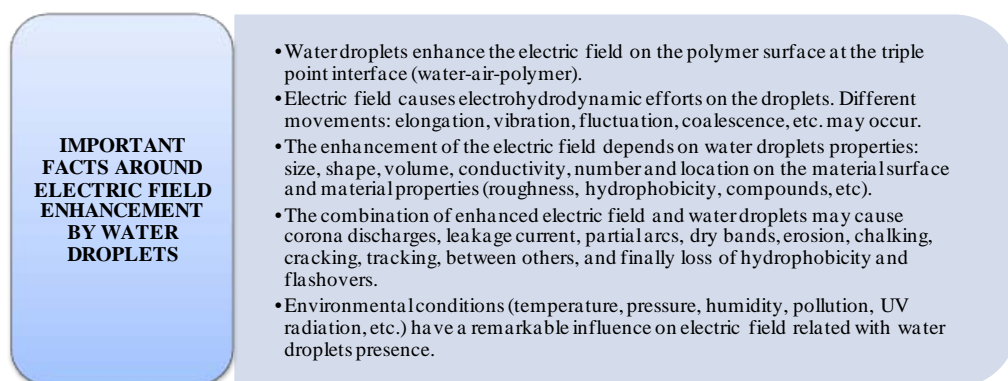


Figure 6.3 Main factors that influence the enhancement of \vec{E}

Regarding the electric field distribution along polymer insulators, it is possible to define lines of force perpendicular or parallel to the material surface. In consequence, the electric stress differs along the geometry of the insulator (Figure 6.4(a)).

The majority of ageing studies involving water droplets have been done using \vec{E} tangential and one droplet located in the centre of the inter-electrode gap. Looking at the Figure 6.4(b) it can be observed that \vec{E} is highly enhanced at the triple point in comparison with the \vec{E} magnitude found in Figure 6.4(c). However, normal \vec{E} has an important effect on the droplets' movements and also, if the electric field is higher at the top of the droplets, the arcs' path must be initiated in this line and move afterwards to the bottom (interface droplet-surface) [226].

The water droplet shape, which is a consequence of the surface hydrophobicity, has strong influence on \vec{E} enhancement at the triple point. Round or hemispherical droplets (hydrophobic surfaces or high contact angles) cause less \vec{E} distortion than elongated or elliptical droplets (hydrophilic surfaces or small contact angles) (Figure 6.5).

In Figure 6.6(a), the electric field between two symmetrical water droplets located in the centre of the electrodes is presented. The influence of the distance between droplets is also shown in Figure 6.6(b). The electric field (\vec{E}) is even more distorted or less homogeneous when two non symmetrical droplets are located on the material surface. The shape of the droplets is also an important factor in the electric field enhancement. If the distance between two droplets placed on surface increases from 0.5 mm to 10 mm, the electric field changes from 4.5 to 30 V/mm, keeping same gap, applied voltage, and shape of droplets.

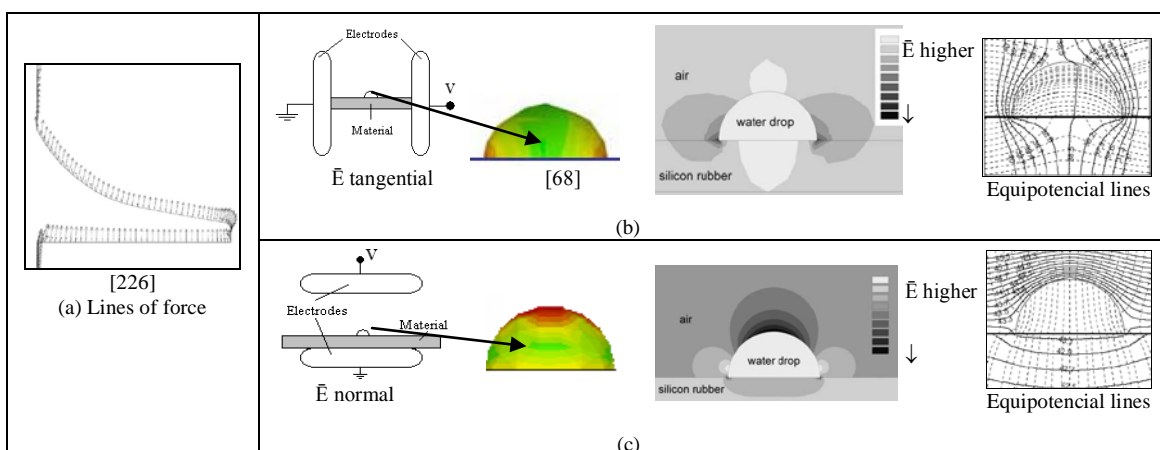


Figure 6.4 Normal and tangential electric field on one droplet located on a polymer insulator surface

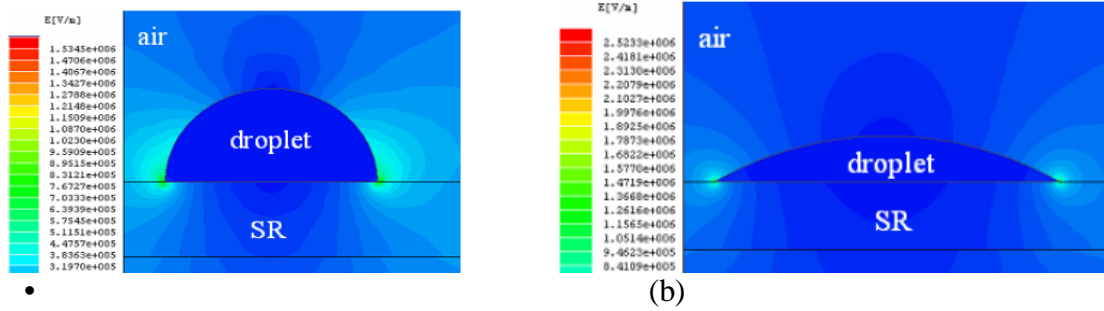


Figure 6.5 Comparison between the electric field on (a) hemispherical and (b) ellipsoidal droplet [223]

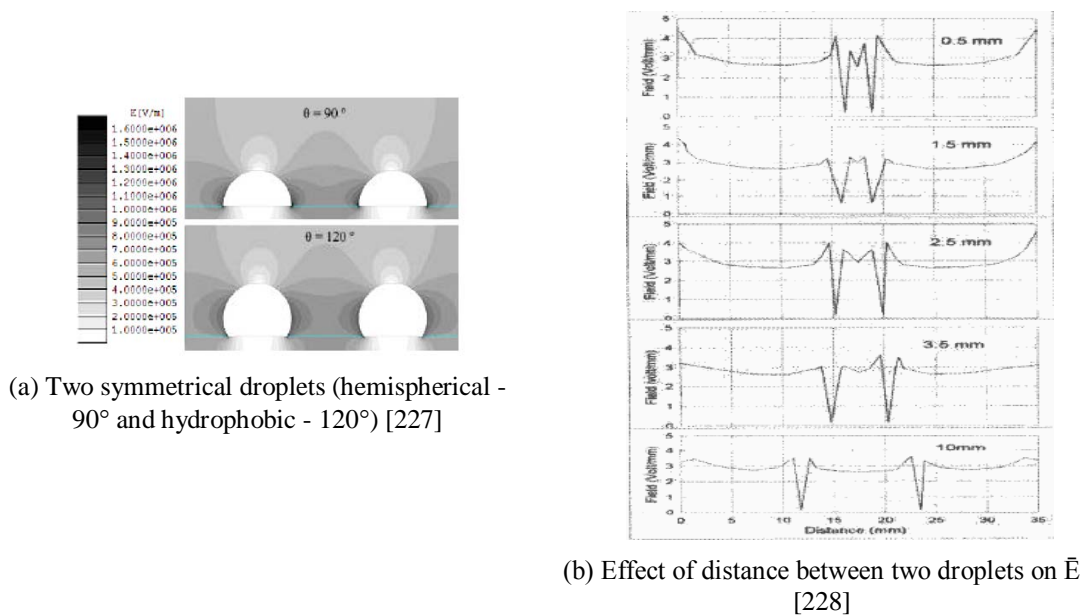


Figure 6.6 Electric field between two symmetrical droplets at the centre of an interelectrode gap

In Table 6.1, some \bar{E} enhanced factors published are summarized. These values were found by the authors using FEM simulations.

In the previous paragraphs electric field behaviour was described looking at single or multiple aligned droplets but the phenomenon is even more complex when unaligned droplets are evaluated. In Figure 6.7, three droplets (equidistant with two aligned with \bar{E} direction) were represented.

When the path is through the centre of the two basic water drops (in top of Figure 6.7), the enhanced factor is as high as 2.1, when the path is far from the two basic drops, drops to 1.2. When the path is through the region without water drops, reduces to the original value of electric field. And when the path is through the third water drop (the one below the 2 basic drops), it is increases again. It reaches another peak when the path is through the

centre of the third droplet. It can be concluded that when the water drops are aligned in the direction of \vec{E} , their effect is much more than those of water drops in other directions. It is important to remark that this is only one case of an infinite number of possibilities.

Table 6.1 Enhance Factors of Electric Field [227, 229-232]

Reference / Characteristics	Simulations	Enhanced Factor
SIR $\epsilon_r = 2.2$ Gap = 30 mm; electrodes on surface Droplets: de-ionized water, 30 – 80 μl , $\epsilon_r = 81$	One hemispherical droplet, volume 30 – 80 μl Two hemispherical droplets, volume 30 – 80 μl (Values were experimentally confirmed)	3,9 to 4,8 5,5 to 6,3
SIR $\epsilon_r = 4$ Gap = 20 mm, electrodes on surface Droplets: $\epsilon_r = 81$	One hemispherical droplet (radius=2,5 mm) One elliptical droplet (base=10mm) One hemispherical droplet, volume 10 - 100 μl	3,9 to 4,5 5,0 3,9 to 4,5
SIR $\epsilon_r = 4$ Gap = 30 mm, electrodes on surface Droplets: 30 μl , $\epsilon_r = 81$	One hemispherical (hs) droplet (radius=2,5mm) One elongated droplet (base=10mm) Two hemispherical aligned droplets, distance 1 mm to 5 mm Three hemispherical aligned droplets, distance 1 mm to 5 mm Four hemispherical aligned droplets, distance 1 mm to 3 mm Five hemispherical aligned droplets, distance 1 mm	3,8 6,8 5,6 to 3,8 8,0 to 7,2 9,5 to 13,5 ~16,0
SIR $\epsilon_r = 4$ Gap = 50 mm, electrodes on both lateral sides of the material	One hemispheric droplet, 5 to 80 μl One elliptical droplet, 5 to 80 μl <i>10 μl droplets</i> Two hemispherical aligned droplets, distance 1 mm to 5 mm Three hemispherical aligned droplets, distance 1 mm to 5 mm Four hemispherical aligned droplets, distance 1 mm to 5 mm Five hemispherical aligned droplets, distance 1 mm to 5 mm <i>20 μl droplets</i> Two hemispherical aligned droplets, distance 1 mm to 5 mm Three hemispherical aligned droplets, distance 1 mm to 5 mm Four hemispherical aligned droplets, distance 1 mm to 5 mm Five hemispherical aligned droplets, distance 1 mm to 5 mm	2,5 to 3,5 2,8 to 4,2 3,1 to 4,5 3,2 to 5,8 3,2 to 6,0 3,2 to 6,5 5,5 to 3,2 6,2 to 3,2 6,8 to 3,3 7,2 to 3,3

(1)The corona onset electric field has a threshold at a specific number of droplets. After this number the value is severely reduced. The max number of droplets depends of the gap distance and volume of the droplets.

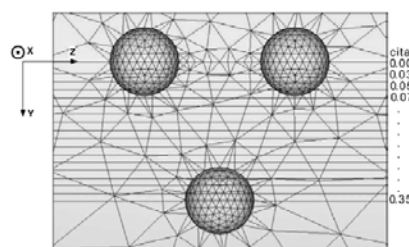


Figure 6.7 3D FEM mesh of three droplets unaligned (equidistant in a triangular disposition) [227]

If an insulator design is considered, looking at the different insulator’s surface disposition, three different types of droplets can be observed: sessile droplets (located at the upper side of the sheds), pendant droplets, (located at the bottom side of the sheds) and clinging droplets (located at the core) (Figure 6.8). In Figure 6.9(a) and (b), the electric field at the high potential end-fitting or near the ground end-fitting, respectively, is shown. The shape of the droplets used in the simulations was the same in all locations, but the different

intensities of \vec{E} are evident. \vec{E} is higher at the high potential end at the triple point of the droplets located on the core. It is important to notice that significant intensities of \vec{E} can also be found in the material bulk [227].

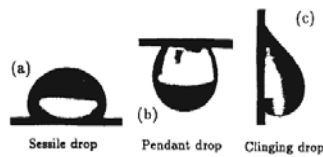


Figure 6.8 Shape of a droplet located on the upper part of a shed (a), at the bottom part (b) and at the core (c)

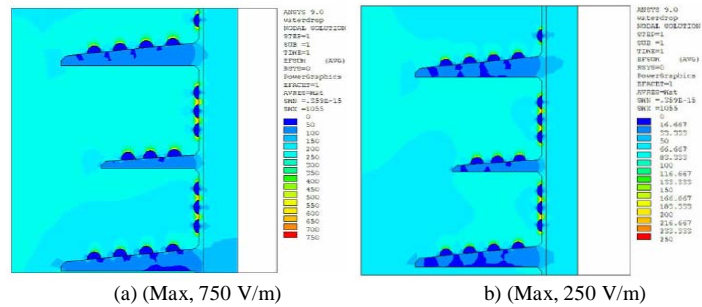


Figure 6.9 Electric field on the sheds at (a) the potential side and (b) the ground side of an insulator covered by water droplets [233]

Considering service conditions, understanding of the influence of pollution on \vec{E} distribution is also an important topic. A simulation/experimental study made on droplets located on polluted surfaces presents the electric field characteristics shown in the Figure 6.10 [234]. It was found that the dynamic behaviour and distortion of droplets on hydrophobic polluted surface is different that the behaviour on clean surfaces. In this study it is proposed that the contaminated layer changes the electric field distribution along the surface and reduce the intensity at the triple point, which might increase the voltage required to start corona discharges.

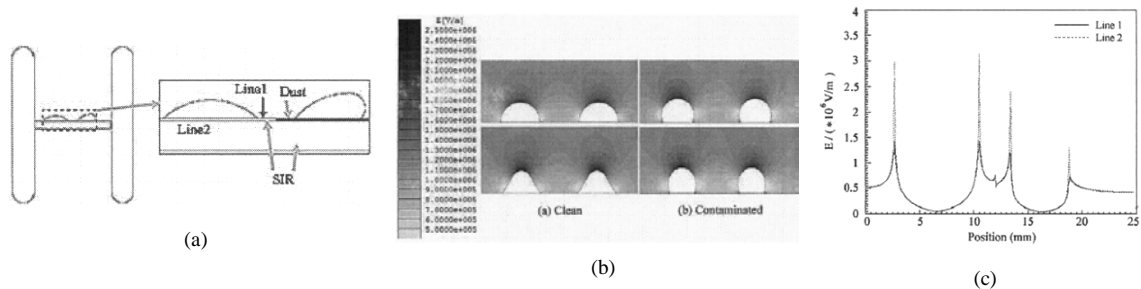


Figure 6.10 Configuration simulated: polluted surface plus droplets. (a) Basic model, (b) Electric field distribution, (c) \vec{E} magnitude along the lines shown in (a) [234]

On polluted insulator surfaces with water droplets present, the conductive contamination is dissolved within the moisture [234]. During ageing, hydrophobicity is lost and in hydrophilic surfaces the water filaments dissolve the conductive pollution layer, reducing

the surface resistance with a conductive electrolyte along a continuous path. The field strength at the triple point of a droplet on a clean surface is higher than on a contaminated surface, which explains why discharges appear on the clean surface first. In the simulation, the pollution was defined with higher permittivity than the polymer surface. Further investigations or simulations are required on this matter.

Coalescence of water droplets is also a phenomenon that disturbs \vec{E} locally (Figure 6.11). When one small and one big water droplet coalesce the resulting water droplet has a very sharp area on the side of the small original droplet. This highly intensifies the electric field in the triple point. If the two droplets are similar in size the effect is less intense.

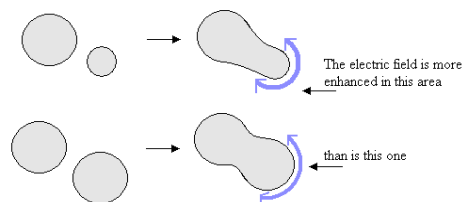


Figure 6.11 Enhancement of \vec{E} when water droplets coalescence

6.3. Electrohydrodynamic Behaviour of Water Droplets under Electric AC Field (Different Movements)

When a water droplet is located on a surface material, between two electrodes, some different movements are presented following the AC voltage phase [167, 224, 234-245] and different movements are followed by the water droplets submitted to DC fields [246-248]. In this research, some references about DC behaviour will be included but the main emphasis will be focused to the AC understanding.

Different references [223, 240] describe the phenomenon of one droplet located in the centre of two electrodes under AC voltage as: when voltage is zero the water droplet is standstill in the centre of the interelectrode distance; during the positive half cycle the droplet tilted towards the positive electrode and the movement is maximum at 90° ; during the negative half cycle the droplet tilted towards the ground electrode and the movement is also maximum at 90° . An explanation of this behaviour is focused on the negative charges induced on the water droplet's surface. But, this summary of the phenomenon does not

fully describe the electrohydrodynamic process involved. This is more complex than that and it will be influenced for many different factors (See Figure 6.1).

6.3.1. Stillness plus Vibration → Elongation → Fluctuation Cycle

Published studies of the electrohydrodynamic behaviour of water droplet under AC field agree that vibration and elongation (or extension) of droplets will be always present. There is no consensus of the specific names given to each particular movement of a water droplet under electric AC field. In references [224, 241, 242, 244, 245] the movement of a water droplet under AC field is defined like a periodic vibration divided in the following phases: *stillness, vibration, elongation, fluctuation*. The main characteristic of the process are:

- Water droplets present double power frequency vibration and power frequency fluctuation.
- The phase vibration/elongation to fluctuation is repeated many times before flashover.
- Vibration is a special fluctuation with smaller amplitude.
- The transition between quiet state to vibration state has no obvious boundary.
- When the electric field (\bar{E}) is increased gradually, vibration starts.
- Contact longitude, between droplet and surface, keeps constant or has a little elongation.
- Increasing \bar{E} further the contact surface is suddenly elongated.
- Vibration comes to be a more violent fluctuation state at power frequency with a new shape.
- Under \bar{E} , corona discharges can occur at the triple point, between water drops or between water drops and electrodes.
- Intensive corona influences the shapes of vibration and fluctuation.

Vibration can be explained by the dielectric polarization of the water droplet under AC stress. The deformation towards one or other electrode can be a result of the location of polarized charges is opposite sides in each positive and negative half-cycle [224].

6.3.2. Resonance or Vibration Modes

Resonance of water droplets can be observed at different frequencies for a given volume [242, 243]. At such frequencies water droplets vibrate more vigorously. The phenomenon

will be influenced by the surface properties of the hydrophobic material [234]. Under AC fields a water droplet deforms strongly only at a particular frequency and manifests resonant vibration according to a natural frequency determined by its size. This frequency becomes lower when the volume of the droplet is increased.

In Figure 6.12, the difference between the behaviour of a droplet at 50 Hz and its resonant frequency (19 Hz @ 30 μ l) is clearly shown [84]. The droplet is deformed and repeated by shrinks and extends twice a cycle of the applied voltage. A water droplet with a specific volume resonates mechanically when the characteristic frequency of the water droplet is twice as much as the frequency of the electric field because electric force has two peaks in one cycle. The water droplet would manifest the maximum elongation at the phase angle after passing the peak value of the voltage and the inertia of the water flow in a droplet should also contribute to the maximum deformation. On the contrary, the water droplet at 50 Hz moves slightly, although the magnitude of the voltage is more than 35 % higher. The influence of the surface hydrophobicity on resonance phenomenon and magnitude of the deformation was also confirmed (Figure 6.13) [70,83]. In the resonant state the width of the water droplet is 1.5 times larger than that in other frequencies.

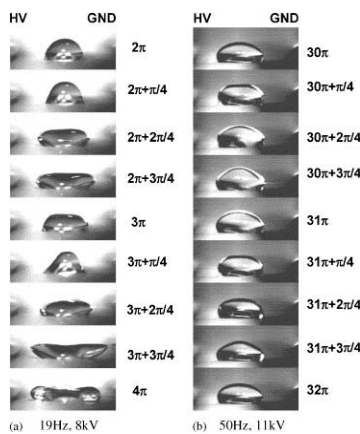
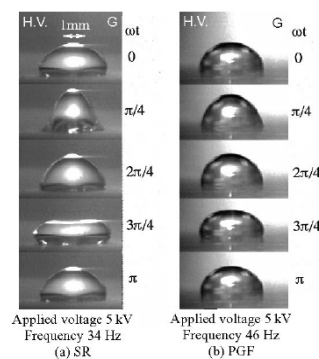


Figure 6.12 Water droplet distortion at 50 Hz and resonance frequency, 19 Hz



SR, silicon rubber; PGF, polydimethylsiloxane-grafted fluoropolymer. Static contact angle: SR = 115°, PGF = 90°, receding contact angle: SR = 65°, PGF = 90°.

Figure 6.13 Water droplet distortion in two different materials

A theoretical approximation was found in [241]. For every droplet volume, several resonances or vibration modes were observed (Figure 6.14) and, adjusting the resonance modes for a free droplets theory to a droplet on a hydrophobic surface, the frequency f_n of the resonance mode n were presented as:

$$f_n = \{ [n (n-1) (n+2) \gamma] / [12V\pi\rho] \}^{1/2} \quad n \geq 2$$

where: V = droplet volume, γ = surface tension and ρ = liquid density. The difference between a free droplet and droplet on a surface under horizontal field is that additional modes must be proposed because more resonance modes are presented (mode 3.5 was proposed).

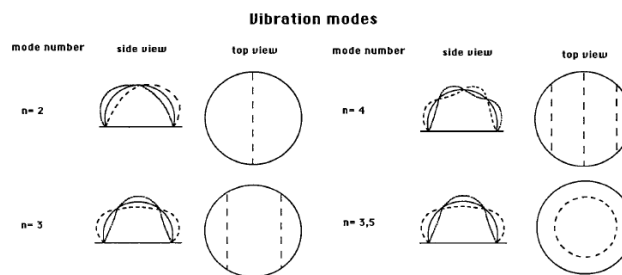


Figure 6.14 Vibration modes of a water droplet located on a hydrophobic surface under AC field [241]

6.3.3. Water Droplet Located out of the Centre of the Inter-Electrode Gap

A water droplet located close to the energized electrode vibrates and then is extended. Just after its extension it tends to move to the centre of the gap inducing flashover. This movement to the centre is not always observed if the droplet is located near to the ground electrode. The flashover voltage is always lowest when the droplet is located close to the high potential electrode compare to any other place [167].

When multiple droplets are aligned, the droplets located at high voltage side begin to vibrate first at a particular value of AC electric field. If the voltage is increased, all the droplets start to vibrate and to extend to the direction of the electric field [224]. If the conductivity of the droplets is high, the same phenomenon occurs but at a very low level of the electric field.

When a water droplet placed on an end of a polymer insulator (see electrodes in configuration k, Table 6.2) [240] starts to vibrate, under an AC field, keeping its quite round shape with no significant deformation; increasing the voltage the droplet starts to elongate at the bottom in the interface area with the solid material and finally is hardly deformed and the tip of the water droplet is drawn up towards the tip of shed (droplet is moved towards the direction of the plane electrode, see Figure 6.15).

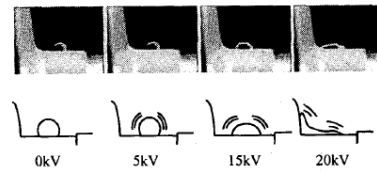


Figure 6.15 Behaviour of a water droplet located at the end of an insulator under an AC field [240]

Positive and negative charges are electrostatically induced at the water droplet tip and are subjected to Coulomb force. This tensile force has the same direction of electric field and is proportional to the instantaneous magnitude of the applied voltage. It induces vibration, a synchronized behaviour with the double of the frequency of the AC stress but not vibration under DC.

The movement of the droplet towards the plane electrode may be explained by the asymmetrical electrode arrangement where the tip electrode is highly stressed in comparison with the plane and the distance between the droplet and this electrode is short so that the tip of the droplet is charged equal to the tip and is attracted towards the plane charged with opposite polarity.

6.3.4. Coalescence

Under an electric field, multiple droplets located on a surface can coalesce and form bigger droplets. After this, the electric field is highly enhanced. Small discharges occur between close small droplets and the intensity of the discharges increases after coalescence. If the conductivity of the droplets is high, corona discharges or arcs will be easily triggered. At the same time if the conductivity is high, during coalescence / drying processes, salty dust can be found on the surface.

6.3.5. Additional Electrohydrodynamic Phenomena

Although the main electrohydrodynamic phenomena were previously described, in some additional process have been presented. When a critical field stress is exceeded additional and different phenomena occur, such as transient structures on the surface, creation of filaments, formation of water paths between droplets, collapsing of several droplets, separation of droplets and ejection of very small droplets from bigger ones. See illustrations in the Figure 6.16. These effects lead to a deformation and rearrangement of the original droplets, wetting a wider area of the insulating surface, minimize the dry

zones of the solid surface and the final creation of a water path between the electrodes becomes more probable. Slip of small droplets can also be presented and it is more likely on rough surfaces [167].

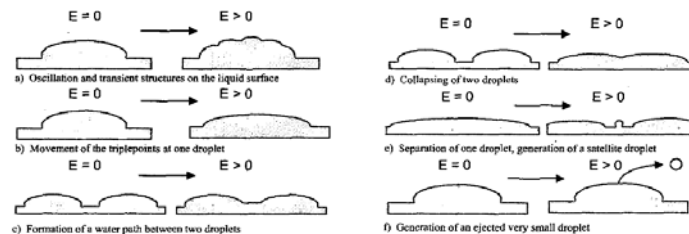


Figure 6.16 Basic patterns of electrically stressed water droplets [167]

6.3.6. Water Droplet Distortions on Surfaces with Reduced Hydrophobicity caused by Sparks

Using sparks to degrade a silicone surface and a 20 μl droplet located in the centre, the top view of the distortion is shown in Figure 6.17(a). If the droplet is located in the interface between degraded and new area, the distortion follows the shape shown in Figure 6.17(b) and, if the droplet is located in a narrow degraded area, a long/thin shape will be found Figure 6.17(c) [249].

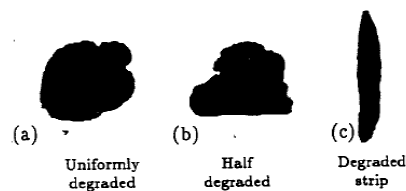


Figure 6.17 Distorted shapes found in non-hydrophobic surfaces

6.3.7. Behaviour of Water Droplets with Electrodes Directly Connected in their Volume

In the literature, a recent study made with electrodes directly introduced into the volume of two aligned droplets [250, 251] found that when the AC current is limited (less than 1 mA), as normally occurs in service, an unstable behaviour can occur. That means that when the energy (current or voltage) is insufficient to maintain the arc the discharge will be repeatedly on/off. In consequence, the phenomenon is electrically unstable and spatially stable. In particular protrusions at the front of the droplets were detected (. Similar results are presented in [252, 253]. As a consequence of the electrodes' shape, and their location

directly in the water droplets all the phenomena associated with charges have important details involment.

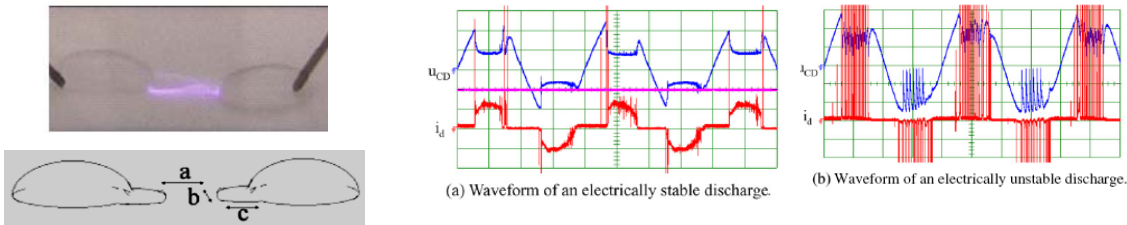


Figure 6.19 Waveform of voltage and current

Figure 6.18 Electrodes inside the droplets and protussions

6.3.8. Elongation and Contraction of a Droplet in AC field (Does this phenomenon exist?)

Two works presented by the same research group [238, 239] report significant deformation of a water droplet located in the middle of two electrodes (Table 6.2, shape g) with elongation and contraction movements in the direction of the electric field (Figure 6.20). The diameter of the water droplet at the positive half-cycle voltage peak was bigger than the diameter at the negative half-cycle voltage peak (6.4 mm vs. 4.3, 40 μl de-ionized water droplet, 22 mm gap, silicon sample, 15 kV_{rms} , 50 Hz, carbon electrodes).

In consequence, the studies present the following conclusion: “It follows that in the positive half-cycle the water drop effectively reduces the insulation path between the electrodes and increases the risk of flashover, for example, during switching surges”. This result was not found in any other publication reviewed.

In Figure 6.21, the behaviour of a 30 μl water droplet with $2.0 \mu\text{Sm}^{-1}$ located on a silicone surface, stainless steel electrodes, gap 30 mm, in one voltage cycle (60 Hz) is shown [85,101]. It was selected between many coincident publications showing the same electrodynamics behaviour. Only under resonance conditions elongation/contraction phenomena was found but not following the same premise (elongation +/contraction -).

Reviewing all the information presented in both papers only one particular condition was found: the electrodes configuration (shape g, Table 6.2) introduces a very high non-uniformity or distortion in the electric field around the droplet. This condition combined

with a short gap between the electrode and the tip of the drop could induce charges at the droplet through invisible or subtle discharges from the tips of the electrodes to the droplet. It could be charged, under critical stress condition, in a specific way to produce elongation (electrodes-droplet attraction) during the positive half-cycle and contraction (electrodes-droplet repulsion) during negative half-cycle. Additionally, these are the only studies where the electrodes are made from carbon, a material which is a good emitter of electrons.

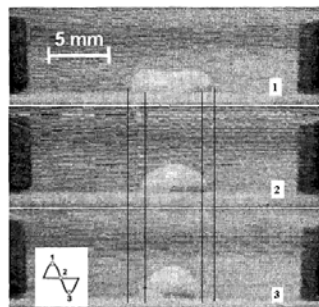


Figure 6.20 Water droplet's behaviour with different diameters at $V_{\max+}$ and $V_{\max-}$. [238]

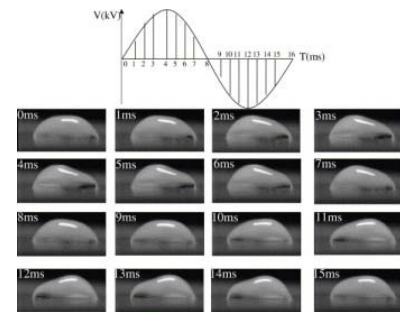


Figure 6.21 Water droplet behaviour following the voltage cycle with agreement in the literature [223]

6.3.9. Water Droplet Movement under DC Voltage [246-248]

The DC droplet distortion does not present vibration or fluctuation. This is characterized by step by step development, asymmetric distortion and 'rise and fall' phenomena. Water droplets do not continuously become longer and longer until lose stability when voltage is increased. The process was summarized as:

- When voltage is increased the droplet base does not elongate until the electric field (\bar{E}) is reached a threshold and a macro-contact angle appears.
- After certain value of \bar{E} the droplet becomes longer and the macro-contact angle decreases. If \bar{E} keeps on increasing the macro-contact angle starts to increase and the process is repeated again.
- 'Rise and fall' points are created on the droplet in certain directions but
- Return to the symmetric position (round) (Figure 6.22).
- Increasing \bar{E} would cause a new 'rise and fall' process, keeping dynamic stability. This is broken because corona causes the injection of space charge and the droplet's electric inner charge equilibrium is broken (Non- equilibrium state).
- Asymmetrical electric forces are equalized by continuous distortion.

- Non-symmetrical droplet's shape occurs distorting of \vec{E} in the droplet tips.
- Corona activity occurs.
- Charge gained by corona discharges neutralizes the surplus free charge in the water droplet, equilibrium is recovered and new space charge is accumulated. A new cycle starts.



Figure 6.22 (a) Asymmetrical distortion, (b) Return to symmetric position

6.3.10. Two Droplets under DC Electric Field.

If two droplets are located beside the electrodes under DC electric field elongation is the most representative part of the process and some differences between positive and negative voltage are found. (See Figure 6.23) [248].

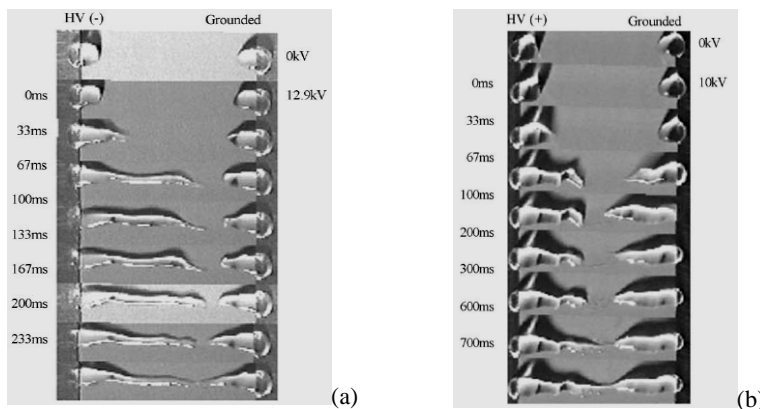


Figure 6.23 Droplets on silicon surface under DC voltage, (a) Negative, (b) Positive

6.4. Corona Discharge Phenomena on Water Droplets

When droplets are located on a material surface if a certain threshold of electric field (\vec{E}) is exceeded, corona discharges occur. These will be the start point of other ageing phenomena: leakage current, dry band arcs and flashover.

The CD phenomenon is principally influenced by the following factors:

- Polymer material's properties (silicone, EPDM, SIR/EPDM alloys, etc).
- Electric field homogeneity (consequence of voltage magnitude, electrodes shapes, electrodes location).
- Water droplets properties (size/volume, conductivity, location, number).
- Environmental conditions (pressure, temperature, humidity).

6.4.1. Water Droplet Corona Onset

The presence of a water droplet on an insulator surface introduces an onset of corona discharge activity if the electric field magnitude exceeds a specific threshold level. This limit depends on: volume and conductivity of the droplet, hydrophobicity condition of the material and atmospheric conditions. After the onset voltage is reached the corona discharges are increasing rapidly with growing voltage.

In a study published in 1995, Phillips et al [221] found the following values for the corona onset although environmental conditions and water droplets properties were not reported:

- *i.) Water droplets on the sheath:* using a 20 μl water droplet on SIR (centred between electrodes), contact angle 88° , between 0 to 0.5 kV/mm no significant changes are found; at 0.58 kV/mm the droplet elongates abruptly; at 0.66 kV/mm further elongation is added; at 0.68 kV/mm the drop is strongly elongated and corona discharge currents start to be sensed Changing the volume of the droplet, the required \bar{E} to corona onset decreases using droplets between 10 – 80 μl and there is no significant changes between 80 – 100 μl . An important reduction on \bar{E} required to corona activity onset was found if the material is less hydrophobic; the onset is $\sim 30\%$ higher if the contact angle of the material is 115° .
- *ii.) Water droplets on the shed:* using droplets between 65 – 125 μl , located on the centre between electrodes, the onset is near 0.86 – 0.96 kV/mm and for droplets of 60 μl or less the onset is higher than 1 kV/mm.

In 2001 [254], similar onset values were also presented for a single droplet submitted to tangential \bar{E} . Additionally, for two droplets located in a 3 cm gap and 2 mm between them,

values between 0.54 – 0.45 kV/mm between 30 – 80 μl , were found. In this condition, the reduction in the onset value is close to 30%.

In a recent work, 2006, [255] an AC voltage was applied on a SIR surface, varying the volume of the droplets between 35 – 100 μl , to find the corona onset activity. On tangential field the onset was 0.36 kV/mm and 0.98 kV/mm for perpendicular arrangement. The author found that the size of the water droplets influences the inception voltage slightly as a larger droplet volume requires a higher electric field. This is an interesting different result and this behaviour is a consequence of the test setup configuration used during the study: the electrodes are embedded in the material's bulk.

- *iii.) Water droplets on the shed/sheath interface region:* in these areas, with water droplet presence, the \bar{E} will be more enhanced than in the two previous regions. In consequence, the degradation is higher.

In Figure 6.24, the effect of the water droplets' conductivity is presented [223]. In this, corona onset voltage decrease when the volume of water droplet increases and also when conductivity is increased (for a constant volume).

The onset corona discharge voltage is also reduced after a flashover by ~30% [81,98]. In [62] the corona onset potential of a water droplet as a function of air pressure is reported. The model and its validation were made using a droplet suspended on a ball of a ball-plane electrode geometry. There are different corona onset mechanisms and they are a result of two different corona onset processes: water drop instability and ionization of the surrounding air.

The onset potential does not remain constant across the entire air pressure range as would be expected if the onset of corona was due to drop instability alone. Instead, water drops have a 'corona onset versus air pressure' trend similar to that shown in Figure 6.25. In the non-constant part of the curve (regions A and B) the onset mechanism is not drop instability but ionization of the surrounding air. At the higher values of air pressure the onset potential remains constant with changes in air pressure (region C).

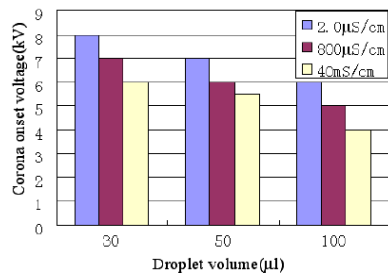


Figure 6.24 Corona onset voltage vs. volume and water conductivity

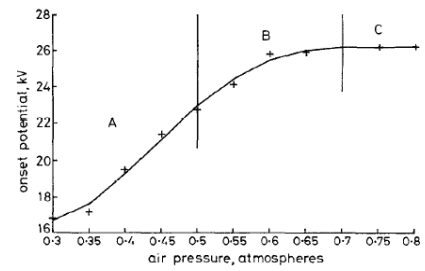


Figure 6.25 Onset as a function of air pressure for a water droplet in a divergent field

6.4.2. Corona from water droplets, leakage current and early ageing state relationship

In Figure 6.26, a relation between corona discharges from water droplets, leakage current and early ageing state is presented. This means that at the beginning of the ageing process of a polymer surface, corona activity on water droplets is the main factor to produce the hydrophobicity loss. It can be used to identify incipient ageing process [42,62].

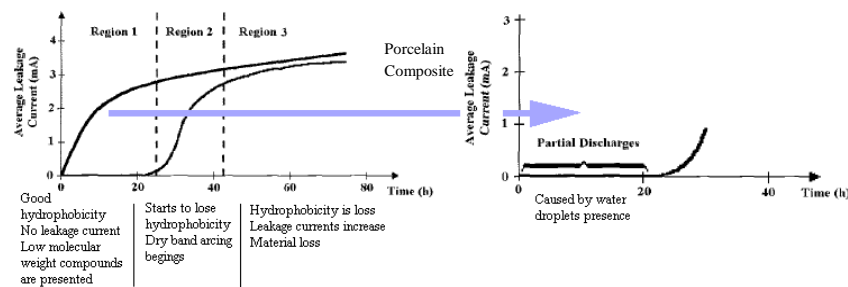


Figure 6.26 Relation of corona discharges under water droplet presence with early stages of degradation

6.5. Leakage Current Behaviour with Water Droplets Presence

Important characteristics of leakage current (LC) originated by an electric field and with water droplets located on a polymer surface are:

Leakage current can be capacitive, resistive, non-linear, non-linear with discharges [112] and particular patterns can be observed giving information of the surface condition. For this reason some groups have been showing the applicability of neural networks, wavelets or other techniques that can be used to identify recurrent waveforms of LC in the diagnosis of composite insulators. A general agreement exists that leakage current has a high harmonic content. In consequence, evaluating the spectrum of harmonics of leakage

current has been used to identify degradation on the outdoor insulators and an important amount of publication has been presented with this objective.

Once again, it is relevant to comment that leakage current is also affected by the environmental conditions and this information should be included to find good correlation between patrons at different locations and systems.

Under wet conditions and pollution, different leakage current stages may be defined: a conductive current during the water layer formation, leakage current during the time that droplets are vibrating (corona discharges time), leakage current during dry band arcs and the last (also, most severe) stage, leakage current during tracking.

Leakage current also presents important differences when AC or DC stress is applied. In the Figure 6.29(I-III), a typical waveform of leakage current during the tracking process is presented. The differences between AC, DC+ and DC- can be observed [66,113].

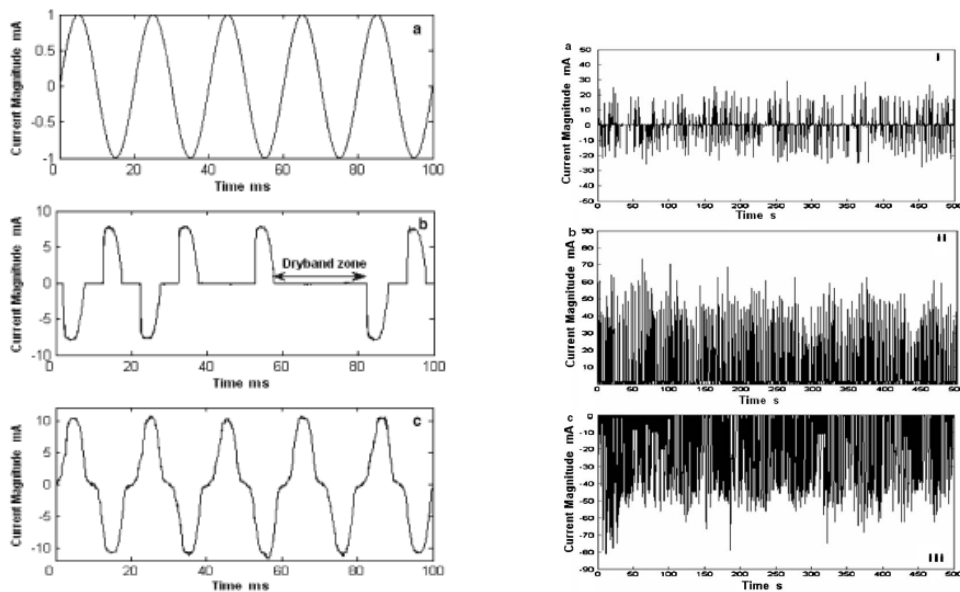


Figure 6.27 Typical leakage current waveform , (a) Before dry band arcs under AC field, (b) During dry band arc under AC field, (c) Tracking under AC field, (I) AC, (II) DC+ and (III) DC

In Figure 6.28 and Figure 6.29, leakage current is presented when droplets are vibrating and the dry band arcs' activity occurs [231]. A good agreement with the surface polymer condition was found by extracting the information of leakage current waveform and its correspondent harmonic components. The authors indicate that the ratio between the third harmonic and the fundamental component can be used as diagnosis parameter.

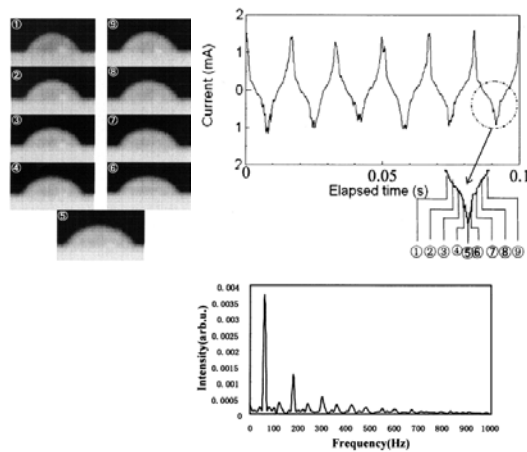


Figure 6.28 Vibration of water droplets, leakage current waveform and frequency analysis

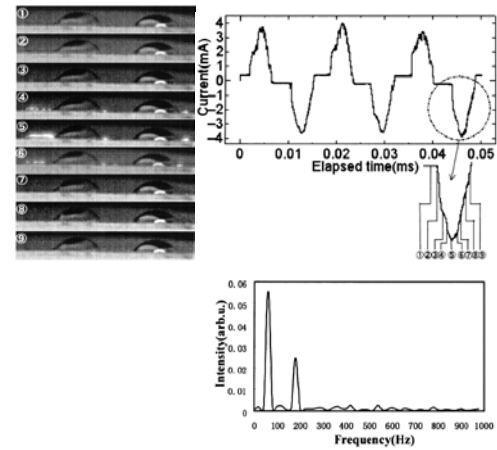


Figure 6.29 Dry band arc activity between water droplets, leakage current waveform and frequency analysis

Two comments can be said about this investigation. In these publications the authors include the correlation between leakage current shape and water behaviour. No additional works were found with this information. The authors present the harmonic decomposition using a single analysis technique losing the temporal information. In this particular case, using a multiresolution analysis technique, by example, wavelets, they can keep the spatial/temporal relation between the three phenomena: water droplets behaviour with standard waveform and harmonic content.

6.6. Flashover Occurrence vs. Water Droplets Presence

Polymers lose their hydrophobicity after long periods of heavy or continuous wetting because water droplets have a strong influence in the electrical breakdown or flashover of a polymer-gas interface [230, 242, 245, 256-258]

- Water droplets enhance the electric field at the triple point, ‘air-polymer-water’ interface, as a consequence of the difference between their relative permittivity magnitudes.
- Droplets are deformed under electric fields due Coulomb and field gradient forces and their new shapes enhance further the electric stress.
- Droplets reduce the distance between electrodes acting as a conductor especially under severe pollution conditions. This enhances the electric stress too.

- The electrohydrodynamic behaviour of the water droplets is a positive feedback phenomenon that finally wets the surface.

During the droplets' electrohydrodynamic changes, different movements like: fluctuations, vibrations, coalescence, slips, etc. are observed. These are the first steps which eventually lead to flashover. In [98], under uniform electric field, one 20 μl water droplet located at the centre of a 20 mm gap of a silicone surface, at 22 °C, 753mmHg and 50% of relative humidity, reduced the flashover voltage by more than 30%. This reduction is greatest for a droplet on a vertical surface (clinging droplets) and least for one on the upper horizontal surface (sessile droplet). The electric field distribution shown in the Figure 6.9 confirmed this. Water droplets located at the core of the insulators exhibit higher intensities of electric field.

The conductivity of water droplets also influences the flashover voltage magnitude. This will be lower at lower conductivities. The breakdown path depends also on the water droplet conductivity. For low-conductivity water, it was across the droplet's surface whereas for high-conductivity water, it was through the droplet [249].

6.6.1. Flashover Behaviour Applying the Similarities with the Theory of Free Droplet under Electric Field

Following the results published in 1990 [220] if the surface is hydrophobic and the electrohydrodynamic behaviour of a droplet in a gap with parallel AC electric field is quantitatively similar to a free droplet and the expected flashover voltage as function of droplet volume (or radio) follows the curve presented in the Figure 6.30. In this curve three different regions can be identified.

Under an AC field the droplet deformation is continuous and smooth, in most cases no water filaments are observed and the vibrations of the droplets spread them along the surface in the field direction. This approximation does not describe the DC phenomenon.

6.6.2. Phases in the Flashover Phenomena of Polymer Insulators

Several hypotheses have been proposed to explain the flashover mechanism of composite insulator. They are looking at finding an explanation between the most important phenomena occurring in low scale to the final stage of fault of the component in the

system. One of the most complete explanations was proposed by Karaday et al [164, 165]. Eight different stages to flashover were identified. They are summarized in the Figure 6.31.

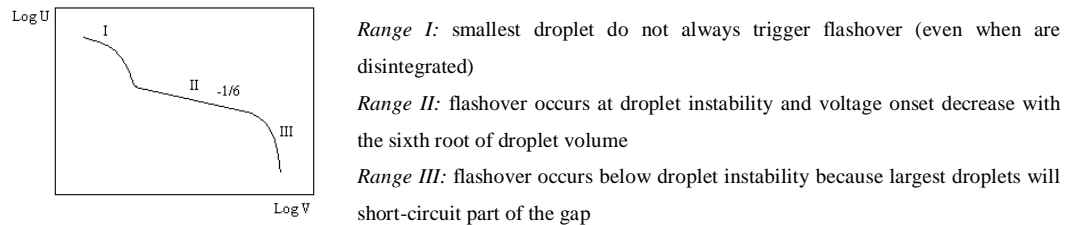


Figure 6.30 Expected flashover voltage (U) vs. drop volume (V) [220]

6.6.3. Shapes and Location of Electrodes Used to Study Water Droplets Behaviour on Polymer Surfaces

Degradation of outdoor composite insulation surfaces, including loss of hydrophobicity, is associated with the presence of water droplets under electric field stress. These phenomena are commonly studied using small rectangular polymer samples and variety of shapes, locations and materials of electrodes [167, 228, 231, 232, 234-239, 259, 260]. It can be inferred that different configurations of electrodes introduce differences in the electric field distribution [1,4,5], charge injection, corona discharges [238, 240, 260], and leakage current [239].

Changes in electrodes properties cause differences in the electric charge induced at the tip of water droplets, and also can introduce conductive charges along the surface. It is conceivable that local enhancement of electric field, water droplet dynamic behaviour, corona discharges properties (inception voltage, magnitude, phase and frequency), and consequently local ageing, could be very much influenced by electrodes characteristics. As result, some misinterpretation of the phenomena may occur. This consideration was first introduced in 1997 [167] and embedded electrodes were proposed and used. Nevertheless, this matter has been received little attention or focus and many different electrodes can be found in the literature.

Pollution of the insulator surface

- Some studies show that after a long term under contamination exposure, one layer, not completely uniform, is formed. Seen for sea and inland pollution.

Diffusion of low molecular weight (LMW) chains

- Hydrophobicity in polymer insulators have a process of loss - recovery cycle of this property. Repellency to the water is recovered when a thin layer of LMW products emerge to the surface.

Wetting of the surface

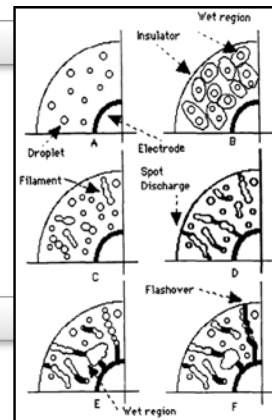
- Migration of pollutant to the droplets and migration of the water into the pollutant exist. Diffusion drives the contaminants through the LMW chains of the polymer layer. Salts are dissolved in water droplets. They start to be conductive. Additionally, water diffuses through polymer and into dry pollution. High resistive layer are formed around droplets. The density of water droplet continues increasing, joining wet regions, producing a high resistive layer covered by conductive water droplets.

Ohmic heating

- Leakage currents drive along droplets or wet paths, temperature is increased, the resistance of the layer is reduced.
- Currents dried the electrolyte and resistance is increased.
- Current is stabilized.
- At the beginning leakage currents are higher (highly capacitive). They are gradually reduced to a small constant value (highly ohmic).
- The surface is not dried and corona discharge activity starts.
- Water droplets coalescence and filaments start to be formed.

Enhancement of the electric field

- Water droplets enhance locally the electric field, elongation, distortion and coalescence occur; filaments are formed. Filaments are conductive regions.
- Big droplets can be separated by smaller droplets. New wet filaments or paths can be formed in the direction of the electric field.



[46]

Arc (or spot) discharges

- Electric fields produce conducting filaments which are surrounded by a high resistive layer.
- The filaments reduce the gap and the electric field is enhanced at the tip of them.
- High electric field intensities produce discharges between filaments (dry bands).
- Hydrophobicity is destroyed.
- Filaments fuse and electric field is even more enhanced.

Formation of wet regions

- Spot discharges destroy hydrophobicity which leads to irregular shape formation in the wet region.
- Wet regions are conductive, with amorphous shape and with defined border.
- Wet regions are surrounded by a high resistance layer. Leakage current is ohmic or active.
- Corona at the electrodes also produces wet regions.
- Local high electric field intensity produce random spot discharges. Several independent dry band arcs appear simultaneously.

Flashover

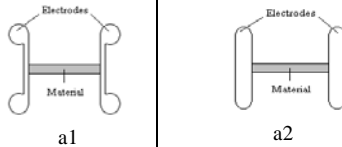
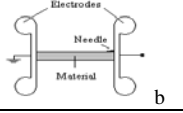
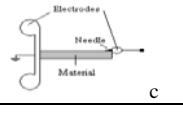
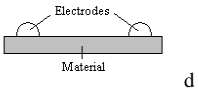
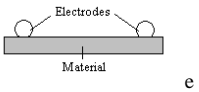
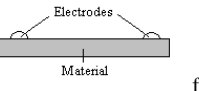
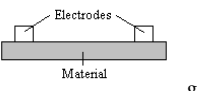
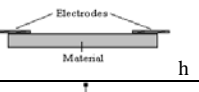
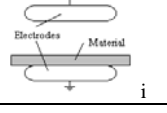
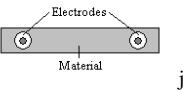
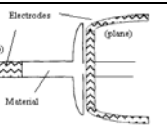
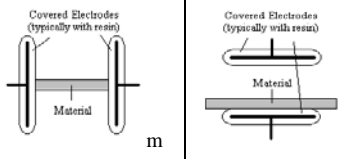
- Filamentation and dry band arc will be always present.
- Flashover occurs when spot discharges increase the length of filaments and they bridge the gap between electrodes.
- Change in filament dimension changes their resistance.
- Arcs destroy hydrophobicity and increases filament's surface. At one point the filaments' resistance is reduced and current is increased. Arc voltage resistance is reduced and an unstable state is reached.

Figure 6.31 Flashover mechanisms

Some shapes and location of electrodes used in the literature are summarized in Table 6.2. The objective of this selection is point out some important differences between cases and not to present a quantitative study about the influence of electrodes on published investigations of water droplet behaviour. In the next chapter main results of a formal

theoretical, including finite element simulations (FEM), and experimental study of electrodes shape and location on electric field distribution, water droplet behaviour and flashover is presented for some specific configurations.

Table 6.2 Some electrodes used in the literature for water droplets under electric field stress studies

Electrodes	Design	Observations
Plane to plane [254, 256]		Electric field (\vec{E}) tangential with the surface. No areas on the electrodes with \vec{E} concentration. \vec{E} tends to be uniform if the contact interface between the electrode and the material is well done.
Plane + needle to plane [237]		Electric field (\vec{E}) tangential with the surface. One area on one electrode with high \vec{E} concentration and corona discharge generation.
Needle to plane [237]		High concentration of \vec{E} in the potential electrode. High level of corona discharges (CD).
Hemispherical		Electric field (\vec{E}) tangential with the surface. No areas on the electrodes with \vec{E} concentration. \vec{E} is intensified in the interface: polymer/electrode/air CD can occur in the interface.
Hydrophobic spheroid		Electric field (\vec{E}) tangential with the surface. No areas on the electrodes with \vec{E} concentration. \vec{E} is intensified in the interface: polymer/electrode/air CD can occur in the interface at higher values of voltage.
Hydrophilic spheroid [237, 240, 258]		Electric field (\vec{E}) tangential with the surface. No areas on the electrodes with \vec{E} concentration. \vec{E} is intensified in the interface: polymer/electrode/air CD occur in the interface at low values of voltage.
Rectangles [238, 239]		Electric field (\vec{E}) tangential with the surface. Areas on the electrodes with \vec{E} concentration. \vec{E} is intensified in the interface: polymer/electrode/air CD can occur at the interface and occur under very low values of voltage at the upper corners of the electrodes.
Planes [231, 232]		Normally are made with aluminium paper or plates. \vec{E} is highly concentrated at the tip of the electrodes.
Plane to plane [261]		Electric field (\vec{E}) perpendicular with the surface. No areas on the electrodes with \vec{E} concentration. \vec{E} tends to be uniform.
Inside the dielectric [167, 235, 236, 262]		\vec{E} tends to be uniform. \vec{E} has bigger influence in the material's bulk. No presence of corona activity around electrodes influencing the surface.
End insulator specimen representation [240]		\vec{E} is close to the \vec{E} generated in real insulators (Scale model). It is no useful when a high number of samples is used in the experiments.
Electrodes covered by dielectric material [263, 264]		All discharge activity around the electrodes is cancel. The applied voltage must to be well estimated to induce the right \vec{E} . ϵ_r of polymer under test and resin are similar. No concentration of \vec{E} will be generated in the interfaces.

7. ELECTROHYDRODYNAMIC PHENOMENA ON POLYMER INSULATORS SURFACE

7.1. Background and Scope of this Sub-Research

In this part of the study the degradation process of polymer insulators surface, seen from a small observation scale, is developed. On the literature reviewed, the main focus of investigations has been the last stages of ageing, characterizing the dry band arc phenomena from all different possible angles. Incipient degradation processes and how they evolve during early stages has not been receiving the same research investment and many aspects are not well understood. Being this early period of the conditioning process for the subsequent degrading development, increasing and improving the knowledge of this can offer additional understanding of the later ageing phenomena.

7.2. Main Goals of this Study

When surface degradation process of polymer insulators is observed from a macro point of view to a more reduced one, it is not difficult to reach the observation that the effect starts from the first moment of their manufacture or, being more conservative, from the moment they are placed in service. Mainly at the early stage of degradation there are uncountable factors which influence the later stage of ageing.

During the development of this work the influence of different factors is evaluated. Some of them are treated more rigorously than others that will only be focused using exploratory experiments. In the first group are included: first corona current pulses, leakage current characteristics, roughness and corona pulse influence on water droplet dynamics, among others. In the second group are: evaporation's influence on contact angle and on surface conditions, and thermal gradient effect.

In early degradation stage, duration of stress in the same place of the insulating material surface is particularly important, even more than the leakage current magnitude. Strong discharges on polymeric surfaces in the presence of moisture are mobile; therefore, it will

not last long enough to cause ageing. Material deterioration depend on a combination of discharges intensity and duration. The effect of small discharges, which appear on a polymeric surface in the presence of water drops over a longer time, is worse than of strong mobile discharges. Having this in mind, knowledge of which are the properties or characteristics of the first leakage current pulses caused by water droplet presence and electric stress give information on the worst conditions for the insulation surface.

At the same time, characterizing the leakage current behaviour before corona pulses start offers information about when polymer surface is starting to behave less like a capacitor and more like a resistor even before dry band arcs start to be part of the ageing process. Electrohydrodynamic behaviour on the surface is influenced by different factors. Studying the influence of roughness versus corona pulses on the dynamic process is an objective to reach. Figure 2.1 summarized the main objectives and lines of investigations which were planned in this research. One route is focusing the electrohydrodynamic phenomena and the other is to evaluate if circuit representation explanations of the processes is an option.

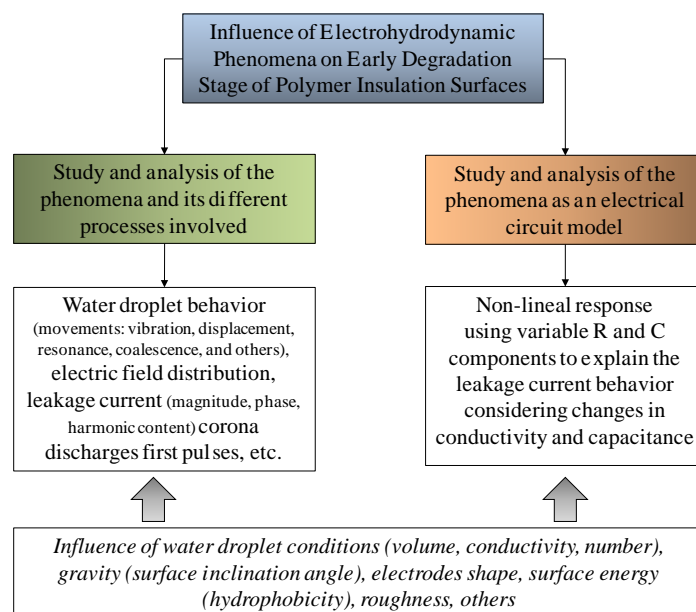


Figure 7.1 Main proposed goals to achieve with this study

7.3. Experimental Techniques and Circuits

Figure 7.2 to Figure 7.5 show the main experimental test arrangements used or implemented to collect the data required to reach the main objectives raised for this work.

In Figure 7.6 to Figure 7.8 the three main parts of the experimental set are presented. It is important to mention that different parts of the whole system are activated for each test performed. This will be explained at the beginning of each test.

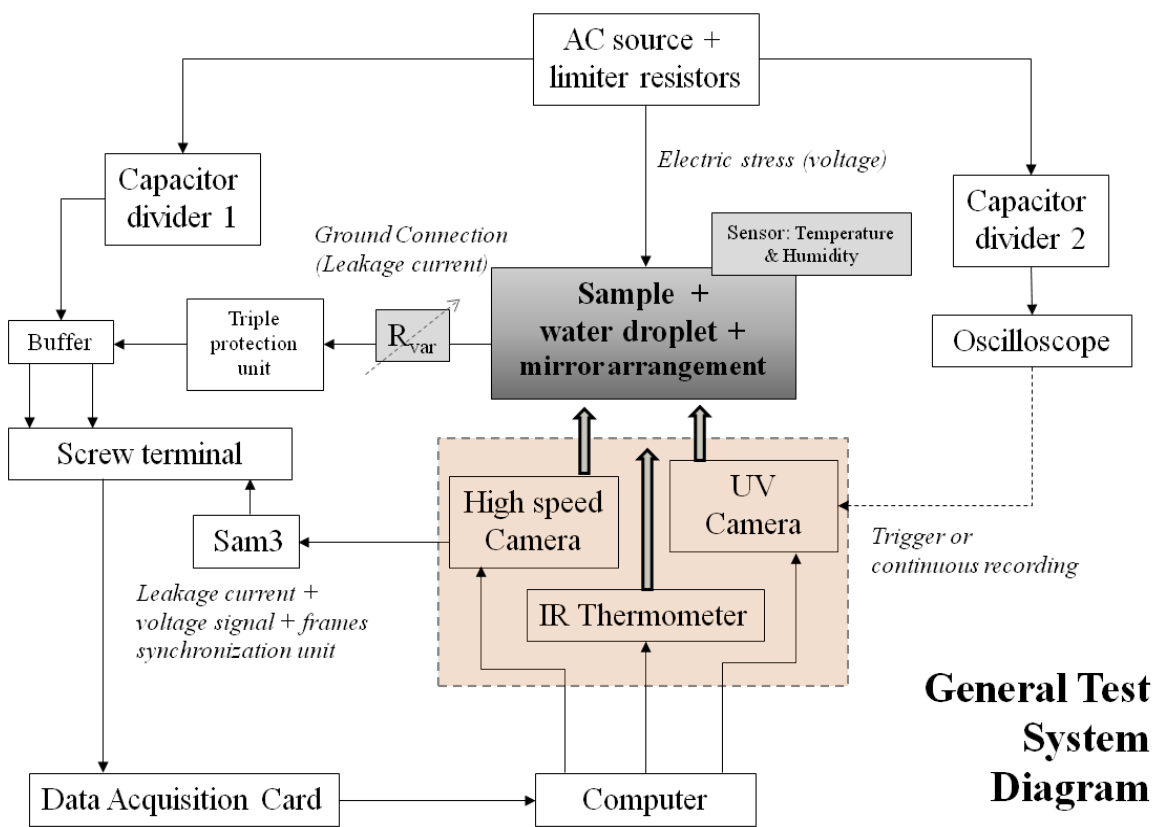


Figure 7.2 Scheme of the general test system implemented

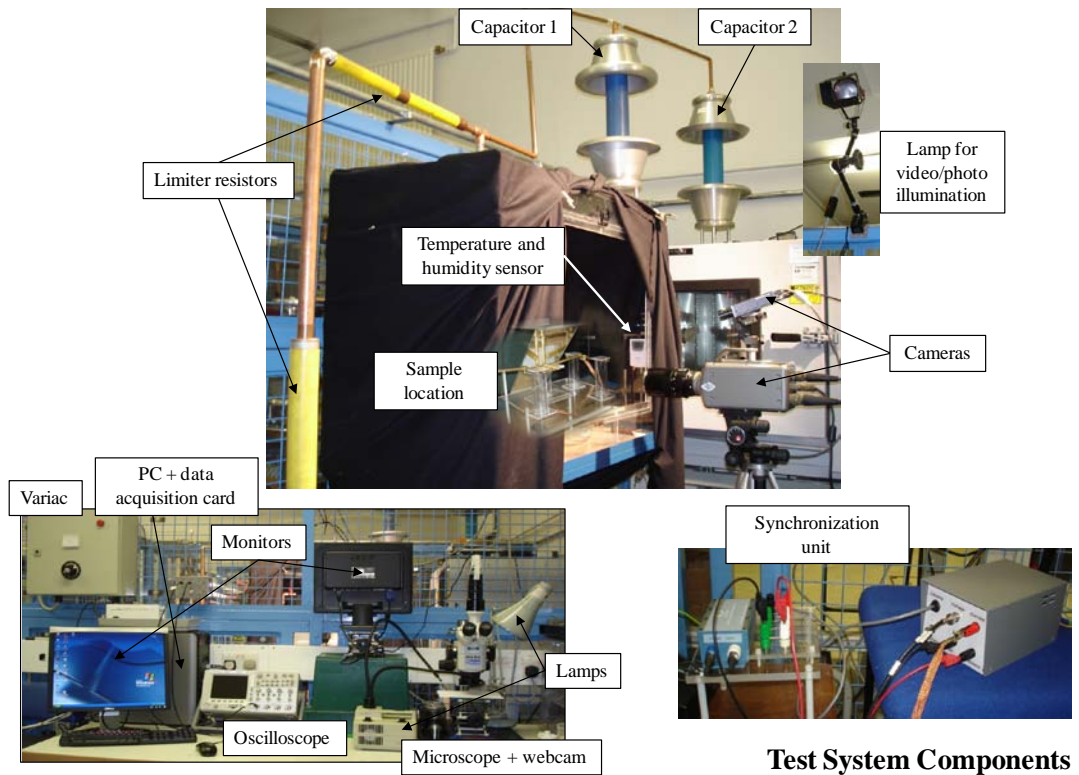


Figure 7.3 View of the main components and instruments used

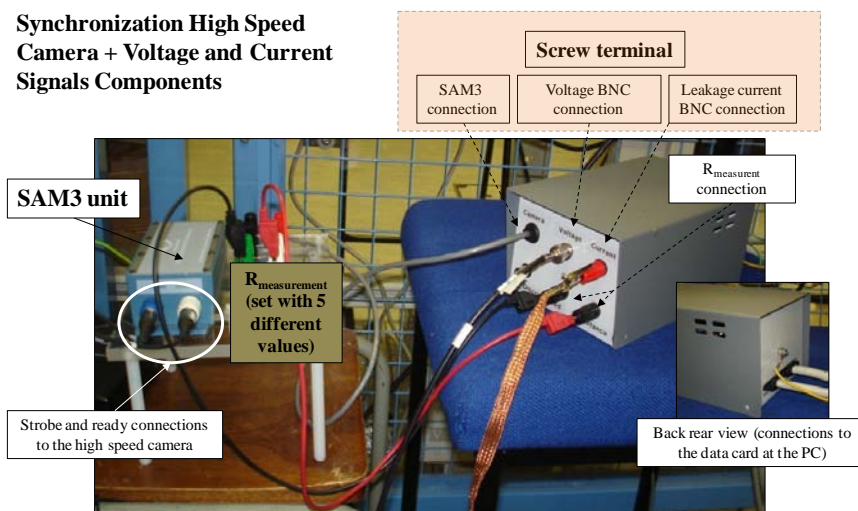


Figure 7.4 Components to collect and synchronized the voltage and leakage current signals with high speed camera frames (buffer and a protection circuit boxes are not included in the image)

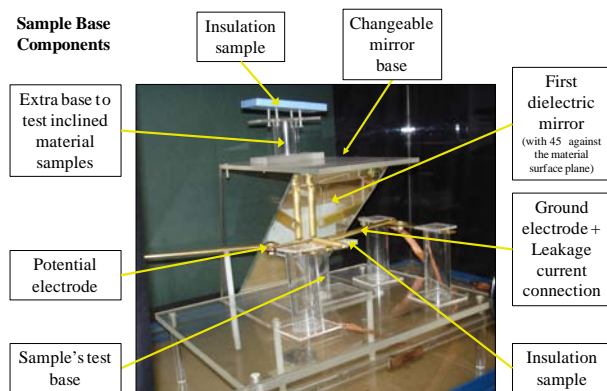


Figure 7.5 View of sample test bases, electrodes, and one side of the mirrors systems. A second mirror was placed in front of this one to reflect the image to the camera for some experiments

Applied voltage signal, leakage current signal and images were synchronized using the high speed camera and the SAM3 unit. Figure 7.6(a) shows the general diagram of this step and Figure 7.6(b) presents the final view of the output. The data of voltage and leakage current signals versus frame number were also stored as Excel files. This gives the possibility of posterior calculation (using Matlab or Excel) of additional values (like power, energy, current pulses, etc) involved during this part of the phenomenon.

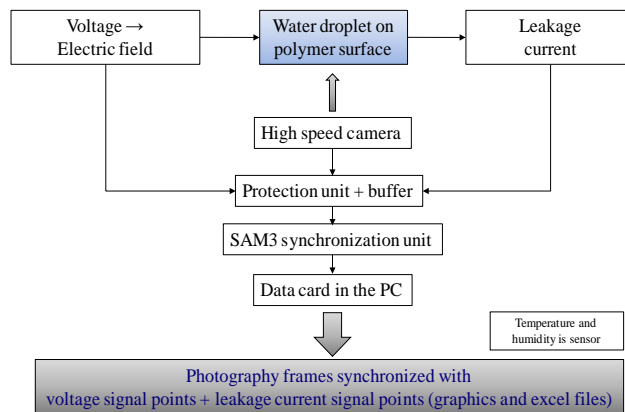


Figure 7.6(a) Sub-scheme for high speed camera and signals recording

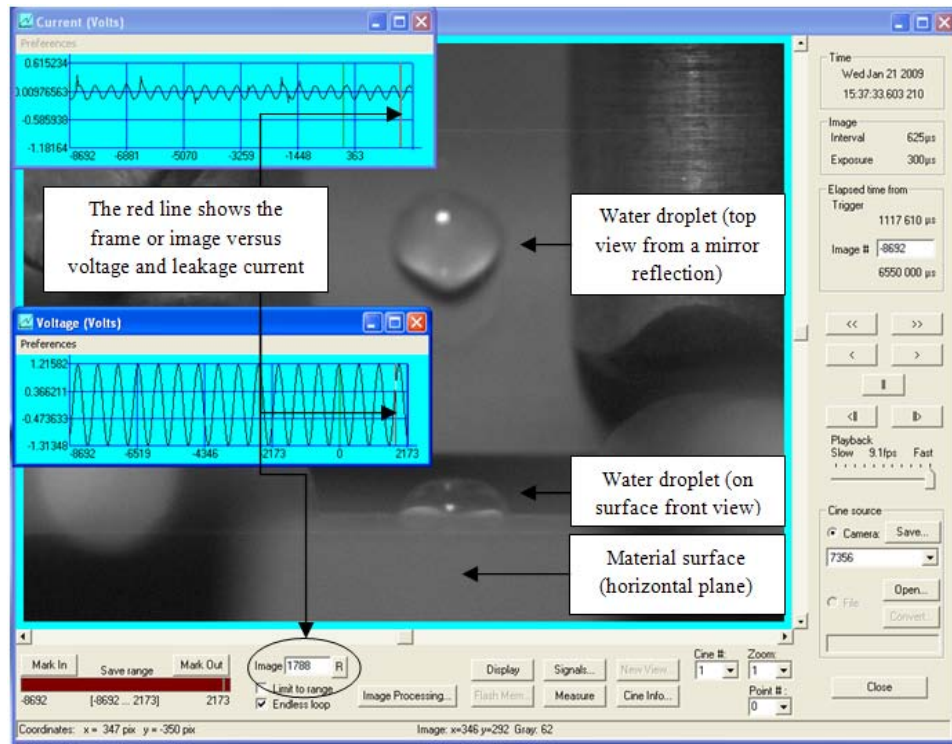


Figure 7.6(b) High speed camera images/videos synchronized with the voltage and leakage current signals

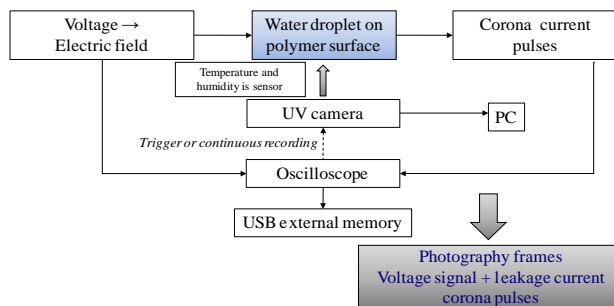


Figure 7.7 Sub-scheme for UV camera and signals recording on the oscilloscope

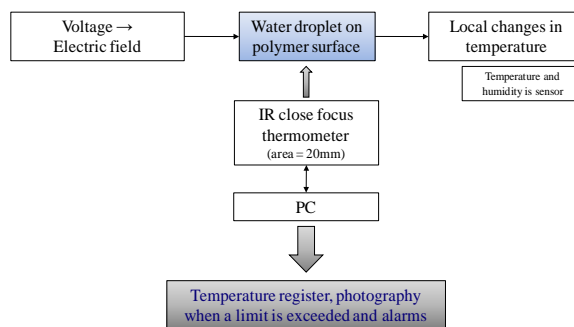


Figure 7.8 Sub-scheme for temperature measurement approximation on sample surface (for comparison with the general environmental conditions surrounding the test area)

7.4. Flashover Test under Dry conditions

To understand better the phenomena caused by water droplets on hydrophobic polymer surfaces is important to understand which processes are activated on dry surfaces and how they behave under an AC electric field, in particular when a flashover occurs.

7.4.1. Test Procedure

Two electrodes with the shape shown in Figure 7.9 were parallel placed on silicone rubber samples (120 x 50 x 8 mm) with 25mm gap. This electrodes' shape selection will be explained in item 7.14 of this chapter. The voltage was increased slowly till the flashover voltage was reached. Five different values were taken changing the sample for each test. The electrodes were cleaned after each discharge to avoid that carbon residues affect the final values.

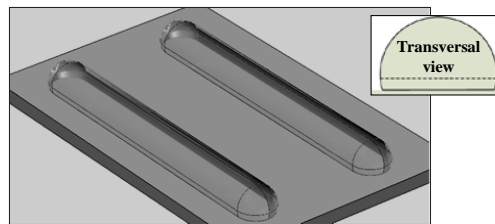


Figure 7.9 Electrodes shape and location on the surface

7.4.2. Results, Phenomena Observed and Analysis

The average value of flashover voltage was 21.8 kVp, corrected to standard environmental conditions. This means, that the electric field is approximately 8.7kV/cm, assuming uniform distribution of it along the interelectrode area.

Explaining surface flashover under dry conditions in a basic way requires considering two different aspects: (1) material surface effects and, (2) interface air/metal electrode/polymer (triple point) behaviour under an electrical field.

Unavoidably, impurities are placed on the surface of the dielectric material. They act as the source of secondary electrons which are produced by the impact of photons and electrons from the leader of the discharge. Because air molecules are very far apart, the surface appears to produce these secondary electrons more efficiently which greatly

increases the value of α (Townsend coefficient), and this causes flashover on the dielectric surface, at a voltage well below the breakdown voltage of the gap in air. The process is, in consequence, more difficult when the material surface is completely clean.

In case of triple points or interface lines (air/electrode/dielectric) it is expected that the adherence is not perfect between the electrodes and the surface leading to irregular micro gas gaps. Even though the electrodes were polished and rounded there still are micro irregularities in contact with the micrometer roughness of the material. This contour will have a higher electric field than the rest of the interelectrode gap and will produce local ionization at much lower voltages than the same gap filled with air. As the voltage across the whole gap increases, the discharge will get more intense and feed electrons and ions into the main gap. These electrons will be multiplied through the normal ionization process, and could cause breakdown at a lower voltages.

It is important to mention that after each flashover test the surface material temporarily loses its hydrophobicity. This condition was observed when water droplets were placed on the interelectrode surface after the flashover occurs. If the water droplet was placed out of the channel discharge path, small contact angles ($< 45^\circ$) were found; if the water droplet was placed on the discharge path, water is extended on the surface as a wet layer. This condition stands for a while (this period depends on the time to rise the voltage during the flashover test and time with corona activity on the surface) and then the material recovers completely its hydrophobic condition. Hydrophobicity recovery time tended to be around few hours to one day.

Looking for a specific explanation, two main causes of this temporary hydrophilic condition of the surface were explored: (1) charges were released and kept on surface, and (2) changes on polymer surface structure occur. In [265] authors found that charges are not the dominant process of hydrophobicity loss of material surfaces and there is almost a general agreement between authors that charge released to the surface is not enough to make this change. On the other hand, different investigations for industrial applications, mainly related with printing, coating, etc, use AC corona treatments to change surface polymer's properties increasing its wettability and adhesiveness. They show that efficiency of short duration corona treatments is limited by the development of a surface layer, composed of oxidation products of the polymer which are weakly bound to the substrate

[266]. This characteristic means they can be easily removed by washing or by waiting time.

Looking deeper in this process it is found that discharge products transfer their activation energy to the polymer by breaking chains and creating radicals. These will rapidly react with the further impinging particles, with the environment, and even in some cases with gas coming from the bulk material. Polar bonds and hydrogen bonds formed in this way will increase the polymer surface energy. The bonds most frequently found are carbonyls and nitrates in smaller amounts: C - , C = O, C - O - O \cdot , C - OOH, NH, NO, NO₂, NO, mainly. The effect of corona treatment increases with time and current until a saturation rate is reached; then oxidation processes are counterbalanced by decarboxilation processes, as revealed by ejection of CO, CO₂ and H₂ molecules emitted from the surface. The chemical changes in the surface are often accompanied by changes in the structure, generally with a loss of crystallinity, which must be attributed to the large number of short chains remaining on the surface [267].

Other fundamental phenomena induced by corona which may contribute to or affect the surface degradation, which required normally more time or intensity, are: (1) Density variations, for instance a decrease induced by oxygen grafting/incorporation or an increase due to crosslinking by active nitrogen, causing surface deformation or change in porosity; (2) Migration phenomena, changing the surface topography, and (3) Sputtering phenomena, or processes whereby atoms are ejected from the surface material due to bombardment by energetic particles localized at the impact/erosion areas of discharges.

The effect of corona on surfaces also depends on polarity. Negative coronas generally appear to be less severe than positive coronas, both for oxidation and etching. Contributing factors are that the energy delivered to the surface by charge neutralization is lower for negative ions than for positive ones and that streamers generated in positive coronas submit the surface to concentrated bursts of high energy ions [267].

Summarizing the process, when a polymer surface is under the effect of corona discharges, the electrons generated by them impact on the surface with high enough energy to break the molecular bonds on the external layer of the surface. The resulting free radicals react rapidly with the oxidizing products of the corona discharge, or with adjoining free radicals on the same or different chain, resulting in a crosslink reaction. Oxidation of a solid

surface increases the surface tension energy, changing hydrophobic properties, allowing wetting by liquids and promoting adhesion. Increasing surface tension making hydrophilic the surface is most assuredly related to the oxidation of the polymer surface resulting in polar groups on it, primarily hydroxyl, carbonyl and amide groups [268].

7.5. Flashover Voltage with Water Droplets on Surface

The study of single water droplets under different conditions (number, volume, location, conductivity, etc) have been evaluated and reported by different authors, mainly focusing the electric field point of view looking at flashover voltage, corona inception voltage and instability of one water droplet. In this part of the work, equivalent tests are presented looking to additional variables and phenomena and using less symmetrical water droplets locations on surface.

7.5.1. One droplet centre between electrodes placed on surface

Test Procedure

Two electrodes, with the shape previously shown (Figure 7.9 Electrodes shape and location on the surface), were placed parallel on silicon rubber samples with a 20mm gap. By using a micro-precision syringe single water droplets were carefully placed on the centre of the gap. The AC voltage was raised slowly, typically at about 1kVp/min until one of either of these phenomena occurs: (1) pulses of leakage current detected through a measuring resistor, $R_m = 12.5 \text{ k}\Omega$ on the oscilloscope, or (2) any displacement or slide is detected in the high speed camera video screen. When one of these conditions is reached, the magnitude of the voltage is recorded. Then, the measuring resistor is short-circuited and the voltage is increased until flashover occurs. Volume and conductivity of the water were varied. Each test was repeated three times and the average value is reported.

Following the same procedure, water droplets were placed close to the potential electrode (Potential or V side), or close to the ground one (Ground side). V side, means 7mm between the energized electrode and the centre of the water droplet; Ground side, means 7mm between the ground electrode and the centre of the water droplet or at 13mm from the energized one.

Although the circuit has a current limiting resistor, precaution was taken to stop the current flow quickly after the flashover to avoid extra degradation of the insulation sample surface. Additionally, after each flashover the electrodes were manually polished and cleaned to avoid that carbon residues affect the next test.

Results, Phenomena Observed and Analysis

Results are presented in Figure 7.10 to Figure 7.12. As can be seen in Figure 7.10, there is a reduction on the corona onset voltage between 30 – 50% when the volume of the droplet is increased and it depends also on the water conductivity, with less variation for deionized water than when the conductivity is higher. There is a tendency of bigger differences when the conductivity is over 1000 μ S/cm and when the volume is higher than 50 μ l.

The current pulse onset voltage occurred always in the positive half of the applied voltage, as it was expected, and this means that the first current pulse is associated with a streamer propagating between the positive charged side of the water droplet and the negative electrode at that moment. If the conductivity of the water is higher, the propagation is facilitated because the resistance is reduced by the high electron mobility and density.

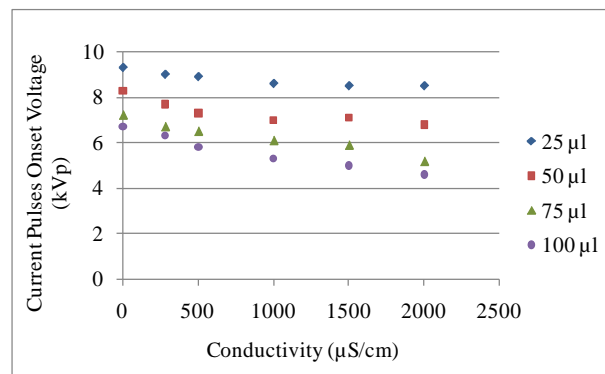


Figure 7.10 Corona Onset Voltage for one centre droplet with different conductivities of the water and volume

Observing the flashover voltage in Figure 7.11, a reduction is also observed and it can be between 15 – 20% when the volume of the droplet is increased and it depends on the water conductivity, with less variation for deionized water than when the conductivity is higher. The same tendency is observed for the flashover voltage as for the corona onset voltage in relation with droplet volume and water conductivity. When the volume of water droplets increases the distance between the border of the droplets and the electrodes is reduced

increasing the corona activity and the risk of flashover. In relation with the conductivity, its influence is more related with donation of charges to the process than enhancement of the electric field. Conductivity, σ , is proportional to the fundamental charge of the electron, its density and mobility. In consequence, water droplets with higher conductivities should have more charges to release helping the discharge process.

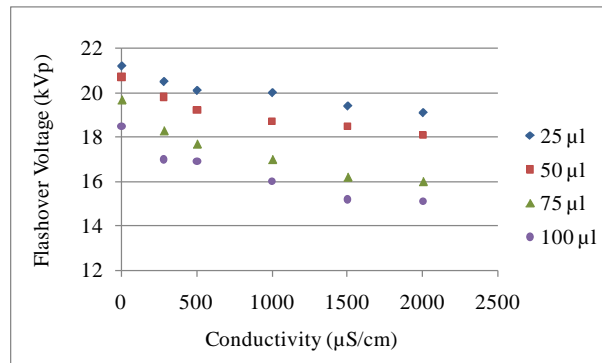


Figure 7.11 Flashover voltage for one centre droplet with different conductivities of the water and volume

In the Figure 7.12 the influence of water droplet position is presented and as is expected, the values of the flashover voltage are significantly reduced when the water droplets are placed close to the potential electrode, higher volume and conductivity. It is worthy to mention that here were excluded the values when the water droplets skates toward the potential electrode at very low voltages caused by corona discharges and very low adherence.

Different phenomena were observed to reach flashover under this condition: (1) it can occur after vibration plus elongation of water droplet; (2) sliding of the droplet can occur before any elongation or movement; (3) some flashovers disintegrate the droplet creating a water layer or path and others do not; (4) some flashovers occur close to the water droplet without cross it; (5) some flashovers eject very small droplets, among the most representative and recurring. Additional experiments were conducted to observe these processes with more details.

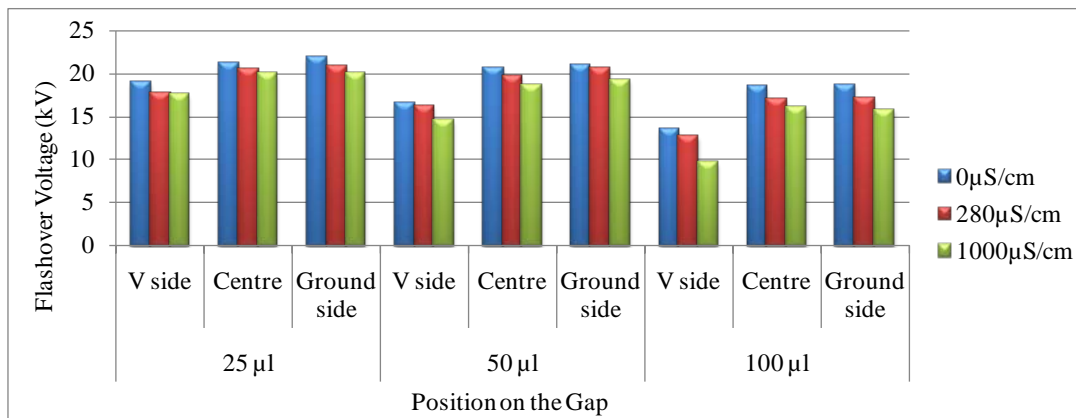


Figure 7.12 Flashover voltage versus water droplet location, conductivity and volume

7.5.2. Single Droplet's Flashover Mechanisms and Water Channel Formation: Elongation followed by multiple flashover discharges before a water channel is formed

Test Procedure

One 50 µl droplet ($\sigma_w=200\mu\text{S}/\text{cm}$) is placed centred on the interelectrode gap ($d=25\text{mm}$). Images and electrical signals (voltage and leakage current) were recorded. The system was set up to take 2100 fps at 768x768 of resolution, a period of 476 µsec for the images, and 250 points per image for each signal.

Figure 7.13 shows the voltage and leakage current of a water droplet under electric field after instability and significant corona discharges started (time considered as 0ms). Previous to this point, only rhythmical movements of the water droplet are observed and small pulses of corona are detected on the leakage current signal with no significant changes of the water droplet shape. Elongation of the water tips towards the electrodes (mainly the potential one) is observed after a threshold voltage is reached (~17.5 kV) although corona discharges appeared around 8kV. The number of positive discharges is significantly higher than negative ones. Voltage behaviour can be analyzed in Figure 7.13 to Figure 7.15 (leakage current is not included once the measurement circuit protection acted after the first flashover. Intermittency of the arc can be easily followed looking at the voltage signal and it was verified looking at the images recorded).

Looking at the prebreakdown time (0-94.86msec) it can be observed that magnitude and number of current pulses on the first quarter of the positive voltage signal is higher in

magnitude and number and when the flashover event is closer the pulses are more coincident with the positive peak of the signal. The flashover is composed of one arc with no reigniting till the next positive semicircle. Four additional times the arc is reignited always at the maximum of the applied voltage positive half cycle. After this, a first discharge in negative polarity occurs (at 204.68 msec, see Figure 7.16 and images). Once this condition of arc ignition occurs in both sides of the voltage the process starts to have multiple arc reignition in both sides, the water droplet elongates considerably shortening the path between electrodes, voltage drops significantly ($<10\text{kV}$) and a dry band arc process with high current takes place. Voltage drop is caused by a drop in the surface resistance increasing the current and drying the wet channel. Some authors define this change from an electrically stable discharge to an unstable one.

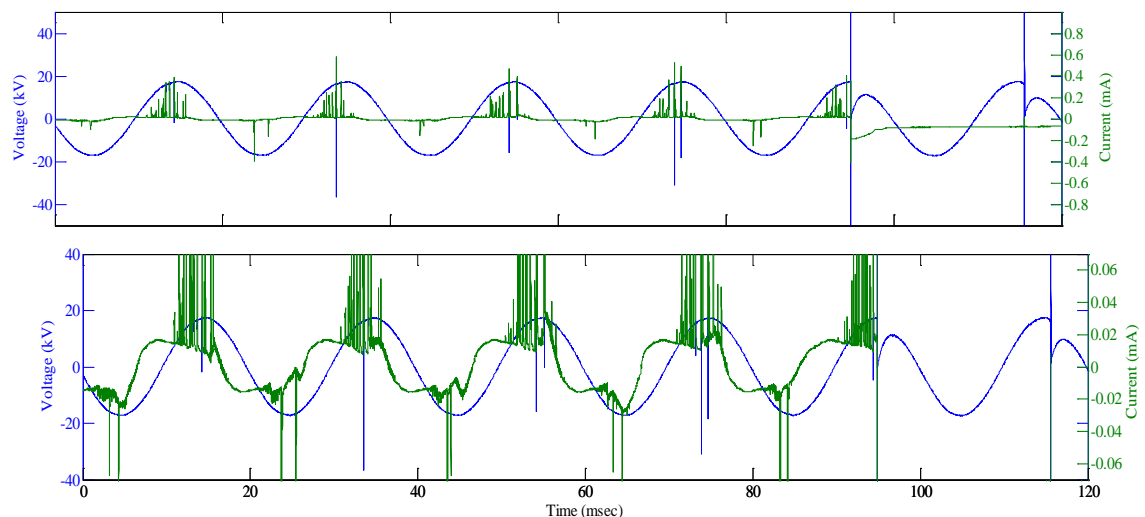


Figure 7.13 Voltage and leakage current followed by a flashover at 94.86 msec at the positive V_{peak} . At the top current pulses are shown; at the bottom a ten times magnification of the current pulses is presented

In the Figure 7.14 the time of the arcs between the initial evaluation time (defined as 0msec) to 300msec is presented; polarity, reignition time and some observations extracted from the images in Figure 7.15 are included as well. Reignition time was extracted from the images/signal synchronization system.

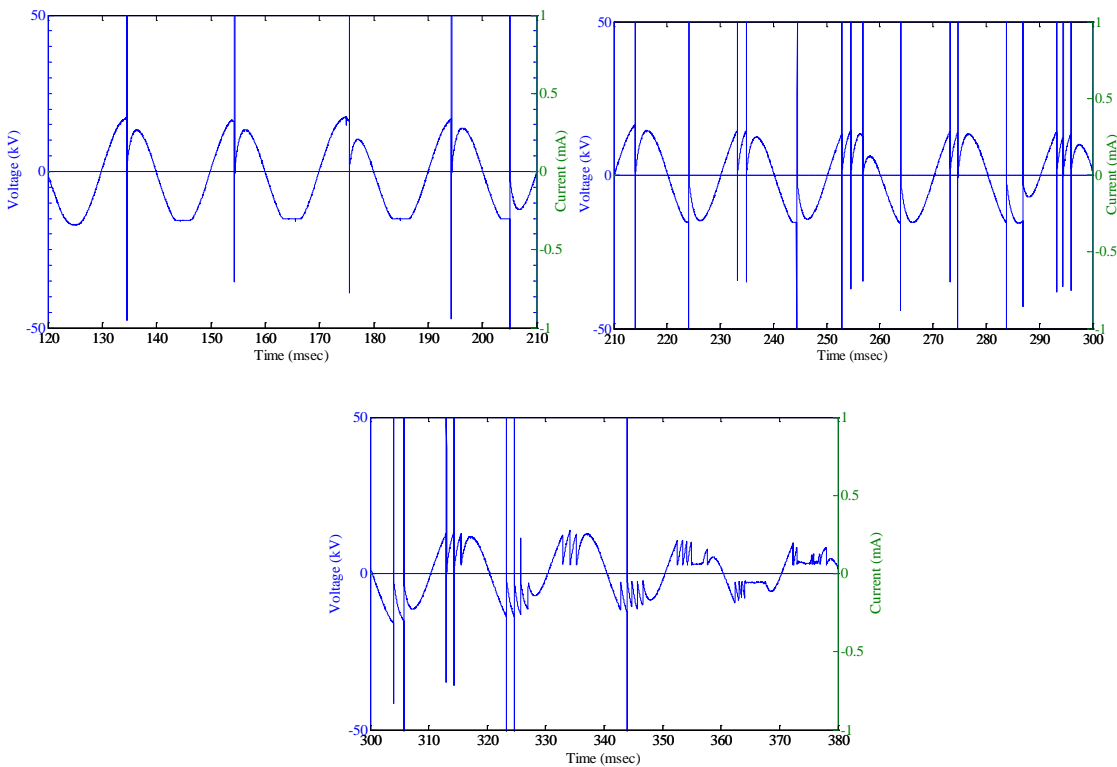


Figure 7.14 Voltage behaviour between 120ms and 380ms

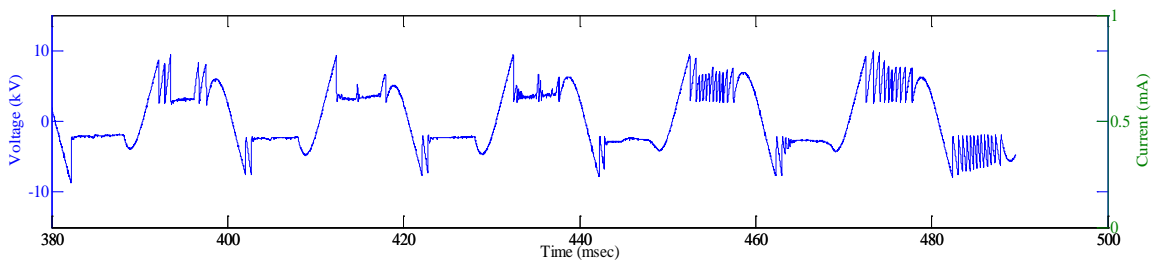


Figure 7.15 Voltage signals between 380ms and 490ms where multiple dry band arcs are observed

As it was described, at the initial stage of the arcing process the main discharges have positive polarity which indicates that there is a particular list of chemical components and ions which be introduced and deposited on the surface. At the same time specific components will be extracted from the most superficial layer of the dielectric.

Table 7.1 Flashovers occurrence time and details crossing over the water droplet

Time (msec)	Positive	Negative	Observations
< 94.86	-	-	Water droplet has an extension tip towards the ground electrode at 12 kV (See circle at 94.86 msec, Figure 7.16). Corona discharges occur surrounding the triple line, mainly at the areas in front of the electrodes and these are more intense at this tip (as described by Taylor cone jet. The full extension of the droplet is 6.97mm.
94.86	x		One discharge per semicircle. Strong vibrations and extensions are observed after each flashover.
115.19	x		
134.23	x		
154.22	x		
175.17	x		
194.21	x		
204.68		x	First pulse in negative polarity.
213.72	x		
223.72		x	
234.67	x		The shape of the droplet starts to be distorted at the contact area losing its round appearance. The tip towards ground electrode grows.
244.19		x	
252.76	x		Consecutive discharges in the same positive semicircle (3 flashovers). Strong turbulence and extensions are observed after each flashover.
254.18	x		
256.56	x		
263.70		x	
272.75	x		Two consecutive discharges in the same positive semicircle.
274.36	x		
283.70		x	Two consecutive discharges in the same negative semicircle.
286.55		x	Extension toward the potential electrode covers more than 75% of the distance (centre/electrode). After this moment multiple flashovers occurs in both polarities. Following a discharge at 303.69msec a water channel is fully formed towards the ground electrode and smaller arcs occurs towards the potential side.

The next images show the process followed by a single water droplet placed on the centre of a 20 mm gap. Strong vibrations and extensions are observed after each flashover.

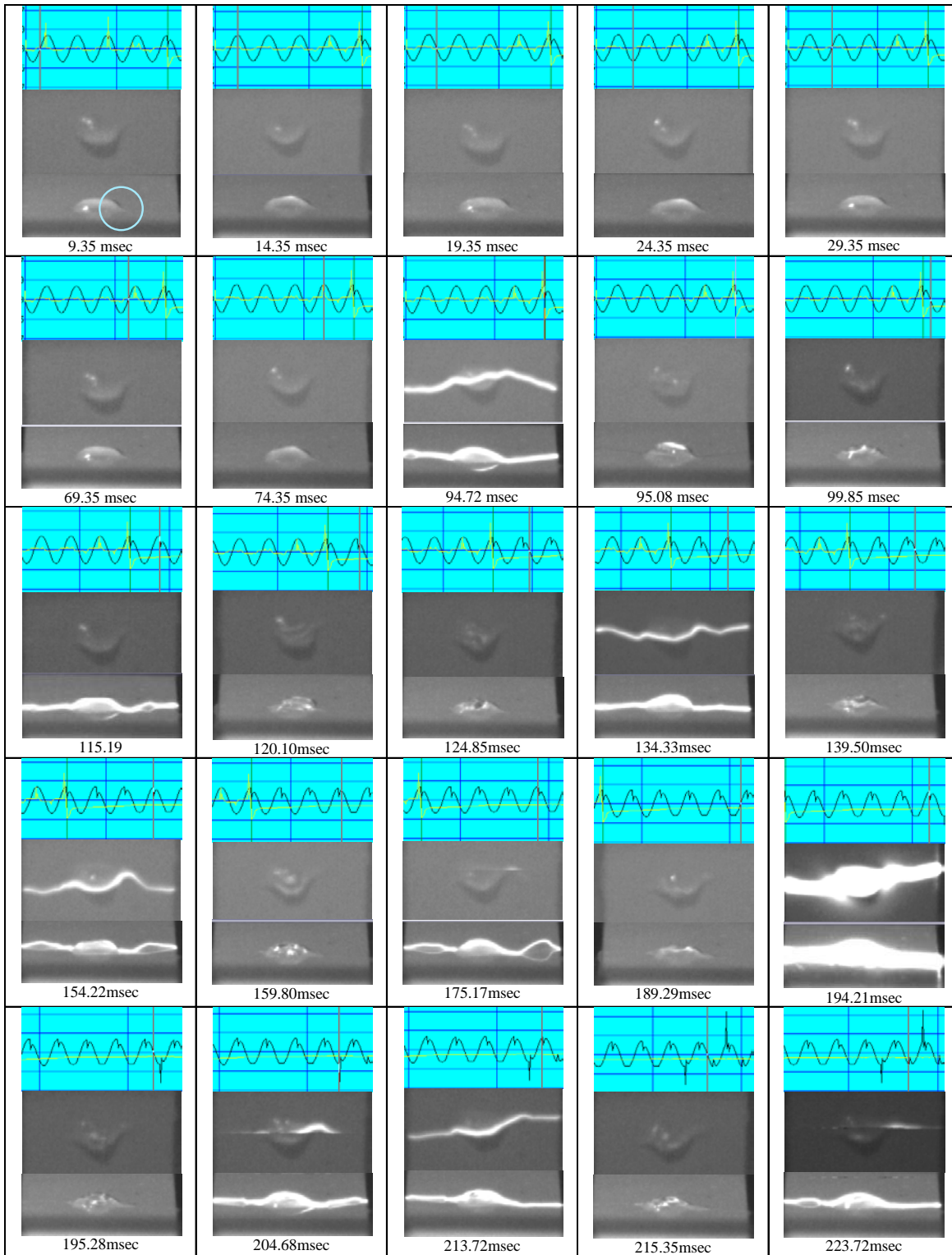


Figure 7.16 Images of the movements after corona inception, and flashover, gap 25mm, 50 μ l droplet

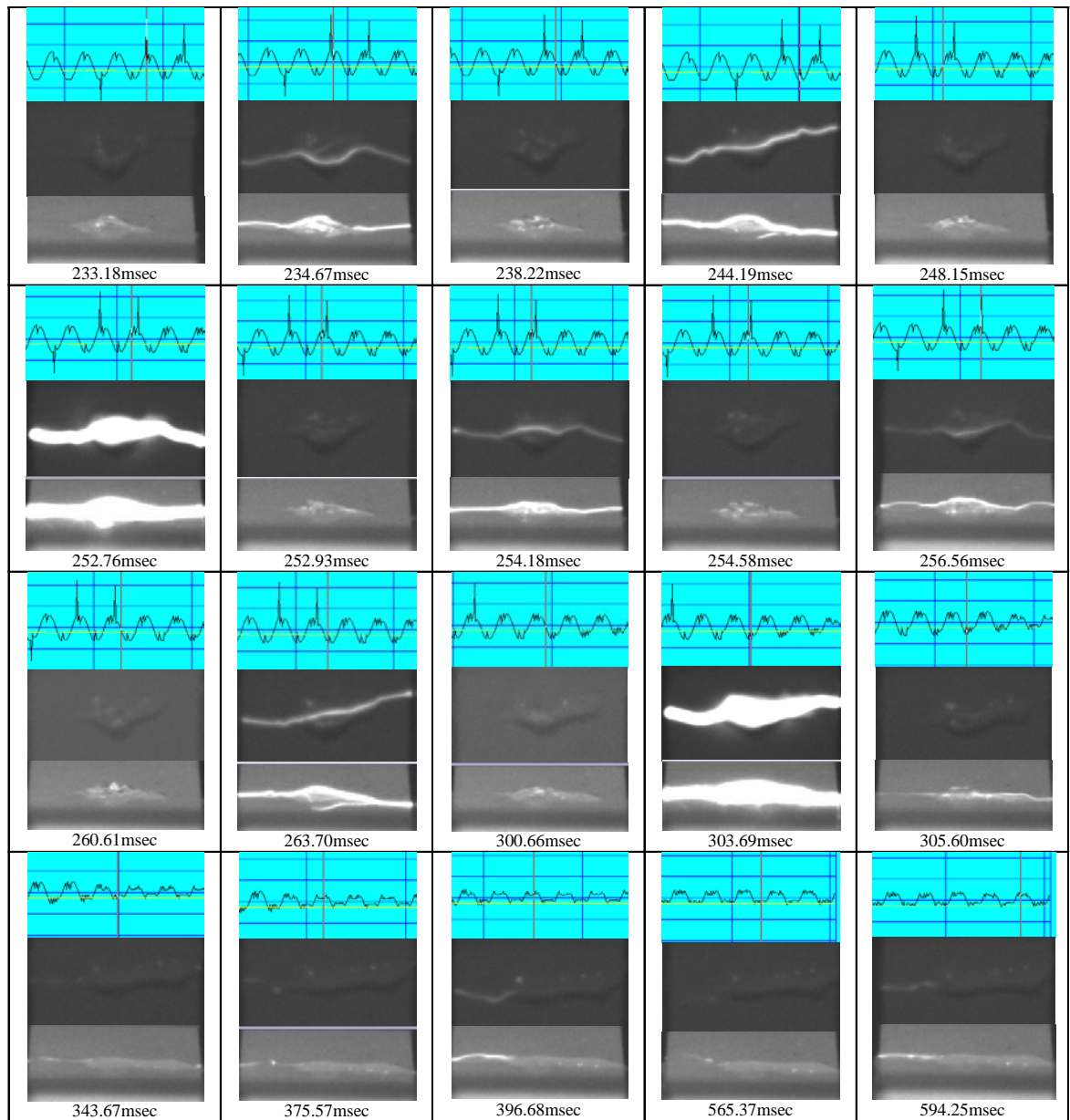


Figure 7.16 (con't) Images of the movements after corona inception, and flashover, gap 25mm, 50 μ l droplet

7.6. Flashover observation between two aligned water droplets

Figure 7.17 shows the leakage current and voltage applied between two aligned water droplets versus elapsed time, where corona discharges, movements and deformation/extension of the water droplets happened. In Figure 7.18 some representative images are presented. In this experiment corona is first observed between the tips of the droplets towards the electrodes and subsequently between water droplets. The formation of the water channel is easily produced and the multiple arcs' ignitions are favoured. Negative pulses on the leakage current with higher magnitude and repetition rate are detected. This is mainly caused by the droplet/droplet discharges.

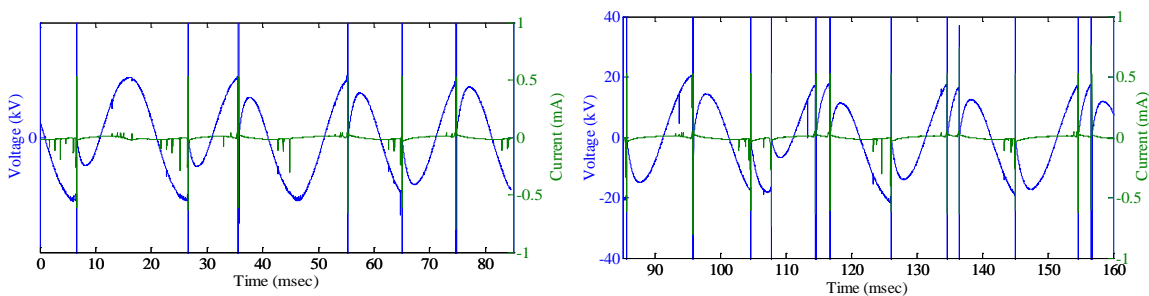


Figure 7.17 Voltage and leakage current signal for flashovers over two droplets

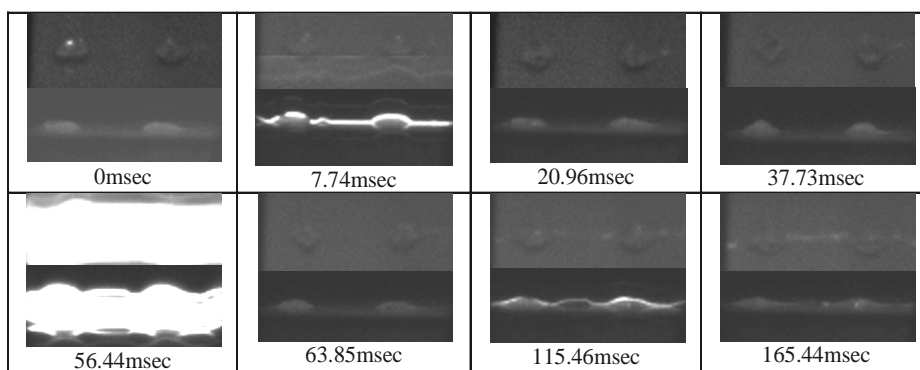


Figure 7.18 Images of the flashovers of two droplets aligned with the electric field

7.7. Flashover observation between different cases of water droplets location, size, volume, surface condition

Some flashover processes under different conditions were observed. Here three cases are included.

Two 75 μ l, 200 μ S/cm, droplets not aligned with the electric field. One on the hydrophobic area of the material and one on a less hydrophobic region.

As can be observed in Figure 7.19 even though the hydrophobic droplet is the one presenting higher dynamic or movements and takes a similar shape than the other droplet, the flashover crosses first through the one placed on the hydrophilic side which is the one closer to the energized electrode. Displacement of the droplets was not detected in any of the droplets, highly probably caused by the big volume, but a strong elongation of the one placed on the hydrophobic part of the material towards the potential electrode was observed creating a tip and changing the shape from symmetrical to asymmetrical. Few corona discharges were detected because the flashover occurred very easily and at a low electric field; discharges were only observed at the tip formed at the droplet located at the hydrophobic area.

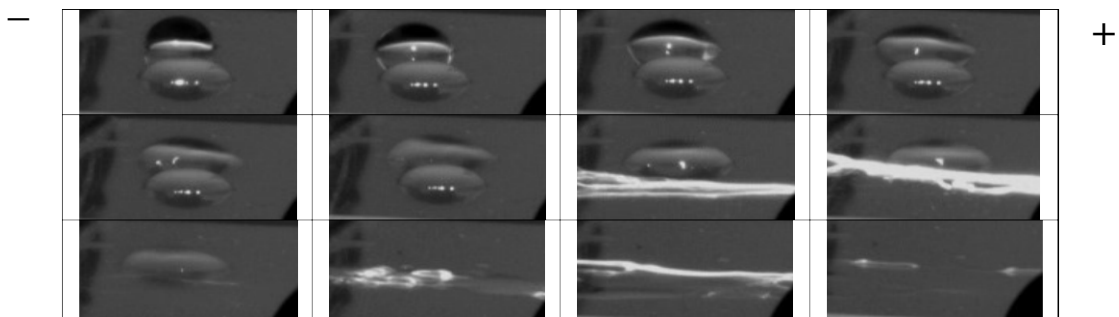


Figure 7.19 Flashover between two water droplets (75 ml) not aligned with the electric field

Two 25 μ l, 200 μ S/cm, droplets not aligned with the electric field. One on the hydrophilic area of the material and one on the hydrophobic part

Figure 7.20 shows a test with two 25 μ l water droplets; one droplet was placed on the hydrophobic area of the surface closer to the potential electrode, and a second droplet was placed on the hydrophobic region slightly moved closer to the ground electrode.

Increasing the voltage, a small elongation of the droplets occurred and an easy path for the flashover was made crossing over the extended droplet placed on the hydrophobic region. It will eventually be dried by the current producing dry band arcs. When this path is completely dried, a significant elongation of the remaining droplet is produced and corona discharges are detected at the tip facing the ground electrode and a displacement of the droplet was produced when the intensity of these discharges increased.

In this case it was not elongation; it was a glide of the complete droplet towards the high potential electrode followed by the cessation of the discharges. This is immediately followed by the displacement of the droplet towards the high potential electrode, and the cycle is reinitiated and repeated consecutively until the flashover occurred. Multiple flashovers were observed crossing over the droplet without fully destroy it, followed by multiple flashovers over the hydrophilic region until finally a fully wetted path is created with the droplet and the drying process started.

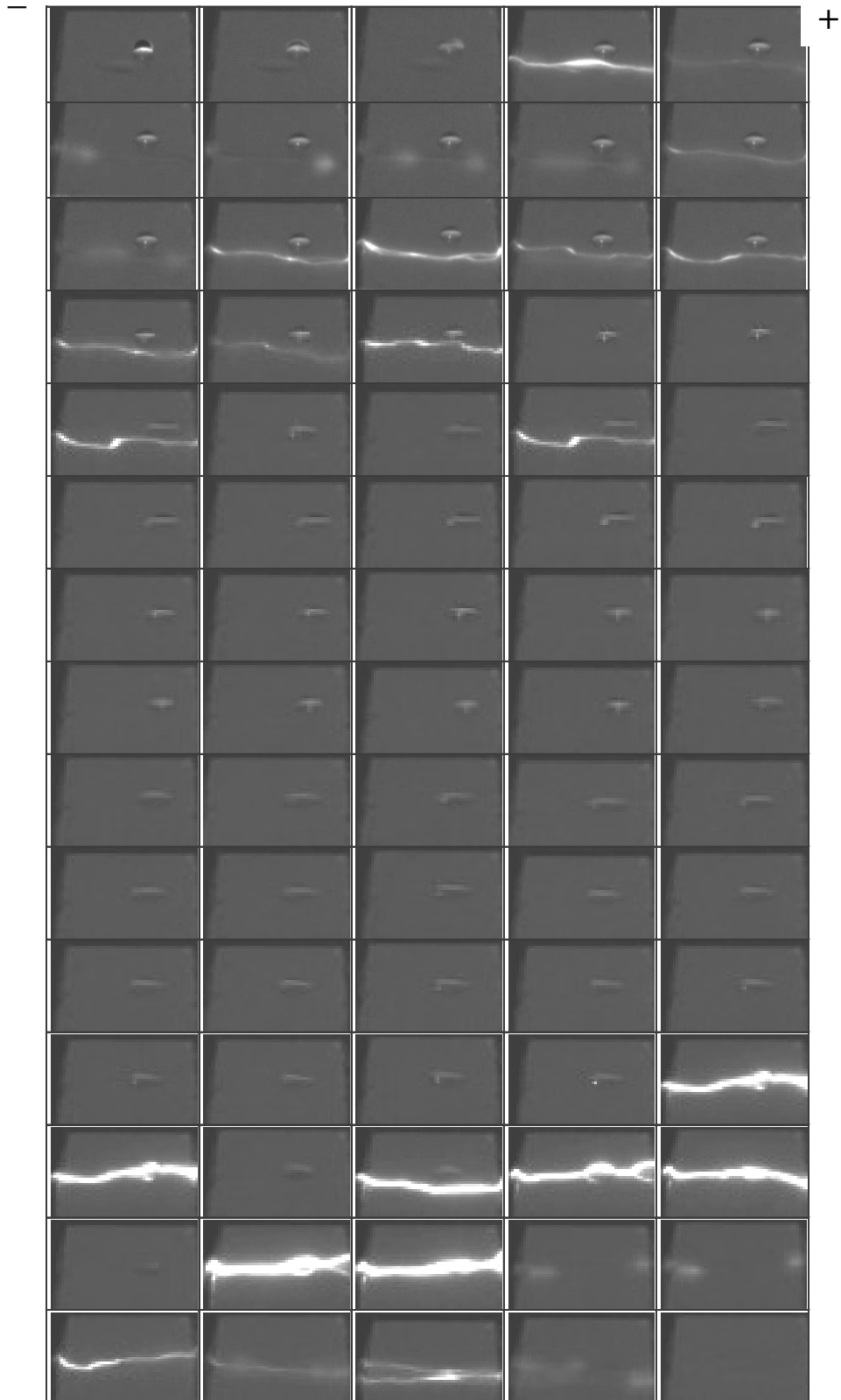


Figure 7.20 Flashover between two water droplets (25 ml) not aligned with the electric field

Three 25 μ l, 200 μ S/cm, droplets in triangle formation

In this case, multiple flashovers occurred crossing the two droplets aligned with the field before the third one is also involved in one discharge. All of them suffered elongation when electric field was applied. Dry band arcs were initiated and sustained on the surface during the drying process. Only when the path between the two aligned droplets is dried was the third droplet extended by a flashover and subsequently dried.

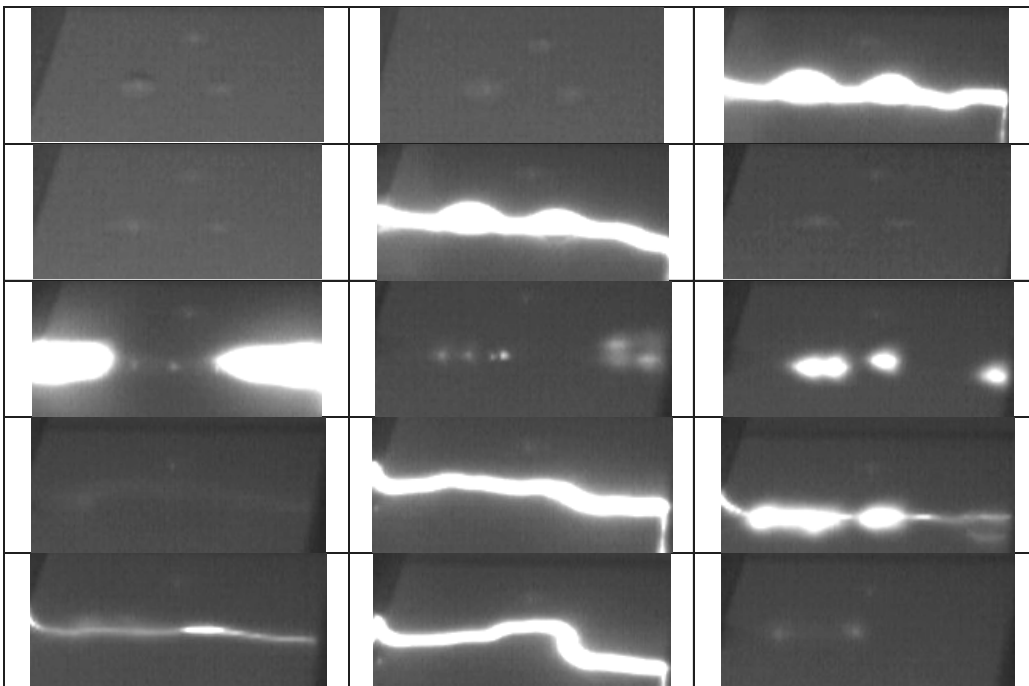


Figure 7.21 Flashover between three water droplets (25 ml) not aligned with the electric field

7.8. Leakage Current Pulses effect on Water Droplets Dynamics versus Surface Roughness

Test Procedure

Different configurations of water droplets (volume, conductivity, number and location) were evaluated for three different surface roughnesses of silicon rubber: A: 0.45 μ m, B: 0.72 μ m and C: 0.93 μ m. Roughness was altered using soft sand paper with uniform movements to minimize the reduction on contact angle final values.

The main configurations used are shown in Figure 7.22.

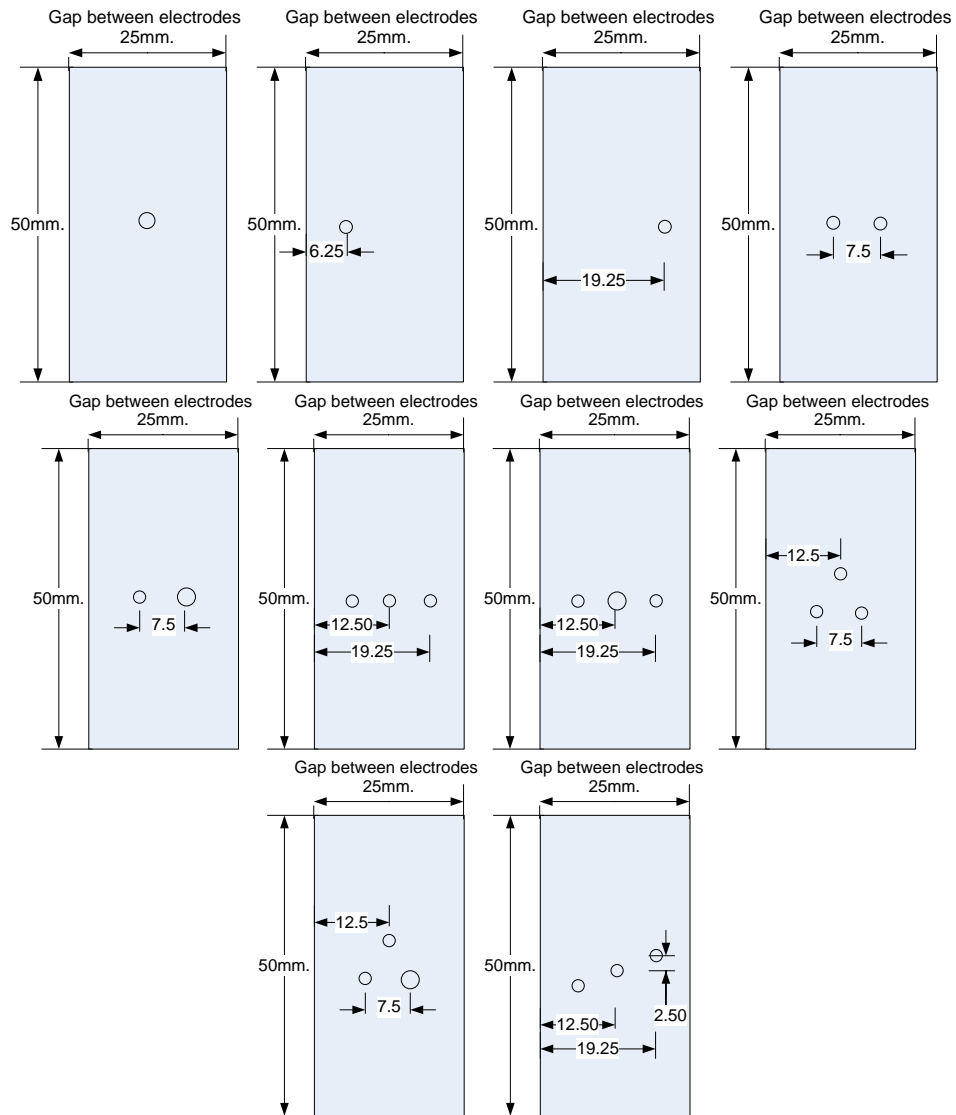


Figure 7.22 Some configurations under study (changes in droplets size means different volume)

During this experiment four consecutive cycles, after the first pulse occurrence, were observed. The first pulse is used to trigger the oscilloscope and immediately is triggered the high speed camera which preserved the information in its buffer. High speed images were recorded at 1200 fps and UV images at 3 fps.

Results, Phenomena Observed and Analysis

The movements reported here are: displacements, coalescence, and elongation in any direction, vibration, and ejections. Contractions were not considered because they introduce less severe alterations on the electric stress distribution on the material surface

and are less responsible of the final flashover or partial arcs. Only some results are included.

Assuming the percentage of all tests as 100%, the behaviour is summarized in Figure 7.23. Elongations are included in a separate figure (Figure 7.24) to improve the visualization of the other movements. Additionally, it was detected that coalescence between water droplets occurred close to the negative peak of the applied voltage and required more than one cycle to complete when the coalescence was caused more by elongation than by displacement or skate of the droplets. Coalescence introduces high inconvenience because it bridges a big part of the interelectrode gap which intensifies the electric field at the triple points and the corona discharge activity with it.

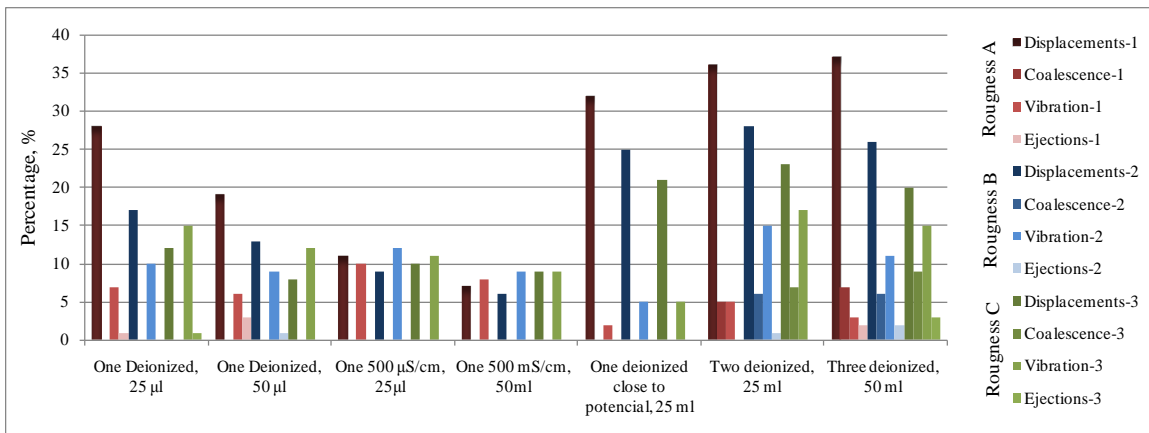


Figure 7.23 Droplets movements: displacements, coalescence, vibration, and ejections (Roughness: A: 0.45µm, B: 0.72µm and C: 0.93µm)

As can be seen in the Figure 7.24 displacements increase when roughness decreases. As a consequence of this, electric field distribution changes and takes higher values mainly because displacements are movements of the water droplets toward the electrodes. This condition will cause flashover at lower values of applied voltages. Surface roughness affects in a positive way the flashover voltage, when the number of droplets is large and with the same volume. Having droplets with different volume there is a tendency to increase the number of coalescences even when the roughness increases. Surface roughness works as a hindrance or barrier to the movement of the droplets, and consequently renders their fluctuation more difficult. The surface roughness hinders the oscillation preventing extension and displacement of droplets reducing the opportunities to

form a conducting path leading to a flashover occurrence following the direction of the applied electric field.

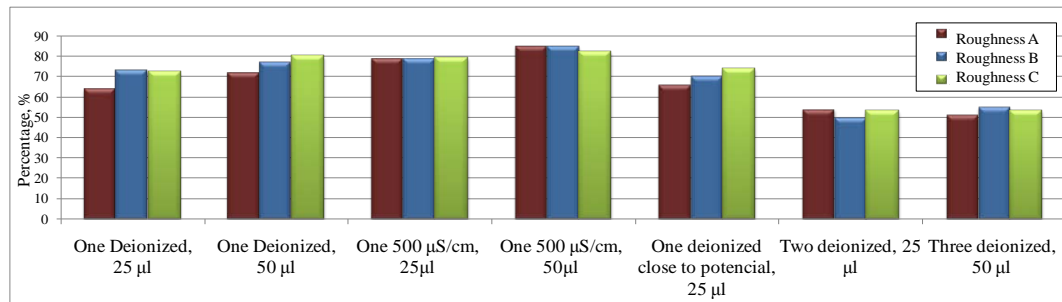


Figure 7.24 Elongation versus roughness (Roughness: A: 0.45 μ m, B: 0.72 μ m and C: 0.93 μ m)

To maintain a balanced view of the impact of roughness it must be remembered that a highly rough material is going to be detrimental and can help the capture of a pollution layer on the surface. Roughness on insulation surfaces must be evaluated and studied concerning its impact on hydrophobicity, the washing of the pollution under natural rain, on tracking resistance and on the coalescence of the droplets, among other characteristics. It does not look as an easy task but, by example, it is possible to think, given their multiple advantages, that using nanofillers in the silicone polymer matrix or nanocoatings applied by different techniques (by example, chemical vapour deposition [269]) this can be achieved.

When surface energy is lowered, hydrophobicity is enhanced. For the simplest case, the surface energy of solid surfaces is evaluated using the contact angle value, θ , given by Young's equation (Eq. (1)):

$$\cos\theta = (\gamma_{SV} - \gamma_{SL})/\gamma_{LV} \quad (1)$$

where γ_{SL} , γ_{SV} , and γ_{LV} are the interfacial free energies per unit area of the solid-liquid, solid-gas, and liquid-gas interfaces, respectively, but this equation is applicable only to flat surfaces and not to rough ones. Wenzel proposed a model describing the contact angle θ' at a rough surface modifying Young's equation as follows (Eq. (2)):

$$\cos\theta' = r(\gamma_{SV} - \gamma_{SL})/\gamma_{LV} = r \cos\theta \quad (2)$$

where r is a roughness factor, defined as the ratio of the actual area of a rough surface to the geometric projected area. Given that r is always larger than unity, the surface

roughness enhances both the hydrophilicity of hydrophilic surfaces and the hydrophobicity of hydrophobic ones.

The Cassie equation describes the contact angle θ' at a surface composed of solid and air. When a unit area of the surface has a wetted solid surface area fraction f (defined as $\Sigma a = \Sigma(a + b)$ in Figure 7.25) with a water contact angle θ , the contact angle on the surface can be expressed by Eq. (3), assuming a water contact angle for air of 180° [15]. The concepts of Wenzel [14] and Cassie [15] are outlined in Fig. 1.

$$\cos\theta' = f\cos\theta + (1 - f)\cos180^\circ = f\cos\theta + f - 1 \quad (3)$$

Johnson Jr. and Dettre have simulated the contact angle of a water droplet on idealized sinusoidal surfaces [270]. During the regime where the Wenzel mode is dominant, they could show that the contact angle and its hysteresis (the difference between the cosine of a receding contact angle and that of an advancing contact angle for a water droplet on a tilted surface) on hydrophobic rough surfaces increase as the roughness factor increases. They also demonstrated that the contact angle continues to increase when the roughness factor exceeds a certain level (~ 1.7), whereas the hysteresis starts to decrease. This decrease in hysteresis occurs as a consequence of the switching of the dominant hydrophobicity mode from Wenzel to Cassie due to the increase of the air fraction at the interface between the solid and water.

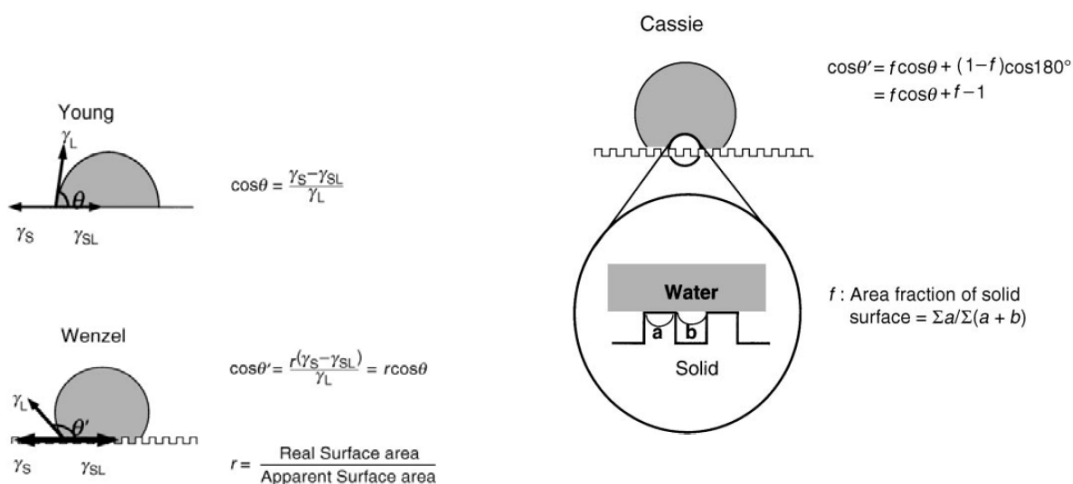


Figure 7.25 Effect of roughness on the hydrophobicity of solid surface following Young/Wenzel/Cassie concepts

Extrapolating this finding and its application to the surface of outdoor polymer insulators, it is possible to think in a surface with sinusoidal roughness, where it looks sufficiently 'rough' to improve hydrophobicity yet being smooth enough to allow the removal of the pollutants during natural washing under rain. Likewise, it could be expected that this structure should reduce the damage from UV radiation having areas that can be protected from them due to their inclination or orientation, mainly in geographical areas where the sun is not incident perpendicularly.

In addition, if the surface roughness can be considered as a valid design option, various theoretical works about hydrophobicity of rough surfaces should be reviewed. A summary of them is presented in reference [270]. The main concepts are:

- Practical contact angles are in good agreement with the calculated values based on fractal analysis.
- How molecular level heterogeneity influences this phenomena and revision of the Cassie equation by considering the line tension (the excess energy in the region of the three-phase (liquid-solid-air) contact line associated with intermolecular and surface-free energy) and contact angle hysteresis.
- General equation for the actual contact angle on a solid surface with roughness in a three-dimensional setting by considering the effects of line tension and the variation in line with the position of the contact line.
- Theoretical effect of gravity on rough solid-liquid interfaces showing that the tension of the interface is enhanced by gravity when gas is adsorbed on it.
- Consider a three-dimensional liquid drop sitting on a rough and chemically heterogeneous substrate under the presence of gravity and line tension.
- Low surface energy and proper surface roughness are indispensable for the processing of super-hydrophobic surfaces.

To the concept of 'roughness' to improve hydrophobicity can be also related with the principle of self-cleaning surfaces, where the particles adhere to the droplets and not to the surface. For a surface to be self-cleaning it must be extremely water repellent and have low particle adhesion and this can only be obtained if the surface has low surface energy and surface texture [271]. This objective has been nowadays highly achieved using nanoparticles.

Finally, it is relevant to mention than roughness cannot be confused with porosity. Under porosity the water will be migrating into the material volume creating a film of water being the material surface degraded and hydrophilic, as can be observed in Figure 7.26.



Figure 7.26 Water droplets on porous surfaces [272]

7.9. First Leakage Current Pulses on Different Water Droplets Arrangements

Test Procedure

Fifteen (15) different configurations of water droplets were studied (changing number, conductivity, location on surface and volume). Only surfaces with the original roughness were tested. Electrodes were cleaned if any flashover occurred during the experiments. Using an oscilloscope 100 msec were captured after the first current pulse was detected. Once the signal has been recorded, as shown in Figure 7.27, each pulse was magnified using the megazoom option of the oscilloscope and the data (voltage and current pulse) was also recorded in excel format. Each file containing the data of the 100 msec of each test is open to extract the values shown in Figure 7.28.

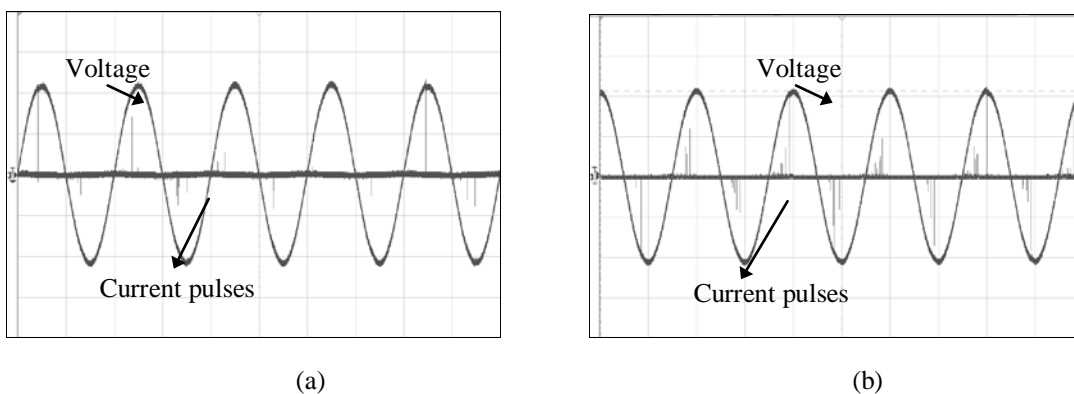


Figure 7.27 Oscilloscope signals: voltage and current pulses; Voltage scale: 10 kV/div; Current scale: 500 μ A/div; Time scale: 2 msec/div, (a) One droplet, 25 μ l, deionized; (b) One droplet, 25 μ l, 500 μ S/cm

After all this information was compiled, different graphics were made to compare peak numbers, magnitude, phases, charge, etc between cases. Equivalently, each file which

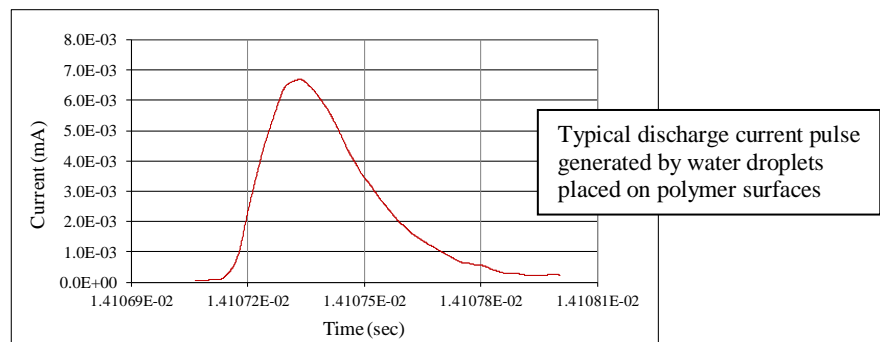
contains the data of each of each pulse is used to plot them and to extract all the information shown Figure 7.29. Finally, using this data, images such as the ones presented in Figure 7.30 are plotted and comparisons between cases are done.

During the development of this experiment it was detected that if the water droplet suffers displacement during the first peak, the following peaks will be different than the case where the water droplet only suffers elongation. This is a consequence of electric field distribution changes and interchange of charges.

Arrangement			Negative						Positive					
Conductivity ($\mu\text{S/cm}$)	Volumen (μl)	Vinception (kV)	Peak- (mV)	Peak- (μA)	Phase- (ms)	Phase- (Hz)	Duration (ns)	Area (pC)	Peak+ (mV)	Peak+ (μA)	Phase+ (ms)	Phase+ (Hz)	Duration (ns)	Area (pC)

Figure 7.28 Information to collect from each current pulse’s excel file recorded from each configuration

The first discharge current peaks for each configuration under study are presented here and the inception voltages are different. Normally, the comparisons have been done looking at the discharges at the same voltage but in this case the interest is in the discharge itself to see the characteristics of the pulses when they are initiated.



Second	Volt	I(Volt)	Current	Charge	Peak	10% peak	90% peak	50% peak
<i>Data recorded with the oscilloscope using Megazoom option</i>				<i>Area under current signal</i>				

t peak	t initial	t final	t total	t 10% peak	t 90% peak	t rise	t 50% rise	t 50% tail	t 50%
			t final - t initial			t 10%peak - t 90%peak			

Figure 7.29 Typical current pulse view after data is recorded and plotted; table shows all the information taken from the pulses plots

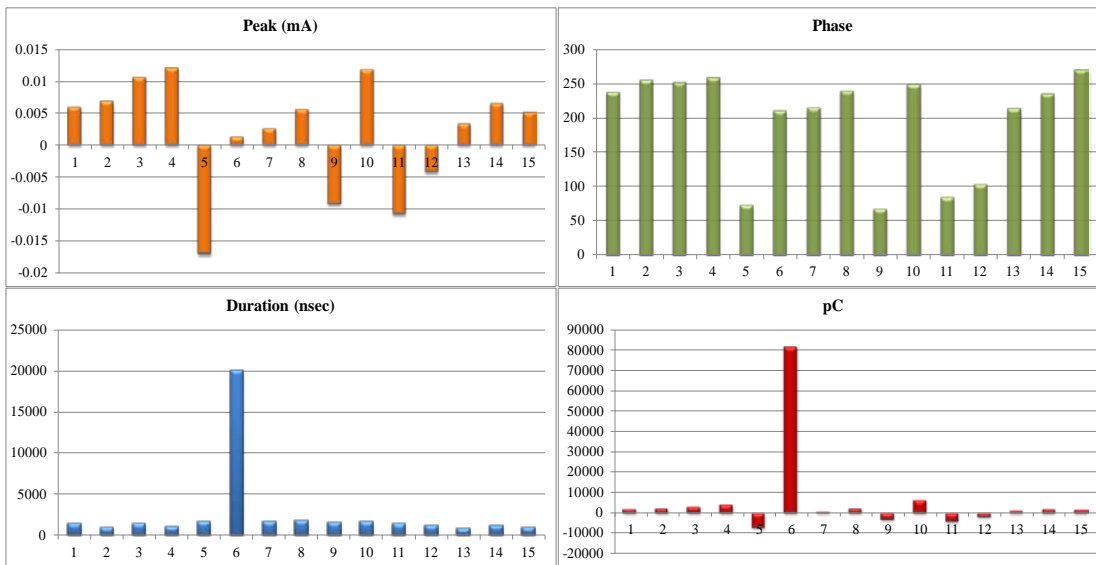


Figure 7.30 Main charts produced for each experiment recorded. These figures will show how many pulses occur for each water droplets configuration studied during 100 msec, sequence of pulses, peaks magnitude, phase, duration and charge of each one

Results, Phenomena Observed and Analysis

Some representative cases are fully described. Observations collected from all cases evaluated are included.

Single distilled water droplet placed on the centre of the 25 mm gap. Cases tested: 25, 50, 75 and 100 µl

Figure 7.31 shows positives and negative pulses detected on each volume tested. The number of pulses which occurs during an elapsed time of 100 msec is similar between cases (5-6). It can be observed that corona current pulses have higher values on the smaller volumes (20 and 50µl). Inception voltages, $V_{inception}$, were 21.6, 19.8, 19.1 and 18.8 kV for 25, 50, 75 and 100 µl, respectively; this fact should explain why the peak values of the pulses are higher on the smallest droplets. At the same time, pulses magnitudes are very similar between 75 and 100 µl droplets, which can be explained because in both cases the distance toward the electrodes was very similar before the electric field was applied. After these pulses occurred the droplets suffered elongation but no sharp tips on the droplets shape were detected. Elongation was small in all cases which caused, principally, a reduction in the contact angle of the droplets. This indicates that after this initial point, even though the droplets had high initial contact angles, they will act like they are placed

on a less hydrophilic surface. Looking at the peak values it can be inferred that the magnitude of the charge released on a small water droplet will be higher if the inception voltage is reached than the charge released by a bigger droplet when the process is initiated but with lower inception voltage, assuming that the duration time of the peaks are similar between them. This can be verified when charge of each current peak is estimated.

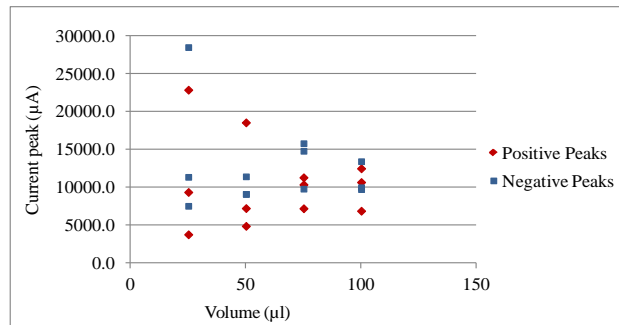


Figure 7.31 Example of one graphic created using the data extracted from the signals recorded (examples shown on Figure 7.27 and Figure 7.29). First peaks detected versus deionized water droplet volume

Single water droplet placed on the centre of the 25 mm gap. Cases tested: 25, 50, 75 and 100 µl and two different conductivities

Figure 7.32 shows the information given by the previous figure using distilled water and its comparison with water droplets with higher conductivity. Looking at the peak for higher conductivity, the number of pulses and their magnitude are smaller in all cases in comparison with distilled water. This can be explained because the conductivity reduces the equivalent resistance of the interelectrode gap and additionally, the charges needed for the process are supplied for the water conductivity and not by the corona pulses. The $V_{\text{inception}}$ for the 25, 50, 75 and 100 µl droplets with higher conductivity were: 19.7, 19.2, 19.4 and 19.1 kV respectively, which tend to be more uniform.

As can be seen in the Figure 7.33, peak magnitudes from deionized water decrease with volume and the fundamental reason should be the magnitude of the inception voltage applied. There is a tendency in the magnitude of the peaks to be smaller when they are positive which can be explained by charges balance. It can be also observed in Figure 7.34, that droplets placed closer to one of the electrodes influences small droplets more than bigger ones; this can be explained by the fact that the left and right gaps between water droplet and electrodes are less different when the bigger droplets are used, mainly

for small interelectrode gaps. This means that when a small deionized droplet is placed close to the ground electrode the distance between the water droplet and the high potential electrode is much bigger than the one for a bigger droplet with higher volume.

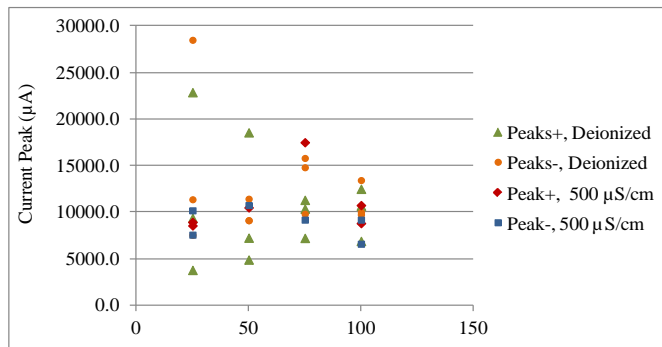


Figure 7.32 Example of one graphic created using the data extracted from the signals recorded (examples shown on Figure 7.27 and Figure 7.29). First peaks detected versus water droplet volume for two different conductivities

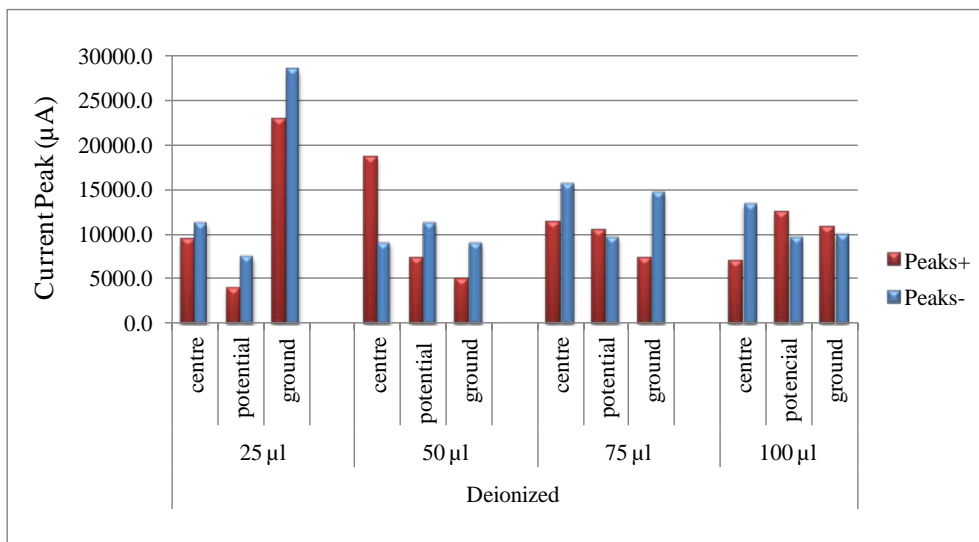


Figure 7.33 First positive and negative peaks for distilled water droplets with four different volumes and placed on different positions in the interelectrode gap

Figure 7.34 shows that water conductivity has strong influence on positive pulses for droplets with the same volume. It looks even higher than the influence of location (for the volume and gaps used in these experiments).

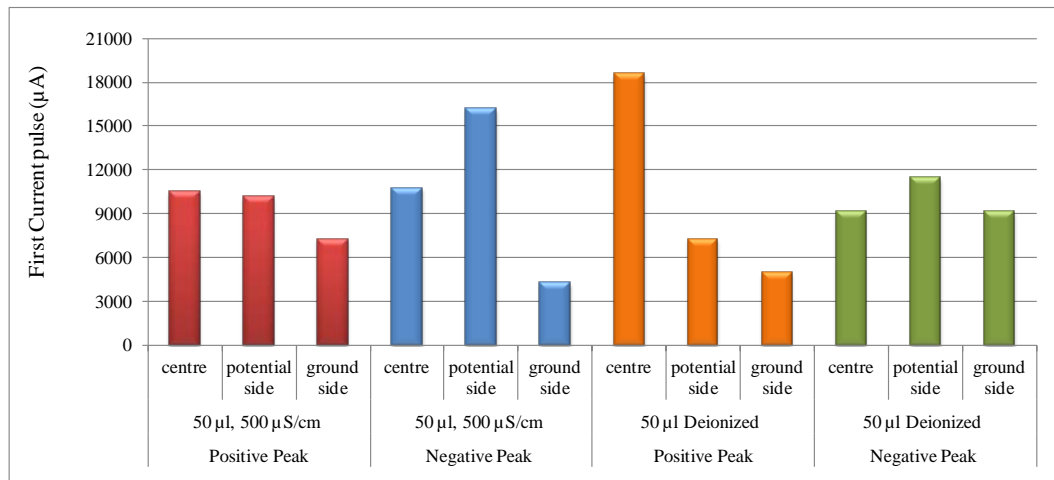


Figure 7.34 First positive and negative peak for 50 µl water droplets with two different conductivities

Figure 7.35 shows charge carried by each first (positive and negative) discharge current pulse for one single droplet placed on different locations: centre, close to potential electrode and close to ground electrode. At the centre and close to the high potential electrode, positive peaks have more charge even though their magnitude is smaller because they last longer.

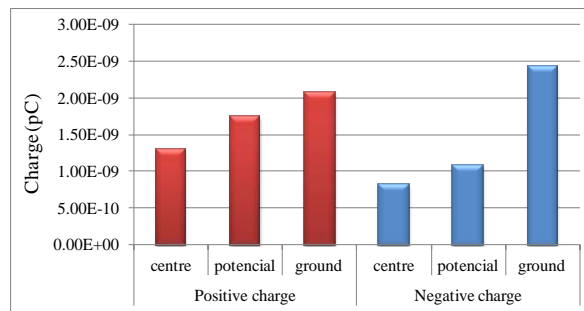


Figure 7.35 Charge of the first positive and negative peaks for a 25 µl, deionized water droplet, placed on centre, close to potential electrode and close to ground electrode.

7.10. Leakage Current Pulses Patterns

Corona discharges have been used as one of the most important tools to diagnose and classified materials and equipment. Nowadays is one of the most important techniques used to establish the condition and monitoring of many types of equipment in service. But this technique has some complications when it is going to be used in the field: (1) there are many factors which can influence the test and the values detected, (2) if requires

sophisticated equipment, (3) interpretation of the results is not always an easy task and people involved requires specific training. Unlike the case of partial discharges in internal insulation whose magnitude is extremely low and easily hidden by the surrounding electromagnetic noise, corona discharges on outdoor insulators present high magnitudes making them easy to detect.

During this test, leakage current pulses were observed using the original setup of the system and the ‘envelope’ option of the oscilloscope. This option was used in [273] with good results for non uniform electric field effect on water droplets in air moving against metal surfaces.

Test Procedure

One x10 oscilloscope probe is incorporated to the measurement system and different values of measuring resistors were used. The applied voltage was held steady at the inception values found during the previous experiment and the oscilloscope was manually triggered to record leakage current pulses accumulated during approximately 5 seconds to create envelop images. Environmental conditions were also recorded.

Results, Phenomena Observed and Analysis

The images obtained are presented for one example for 25 µl and 500 µS/cm water droplets and one example for a 25 µl deionized droplet.

Environmental conditions:	Initial	Final
Temperature (°C)	22.5 ± 0.1	23 ± 0.1
Humidity (%)	35	35
Pressure (mmHg)	741	741

Case i) 50 µl, deionized, water droplet

As can be observed in the Figure 7.36 current pulses start on the positive half cycle with an almost uniform pattern and two different times, before 4 msec and between 4 and 6 msec, which coincides with the peak of the voltage. After some elapsed time the magnitude of the pulses increases and pulses also occur in the negative half cycles. For deionized water droplets the discharges in the negative half take the same shape and magnitudes, with lower repetition rates than the ones observed on the positive one, when there is a drying process occurring with stable arcing.

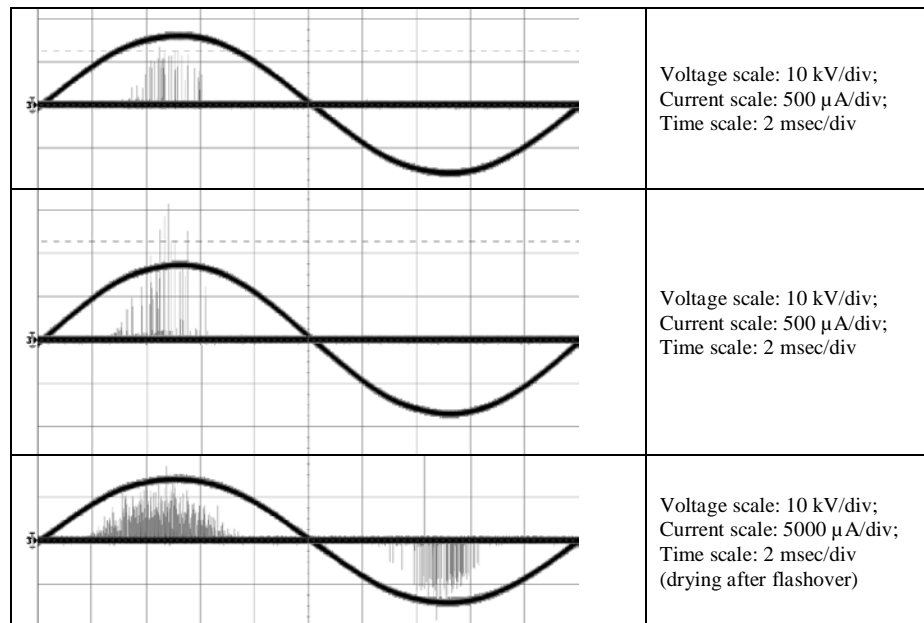


Figure 7.36 Changes on current pulses envelopes with elapse time (5 sec each graphic) for 50 μ l, deionized water droplet

Case ii) 25 μ l, 500 μ S/cm, water droplet

Figure 7.37 shows the envelopes of this case. At the beginning large discharges occur during the positive half cycle between 4 and 6 msec of the cycle. After a while the magnitude of these discharges increases and negative discharges with high amplitude and lower repetition rate also appeared at the peak of the voltage. Simultaneously, a second cluster of discharges in the positive half at 1.5-2 msec whose magnitude is less than 25% of the initial ones located at the peak. If a flashover occurs and a drying process starts, pulses are observed on both half cycles, close to the peaks of the applied voltage and the magnitude tends to be constant during the negative half cycle for low conductivity water droplets.

On the contrary, if the conductivity increases both half cycles, show peaks with different values. Initially, positives present higher magnitude and after a while the process starts to present a lower repetition rate of pulses and the amplitude of them is higher in the negative polarity. This occurs when drying process is developing.

Cases tested can be compared and analyzed and different patterns can be found depending on water droplet conditions: incipient corona discharges, large discharges, arcing between

droplets, arcing between one of the electrodes and the droplet, drying of the water channel or full flashovers, etc.

All cases presented in the Figure 7.22 were evaluated. These results and the compilation of cluster and their relation with the different phenomena developed on the surface will be summarized in a paper. This test can be used to analyze discharges on polymers in a similar way that it is done using partial discharge detection and measures but in an easier way. Evaluation of the current pulse clusters, repetition, phase and magnitude using this method seems to be easier than the traditional technique which requires more sophisticated equipment and more expertise.

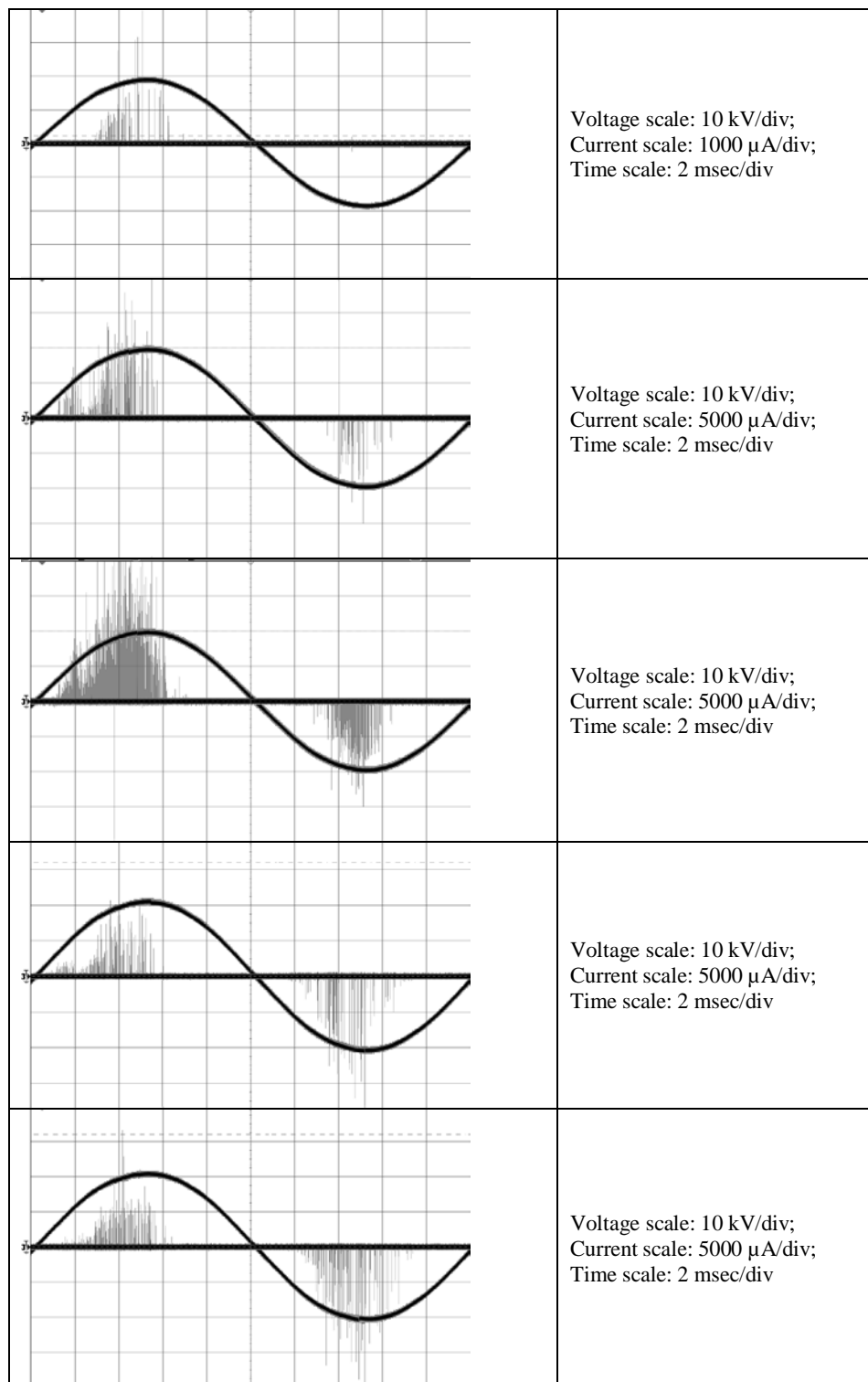


Figure 7.37 Changes on current pulses envelopes with elapse time (5 sec each graphic) for 25 μ l, 500 μ S/cm, water droplet

7.11. Electric Field 3D FEM Analysis of Water Droplets under Different Condition

Different three-dimensional configurations were evaluated to determine where the electric field is enhanced and where the maximum value is going to be placed. Special considerations were taken to improve the mesh around the water droplets to obtain the closest values. Final values were used to analyze and explain some of the differences found on the initial leakage current pulses. Electric field distribution is enhanced with displacements, with coalescence of water droplets with different volumes and even with only movements which cause changes on contact angles. This is a fully dynamic process where changes on electric field distribution create changes on the droplets dynamic and shape and this will cause changes on the electric field distribution creating a cycle.

In the literature there are not significant contributions to model the mentioned dynamic process. Dirk Langemann is the author with the most relevant contributions founded in this topic [274-278]; his last publication is the first founded work which links the electric problem with the mechanical one in a calculation cycle.

For the simulations only hemispherical water droplets were considered. This simplification of the problem can be assumed as the start point of the process. Some images from the simulations are presented as an example in Figure 7.38.

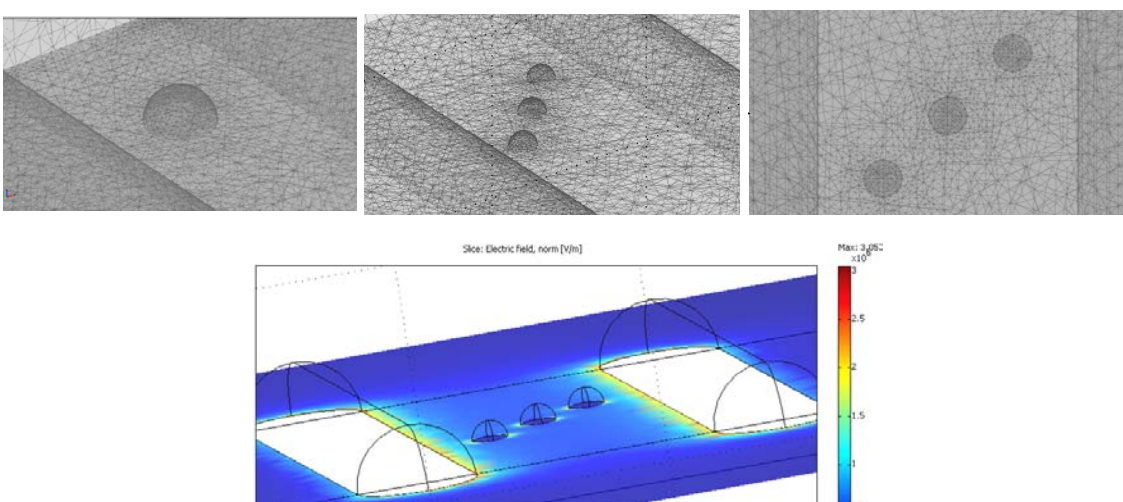


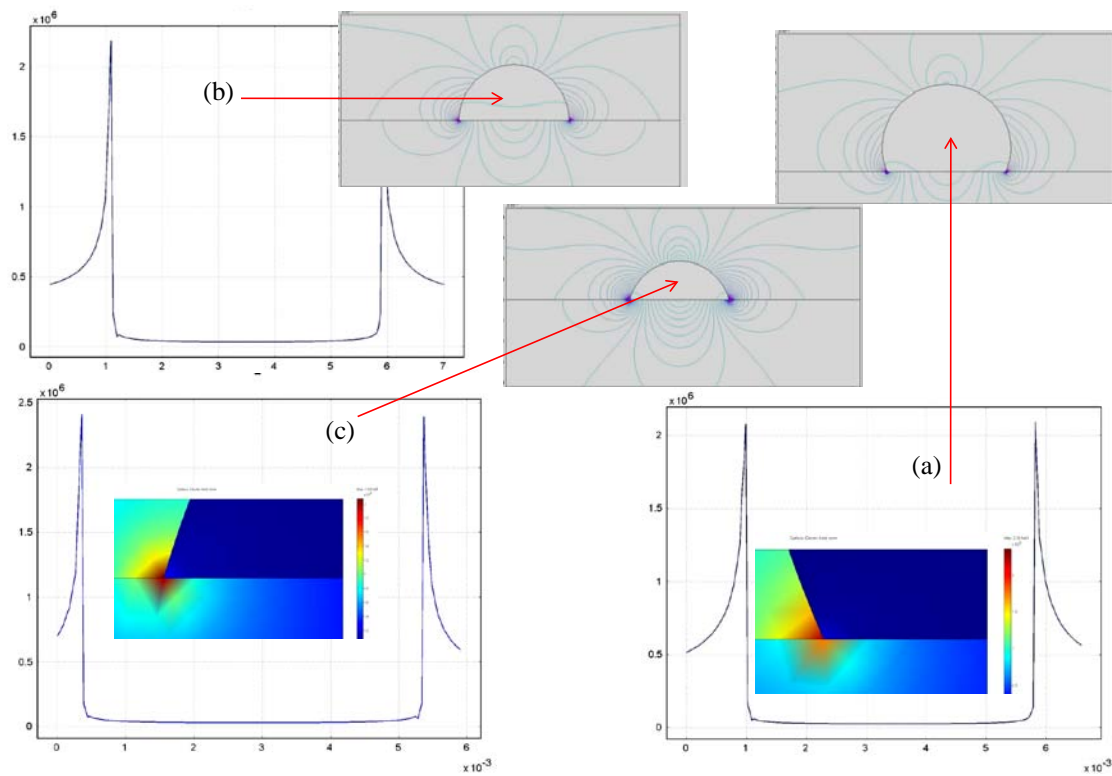
Figure 7.38 Three-dimensional electric field FEM simulations examples

Figure 7.39 presents the enhancement factors of electric field (E_{\max}/E_0) for water droplets with different contact angle: $<90^\circ$ (hydrophilic), 90° (hemispherical) and $>90^\circ$ (hydrophobic). Here the simulation was done in 2D which is enough to see the behaviour of one water droplet. As can be observed, the difference between the water droplets shapes, specifically their contact angle, used for the simulations is going to have an enormous impact on the final results.

The values are presented using the enhance factor of the electric field considering as the normal one the magnitude of the field for a uniform distribution along the surface between the interelectrode gap. Values for some basic simulated configurations are summarized in Table 7.2.

Table 7.2 Electric field enhancement factor for different basic configurations

Cases	E_{\max}/E_0	Observations
2 aligned droplets	3.2	The factor increases when the distance is closer between then or when one is too close to the potential electrode.
3 aligned droplets	6.4	Interaction between droplets is higher when they are closer.
3 aligned droplets closer	8.1	
3 droplets in diagonal	3.7	Prevalent effect of the one closer to potential
3 droplets in triangle (1/2)	3.8	Prevalent effect of 2 aligned. Enhancement factor is 1.5 times higher along the line crossing the 2 droplets than crossing the single one.
5 droplets aligned	13.7	Path free between electrodes is highly reduced
5 droplets (2/1/2)	4.7	Prevalent effect of 2 aligned
7 droplets (2/3/2)	9.3	Prevalent effect of 3 aligned



CASES:	Enhancement Factor
(a) One hydrophobic droplet	6.42
(b) One hemispherical droplet	6.87
(c) One hydrophilic droplet	7.48

Figure 7.39 Enhancement factors (E_{max}/E_0) for water droplets with different contact angle

7.12. Effects of Water Droplet Evaporation under no Electric Stress

Evaporation of water droplets has not been considered on material surface degradation studies. In this research two main questions were formulated:

- (1) What is the influence of water droplet evaporation on contact angles having in mind that under tropical environmental conditions it can be an important influencing factor?
- (2) What is on the insulation surface after water droplets have dried that can influence subsequent phenomena?

Exploratory experiments were carried on to find some answers.

7.12.1. Evaporation rate versus water droplet volume and conductivity

The process will be evaluated with and without electric field stress.

With no electric field stress

Water droplet evaporation time, at 21°C, 34% humidity, and 767.31 mmHg of atmospheric pressure, was estimated recording the drying process of sessile drops placed on a clean silicone rubber surface. Top and front views were observed simultaneously as can be seen in Figure 7.40. Six different volumes and two water conductivities are reported in Figure 7.41.



Figure 7.40 100, 150 and 200 µl water droplets: (a) top view, and (b) front view, recorded using one camera and one mirror arrangement

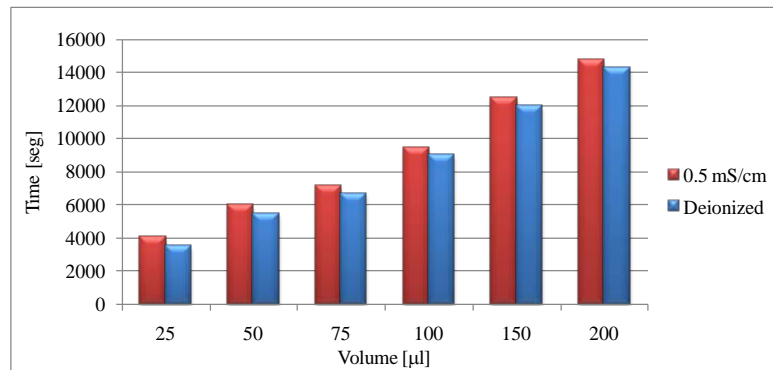


Figure 7.41 Time to dried sessile water droplets with different volumes and conductivities (21°C, 34% humidity and 767.31mmHg)

Rate of evaporation is affected proportionally by: (1) temperature (indicator of kinetic energy); (2) pressure and (3) surface area, and affected inversely by: (1) Intermolecular Forces (which are affected by concentration of dissolved substances as salts and dissolved gases as N₂, O₂, CO₂), (2) Humidity and (3) Wind.

How fast something evaporates is due to its vapour pressure. Adding anything to a solution lowers the vapour pressure. The relationship is called Raoult's Law.

Changes on contact angles can be detected looking at the effect on the water droplet dimension factor which relates its base with its height, $D_{\text{factor}} = \text{base}_{\text{wd}}/\text{height}_{\text{wd}}$. Values lower than 2 means hydrophobic angles ($> 90^\circ$), equal to 2 means hemispheres ($=90^\circ$) and values higher than 2 indicate hydrophilic angles ($< 90^\circ$). Figure 7.42 shows D_{factor} evolution along one hour for a water droplet with conductivity equal to 0.5 mS/cm. Behaviour of D_{factor} using deionized water droplets follows the same tendency but they are approximately 6.5% smaller than conductive water (0.5 mS/cm) at 0 min, and approximately 4% at 60 min. This result indicates that conductive water reduces contact angle values but evaporation rate reduction tends to reduce changes in D_{factor} after the same elapsed time. This must be carefully observed because when conductive water is used D_{factor} will reach higher values than deionized water droplets but after longer elapsed time.

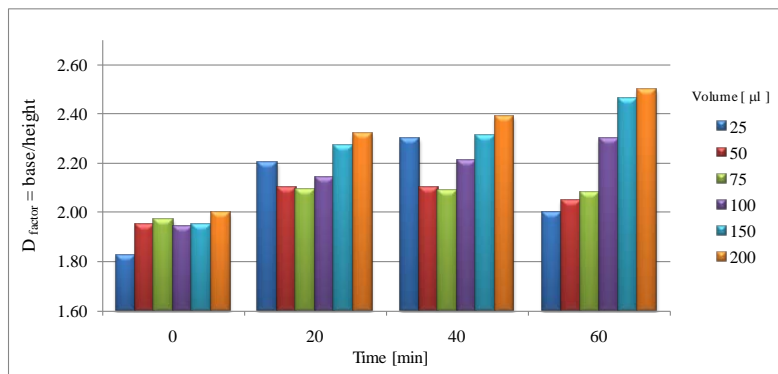


Figure 7.42 Conductive water droplets (0.5 mS/cm) dimensional factor ($D_{\text{factor}} = \text{base}_{\text{wd}}/\text{height}_{\text{wd}}$)

With this exploratory experiment one important observation can be extracted: if evaporation changes contact angle of water droplets placed on silicon rubber, droplets which initially are not having enough electric field intensity to initiate corona discharges can reach a shape/volume/conductivity combination where electric field can be enhanced and exceed the discharges initiation threshold, mainly for droplets with big volumes. Additional to this another fact must be considered during the analysis: when droplets are evaporating their dimensions are diminishing and even so they are having hydrophilic angles, they are in general smaller making it more difficult to reach high electric field concentrations. Figure 7.43 shows height and base dimensions separately and these considerations can be easily observed.

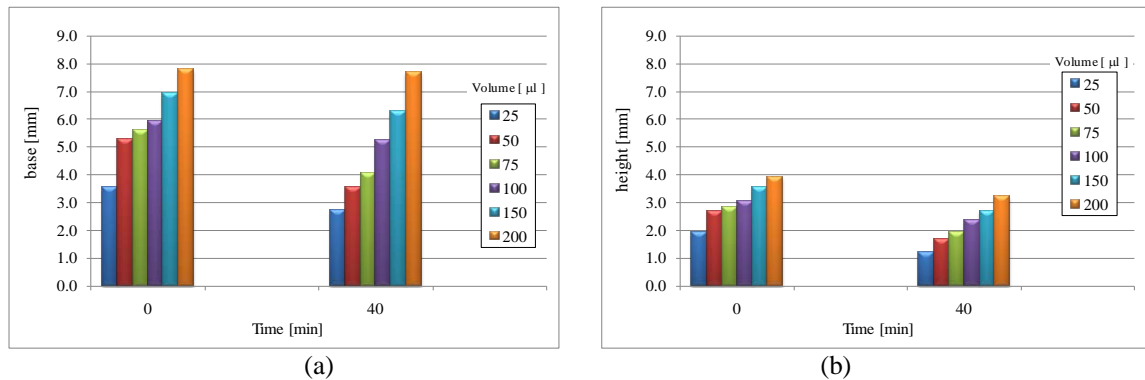


Figure 7.43 Water droplets dimensions at 0 min and after 40 min after been placed on surface (water conductivity = 0.5 mS/cm)

The characteristics of an evaporating sessile droplet vary with its surface contact conditions [279]. Evaporation of water droplets on hydrophobic surfaces has three distinct regimes: constant contact area mode, constant contact angle mode and mixed mode. One time is also defined: pinning time (t_{pin}), which is the total time the contact diameter (base) remains fixed during droplet evaporation. In the case of PDMS surfaces t_{pin} is about 40% of the total evaporation time and corresponds to the constant contact area stage, given above, as the initial mode of an evaporating droplet on a hydrophobic surface. This time can reach 75% of the total evaporation time when surface is hydrophilic [280]. The edge shrinking velocity of the droplet shows nonlinear characteristics; the edge of droplet shrinks extremely fast at the last period of total evaporating time.

7.12.2. Residues on surfaces after water droplet evaporation under no electric field

The drying process of one tap water droplet, 25 µl and contact angle equal to 108° , on silicone rubber surface was observed using a microscope (See Figure 7.44). After the water droplet evaporates completely a stain remains. This stain concentrates more solid particles at the edges and dries faster once the contact area liquid/solid is smaller than the perimeter created by the particles at the external ring.

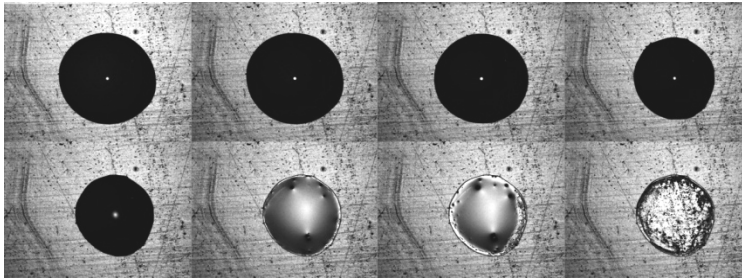


Figure 7.44 25 µl tap water droplet evaporation process

A second similar droplet was placed on the stain left by the first evaporated droplet, as is shown in the Figure 7.45. Looking at the final image it can be seen that a second stain overlap the original and higher concentration of solids is retained on it, mainly at its edge or perimeter. Some papers describe this phenomenon which occurs for a wide range of surfaces, solvents and solutes. There are now reviewed.

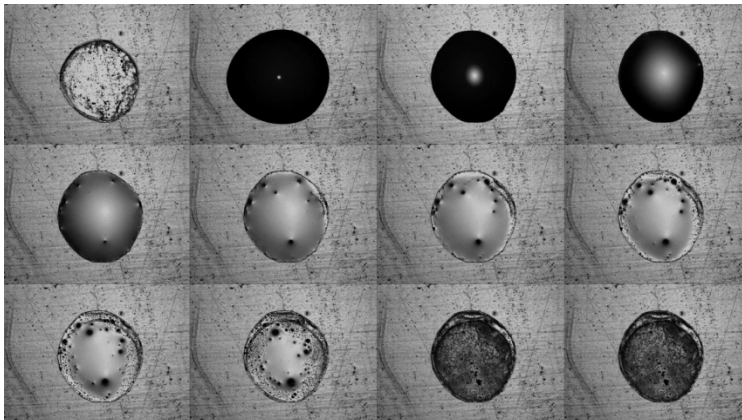


Figure 7.45 Evaporation process of 25 µl tap water droplet placed on the first evaporated water droplet stain

Solids dispersed in an evaporating or drying droplet tends to migrate to the edge of the droplet and form a solid ring [281]. This phenomenon produces stains with solids concentrations higher at the perimeter of it giving the deposit a ringlike appearance (phenomenon known as “coffee-stain effect”). This is explained in [281] by an outward flow in a drying droplet of liquid which is produced when the contact line is pinned so that liquid that is removed by evaporation from the edge must be replenished by a flow of liquid from the interior. This theory relies only on the generic property of the material/liquid interaction or surface energy, the presence of roughness or chemical heterogeneities which establish geometrical constrains making the droplet to maintain an equilibrium drop shape with a fixed boundary.

In [282] the evaporation of saturated NaCl solutions on a hydrophilic surface results in the formation of small cubic crystals at the liquid-air interface (Figure 7.46(a)). The growth of these crystals decreases the liquid-vapour interfacial tension, leading to the observation of a slight spreading (its radius increases by about 10%) of the droplet. The spreading is less pronounced than for a Na₂SO₄ (Sodium sulphate) solution, probably because of the higher solubility of NaCl. At the end of drying, ringlike crystalline deposit in the border is observed (Figure 7.46(b)). On a hydrophobic surface, contrary to what happens for the hydrophilic case, the NaCl crystallization appears not at the liquid-air interface but rather at the solid-liquid interface. At the end of the evaporation a *cauliflower-like* structure is observed to grow on top of the cubic crystals at the droplet edge (Figure 7.43). Sodium chloride crystals prefer to grow in contact with a non-polar environment such as air or a silanized solid surface [282].

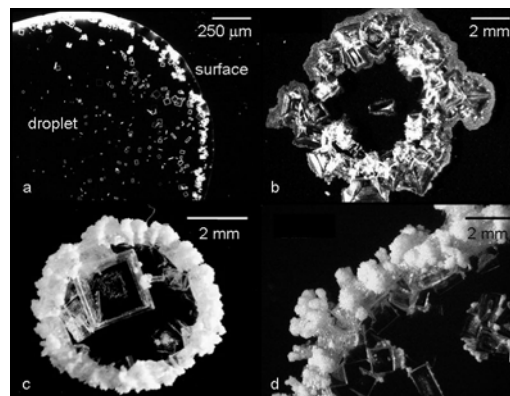


Figure 7.46 Crystallization during evaporation of saturated NaCl droplets. Hydrophilic surface: (a) growth of cubic crystal at the liquid-air interface, (b) ringlike crystalline deposit surrounded by a small spreading film. Hydrophobic surface: (c) crystallization pattern, (d) close-up of the cauliflowerlike morphology on the border [282]

Looking at these exploratory experimental results and the theory involved, it can be concluded that polymer insulators surface will be conditioned for changing behaviour from the first moment of its installation and immediately after the first water droplets placed on it are evaporated. Once placed in service, pollutants will be deposited on the insulators surface and ringlike stains (with or without salty crystals placed at the perimeters), corona discharges and electrohydrodynamic phenomena will be influenced and the degradation process as a whole will be more complex and intricate than is regularly presented by researches where ideal conditions are currently simulated. This is

important to point out that this initial surface conditioning could introduce significant modification on the early stage of ageing.

7.13. Thermal Gradient Effect

This second exploratory experiment was done using an infrared thermometer. In this part, five (5) different flashovers between tap water droplets, conductive water droplets, droplets and one electrode, etc were created on five (5) different samples. The maximum value of thermal gradient detected on the surface was $4.3^{\circ}\text{C}\pm 0.1^{\circ}\text{C}$ (IR thermometer at 25 cm from the surface). Obvious limitations of this method to detect the proper thermal gradients occurring on the material surface under corona discharges or leakage current pulses are: (1) the whole interelectrode area is considered and not the region where the bigger increment is happening, and (2) the response of the thermometer cannot detect very fast transient increment that can occur during the flashovers. But even under these two main limitations, the thermal changes are enough to indicate that water droplets dynamic will change because temperature is changing in some areas surrounding the water droplets.

On a thermal gradient, the drop will move from the warm side to the cool side. It does this because liquid-gas surface tension is affected by temperature. As temperature increases, surface tension decreases, and vice versa.

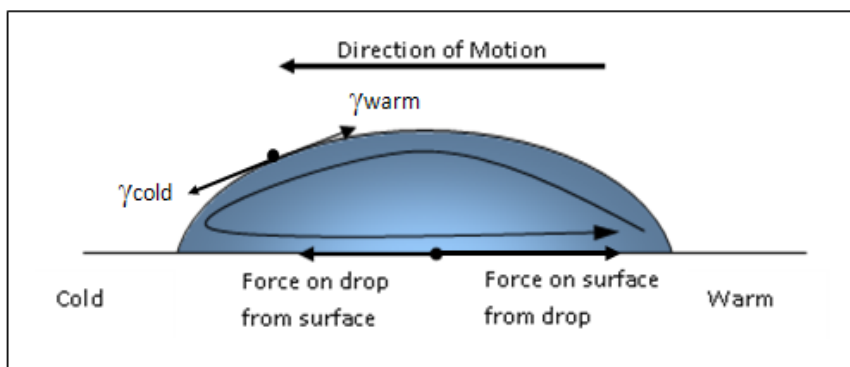


Figure 7.47 Effect of thermal gradient on water droplets dynamic and forces

On each area element at the liquid-gas interface, there are two forces pulling in opposite directions trying to reduce the surface area of the droplet. Since surface tension decreases

with increasing temperature, the tension pulling in the cold direction (γ_{cold}) is stronger than the one pulling in the warm direction (γ_{warm}). This results in a flow around the edge of the droplet, as shown in Figure 7.47. This flow pushes against the surface under the bottom of the droplet and the reaction force from the surface pushes the droplet along the thermal gradient. If temperature affects contact angles, then the two sides of the drop could have different contact angles and increasing subsequently the electric field intensity. This could introduce an additional force on the droplet affecting the dynamic of it.

Some sources of thermal gradients on polymer insulators surface are shown on Figure 7.48.

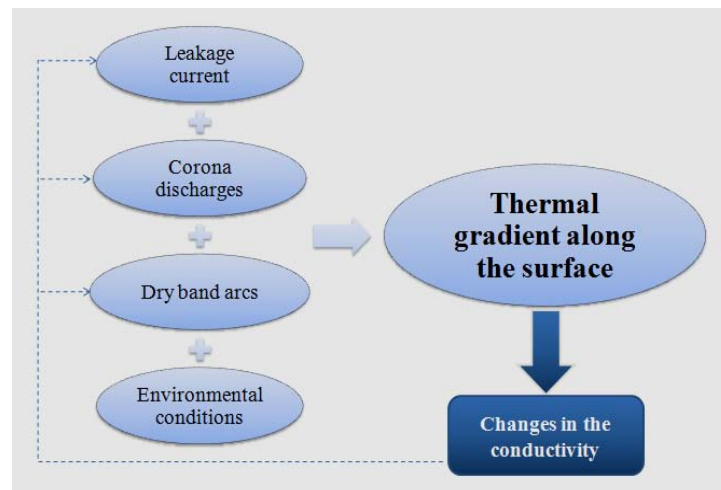


Figure 7.48 Sources of thermal gradients on polymer insulators surface

7.14. Electrode Shape Effects on Test Results

The study was focused on metal electrodes shapes and their influence on electric field distribution, water droplet behaviour and leakage current characteristics. Keeping the gap distance constant, five different shapes of elongated electrodes (flat, three different circle-sections, and rectangular bars) were simulated using Finite Element Analysis (FEM) and four of them were experimentally tested. Contact angles of water droplets were monitored using a high speed camera. Images were synchronized with leakage current and voltage signals.

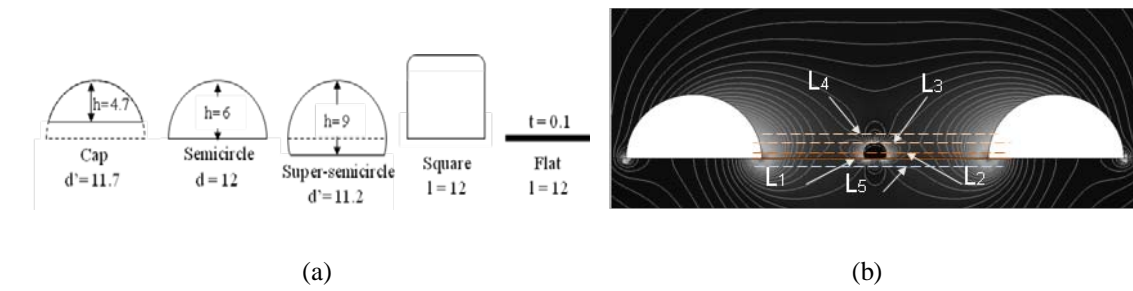


Figure 7.49 (a) Electrode cross-section shapes under study (d; diameter; d': base; h: height; l: length; t: thickness, all in mm); (b) Electric field intensity with semicircle bar electrodes and a centred water droplet under 15 kV. LX: height for the analysis (L1 = 0 mm; L2 = 1 mm; L3 = 2 mm; L4 = 3 mm; L5 = 0.5 mm)

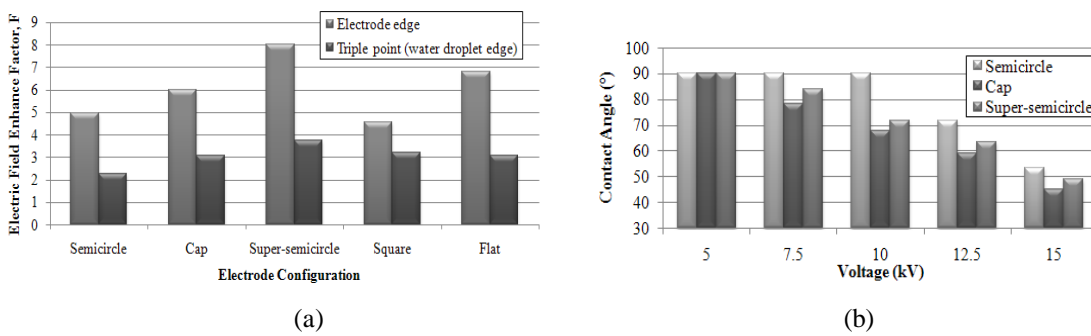


Figure 7.50 (a) Electric field enhance factors (F) along the material surface; (b) Contact angle versus applied voltage (Ground electrode side)

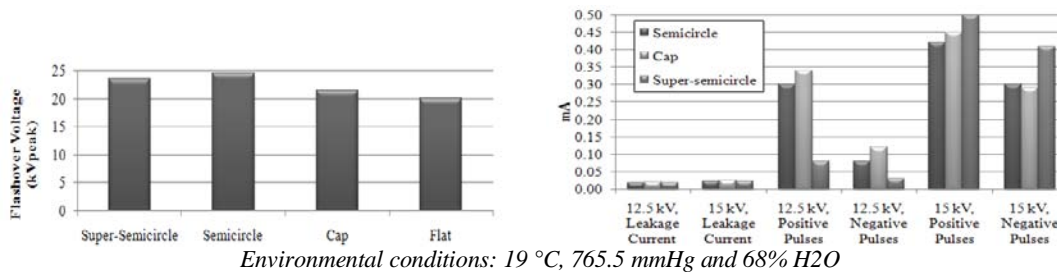


Figure 7.51 (a) Changes of flashover voltages caused by different electrodes shapes; (b) Leakage current and pulses at leakage current signal

Experimental tests have been carried out previously to study water droplet behaviour under electric fields, but ill-defined conditions introduce barriers to comparison of phenomena.

Different conditions and results are introduced by the experimental use of various electrode geometries. Semicircular bar electrodes cause reproducible distortion in the electric field distributions, leakage currents, phase angles between leakage current and voltage, contact angles and water droplet displacement. Additional configurations will be

required to develop an understanding of phenomenon and service conditions, but results may not be directly comparable to published work.

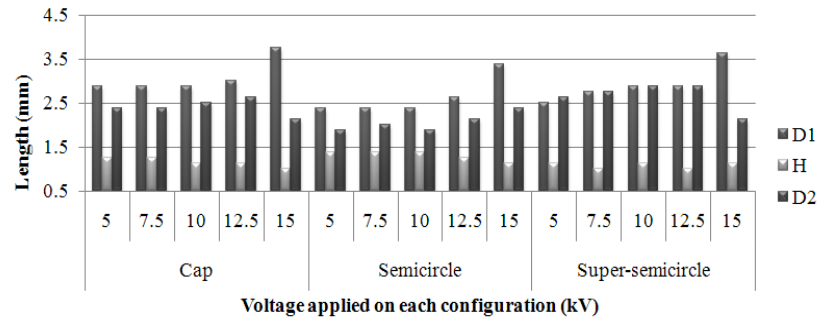


Figure 7.52 Water droplet dimensions versus applied voltage. D1 is the drop length on the axis between the electrodes, H is the droplet height and D2 is the width of the droplet parallel to the length of the electrodes

8. CONCLUSIONS

Following the structure originally given to this work the following main conclusions can be extracted:

Nowadays, polymer insulators monitoring and diagnosis in service relies on visual inspections and leakage current detection and analysis. Main efforts have been done by EPRI, STRI, and CIGRE to compiled data, which is the first step to make an asset management plan based on condition and risk. For distribution the situation is even more critical because utilities do not record information of these assets.

All deterioration forms, damage and additional conditions reported on the literature were included here to offer a full visual inspection manual that can be followed by the utilities. In parallel all monitoring and diagnosis techniques were included, described and catalogued to help the professionals in charge to understand the kind of information that can be collected by each one, and how much training is required to interpret the final values. All information and data required and all main steps that must be followed to start with a formal condition based asset management plan are listed. Implementing them is a warranty of be able to formulate health indexes, risk levels and investment plans for refurbishing or new installations in the future.

Diagnosis of MV EPDM insulators recovered from service under different environmental conditions and very low electrical stress demonstrate how influential UV radiation and pollution level and type on the surface degradation of these assets are. At the same time, it is important to mention that manufacturing mistakes can enhance the failure rate even in distribution insulators. As a result, quality control on insulators during their manufacturer process or during reception is vital to guarantee the proper life time.

For the cases under study, severe coastal pollution and biofilms are introducing important changes on EPDM surface at the lower side of the insulators. UV radiation is the main ageing factor acting at the top side. Although hydrophobicity is completely lost, this is not a reason to replace the insulators. The two main bases for this statement are: (1) dielectric

behaviour was shown to be good enough for the 11 kV system (insulators are for 15 kV lines), and (2) EPDM insulators must be treated as hydrophilic surfaces and not as silicone rubber, following EPRI recommendations.

Two new methods were presented to evaluate polymer insulators: (1) dielectric impedance on full samples and (2) roughness versus static contact angle relation. The first technique showed promising results where differences on surface condition can be detected under dry and wet conditions, but also difference on material formulation can be detected. As a consequence this can be also used as a reception test for utilities. Additional studies are needed and comparison of this technique with the traditional dielectric spectroscopy on small samples looks relevant. The second test presented showed novel results where roughness and static contact angle are directly related, if roughness increases the static contact angle also increases and different relations can be found for different prevailing ageing factors. An additional relation between HC hydrophobicity classification and roughness should offer interesting information but sampling must be carefully selected. In our studies this relation does not exist because all insulators surfaces had HC7.

Following the experimental part developed on SiR samples, looking at the degradation process at small scale and the variables involved, an early ageing state diagram is proposed. Taking as a base a previous diagram published in [167]. Following the results of this work, additional considerations to that model can be included:

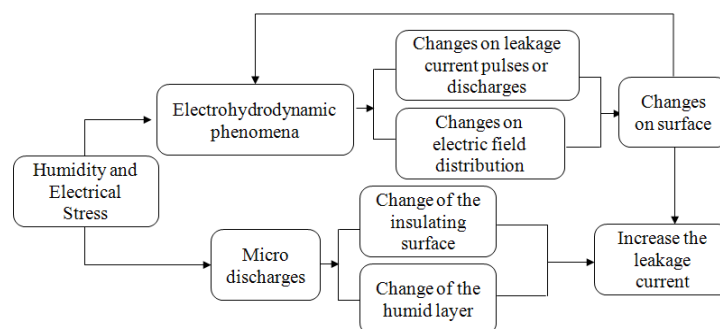


Figure 8.1 Proposal for the early ageing stage of polymer insulators

In this proposal the influence of the electrohydrodynamic processes on the leakage current pulses and electric field is included, and the changes on surface (roughness, etc) are

included as well, because its effect on the electrohydrodynamic processes. Electrohydrodynamic changes leakage current pulses and microdischarges as well, but also changes the electric field distribution. Both will act on the material surface and this can change in a positive way the electrohydrodynamic processes and discharges, but also in a negative way when the leakage current is increased.

In Figure 8.2 Early stage additional loops or steps that occur on early stage of degradation are shown were some interaction between process are presented. With this diagram the dependability between processes is highlighted to show the importance of have in mind the high level of synergy which dominates the surface ageing of polymer surfaces.

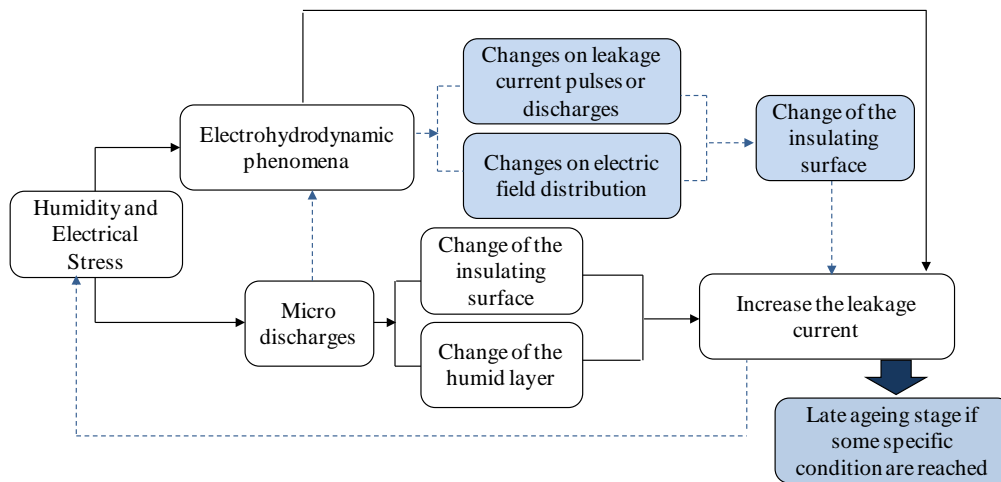


Figure 8.2 Early stage diagram including additional loops. In black is presented the original diagram found in [167], in blue the additional proposed steps

Leakage current pulses and their behaviour in time give information about the early ageing stage of polymer surfaces under humidity and electric field stress. Important information can be obtained from these pulses and it is a simple test. The methodology used here can be improved and automated.

Three additional phenomena were experimentally commented in this work: (1) influence of evaporation rate and residues, (2) thermal gradients, and (3) electrodes shape and location effects on tests. The first two phenomena can be integrated on the early ageing state but further investigation is needed.

FUTURE WORK

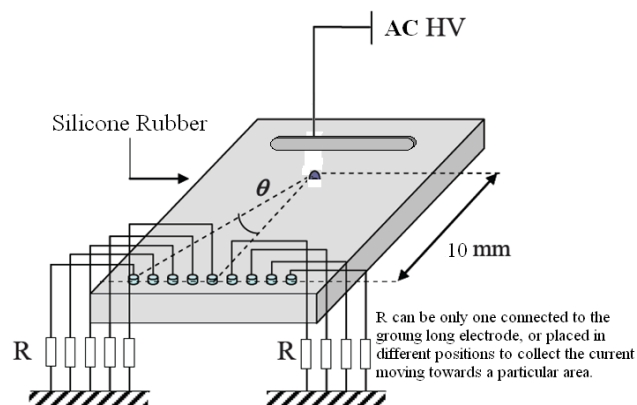
1. Energy Involved in Water Droplets Corona Discharges

Having recorded the leakage current and voltage for different cases and configurations of the phenomena, the calculation and analysis of energy involved in each process is possible. This can give additional information about the conditions that can introduce the more severe conditions and cause more severe damage of the surface.

Analysis of the harmonic content of leakage current and frequency spectrum analysis of current pulses can be done. Both details allow a much better classification and additional understanding of the phenomena.

2. Chemical Compounds Released by Water Droplets Corona Discharges Using Capillary Ion Electrophoresis

Study the transport of the gaseous products from a surface discharge along an insulating surface, in correlation with the properties of the discharges. Having in mind that the results of corona/current pulses discharges involve different polarities, with different magnitudes, repetition rates and charges and that them influence the type of chemicals compounds that can be release to the surface an experiment proposed in the literature offers the opportunity to do it in an easy way [283].



Using the instantaneous voltage \times current method, the mean power P is evaluated; this value, divided by the applied rms voltage gives the mean active discharge current which is used for comparison of the laws characterizing the diffuse component of the surface discharge: (1) Townsend law relating the total mean current to the applied voltage, Warburg law describing the current repartition inside the discharge gap). Space resolved

surface energy W_s is simply deduced from measurements of the contact angle of distilled water droplets (10 μl volume) deposited on the surface after its exposure to the discharge, using the $W_s = \gamma LV (1 + \cos\alpha)$ relation with $\gamma LV = 72.8 \text{ mJ.m}^{-2}$ for distilled water. Space resolved chemical analyses are performed by capillary ion electrophoresis on the products collected in 10 μl pure water droplets first deposited with a syringe on local sites of discharge treated surfaces and then taken off in the same way. Comparisons can be done in concentrations if deionized water is used and taken after the discharges for the chemistry analysis. With this experiment the chemistry involved and release on the surface could be possibly related with the current pulses type or patrons.

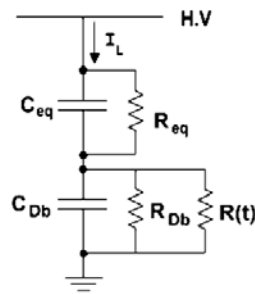
3. Dynamic 2D Electric Field Distribution Calculation Considering the Movements of Water Droplets (Displacement, Elongation, Coalescence, Distortion)

A loop between electric field distribution and its effect on water droplets dynamic and subsequently the effect of this dynamic on the electric field distribution should be proposed. Using the images recorded using the high speed camera and the models proposed in [275-278] and other dynamic model for water droplets on the literature a loop in the calculation could be feasible to develop. The task is not an easy one having in mind that for a droplet moving in two dimensions, at least five functions time dependable are needed to describe its behaviour: elongation to the right, elongation to the left, contact angle right side, contact angle left side and high, but this only describe one non symmetrical elongation and not some of the highly distorted shapes than droplets under electric field can present. Looking at the complication, selection of the proper simplifications is important.

The equations and the loop in the program can be implemented in Matlab. This software also has the tool to make the needed graphics. Once the complete theory, equations and validation of the program in 2D is complete, the problem in three dimensions can be raised.

4. Model of Leakage Current Pulses produce by Water Droplets Corona Discharges under AC Stress

Multiple leakage current signals were recorded with their images and voltage applied. Validation of the following proposed model for corona discharges could be done and adjusted [284].



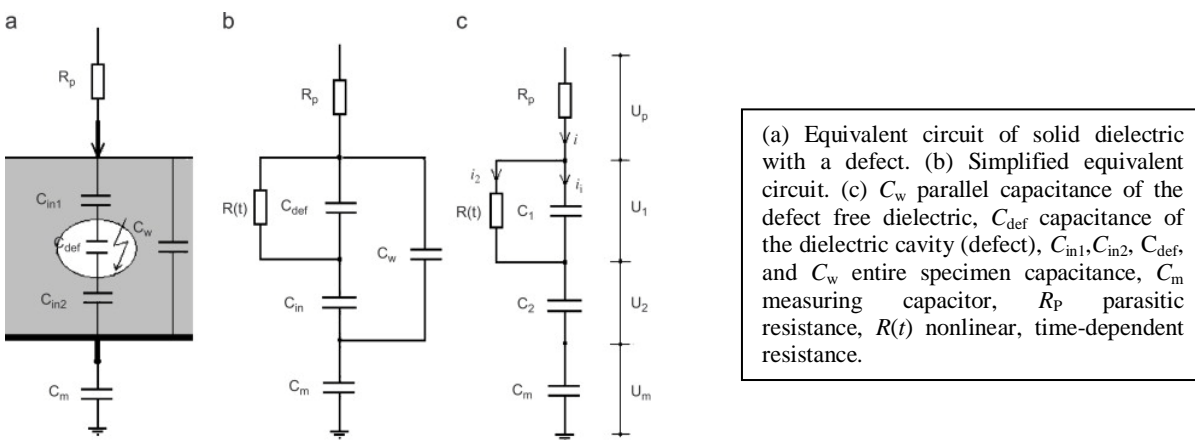
where C_{eq} and R_{eq} are the capacitance and resistance of the insulator not involving the dry band and C_{Db} and R_{Db} are the capacitance and resistance of the dry band region, respectively. Various references in the bibliography have demonstrated that, on the insulator's surface and specifically on the dry band not subject to arcing, partial discharges also occur. The effect of partial discharges on the equivalent circuit of the insulator is also represented by $R(t)$, which short-circuits for this occasion a rather small part of the dry band resistance. Because not all dry band is short-circuited, but only a part, $R(t)$ at the time when partial discharges occur represents the non-short-circuited part of the dry band.

The effect of partial discharges on the equivalent circuit of the insulator is also represented by $R(t)$, which short-circuits for this occasion a rather small part of the dry band resistance. Because not all dry band is short-circuited, but only a part, $R(t)$ at the time when partial discharges occur represents the non-short-circuited part of the dry band. Resistance $R(t)$ that short-circuits a small or considerable part of the dry band, due to partial discharges or arcs respectively, is a non-linear time dependent resistance. The following formula is proposed for $R(t)$:

$$R(t) = K1 - [K1 - (r_{arc} + r1)] \cdot e^{a1*(t-t1)^2} - [K1 - (r_{pd} + r2)] \cdot e^{a2*(t-t2)^2}$$

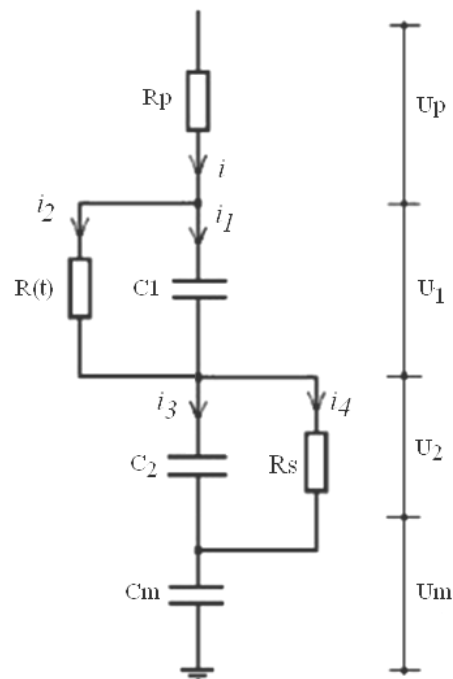
where $K1$ is a constant, usually of the order of $10^{12} \Omega$, $r1$ and $r2$ are the resistances of the non-short-circuited part of the dry band in the case of an arc or a partial discharge

respectively, and r_{pd} , r_{arc} are the resistances of the partial discharges and arcs, respectively, when one of them is in progress. The constants a_1 and a_2 determine the time duration of the pulses, and have values of the order of 10^{14} . Time parameters t_1 and t_2 correspond to the initial time when partial discharges and arcs occur, respectively. This model proposed in [284] takes as a base the well known models for partial discharges and adjusts them for porcelain insulators with dry band arcs and present the equation development and forms to calculate some of the parameters; in [285] the concept was applied satisfactorily to adjust the model for internal partial discharges as well.



When solid dielectrics are stressed in air, the surface layer of the solid, which has a thickness $\sim 30\text{\AA}$, and the surrounding air contribute to the discharges and when they break the space there is a gradual increase in the electric charge flow and consequently there is an increase in the overall capacitance of the dielectric. These changes in capacitance can be detected as disturbance or steps in the voltage. These steps appear as soon as the charges introduced by discharges flow and these are periods of high conductivity.

With the previous information and the theory of superficial discharges on polymers the following model is proposed:



The proposed model: $R(t)$ nonlinear, time-dependent resistance; C_1 , specimen capacitance where corona takes place; C_2 , specimen capacitance free of discharges, R_s , pollution representation; C_m measuring capacitor, R_p parasitic resistance.

If parasitic elements are neglected and C_m as well, the circuit is pretty similar with the one proposed initially where the dry band part is deactivated. Equations and validation is for a next step.

9. PUBLISHED PAPERS

1. E. Da Silva and S. M. Rowland, "*Natural, Rotationally Asymmetric Ageing of Composite Insulators,*" in *IEEE-DEIS International Symposium on Electrical Insulation, ISEI.* Vancouver, Canada, 2008.
2. E. Da Silva and S. M. Rowland, "*In-Service Surface Degradation of MV Composite Insulators under Severe Environmental Conditions and Low Electric Stress,*" in *IEEE-DEIS Conference on Electrical Insulation and Dielectric Phenomena, CEIDP.* Quebec, Canada, 2008.
3. E. Da Silva and S. M. Rowland, "*Dielectric Impedance as a Tool to Diagnose MV Composite Insulators,*" in *International Symposium on High Voltage Engineering, ISH.* Cape Town, South Africa, 2009.
4. A. Tzimas, E. D. Silva, and S. M. Rowland, "*A Framework to Assist Asset Management of Composite Insulators,*" in *International Electrical Insulation Conference, INSUCON.* Birmingham, UK, 2009.
5. E. Da Silva and S. M. Rowland, "*The Dependency of Water Droplet Behaviour and Leakage Current Pattern on Electrode Configuration,*" in *IEEE-DEIS Conference on Electrical Insulation and Dielectric Phenomena, CEIDP.* Virginia Beach, USA, 2009.
6. A. Tzimas, E. Da Silva Domingues and S.M. Rowland. "*Framework on Ageing of Composite Insulators to Assist Asset Management with examples from service*". in *IEEE-DEIS International Symposium on Electrical Insulation, ISEI.* San Diego, USA, 2010.

Papers in progress to be send to Journals

1. E. Da Silva and S M Rowland, "New Diagnosis Method of MV EPDM insulators aged in service under natural conditions".
2. E Da Silva and S M Rowland, "Electric field FEM simulations of water droplets on polymer surfaces under different conditions".
3. E Da Silva and S M Rowland, "Correlation of static contact angle versus roughness and dynamic contact angle versus hydrophobicity on SiR surfaces".
4. E Da Silva and S M Rowland, "Leakage current pulses behaviour versus electrohydrodynamic processes on polymer insulator surfaces".
5. A. Tzimas, E Da Silva and S M Rowland, "Composite insulators' assets management plan".

10. REFERENCES

- [1] H. Kloes and D. Koenig, "Multifactor-Surface-Tests of Organic Insulating Materials in the Early Stage of Degradation," in *IEEE International Symposium on Electrical Insulation* Montreal, Canada, 1996, pp. 296-299.
- [2] "BSI PAS 55-1: Asset management. Specification for the optimized management of physical assets," 2008.
- [3] S. Chapel, "Asset Management White Paper," S. Chapel and Associates June 7th, 2009.
- [4] R. Brown, "Reliability and Distribution Asset Management," in *Electric Energy T&D Magazine* Quebec, Canada Jaguar Media Inc., 2004, pp. 50-53.
- [5] S. Rahman, "Municipal Infrastructure Asset Management," Municipal and Community Affairs - Government of the Northwest Territories, , Yellowknife, Canada, 2007.
- [6] D. Perez, G. Hurtado, and M. delRey, "Nuevas alternativas en la gestión de activos para compañías de transporte y distribución de energía eléctrica en mercados liberalizados," *Anales de Mecánica y Electricidad*, pp. 5-14, Sep/Oct 2004.
- [7] M. Chan, "Asset Management - Optimizing Project Portfolio," in *IEEE PSCE* Atlanta, USA, 2006.
- [8] T. Hjartarson, B. Jesus, D. T. Hughes, and R. M. Godfrey, "Development of health indices for asset condition assessment," in *IEEE PES Transmission and Distribution Conference and Exposition*, Oakville, Canada, 2003, pp. 541-544.
- [9] J. Lúcio, J. Nuñez, and R. Teive, "Asset Management into Practice: A Case Study of a Brazilian Electrical Energy Utility," in *The 15th International Conference on Intelligent System Applications to Power Systems*, Curitiba, Brazil, 2009, pp. 1-6.
- [10] R. P. Hoskins, A. T. Brint, and G. Strbac, "A structured approach to Asset Management within the electricity industry," *Utilities Policy*, vol. 7, pp. 221-232, 1999.
- [11] S. Chapel and J. Lesser, "Keys to Transmission and Distribution Reliability," in *Public Utilities Fortnightly* Vienna: Public Utilities Reports, Inc., 2004, pp. 58-60.
- [12] C. Feinstein and S. Chapel, "Creating a New Distribution Asset Management & Infrastructure Planning Function at AEP," EPRI, 1999.
- [13] P. Dyer and D. Openshaw, "Techniques for Modeling and Monitoring Critical Conditions," in *17th International Conference on Electricity Distribution (CIRED)* Barcelona, Spain, 2003, pp. 1-7.
- [14] A. Afonso and E. Sarno, "Una Visión Holística para la Gerencia de Activos en Sistemas de Distribución," Mexico: Instituto de Investigaciones Electricas - Bearing Point, 2006, p. [www.iie.org.mx/.../UnaVisionHolistica para laGerencia deActivos enSistemas de Distribucion 12102006MTY.pdf](http://www.iie.org.mx/.../UnaVisionHolistica%20para%20laGerencia%20deActivos%20enSistemas%20deDistribucion%2012102006MTY.pdf)
- [15] R. E. Brown and B. G. Humphrey, "Asset management for transmission and distribution," *Power and Energy Magazine, IEEE*, vol. 3, pp. 39-45, May-June 2005.

- [16] Tumiran, "Development of CMMS (Computerized Maintenance Management System) in Yogyakarta Electric Power Distribution Network Company To Support The Strategic Maintenance," in *2008 International Conference on Condition Monitoring and Diagnosis* Beijing, China 2008, pp. 1-6.
- [17] O. Tor and M. Shahidehpour, "Power Distribution Asset Management," in *IEEE Power Engineering Society General Meeting* Montreal, Canada, 2006, pp. 1-7.
- [18] J. Smith, B. Quak, and E. Gulski, "Integral Decision Support for Asset management of Electrical Infrastructures," in *IEEE International Conference on Systems, Man and Cybernetics* Taipei, Taiwan, 2006, pp. 2622-2628.
- [19] G. Anders, S. Otal, and T. Hjartarson, "Deriving Asset Probabilities of Failure: Effect of Condition and Maintenance Levels," in *Power Engineering Society General Meeting, IEEE*, Montreal, Quebec, 2006, pp. 1-7.
- [20] S. Chapel, "Transmission and Distribution Infrastructure Management Must Enter a New Age," *Natural Gas & Electricity*, pp. 23-28, 2008.
- [21] S. Birlasekaran and G. Ledwich, "Asset Management of Power Apparatus," in *1st World Congress on Engineering Asset Management*, Queensland, Australia 2006, pp. 1-9.
- [22] L. Bertling, R. Allan, and R. Erickson, "A Reliability-Centered Asset Maintenance Method for Assessing the Impact of Maintenance in Power Distribution Systems," *IEEE Transaction on Power Systems*, vol. 20, pp. 75-82, 2005.
- [23] L. Bertling, R. Erickson, and R. Allan, "Impact of Maintenance Strategy on Cost and Reliability of Distribution Systems," in *17th International Conference on Electricity Distribution (CIRED)* Barcelona, Spain, 2003, pp. 1-6.
- [24] P. Hilber, "Maintenance Optimization for Power Distribution Systems," in *Electromagnetic Engineering, School of Electrical Engineering*. vol. PhD Stockholm, Sweden,: Royal Institute of Technology, 2008, p. 125.
- [25] M. Tapper, S. Jansson, and K. Oberger, "RCM for Electrical Distribution Systems - The Swedish Solution," in *17th International Conference on Electricity Distribution (CIRED)* Barcelona, Spain, 2003, pp. 1-3.
- [26] A. Phillips, "Review for the State of the Art and Application of Polymer Materials / Insulation used in Distribution Class (12 - 46 kV class) Substation," EPRI, 2003.
- [27] K. Goly, "A Business-Based Approach to Developing an Effective Program." vol. 2010: ReliabilityWeb.com.
- [28] T. Hjartarson and S. Otal, "Predicting Future Asset Condition Based on Current Health Index and Maintenance Level " in *IEEE 11th International Conference on Transmission & Distribution Construction, Operation and Live-Line Maintenance (ESMO)* New Mexico, USA, 2006, pp. 1-8.
- [29] D. T. Hughes, "The Use of "Health Indices" to Determine End of Life and Estimate Remnant Life for Distribution Assets," in *17th International Conference on Electricity Distribution*, Barcelona, Spain, 2003, pp. 1-4.
- [30] T. Hjartarson, "Asset Sustainability: From Condition and Risk," in *Asset Management Conference* Monterrey, Mexico, 2006.
- [31] Y. Tsimberg, "Assessing Condition of Overhead Lines Using Best Asset Management Practices," IEEE WG Meeting of Management of Existing Overhead Lines (Kinectrics Inc Director presentation), Calgary, Alberta, Canada, 2009.
- [32] A. Naderian, S. Cress, R. Piercy, F. Wang, and J. Service, "An Approach to Determine the Health Index of Power Transformers," in *IEEE International Symposium on Electrical Insulation* Vancouver, BC, Canada, 2008, pp. 192-196.

- [33] K Lightfoot and B Woodrow, "Maintenance and Inspection Overview. Engineering Instruction EI 10-0001," EDF Energy Networks, p.p. 18, 2006.
- [34] "Hydro One Distribution's Asset Condition Assessment (ACA)," Hydro One Distribution and Acres International Consultant. Ontario Energy Board, Ontario, 2006.
- [35] I. Hathout, "Maintenance Prioritization of Existing Transmission Lines Using Priority Risk Indices (PRI)," in *9th International Conference on Probabilistic Methods Applied to Power Systems* Stockholm, Sweden 2006, p. 7.
- [36] J. Osztermayer, H. Zhang, and K. Feser, "Enhanced Competitiveness with a Modern Asset Management System, ," in *International Symposium on Modern Electric Power Systems* Wroclaw, Poland, 2002, pp. 64-69.
- [37] Kinectrics-Inc., "Distribution Asset Condition Assessment for Toronto Hydro Electrical Systems Limited," Report N°: K-012905-RA-0002-R00, Toronto, ON, Canada, 2007.
- [38] "Planning for the Future of Our Networks," EDF Energy Networks Ltd, pp. 60, <http://edfenergynetworks.dialoguebydesign.net/bgo/background.asp>, 2008.
- [39] S. J. Gusavac, M. D. Nimrihter, and L. R. Geric, "Estimation of overhead line condition," *Electric Power Systems Research*, vol. 78, pp. 566-583, 2008.
- [40] I. Al-Hamoudi and Z. Al-Hamouz, "Reliability and Cost Effectiveness of Silicone Rubber Insulators in the Eastern Coastal Industrial Area of Saudi Arabia," in *2003 IEEE ESMO - 2003 IEEE 10th International Conference on Transmission & Distribution Construction, Operation & Live-Line Maintenance Proceedings*, 2003, pp. 156-168.
- [41] B. Woodrow, "Inspection and Maintenance Frequency Schedule. Engineering Instruction EI 10-0002 (Version: 1.1)," EDF Energy Networks, p.p. 69, 2006.
- [42] A. Phillips and T. Shaw, "Field Guide - Visual Inspection of NCI, Revision 1 (1008739)," EPRI, Palo Alto, CA, USA, 2004.
- [43] "STRI - Guide 5, 2005, Guide for Visual Identification of Deterioration & Damages on Suspension Composite Insulators," STRI, Ludvika, Sweden. 2005.
- [44] "STRI - Guide 1, 92/1, Hydrophobicity Classification," STRI, Ludvika, Sweden. 1992.
- [45] "STRI - Guide 3, 2005, Composite Insulator Status Program: Field Inspection of Composite Line Insulators," STRI, Ludvika, Sweden. 2005.
- [46] J. Burnham, "Guideline for Visual Identification of Damaged Polymer Insulators, <http://ewh.ieee.org/soc/pes/iwg/NCIEvaluation/POLYMERDAMAGEGUIDELINE.doc>." vol. 2009, 1998.
- [47] S. Gubanski, A. Dornfalk, J. Andersson, and H. Hillborg, "Diagnostic Methods for Outdoor Polymeric Insulators," *IEEE Transaction on Dielectric and Electrical Insulation*, vol. 14, pp. 1065-1080, 2007.
- [48] A. Phillips, "Application of Polymer Insulators (NCI): Workshop Presentations (1002660)." EPRI, Palo Alto, CA, USA, 2003.
- [49] IEEE, "IEEE Std 1572 Guide for Application of Composite Line Post Insulators," 2004.
- [50] "IEEE-ESMOL Subcommittee 15.07. Energized Line Working with Polymer Insulators for Voltages 60kV and above," in *11th International Conference on Transmission & Distribution Construction, Operation and Live-Line Maintenance (ESMO)*, New Mexico, USA 2006.

- [51] A. Phillips, "Field Guide: Visual Inspection of Polymer Insulators. Technical Update, May 2006, (1013283) " EPRI, Palo Alto, CA, USA. 2006, pp. 104.
- [52] R. Gorur, "Condition Assessment of Polymer Insulators," PSERC Seminar Presentation, 2006, p. 37.
- [53] O. dePaiva and M. Filho, "Reviewing 10 Years of Operating Experience with Composite Insulators at CHESF," in *World Congress & Exhibition on Insulators, Arresters & Bushings*, Crete, Greece, 2009, pp. 1-9.
- [54] L. Zhao, C.Li, J. Xiong, S. Zhang, J. Yao, and X. Chen, "Online Hydrophobicity Measurement for Silicone Rubber Insulators on Transmission Lines," *IEEE Transaction on Power Delivery*, vol. 24, pp. 806-813, 2009.
- [55] C. Li, X. Huang, and L. Zhao, "Image Analysis on the Surface Hydrophobicity of Polluted Silicone Rubber Insulators," in *International Conference on Condition Monitoring and Diagnosis* Beijing, China, 2008, pp. 1-3.
- [56] D. Thomazini, "Classificação da hidrofobicidade em isoladores elétricos poliméricos de alta tensão (Hydrophobicity classificationHV polymer insulators), in Portuguese " in *Sistemas Electricos de Potencia*. vol. PhD Sao Paulo: University of São Paulo, 2009, p. 149.
- [57] D. Thomazini¹, M. V. Gelfuso, and R. A. C. Altafim, "Analysis of Entropy and Fractal Dimension to Classify the Hydrophobicity in Polymeric Insulators," in *International Symposium on Electrical Insulating* Yokkaichi, Mie, Japan, 2008, p. 4.
- [58] Igor Gutman, "STRI Guidelines for Diagnostics Of Composite Insulators: for Visual Inspections; for Hydrophobicity; for IR Helicopter Inspections," in *Suspension and post composite insulators: manufacturing, technical requirements, test methods, service experience, diagnostics* St. Petersburg, 2004, pp. 88 - 91.
- [59] IEC, "Technical Specification Guidance on the measurement of wettability of insulator surfaces, First edition 2003-06." vol. IEC TS 62073, 2003.
- [60] E. da Costa, T. Ferreira, M. Neri, I. Queiroz, and A. Germano, "Characterization of polymeric Insulators using Thermal and UV Imaging under Laboratory Conditions," *IEEE Transaction on Dielectrics and Electrical Insulation*, vol. 16, pp. 985-992, 2009.
- [61] M. Farzaneh, "Outdoor Insulators: Overview of In-Service Experience, Inspection Practice and Future Challenges," in *IEEE-EIC Electrical Insulation Conference* Montreal, QC, Canada, 2009.
- [62] S. Gubanski, A. Dernfalk, J. Andersson, and H. Hillborg, "Diagnostic Methods for Outdoor Polymeric Insulators," *IEEE Transaction on Dielectric and Electrical Insulation*, 2007.
- [63] W. L. Vosloo, G. R. Stolper, and P. Baker, "Daylight corona discharge observation and recording system," in *10th International Symposium on HV Engineering*. vol. 6 Montréal, Québec, Canada, 1997, pp. 161-164.
- [64] P. Lindner, "Inspection for corona and arcing with the Daycor camera," in *Proc. 2005 World Insulator Congress and Exhibition* Hong Kong, China, 2005.
- [65] Armando H. Shinohara, Danilo M.F. Santana, Pietro P.J.C. Oliveira, Rodrigo J.G. Silva, Otávio H. Magalhães, Cidrack G. Silveira, Helen J. Khoury, José F.A.G. Wavrik, Flávio M.A.C. Branco, Marco A. Leite, and Tereza C. Galindo, "Defects Detection in Electrical Insulators and Breaker for High Voltage by Low Cost Computed Radiography Systems," in *International Symposium on Digital industrial Radiology and Computed Tomography*, Lyon, France, 2007.

- [66] J. Angelini, G. Costa, A. Formiga, P. Mendonca, A. Shinohara, and T. Ferreira, "Deterioration of Polymeric Insulators Using Exclusive Agents," in *20th International Conference on Electricity Distribution (CIRED)* Prague, 2009.
- [67] D. R. de Mello, E. Acioli, and N. Góis, "Location of Internal Faults in Electrical Equipment Using Digital X-Ray Technology " in *16th World Conference on Non Destructive Testing* Montreal, Canada, 2004.
- [68] W. Cardoso, R. daSilva, V. Swinka-Filho, and T. Loddi, "Detecção de Defeitos em Isoladores Poliméricos por meio da Radiografia Digital e Reconhecimento de Padrões (Composite insulators' defect detection using digital X-rays and patrons identification) " *Espaço Energia*, vol. 2, pp. 1-7, 2005.
- [69] W. Cardoso, K. Geus, R. daSilva, and V. Swinka-Filho, "Detecção automática de vazios em isoladores poliméricos por tomografia industrial 3D (Automatic detection of flaws in polymer insulators using 3D industrial tomography)," *Espaço Energia*, vol. 11, pp. 1-6, 2009.
- [70] P. Mendonça and A. Shinohara, "A Experiência da Celpe no Uso da Radiografia Digital como Técnica de Diagnóstico de Falhas em Materiais Poliméricos," in *III Simpósio Brasileiro de Sistemas Elétricos (SBSE)*, Belem, PA, Brazil, 2010, p. 6.
- [71] N. Qaddoumi, A. El-Hag, M. Al Hosani, I. Al Mansouri, and H. Al Ghufli, "Detecting Defects in Outdoor Non-ceramic Insulators using Near-field Microwave Non-destructive Testing," *IEEE Transaction on Dielectric and Electrical Insulation*, vol. 17, pp. 402-407, 2010.
- [72] A. Lopes and I. daSilva, "Estudo da Distribuição de Campo Elétrico em Isoladores Poliméricos: uma abordagem computacional e experimental," in *SBSE - Simpósio Brasileiro de Sistemas Elétricos* Belo Horizonte - MG - 27 a 30 de abril, 2008, p. 6.
- [73] V. T. Kontargyri, I. F. Gonos, N. C. Iliá, and I. A. Stathopoulos, "Simulation of the electric field on composite insulators using the finite elements method," *WSEAS Transactions on Circuits and Systems*, vol. 3, pp. 1318-22, 2004.
- [74] F. Goodman, "EPRI - Advanced Distribution Monitoring. Definition of Requirements. 1010667," EPRI, Palo Alto, CA, USA. 2005.
- [75] N.C. Gois, J.A.D. Rossi, F.E. Nallin, J.A. Petrachim, and J.M.G. Angelini, "Aplicacao de sensor para monitoriamento da degradacao de isoladores polimericos de epdm na coelba," in *Seminario Nacional de Producao e Transmissao de Energia Eletrica* Rio de Janeiro, 2007.
- [76] P. Mendonça, J. Angelini, F. Nallim, E. Costa, T. Ferreira, and A. Germano, "Monitoramento de Isoladores Polimericos em Linhas de Transmissao atraves de Sensor de Corrente de Fuga," in *SBSE2010 - Simpósio Brasileiro de Sistemas Elétricos*, Belem, Brazil, 2010, p. 6.
- [77] N. Anami, Y. Zhu, S. Hashimoto, M. Otsubo, C. Honda, O. Takenouchi, and Y. Hashimoto, "Evaluation of dry band arc on the polymeric insulator using differential technique and distortion factor of leakage current," in *Electrical Insulation and Dielectric Phenomena, 2003. Annual Report. Conference on*, 2003, pp. 414-417.
- [78] C.Muniraj and S.Chandrasekar, "Analysis of Leakage Current on Polluted Polymer Insulator by High Resolution Spectrum Estimation method," in *Third International Conference on Power Systems*, Kharagpur, India, 2009, p. 5.
- [79] S. Chandrasekar, C. Kalaivanan, A. Cavallini, and G. Montanari, "Investigations on leakage current and phase angle characteristics of porcelain and polymeric

- insulator under contaminated conditions," *Dielectrics and Electrical Insulation, IEEE Transactions on*, vol. 16, pp. 574-583, 2009.
- [80] M. Amin, S. Amin, and M. Ali, "Monitoring of Leakage Current for Composite Insulators and Electrical Devices," *Rev. Adv. of Material Science*, vol. 21, pp. 75-89, 2009.
- [81] R. Gorur, R. Olsen, and S. Venkataraman, "Prediction of Flashover Voltage of Insulators using Low Voltage Surface Resistance Measurement," PSERC, publication 06-42, Arizona, USA, November, 2006, pp. 1-65.
- [82] S. Venkataraman and R. S. Gorur, "Prediction of flashover voltage of non-ceramic insulators under contaminated conditions," *Dielectrics and Electrical Insulation, IEEE Transactions on*, vol. 13, pp. 862-869, 2006.
- [83] S. Venkataraman, R. S. Gorur, and A. P. Mishra, "Impact of weathering on flashover performance of nonceramic insulators," *Dielectrics and Electrical Insulation, IEEE Transactions on*, vol. 15, pp. 1073-1080, 2008.
- [84] R. Gorur, H. Schneider, J. Cartwright, Y. Beausajour, K. Kondo, S. Gubanski, R. Hartings, M. Shah, J. Mc.Bride, C. de Turreil, and Z. Szilagyi, "Surface Resistance Measurements on Nonceramic Insulators," *IEEE Transaction on Dielectric and Electrical Insulation*, vol. 16, pp. 801-805, 2001.
- [85] V. Gonçalves and G. Nagano., "Inspeção Instrumentalizada em redes de distribuição urbana e rural em 15 e 34,5 kV," in *International Electricity Distribution Congress (CIDEL)* Buenos Aires, Argentina, 2006, p. 7.
- [86] A. Phillips, "EPRI - Damage Detection of Polymer Insulators Using Vibration Response: Evaluation of Remote Excitation Techniques (Rep.100202) " 2004.
- [87] F. Ju, L. Xidong, Y. Yu, W. Chengsheng, and C. Ling, "Application of Acoustic Emission Technology on Structure Design and Quality Control of Composite Insulators," in *6th International Conference on Properties and Applications of Dielectric Materials*, Xi'an, China, 2000, pp. 358-361.
- [88] A. Dernfalk, "Diagnostic methods for composite insulators with biological growth, Ph.D Thesis," Göteborg, Sweden: Chalmers University of Technology, 2004.
- [89] A. Larsson, A. S. Kröll, D. Dernfalk, and S. M. Gubanski, "In-situ diagnostics of high-voltage insulation using laser-induced fluorescence spectroscopy," *IEEE Transaction on Dielectric and Electrical Insulation*, vol. 9 pp. 274-281, 2002.
- [90] S. Bakhtiari, S. Ganchev, N. Qaddoumi, and R. Zoughi, "Microwave Non-Contact Examination of Disbond and Thickness Variation in Stratified Composite Media " *IEEE Trans. Microwave Theory and Techniques*, vol. 42, pp. 389-395, 1994.
- [91] A. Chunghtai, D. Smith, L. Kumosa, and M. Kumosa, "FTIR Analysis of Non-ceramic Composite Insulators," *IEEE Transaction on Dielectric and Electrical Insulation*, vol. 11, pp. 585-596, 2004.
- [92] D. M. Hepburn, "Infrared spectroscopy and allied techniques," in *Materials Characterisation - How Can We Do It? What Can It Tell Us? (Ref. No: 1997/150)*, *IEE Colloquium on*, 1997, pp. 1/1-1/4.
- [93] P. D. Blackmore, D. Birtwhistle, G. A. Cash, and G. A. George, "Condition assessment of EPDM composite insulators using FTIR spectroscopy," *Dielectrics and Electrical Insulation, IEEE Transactions on*, vol. 5, pp. 132-141, 1998.
- [94] D. Birtwhistle, P. Blackmore, G. Cash, G. George, T. Gillespie, and A. Krivda, "Application of Advanced Chemical Analysis Techniques to the Assessment of Composite Insulator Condition," in *Cigre Session 2000 Paris*, France.

- [95] R. Sundararajan, A. Mohammed, N. Chaipanit, T. Karcher, and Z. Liu, "In-service aging and degradation of 345 kV EPDM transmission line insulators in a coastal environment," *Dielectrics and Electrical Insulation, IEEE Transactions on*, vol. 11, pp. 348-361, 2004.
- [96] D. Birtwhistle, G. Cash, G. A. George, and D. Hinde, "New Techniques for Estimating the Condition of High Voltage Polymeric Insulators," in *Engineering Asset Management*, 2006, pp. 949-956.
- [97] D. Birtwhistle, P. Blackmore, A. Krivda, G. Cash, and G. George, "Monitoring the condition of insulator shed materials in overhead distribution networks," *Dielectrics and Electrical Insulation, IEEE Transactions on*, vol. 6, pp. 612-619, 1999.
- [98] D. Birtwhistle, P. Blackmore, G. Cash, T. Gillespie, and A. Krivda, "Application of Advanced Chemical Analysis Techniques to the Assessment of Composite Insulator Condition," *Cigre*, vol. 15-307, 2000.
- [99] W. Broughton and M. Lodeiro, "Review of surface characterisation techniques for adhesive bonding," National Physical Lab., Ed. Teddington (United Kingdom), 2002.
- [100] M. Amin and M. Salman, "Aging of polymeric insulators (an overview)," *Reviews on Advanced Materials Science*, vol. 13, pp. 93-116, 2006.
- [101] H. Homma, T. Kuroyagi, K. Izumi, C. L. Mirley, J. Ronzello, and S. A. Boggs, "Evaluation of Surface Degradation of Silicone Rubber Using Gas Chromatography/Mass Spectroscopy," *IEEE Transactions on Power Delivery*, vol. 15, pp. 796-803, 2000.
- [102] I. Gutman, L. Stenström, D. Gustavsson, D. Windmar, and W.L. Vosloo, "Optimized use of HV composite apparatus insulators: field experience from coastal and inland test stations," in *Cigre Session 2004*, Paris, 2004, p. 10.
- [103] L. Meyer, T. Mustafa, F. Molina, and C. Oldoni, "Desenvolvimento e Aplicação de uma Estação de Monitoramento de Sistemas Isolantes," in *SBSE - Simposio Brasileiro de Sistemas Electricos* Belem, Brazil, 2010, p. 4.
- [104] R. Houlgate, "Natural Testing of Composite Insulators at Dungeness Insulators Testing Station," *SEE Seminar Non Ceramic Outdoor Insulation*, 1993, pp. 161-165.
- [105] I. Gutman, H. Wieck, D. Windmar, L. Stenstrom, and D. Gustavsson, "Pollution measurements to assess the performance of naturally exposed silicone rubber composite insulators," *STRI*, 2006.
- [106] A. Phillips, "EPRI - Promising Technologies for the Inspection of Polymer Insulators: Technology Review and Evaluation (1002025)," EPRI, Palo Alto, CA, USA2003.
- [107] M. Carnero, "Selection of condition monitoring techniques using discrete probability distributions: a case study," *Proc. IMechE Vol. 223 Part O: J. Risk and Reliability*, pp. 99-117, 2009.
- [108] A. Schwalm, A. Bernstorf, T. Baker, and T. Grisham, "IEEE Task Force: Insulators Working Group 101, Panel Final Presentation," in *IEEE/PES 2010 Transmission and Distribution Conference and Exposition*, New Orleans, Louisiana 2010.
- [109] IEEE-PES, "Guide for Cleaning Insulators." vol. IEEE Std 957™-2005.
- [110] T. Ferreira, A. Germano, E. da Costa, J. Angelini, F. Nallim, and P. Mendonça, "Isoladores Poliméricos Envelhecidos Naturalmente: Lavagens e suas

- Conseqüências (Polymer Insulators Aged Naturally: Washing and its Consequences, in Portuguese)," in *Simpósio Brasileiro de Sistemas Elétricos* Belen, PA, Brazil, 2010, pp. 1-6.
- [111] F. Gomes, "Lavagem De Isoladores em Instalações Energizadas," in *CIER - Jornadas de Integracion Electrica Regional* Fortaleza, Brasil, 2004, p. 5.
- [112] Ampla, Coelce, and Endesa-geração, "Sistema de Lavagem Ecologicamente Correta," <http://www.encontroendesa.com.br/apresentacoes/14.40%20-%20Sistema%20de%20Lavagem.pdf>." vol. (Access year 2010) Fortaleza, CE, Brazil: 2do Encontro de Pesquisa & Desenvolvimento Endesa Brasil, Abril, 2010.
- [113] A. Phillips, "EPRI Polymer Insulator Failure Database: 2005 Analysis (Doc number: 1010236)"
" EPRI, Technical Update, June 2005.
- [114] A. Tzimas, E. D. Silva, and S. M. Rowland, "A Framework to Assist Asset Management of Composite Insulators," in *International Electrical Insulation Conference, INSUCON*. Birmingham, UK, 2009.
- [115] E. da Costa, T. Ferreira, M. Neri, I. Queiroz, and A. Germano, "Characterization of polymeric Insulators using Thermal and UV Imaging under Laboratory Conditions," *IEEE Transaction on Dielectric and Electrical Insulation*, vol. 16, pp. 985-992, 2009.
- [116] A.J. Phillips and C.S. Engelbrecht, "The Feasibility of Using Daytime Corona Inspection to Identify Contaminated Insulators That Needs to be Washed," *Water and Energy Abstracts*, vol. 19, 2009.
- [117] W.Giménez, H. Pascual, L. Neira, F. Pérez, D. Cairol, J. Ramos, G. Alonso, and J. Moya, "TCT en Líneas de A.T. con Aisladores Poliméricos " in *IV Congreso Internacional Trabajos Con Tensión Y Seguridad En Transmisión y Distribución De Energía Eléctrica*, Buenos Aires, Argentina, 2009.
- [118] C. Yangchun and L. Chengrong, "Online detecting composite insulators by two dimensions electric field distribution," in *Electrical Insulation, 2006. Conference Record of the 2006 IEEE International Symposium on*, 2006, pp. 132-135.
- [119] S. Gorur and S. Sivasubramaniyam, "Defects in Nonceramic Insulators: Can They be Detected in a Timely Manner?," Ofil, Ed., 2004.
- [120] L. Chengrong, Z. Linjie, X. Jun, Z. Shuqi, and Y. Jisha, "Influence of seasons on hydrophobicity of silicone rubber insulators in semi-wet warm-temperature zone of china," *Dielectrics and Electrical Insulation, IEEE Transactions on*, vol. 15, pp. 1081-1088, 2008.
- [121] "IEC Std -TS 62073, Guidance on the measurement of wettability of insulator surfaces," International Electrotechnical Commission, 2003.
- [122] M. Amin, M. Akbar, and S. Amir, "Hydrophobicity of Silicone Rubber Used for Outdoor Insulation (An Overview)," *Rev. Adv. of Material Science*, vol. 16, pp. 10-26, 2007.
- [123] I. Lopes, S. Jayaram, and E. Cherney, "Partial discharge measurement as a diagnostic tool of the early ageing of silicone rubber insulation," in *Power Engineering Society General Meeting, 2003, IEEE*, 2003, p. 206 Vol. 1.
- [124] A. H. El-Hag, "Leakage current characterization for estimating the conditions of non-ceramic insulators' surfaces," *Electric Power Systems Research*, vol. 77, pp. 379-384, 2007.
- [125] M. Otsubo, T. Hashiguchi, C. Honda, O. Takenouchi, T. Sakoda, and Y. Hashimoto, "Evaluation of insulation performance of polymeric surface using a

- novel separation technique of leakage current," *Dielectrics and Electrical Insulation, IEEE Transactions on*, vol. 10, pp. 1053-1060, 2003.
- [126] I. A. D. Giriantari and T. R. Blackburn, "Characterisation of Surface Partial discharges on SiR insulators under high humidity and pollution conditions " in *International Symposium on High Voltage* Bangalore, India, 2001.
- [127] R. Sundararajan, A. M. Kannan, E. Romero, and I. Molina, "Characterization of Aging and Degradation of 28kV Polymeric insulators using Electrical Impedance Spectroscopy," in *Electrical Insulation and Dielectric Phenomena, 2006 IEEE Conference on*, 2006, pp. 461-464.
- [128] J. Ramirez, E. Da Silva, J. C. Rodriguez, and M. Martinez, "Evaluation of 400 kV Silicone Insulators Aged under Natural Tropical Conditions," in *IEEE Electrical Insulation and Dielectric Phenomena (CEIDP) Quebec*, Canada, 2008, pp. 276-279.
- [129] M. Ehsani , G. R. Bakhshandeh, J. Morshedian, H. Borsi , E. Gockenbach , and A. A. Shayegani, "The dielectric behavior of outdoor high-voltage polymeric insulation due to environmental aging," *European Transaction on Electrical Power*, vol. 17, pp. 47-59, 2006.
- [130] S. M. Rowland, Y. Xiong, J. Robertson, and S. Hoffmann, "Aging of silicone rubber composite insulators on 400 kV transmission lines," *Dielectrics and Electrical Insulation, IEEE Transactions on*, vol. 14, pp. 130-136, 2007.
- [131] J. Ramirez, E. Da Silva, J. Rodriguez, and M. Martinez, "Evaluation of 400 kV Silicone Insulators Aged under Natural Tropical Conditions," in *Conference on Electrical Insulation Dielectric Phenomena Quebec*, Canada, 2008, pp. 276-279.
- [132] P. delValle, M. Deorsola, and M. d. Pozo, "Evaluación del Efecto de la Contaminación Sobre Aisladores Poliméricos Retirados de Servicio," in *XIII ERIAC-Décimo Tercer Encuentro Regional Iberoamericano de CIGRÉ* Puerto Iguazu, Argentina, 2009, p. 8.
- [133] G. Cash, G. George, P. Blackmore, and D. Birtwhistle, "In-situ assessment of composite insulator surface condition," in *Dielectric Materials, Measurements and Applications, Seventh International Conference on (Conf. Publ. No. 430)*, 1996, pp. 285-288.
- [134] F. Noronha, J. M. G. Angelini, N. C. Góis, and L. H. I. Mei, "Performance development requirements for elastomers of electric power network insulators," *Journal of Materials Processing Technology*, vol. 162-163, pp. 102-108, 2005.
- [135] P. A. Sorichetti, C. L. Matteo, O. A. Lambri, G. C. Manguzzi, L. M. Salvatierra, and O. Herrero, "Structural Changes in EPDM Subjected to Ageing in High Voltage Transmission Lines," *Dielectrics and Electrical Insulation, IEEE Transactions on*, vol. 14, pp. 1170-1182, 2007.
- [136] T. Sorqvist and A. E. Vlastos, "Performance and ageing of polymeric insulators," *Power Delivery, IEEE Transactions on*, vol. 12, pp. 1657-1665, 1997.
- [137] Y. Bok-Hee and H. Chang-Su, "Surface characterization of silicone polymer used as an outdoor insulator by the measurement of surface voltage decay," *Surface and Interface Analysis*, vol. 33, pp. 954-9, 2002.
- [138] Z. Yong, K. Haji, M. Otsubo, and C. Honda, "Surface Degradation of Silicone Rubber Exposed to Corona Discharge," *Plasma Science, IEEE Transactions on*, vol. 34, pp. 1094-1098, 2006.
- [139] A.J.P. Silveira, D. Ramalho de Mello, G. Aguiar, L. Viviani, L.T. Murad, and P. A. M. Cardoso, "Isoladores Poliméricos; As Experiências da Enersul - Rede Energia e

- da Escelsa - Grupo Energias do Brasil No Uso Destes Isoladores em Suas Linhas de 138 kV," in *XIII ERIAC - Décimo Tercer Encuentro Regional Iberoamericano de Cigré* Puerto de Iguazú - Argentina, 2009.
- [140] H. Liu, G. Cash, D. Birtwhistle, and G. George, "Characterization of a Severely Degraded Silicone Elastomer HV Insulator - an Aid to Development of Lifetime Assessment Techniques," *IEEE Transaction on Dielectric and Electrical Insulation*, vol. 12, pp. 478-485, 2005.
- [141] H. Liu, G. Cash, D. Birtwhistle, and G. George, "Characterization of a severely degraded silicone elastomer HV insulator-an aid to development of lifetime assessment techniques," *IEEE Transaction on Dielectrics and Electrical Insulation*, vol. 12, pp. 478-486, 2005.
- [142] "EDF Energy Networks, Webmail: <http://edfenergynetworks.dialoguebydesign.net/docs/PlanningForTheFuture.pdf>," 2009.
- [143] "Met Office UK, Website: <http://www.metoffice.gov.uk/climate/uk/averages/19712000/mapped.html>."
- [144] "UK National Ammonia Monitoring Network 2007 Annual Report, Webpage: <http://www.uk-pollutantdeposition.ceh.ac.uk>," 2009.
- [145] "Air Pollution Information System, Website: <http://www.apis.ac.uk/index.html>," 2009.
- [146] "BBC, UK Climate Webpage: <http://www.bbc.co.uk/schools/gcsebitesize/geography/weather/climaterev4.shtml>," 2009.
- [147] "BWEA, Website, http://www.bwea.com/images/misc/noabl_c.gif," 2009.
- [148] "Centre for Ecology & Hydrology, "National Hydrological Monitoring Programme Webpage: http://www.ceh.ac.uk/data/nrfa/documents/Hydrological_Review_2006.pdf," 2009.
- [149] "Contemporary Energy Ltd, Website: <http://www.contemporaryenergy.co.uk/windmap.htm>," 2009.
- [150] "Protection UK, Website: <http://www.environmental-protection.org.uk/air-quality-and-climate/air-quality/sources/>," 2009.
- [151] "GreenFacts, Website: <http://www.greenfacts.org/en/dioxins/index.htm>," 2009.
- [152] "UK Air Quality Archive, Website: <http://www.airquality.co.uk/laqm/documents/Backgroundmaps20090202.pdf>," 2009.
- [153] "UK Air Quality Archive, UK Air Quality Archive, Website: http://www.airquality.co.uk/reports/cat09/0807231621_dd12006mapsrep_v2.pdf," 2009.
- [154] "National Atmospheric Emissions Inventory - AEA Group, Webpage: http://www.airquality.co.uk/reports/cat07/0910211141_DA_AQ_Inventory_Report_2007_maintext_Issue1.pdf," 2009.
- [155] A. Stewart and N. Murray, "Inspection and Assessment Utility Practices," Management of Existing Overhead Lines WG Meeting, Panel Session, Disney Contemporary Resort, Orlando, FL, USA, January 2010, p. 22.
- [156] "UK Pollutant Deposition, Webpage: <http://www.uk-pollutantdeposition.ceh.ac.uk/image/tid/45>," 2005.
- [157] National Atmospheric Emissions Inventory - AEA Group, "Webpage: http://www.airquality.co.uk/reports/cat07/0910211141_DA_AQ_Inventory_Report_2007_maintext_Issue1.pdf," 2009.

- [158] European Commission, "Webpage: http://re.jrc.ec.europa.eu/pvgis/countries/europe/g13y_uk_ie.png," 2009.
- [159] Solar Trade Association, "www.solartradeassociation.org.uk," 2009.
- [160] EDF Energy, "Webpage: <http://www.eeegr.com/uploads/DOCS/431-20070718140558.pdf>," 2009.
- [161] EDF Energy Networks, "Website: <http://edfenergynetworks.dialoguebydesign.net/docs/PlanningForTheFuture.pdf>," 2009.
- [162] Ocipenergy, "Website: www.ocipenergy.com/wind/noabl-wind-speed.php," 2009.
- [163] NEF-National Energy Foundation, "Webmail: <http://www.nef.org.uk/greencompany/images/active-windmap.gif>," 2009.
- [164] G. G. Karady, M. Shah, and R. L. Brown, "Flashover mechanism of silicone rubber insulators used for outdoor insulation-I," *Power Delivery, IEEE Transactions on*, vol. 10, pp. 1965-1971, 1995.
- [165] M. Shah, G. G. Karady, and R. L. Brown, "Flashover mechanism of silicone rubber insulators used for outdoor insulation-II," *Power Delivery, IEEE Transactions on*, vol. 10, pp. 1972-1978, 1995.
- [166] K. Portella, F. Piazza, P. Inone, S. Ribeiro, M. Cabussú, D. Pedreira, and C. Sobreira, "Atmospheric pollution (coastal and industrial) effects on electric energy distribution insulators in Salvador, Brazil, Metropolitan Region," *Quimica Nova*, vol. 31, pp. 340-348, 2008.
- [167] S. Keim, D. Koenig, and V. Hinrichsen, "Experimental investigations on electrohydrodynamic phenomena at single droplets on insulating surfaces," in *Electrical Insulation and Dielectric Phenomena, 2003. Annual Report. Conference on*, 2003, pp. 133-136.
- [168] J. Liebman and A. Greenberg., *Molecular Structure and energetic: volume 1, Chemical bonding models*. vol. 1. New York, USA: VCH, 1987.
- [169] W. Reusch, "Virtual Textbook of Organic Chemistry. [www.cem.msu.edu/~reusch/VirtualText/react1.htm#rx2] " University of Michigan, Michigan, USA, (1999. Most recent revision 7/16/2007).
- [170] J. A. Bousquet and J. P. Fouassier, "Mechanism of photo-oxidation of an elastomer," *Polymer Degradation and Stability*, vol. 5, pp. 113-133, 1983.
- [171] R. J. Arhart, "The chemistry of ethylene propylene insulation. I," *Electrical Insulation Magazine, IEEE*, vol. 9, pp. 31-34, 1993.
- [172] M. Otsubo, T. Hashiguchi, S. Yamashita, N. Anami, C. Honda, O. Takenouchi, K. Tsurugida, Y. Hashimoto, and M. Nakamura, "Discharge and emission spectra on the surface of polymer insulator materials in salt fog aging test," in *Electrical Insulation and Dielectric Phenomena, 2001 Annual Report. Conference on*, 2001, pp. 620-623.
- [173] T. P. Duguid, "Accelerated Ageing of Composite Insulator Materials," in *C.I.R.E.D. Liege, Belgium*, 1991.
- [174] V. Moreno and R. Gorur, "Corona-Induced Degradation of Nonceramic Insulator Housing Materials," in *IEEE Conference on Electrical Insulation and Dielectric Phenomena*, Ontario, Canada, 2001.
- [175] A. Skopec, L. Moron, and P. Zylka, "Time-domain Temperature Variations of a Composite Insulator Surface Exposed to Arc Discharges " *IEEE Transaction on Dielectrics and Electrical Insulation*, vol. 11, pp. 369-377, 2004.

- [176] R. Sarathi and S. Chandrasekar, " Investigation of Tracking Phenomena in Silicone Rubber Using Moving Average Current Technique," *Journal on Plasma Science & Technology*, vol. 6, pp. 2514-2520, 2004.
- [177] R. Sarathi and U. Maweswar, " Analysis of Surface Degradation of Silicone Rubber Due to Tracking - A Physica Approach " *Journal of Applied Polymer Science*, vol. 88, pp. 2392-2399, 2003.
- [178] S. Chandrasekar, R. Sarathi, and M. Danikas, "Analysis of Surface Degradation of Silicone Rubber Insulation due to Tracking under Voltage Profiles," *Journal Springer Berlin / Heidelberg*, vol. 89, pp. 481-501, 2007.
- [179] S. Pereira, R. d. Costa, S. Barbosa, and G. Almeida, "Tracking Degradation and Pyrolysis of EPDM insulators," *IEEE Transaction on Electrical Insulation*, vol. 24, pp. 99-105, 1989.
- [180] S. Wallström and S. Karlsson, "Biofilms on silicone rubber insulators; microbial composition and diagnostics of removal by use of ESEM/EDS: Composition of biofilms infecting silicone rubber insulators," *Polymer Degradation and Stability*, vol. 85, pp. 841-846, 2004.
- [181] X. Wang, S. Kumagai, and N. Yoshimura, "Acid Rain Affecting the Electrical Properties of Outdoor Composite Dielectric Materials.," *Japan Journal Applications Physics, Part 1*, vol. 37, pp. 6476 - 6481, 1998.
- [182] Q. Zhao, X. Li, and J. Gao, "Aging of ethylene-propylene-diene monomer (EPDM) in artificial weathering environment," *Polymer Degradation and Stability*, vol. 92, pp. 1841-1846, 2007.
- [183] A. Krivda, G. Cash, D. Birtwhistle, and G. George, "Diagnostics of EPDM polymer insulators," in *Electrical Insulation and Dielectric Phenomena, 1999 Annual Report Conference on*, 1999, pp. 682-686 vol.2.
- [184] J. Kim, M. K. Chaudhury, and M. J. Owen, "Modeling hydrophobic recovery of electrically discharged polydimethylsiloxane elastomers," *Journal of Colloid and Interface Science*, vol. 293, pp. 364-375, 2006.
- [185] T. Berger, S. Sundhararajan, and T. Nagaosa, "Influence of temperature on the hydrophobicity of polymers," in *IEEE Conference on Electrical Insulation and Dielectric Phenomena Minneapolis, USA, 1997*, pp. 394-397.
- [186] M. Fernando and S. Gubanski, "Performance of Nonceramic Insulators Under Tropical Field Conditions," *IEEE Trans. Power Delivery*, vol. 15, pp. 355-360, 2000.
- [187] C. Liwen and R. Hackam, "Low molecular weight fluids in EPDM," in *Electrical Insulation and Dielectric Phenomena, 1997. IEEE 1997 Annual Report., Conference on*, 1997, pp. 423-426 vol.2.
- [188] W L Vosloo, I Gutman, and R. Hartings, "Long-term service testing of insulators at a test tower in South Africa
". vol. 2008, 2001.
- [189] J. Ramirez, M. Sabino, E. Da Silva, J. Rodriguez, M. Martinez, J. Bermudez, J. Ren, and A. Ferraz, "Studies on polymeric insulators for transmission systems under natural aging conditions," in *Electrical Insulation and Dielectric Phenomena, 1998. Annual Report. Conference on*, 1998, pp. 719-722 vol. 2.
- [190] J. Insogna, H. Alonso, and R. Ferrelli, "Experiencias con aisladores organicos de EPDM - Su reemplazo con tensión," in *Conferencia de la Comision de la Integracion Energetica Regional - Comite Argentino, Cacier 2005*, Buenos Aires, Argentina, 2005, p. 11.

- [191] E. Da Silva and S. M. Rowland, "Natural, Rotationally Asymmetric Ageing of Composite Insulators," in *Electrical Insulation, 2008. ISEI 2008. Conference Record of the 2008 IEEE International Symposium on*, 2008, pp. 530-534.
- [192] S. Narita, A. Sawada, and L. Stenstrom, "Design and testing of polymer-housed surge arresters with special emphasize on seismic stresses and selection of specific creepage in costal areas," in *Cigre SC A3 & B3 Joint Colloquium Tokyo, Japan*, 2005.
- [193] "Comsol Multiphysic Manual. Multiphysics Modeling and Engineering Simulation Software," Version 3.2, ed, 2007.
- [194] STRI, "Guide 1, 92/1, Hydrophobicity Classification," 1992, p. 9.
- [195] STRI, "Guide 5. Guide for Visual Identification od Deterioration & Damages on Suspension Composite Insulators," 2003, p. 19.
- [196] T.P. Nguyen and V. H. Tran, "Dielectric properties of poly(phenylene-vinylene) thin films," *Materials Science and Engineering*, vol. B31, pp. 255-260, 1995.
- [197] W. S. Zaengl, "Applications of dielectric spectroscopy in time and frequency domain for HV power equipment," *Electrical Insulation Magazine, IEEE*, vol. 19, pp. 9-22, 2003.
- [198] J. W. Schultz, "Dielectric Spectroscopy in Analysis of Polymers " in *Encyclopedia of Analytical Chemistry: Applications, Theory, and Instrumentation, 15 Volume Set*, R. A. Meyers, Ed.: John Wiley & Sons, Ltd, 2006.
- [199] F. Yakuphanoglu, M. Okutan, Q. Zhuang, and Z. Han, "The dielectric spectroscopy and surface morphology studies in a new conjugated polymer poly(benzobisoxazole-2,6-diylvinylene)," *Physica B: Condensed Matter*, vol. 365, pp. 13-19, 2005.
- [200] S. Syropoulou, "Characterisation of surface treatments on concrete by AC impedance spectroscopy " *SURFACE COATINGS INTERNATIONAL. PART B : COATINGS TRANSACTIONS*, , vol. 88, pp. 61-66, 2005.
- [201] T. Tokoro, "Dielectric Measurements of Degradation Condition of Polymer Material Surface," in *ISEIM Japan*, 2005, pp. 576-579.
- [202] D. K. Das-Gupta and P. C. N. Scarpa, "Modeling of dielectric relaxation spectra of polymers in the condensed phase," *Electrical Insulation Magazine, IEEE*, vol. 15, pp. 23-32, 1999.
- [203] J. Ross Macdonald and J. A. Garber, "Analysis of Impedance and Admittance Data for Solids and liquids," *J. Electrochem. Soc.: ELECTROCHEMICAL SCIENCE AND TECHNOLOGY*, vol. 124, 1977.
- [204] S. Baltianski and Y. Tsur, "Analysis of Impedance Spectroscopy Data—Finding the Best System Function," *Journal of Electroceramics*, vol. 10, pp. 89-94, 2003.
- [205] A. Schwake, H. Geuking, and K. Cammann, "Application of a New Graphical Fitting Approach for Data Analysis in Electrochemical Impedance Spectroscopy," *Electroanalysis*, vol. 10, pp. 1026-1029, 1998.
- [206] E. Correa, S. Peñaranda, J. Castaño, and F. Echeverría, "Concrete deterioration in Colombian urban atmospheres," *Revista Facultad de Ingeniería Universidad de Antioquia*, vol. 52, pp. 41-46, 2010.
- [207] M. Krüger, A. Kraetge, M. Koch, K.Rethmeier, M. Pütter, L. Hulka, M. Muhr, and C. Summereder, "New Diagnostic Tools for High Voltage Bushing," in *VI WORKSPOT- International Workshop on Power Transformers*, Foz do Iguacu, Brasil, 2010, p. 13.

- [208] E. Da Silva and S. M. Rowland, "Dielectric Impedance as a Tool to Diagnose MV Composite Insulators," in *International Symposium on High Voltage Engineering, ISH*. Cape Town, South Africa, 2009.
- [209] A. Ghorbani, C. Camerlynck, and N. Florsch, "CR1Dinv: A Matlab program to invert 1D spectral induced polarization data for the Cole-Cole model including electromagnetic effects," *Computers & Geosciences*, vol. 35, pp. 255-266, 2009.
- [210] G. Song, "Equivalent circuit model for AC electrochemical impedance spectroscopy of concrete," *Cement and Concrete Research*, vol. 30, pp. 1723-1730, 2000.
- [211] M. Flanagan, "Model Circuits for Michael Thomas Flanagan's Java Library Impedance Spectroscopy, <http://www.ee.ucl.ac.uk/~mflanaga/java/ImpedSpecSimulation.html>," UCL (University College London), UK, 2008.
- [212] J. Xiang, D. Cheng, F. S. Schlindwein, and N. B. Jones, "On the adequacy of identified Cole-Cole models," *Computers & Geosciences*, vol. 29, pp. 647-654, 2003.
- [213] J. Xiang, N. B. Jones, D. Cheng, and F. S. Schlindwein, "Direct inversion of the apparent complex-resistivity spectrum," *Geophysics*, vol. 66, pp. 1399-1404, 2001.
- [214] "International Organization for Standardization, ISO 4287-1997: Geometrical Product Specifications (GPS) -- Surface texture: Profile method -- Terms, definitions and surface texture parameters," 1997.
- [215] M. F. Noel and G. J.-M. Riquel, "Evaluation of diagnostic techniques for non-ceramic outdoor high voltage insulators," in *IEEE Conference on Electrical Insulation and Dielectric Phenomena* Arlington, TX 1994, pp. 639 - 644
- [216] D. De-Mello, R. Garcia, J. Mendonca, and J. Oliveira, "A comparative study between hydrophobicity and roughness measurements on the composite insulators housing," in *International Symposium on High Voltage Engineering* Cape Town, South Africa, 2009, p. 4.
- [217] E. Da Silva, "EDF Energy 11 kV EPDM Insulation Recovery Process and Diagnosis (Part I)," University of Manchester, September 2007.
- [218] E. Da Silva, "Improved condition monitoring of composite insulator - First Year," University of Manchester, January 2008.
- [219] E. Da Silva, "Improved condition monitoring of composite insulator - Second Year," University of Manchester, 2009.
- [220] T. Schutte and S. Hornfeldt, "Dynamics of electrically stressed water drops on insulating surfaces," in *Electrical Insulation, 1990., Conference Record of the 1990 IEEE International Symposium on*, 1990, pp. 202-207.
- [221] A J Phillips, I R Jandrell, and J. P. Reynders, "The effect of changes in volume and air density on the corona onset potential of water drops," in *Ninth International Symposium On High Voltage Engineering*, Graz, Austria, 1995.
- [222] J. Taylors, "Disintegration of Water Drops in an Electric Field," *Proc. R. Soc. Academy*, vol. 280, pp. 383-397, 1964.
- [223] Y. Zhu, K. Haji, M. Otsubo, C. Honda, and N. Hayashi, "Electrohydrodynamic behaviour of water droplet on an electrically stressed hydrophobic surface," *J. Phys. D: Appl. Phys.*, vol. 39, pp. 1970-1975, 2006.
- [224] Y. Mizuno, M. Iwatani, M. Nagata, K. Naito, K. Kondo, and S. Ito, "Behavior of water droplets on silicone rubber sheet under AC voltage application," in *Electrical*

- Insulation and Dielectric Phenomena, 1998. Annual Report. Conference on, 1998, pp. 96-99 vol. 1.*
- [225] M. Fontelos and U. Kindelán, "Evolution of Neutral and Charged Droplets in an Electric Field," in *XXII ICTAM, Adelaide, Australia, 2008*, p. 2.
- [226] T. Braunsberger, A. Dziubek, W. Kodoll, U. Schoumann, and M. Kurrat, "PD between water drops influencing hydrophobic processes on SI and EP-resin systems," in *The XIIIth International Symposium on High Voltage Engineering Delft University of Technology, Delft, Netherlands, 2002*.
- [227] Z. Guan, L. Wang, B. Yang, X. Liang, and Z. Li, "Electric Field Analysis of Water Drop Corona," *IEEE Transaction on Power Delivery*, vol. 20, pp. 964-969, 2005.
- [228] R. Sundararajan, S. Sundhur, and T. Asokan, "Electrohydrodynamics of water droplets on polymer surfaces," in *Industry Applications Conference, 1999. Thirty-Fourth IAS Annual Meeting. Conference Record of the 1999 IEEE*, 1999, pp. 1817-1824 vol.3.
- [229] H. El-Kishky and R. S. Gorur, "Electric field computation on an insulating surface with discrete water droplets," *Dielectrics and Electrical Insulation, IEEE Transactions on*, vol. 3, pp. 450-456, 1996.
- [230] Z. Cheng, X. Liang, Y. Zhou, S. Wang, and Z. Guan, "Study of water droplet discharge by electric field computation and high-speed video," in *Properties and Applications of Dielectric Materials, 2003. Proceedings of the 7th International Conference on, 2003*, pp. 820-823 vol.2.
- [231] Y. Zhu, S. Yamashita, N. Anami, M. Otsubo, C. Honda, S. Hashimoto, and Y. Hashimoto, "Leakage current analysis and electric field calculation in salt fog ageing test on polymer insulation material," in *Electrical Insulation and Dielectric Phenomena, 2003. Annual Report. Conference on, 2003*, pp. 92-95.
- [232] Y. Zhu, S. Yamashita, N. Anami, M. Otsubo, C. Honda, and Y. Hashimoto, "Corona discharge phenomenon and behavior of water droplets on the surface of polymer in the AC electric field," in *Properties and Applications of Dielectric Materials, 2003. Proceedings of the 7th International Conference on, 2003*, pp. 638-641 vol.2.
- [233] P. Waluyo and S. Pakpahan, "Influences of water droplet size and contact angle on the electric field and potential distributions on an insulator surface," in *8th International Conference on Properties and applications of Dielectric Materials, Edinburgh, UK, , 2006*, pp. 889-892.
- [234] H. Gao, Z. Jia, Z. Guan, and J. Yang, "The Effect of Water Droplets on Hydrophobic Contaminated Surface under AC Field Voltage Application," in *IEEE CEIDP USA, 2005*, pp. 124-127.
- [235] S. Keim and D. Koenig, "Study of the behavior of droplets on polymeric surfaces under the influence of an applied electrical field," in *Electrical Insulation and Dielectric Phenomena, 1999 Annual Report Conference on, 1999*, pp. 707-710 vol.2.
- [236] S. Keim and D. Koenig, "The dynamic behaviour of water drops in an AC field," in *Electrical Insulation and Dielectric Phenomena, 2001 Annual Report. Conference on, 2001*, pp. 613-616.
- [237] N. Arise, H. Nishioka, Y. Okraku-Yienkyi, M. Otsubo, and C. Honda, "Behavior of water droplet on polymer material and the influence on discharge characteristics," in *Electrical Insulation and Dielectric Phenomena, 1999 Annual Report Conference on, 1999*, pp. 455-458 vol.2.

- [238] A. Krivda and D. Birtwhistle, "Electrohydrodynamic phenomena related to water drops on polymer surfaces," in *7th International Conference on Solid Dielectrics*, I. I. C. o. C. a. B. i. S. Dielectrics, Ed. Eindhoven, Netherlands: IEEE, 2001, pp. 345 - 350.
- [239] A. Krivda and D. Birtwhistle, "Breakdown between water drops on wet polymer surfaces," in *Electrical Insulation and Dielectric Phenomena, 2001 Annual Report Conference on*, 2001, pp. 572-580.
- [240] K. Katada, Y. Takada, M. Takano, T. Nakanishi, Y. Hayashi, and R. Matsuoka, "Corona discharge characteristics of water droplets on hydrophobic polymer insulator surface," in *Properties and Applications of Dielectric Materials, 2000. Proceedings of the 6th International Conference on*, 2000, pp. 781-784, Vol.2.
- [241] Y. Higashiyama, T. Yamada, and T. Sugimoto, "Vibration of water droplet located on a hydrophobic sheet under the tangential AC field," in *Industry Applications Conference, 1999. Thirty-Fourth IAS Annual Meeting. Conference Record of the 1999 IEEE*, 1999, pp. 1825-1830 vol.3.
- [242] Y. Higashiyama, T. Yamada, and T. Sugimoto, "Effect of resonance of a water droplet located on a hydrophobic sheet on AC flashover," in *Industry Applications Conference, 2002. 37th IAS Annual Meeting. Conference Record of the*, 2002, pp. 2198-2203 vol.3.
- [243] T. Yamada, T. Sugimoto, Y. Higashiyama, M. Takeishi, and T. Aoki, "Resonance phenomena of a single water droplet located on a hydrophobic sheet under AC electric field," *Industry Applications, IEEE Transactions on*, vol. 39, pp. 59-65, 2003.
- [244] Y. Mizuno, M. Nagata, K. Naito, K. Kondo, S. Ito, and Y. Koshino, "Water droplet behavior and discharge activity on silicone rubber surface energized by AC voltage," in *Electrical Insulation and Dielectric Phenomena, 2001 Annual Report Conference on*, 2001, pp. 624-627.
- [245] Y. Higashiyama, T.-i. Takada, and T. Sugimoto, "Resonant vibration and flashover phenomena of a water droplet located on a hydrophobic sheet under ac field," *Journal of Electrostatics*, vol. 63, pp. 883-889, 2005.
- [246] Y. Higashiyama, S. Yanase, and T. Sugimoto, "Behavior of water droplets located on a hydrophobic insulating plate under DC field," in *Industry Applications Conference, 1998. Thirty-Third IAS Annual Meeting. The 1998 IEEE*, 1998, pp. 1808-1813 vol.3.
- [247] Claudia Roero, "Contact angle measurements of sessile drops deformed by a DC electric field, ," in *4th International Symposium on Contact Angle, Wettability and Adhesion*, , Philadelphia, USA,, 2004.
- [248] Y. Higashiyama, S. Yanase, and T. Sugimoto, "DC corona discharge from water droplets on a hydrophobic surface," *Journal of Electrostatics*, vol. 55, pp. 351-360, 2002.
- [249] D. A. Swift, "Flashover of an insulator surface in air due to polluted water droplets," in *Properties and Applications of Dielectric Materials, 1994., Proceedings of the 4th International Conference on*, 1994, pp. 550-553 vol.2.
- [250] F. C. Lin and S. M. Rowland, "Study on low current arcs on surfaces of dielectric materials," in *Electrical Insulation and Dielectric Phenomena, 2005. CEIDP '05. 2005 Annual Report Conference on*, 2005, pp. 136-139.

- [251] S. M. Rowland and F. C. Lin, "Stability of alternating current discharges between water drops on insulation surfaces," *Journal of Physics D (Applied Physics)*, vol. 39, pp. 3067-76, 2006.
- [252] A. Moukengue Imano and A. Beroual, "Discharges current characteristics of water droplets on dielectric solid surface under AC voltage stress 16th international symposium on high voltage engineering," in *16th International Symposium on High Voltage Engineering*, Cape Town, South Africa, 2009.
- [253] A. Moukengue Imano and A. Beroual, "Behaviour of corona discharges between a metal electrode and water surface under AC voltage stress," in *16th International Symposium on High Voltage Engineering*, Cape Town, South Africa, 2009.
- [254] I. J. S. Lopes, S. H. Jayaram, and E. A. Cherney, "A study of partial discharges from water droplets on a silicone rubber insulating surface," *Dielectrics and Electrical Insulation, IEEE Transactions on*, vol. 8, pp. 262-268, 2001.
- [255] Y. Zhu, M. Otsubo, C. Honda, and S. Tanaka, "Corona Discharge from Water Droplet on Electrically Stressed Polymer Surface," *Japanese Journal of Applied Physics, Part 1* vol. 45, pp. 234 - 238, 2006.
- [256] Z. X. Cheng, X. D. Liang, Y. X. Zhou, S. W. Wang, and Z. C. Guan, "Observation of corona and flashover on the surface of composite insulators," in *Power Tech Conference Proceedings, 2003 IEEE Bologna*, 2003, p. 6 pp. Vol.2.
- [257] M. G. Danikas, "Water Droplets on Polymeric Surfaces Under the Influence of Uniform Electric Fields: An Investigation with Horizontal and Inclined Test Electrode Arrangements," in *Electrical Insulation, 2008. ISEI 2008. Conference Record of the 2008 IEEE International Symposium on*, 2008, pp. 672-675.
- [258] M. G. Danikas, P. Rakitzis, and K. Karakoulidis, "Study of parameters related to deterioration phenomena due to water droplets on polymeric surfaces," *Journal of ELECTRICAL ENGINEERING*, vol. 57, pp. 130-7, 2006.
- [259] H. J. Kloes and D. Koenig, "Basic investigations of the performance of droplets on electrically stressed polymer surfaces," in *Electrical Insulation and Dielectric Phenomena, 1997. IEEE 1997 Annual Report., Conference on*, 1997, pp. 374-377 vol.2.
- [260] T. Braunsberger and e. al, "Partial Discharge Processes at Sessile Water Drops on Insulating Surfaces," in *XVI ICGDA, China*, 2006, p. 4.
- [261] R. Sarathi, G. Nagesh, and K. Vasudevan, "Classification of Discharges Initiated by Liquid Droplet on Insulation Material under AC Voltages Adopting UHF Technique," *World Academy of Science, Engineering and Technology*, vol. 39, pp. 177 - 182, 2008.
- [262] S. Feier-Iova and V. Hinrichsen, "Partial discharge inception voltage of water drops on insulating surfaces stressed by electrical field," in *Electrical Insulation Conference, 2009. EIC 2009. IEEE*, 2009, pp. 21-25.
- [263] Arkadiusz Dziubek, Tobias Braunsberger, and M. Kurrat, "Effects of water drop corona at dew layers on silicone rubber," in *The 14th International Symposium on High Voltage Engineering*, Beijing, China, 2005.
- [264] T. Braunsberger and M. Kurrat, "Cyclic Water Drop Corona on Silicone Rubber Samples," in *The 15th International Symposium on High Voltage Engineering*, Ljubljana, Slovenia, 2007.
- [265] M. Rahman, R. Thottappillil, M. Berg, and H. Hillborg, "Comment on 'Effect of surface charge on hydrophobicity levels of insulating materials'," *Generation, Transmission and Distribution, IEE Proceedings-*, vol. 149, pp. 300-304, 2002.

- [266] P. Molinie and M. Goldman, "Evolution of the surface layer appearing with the corona ageing of epoxy samples," in *ICSD'95, Proceedings of the 1995 IEEE 5th International Conference on Conduction and Breakdown in Solid Dielectric*, Leicester, UK, 1995, pp. 482-486.
- [267] M. Goldman, A. Goldman, and R. S. Sigmond, "The corona discharges, its properties and specific uses," *Pure & Applied Chemistry*, vol. 57, pp. 1353 -1362, 1985.
- [268] 3DT-LLC, "Plasma & Corona Treating Systems, <http://www.3dtllc.com/index.html>," 2010.
- [269] M. M. Higashikoji, M.; Ohtsuka, S.; Hikita, M.; Ikeda, H.; Gavillet, J.; Ravel, G.; Da Silva, E.; Frechette, M.; , "Evaluation of Pollution Characteristic of Polymer Insulating Material with Surface Nano-Coating by a New Automatic Artificial Pollution Acceleration Test System " in *IEEE Conference on Electrical Insulation and Dielectric Phenomena, CEIDP*, Quebec, Canada, 2008, pp. 212-215.
- [270] Akira Nakajima, Kazuhito Hashimoto, and T. Watanabe, "Recent Studies on Super-Hydrophobic Films," *Monatshefte für Chemie* pp. 31-41 2001.
- [271] B. P. v. d. Wal, "Static and dynamic wetting of porous Teflon® surfaces," in *Department of Polymer Chemistry*. vol. PhD Netherlands: University of Groningen, 2006, p. 120.
- [272] E. Da Silva and S. M. Rowland, "In-Service Surface Degradation of MV Composite Insulators under Severe Environmental Conditions and Low Electric Stress," in *Electrical Insulation and Dielectric Phenomena, 2008. CEIDP 2008. Annual Report Conference on*, 2008, pp. 224-227.
- [273] D. D. Hinde and D. Birtwhistle, "Water drop to Metal and Water drop to Water drop Corona Discharges," in *XVII International Conference on Gas Discharges and their Applications*, Cardiff University, Cardiff, UK, 2008.
- [274] D. Langemann, "A droplet in a stationary electric field," *Mathematics and Computers in Simulation*, vol. 63, pp. 529-539, 2003.
- [275] D. Langemann, "The free transmission problem for a water droplet," Berlin, Germany, 2004, pp. 387-93.
- [276] D. Langemann, "Pseudo-transient processes in the numerical simulation of a water droplet in an electric field," *PAMM*, vol. 5, pp. 679-680, 2005.
- [277] D. Langemann, "Modelling a droplet moving in an electric field," *Mathematics and Computers in Simulation*, vol. 68, pp. 157-169, 2005.
- [278] D. Langemann and M. Krüger, "3D model of a droplet in an electric field," *Mathematics and Computers in Simulation*, vol. 66, pp. 539-549, 2004.
- [279] D. Shin, S. Lee, C. Choi, and S. Retterer, "The evaporation and wetting dynamics of sessile water droplets on submicron-scale patterned silicon hydrophobic surfaces," *Journal of Micromechanics and Microengineering*, vol. 20, p. 6, 2010.
- [280] D. Shin, S. Lee, J. Jung, and J. Yoo, "Evaporating characteristics of sessile droplet on hydrophobic and hydrophilic surfaces " *Microelectronic Engineering* vol. 86, pp. 1350-1353, 2009.
- [281] R. D. Deegan, O. Bakajin, T. F. Dupont, G. Huber, S. R. Nagel, and T. A. Witten, "Contact line deposits in an evaporating drop," *Physical Review E*, vol. 62, p. 756, 2000.
- [282] N. Shahidzadeh-Bonn, S. Rafa, D. Bonn, and G. Wegdam, "Salt Crystallization during Evaporation: Impact of Interfacial Properties," *Langmuir*, vol. 24, pp. 8599-8605, 2008.

- [283] E. Odic, A. Goldman, M. Goldman, M. Dhainaut, and R. Dussart, "Current distribution of AC surface discharges and associated chemistry," *Journal of Electrostatics*, vol. 64, pp. 477-484, 2006.
- [284] P. T. Tsarabaris, C. G. Karagiannopoulos, and N. J. Theodorou, "A model for high voltage polluted insulators suffering arcs and partial discharges," *Simulation Modelling Practice and Theory*, vol. 13, pp. 157-167, 2005.
- [285] C. Karagiannopoulos, "A model for dielectrics experiencing partial discharges under high electric fields.," *Jornal of Electrostatic*, vol. 65, pp. 535-541, 2007.